The use of a reverse genetics system to identify the functional domains of NS2 during Bluetongue Virus replication.

Victoria Alice Kate Easton

Thesis submitted in accordance with the requirements for the degree of

Doctor of Philosophy

University of London

January 2015

Department of Pathogen Molecular Biology

Faculty of Infectious and Tropical Diseases

LONDON SCHOOL OF HYGIENE & TROPICAL MEDICINE

Funded by BBSRC

London School of Hygiene & Tropical Medicine
Keppel Street, London WC1E 7HT
www.lshtm.ac.uk

Registry
T: +44(0)20 7299 4646
F: +44(0)20 7299 4656
E: registry@lshtm.ac.uk

DECLARATION OF OWN WORK

All students are required to complete the following declaration when submitting their thesis. A shortened version of the School's definition of Plagiarism and Cheating is as follows (*the full definition is given in the Research Degrees Handbook*):

"Plagiarism is the act of presenting the ideas or discoveries of another as one's own. To copy sentences, phrases or even striking expressions without acknowledgement in a manner which may deceive the reader as to the source is plagiarism. Where such copying or close paraphrase has occurred the mere mention of the source in a biography will not be deemed sufficient acknowledgement; in each instance, it must be referred specifically to its source. Verbatim quotations must be directly acknowledged, either in inverted commas or by indenting" (University of Kent).

Plagiarism may include collusion with another student, or the unacknowledged use of a fellow student's work with or without their knowledge and consent. Similarly, the direct copying by students of their own original writings qualifies as plagiarism if the fact that the work has been or is to be presented elsewhere is not clearly stated.

Cheating is similar to plagiarism, but more serious. Cheating means submitting another student's work, knowledge or ideas, while pretending that they are your own, for formal assessment or evaluation.

Supervisors should be consulted if there are any doubts about what is permissible.

DECLARATION BY CANDIDATE

I have read and understood the School's definition of plagiarism and cheating given in the Research Degrees Handbook. I declare that this thesis is my own work, and that I have acknowledged all results and quotations from the published or unpublished work of other people.

I have read and understood the School's definition and policy on the use of third parties (either paid or unpaid) who have contributed to the preparation of this thesis by providing copy editing and, or, proof reading services. I declare that no changes to the intellectual content or substance of this thesis were made as a result of this advice, and, that I have fully acknowledged all such contributions.

I have exercised reasonable care to ensure that the work is original and does not to the best of my knowledge break any UK law or infringe any third party's copyright or other intellectual property right.

To be completed by the candidate

NAME IN FULL: Victoria Alice Kate Easton

STUDENT ID NO: 224566

SIGNED:…… DATE: ……

Abstract

Bluetongue is a non-contagious arthropod transmitted viral infection of ruminants, especially sheep where mortality can reach up to 70%. Bluetongue Virus (BTV) has a genome of 10 double-stranded RNA segments which encode for 7 structural (VP1-7) and 4 non-structural proteins (NS1-4). A characteristic of BTV infected cells is viral inclusion bodies (VIBs), consisting mainly of NS2. The VIBs are the sites of immature virus assembly where the structural proteins VP3 and VP7, the transcription complex proteins (VP1, VP4, and VP6) and the BTV ssRNA are recruited and assembled. NS2 is a multifunctional protein which is thought to be essential during *in vivo* replication.

Three putative ssRNA binding domains have been identified in NS2; mutations to these regions have been designed to disrupt ssRNA binding. Two systems have been used to study these mutations: a novel BTV reverse genetics system to rescue and characterise the effect of the mutations *in vivo* through analysis of virus growth, protein production and VIB formation; and a baculovirus protein expression system used to assess the structural changes of NS2, if any, oligomerisation and BTV ssRNA binding activity.

This thesis presents the first *in vivo* and *in vitro* investigations into the ssRNA binding domains. The accumulated data demonstrated that mutation of the N-terminal domain had the most significant effect on BTV replication, its involvement in oligomerisation and BTV ssRNA binding. In contrast, the effect of the mutation of the middle and C-terminal RNA binding domains were less severe but still exhibited detectable differences in replication. In conclusion, NS2-ssRNA binding was shown to be essential for BTV replication.

Table of Contents

Abbreviations

AA – Antibiotic/Antimycotics

AcMNPV - *Autographa californica* multicapsid nucleopolyhedrovirus

AHSV- African horse sickness virus

APRV – Aedes Pseudoscutellaris Reovirus

ATPase – Adenosine triphosphatase

BHK – Baby hamster kidney cell

bp – Base pair

BSR – Baby hamster kidney cell sub-clone

BTV – Bluetongue virus

CFA – Cell free assay

CK2 – Casein kinase 2

CLP – Core like particle

CTFV – Colorado tick fever virus

Cryo-EM - Cryo-electron microscopy

DdRp – DNA dependent RNA polymerase

DISC –Disabled infectious single cycle

DIVA – Differentiate infected from vaccinated animal

dsRNA – Double stranded RNA

EHDV – Epizoonotic haemorrhagic disease

EMSA – Electrophoretic mobility shift assay

FCS – Foetal calf serum

HIV – Human immunodeficiency virus

hpi – Hours post infection

hpt – Hours post transfection

IFA – Immuno fluorescence assay

Kb – Kilo base pair

kDa – Kilo Dalton

KSHV – Kaposi's sarcoma-associated herpesvirus

LB – Luria Bertani

NMP – Nucleotide monophosphate

NTP – Nucleotide triphosphate

NTPase – Nucleotide triphosphate phosphohydrolase

PCR – Polymerase chain reaction

RdRp – RNA-dependent RNA polymerase

RG – Reverse genetics

RT-PCR – Reverse transcription polymerase chain reaction

SAXS – Small angle X-ray scattering

sRNA – single stranded RNA

VIB – Virus inclusion bodies

VLP – Virus like particle

WT- Wild type BTV-

95% CI – 95% confidence interval

Acknowledgments

I would like to thank my PhD supervisor Professor Polly Roy, whose dedication and knowledge are astounding and a source of inspiration. Her advice and encouragement were greatly appreciated. I would also like to thank the entire Roy lab for their support and friendship, especially Dr Meredith Stewart, Dr Cristina Celma and Dr Priya Bhattacharya for the countless ways in which they have helped me over the past 4 years. I would like to think the BBSRC for funding this research.

Thanks go to all my friends and family. I would not have been able to do this without your un-wavering support and belief. Special thinks go to Tristan De Luc and Sarah Rawle for letting me live with them. I don't always think I was the best lodger but they made coming home at the end of the day all the more welcome. Finally I would like to thank David Sadler, whose grasp of English grammar far outstrips my own and who looked after me when I couldn't look after myself.

I couldn't have done this without all your help.

Thank you.

Figures and Tables

Chapter 1

Chapter 2

Chapter 3

Chapter 4

Chapter 5

Chapter 1

Introduction

1. Introduction

Bluetongue virus (BTV) is the prototype virus of the *Orbivirus* genus in the *Reoviridae* family. It is a non-contagious, arthropod transmitted virus which infects sheep, especially fine wool breeds[1], with mortality reaching up to 70% [2,3]. Cattle, goats, wild ruminants and carnivores are also infected with BTV [4,5]. There are 27 distinct serotypes, including the recently identified BTV-25 from Switzerland, BTV-26 from Kuwait [6–8] and BTV-27 from France [9]. The virus, originally endemic in sub-Saharan Africa, has spread to every continent except Antarctica [10]. BTV is of great economic importance with an estimated 1 million sheep deaths in Europe since 1998 [11,12] and costs an estimated $125 million annually in the US: due to disruption to the movements of animals and their products [13]. Within the UK, a large scale outbreak similar to that seen in Belgium during the 2006-200 outbreak would result in 1% losses of cattle and 12% losses of sheep; costing £180 million [14]. Cattle productivity losses would cost an estimated £95 million/year. Vaccination in response to an outbreak in the UK was estimated to cost £35 million, while the cost of education for vets and farmers is an estimated £5 million a year in lost working hours [14].

1.1 Genus and Family

The *Reoviridae* family consists of viruses of icosahedral structure between 60 and 90 nm in diameter with a segmented (9-12) double stranded RNA (dsRNA) genome. Originally, the *Reoviridae* were defined as having 10-12 segments of linear dsRNA [15], but the isolation of Aedes Pseudoscutellaris Reovirus (APRV) from *Aedes*

pseudoscutellaris mosquito cells showed that this 9 segmented dsRNA virus exhibited significant sequence similarity with members of the *Reoviridae* family, especially cypoviruses, fijiviruses and oryzaviruses [16]. The target for this phylogenetic analysis of reoviruses is the RNA-dependent RNA polymerase (RdRp) of member viruses because it was considered the only gene which allows relevant analysis within this family [17]. Recently, other conserved segments such as those coding for the core and sub-core shell proteins have been used for phylogenetic analysis due to their similarity with equivalent segments within the *Reoviridae* family [18].

The *Reoviridae* are usually regarded as non-enveloped, although some can acquire a transient membrane envelope during morphogenesis [19] or cell exit, which was first seem in Colorado Tick Fever Virus (CTFV) in 1968 [20].

The *Reoviridae* have two subfamilies: *Spinareovirinae*, which have a turreted core protein; and the *Sedoreovirinae*, which have a smooth non- turreted core protein [21,22]. The turreted proteins are the viral capping enzyme while the non-turreted capping enzyme is contained within the subcore. Phylogenetic analysis of the RdRp has shown that the *Spinareovirinae* and the *Sedoreovirinae* cluster separately [23].

There are 15 genera within the family, of which the *Orbivirus* genus is the largest, consisting of 22 species and many unclassified isolates [24]. Orbiviruses are composed of a 10 segmented dsRNA genome enclosed within 3 concentric layers and are transmitted between hosts by invertebrate vectors including ticks, mosquitoes and biting midges [23]. BTV is the prototype virus of the genus *Orbivirus*. It has been studied extensively, is economically important and is the genus model for structure and

replication. 27 BTV serotypes have been reported. Phylogenic analysis of VP2, the primary serotype determinant, demonstrated that these serotypes form 10 lineages or nucleotypes [25]

Other economically important orbiviruses include African horse sickness virus (AHSV) and epizoonotic haemorrhagic disease virus (EHDV). AHSV has a mortality of up to 95% [26] and is able to spread outside the endemic area of sub-Saharan Africa to cause outbreaks in the Near and Middle East (1959–63)[1] , Spain (1987–90) [27] and Portugal (1989) [1]. EHDV infects wild deer and ruminants like domestic cattle [28 29] . Mortality in EHDV can reach up to 67% in white tail deer [30]. These viruses are economically important due to their high mortality; severe clinical signs including swelling of the head and neck, ulcers, lameness, fever and haemorrhages [31], production losses and the ban of trading livestock, ova and semen imposed on affected countries.

1.2 Disease, distribution and control

Bluetongue disease is characterised by changes to the mucous linings of the mouth and nose [13]. Clinical signs can vary by species and although symptoms are generally more severe in sheep, cattle can also show signs of disease.

Clinical signs of BTV infection in sheep vary greatly, but can include; eye and nasal discharges, swelling of the neck and head, ulcerations in the mouth, increased body temperature, lameness and haemorrhages under the skin. The “blue tongue”, after which the disease is named, is rarely a clinical sign of infection. Flock mortality may reach as high as 70% and those that survive may lose condition and experience

reduced wool and meat production. Severity of disease is related to the speed of onset and duration of pyrexia and not the titre of viremia [32].

BTV is transmitted by the *Culicoides* biting midges to animals during a blood meal [33]. Virus distribution is therefore based on the habitat of these biting midges, usually found between latitudes 40˚N and 35˚S [11]. Transmission is seasonal, with most occurring during summer and autumn when vectors are abundant. Vertical transmission is also a route of infection, with BTV shown to cross the placenta and infect foetuses in utero [34] and is a possible overwintering mechanism for BTV [34,35]. Vertical transmission can result in tetragenic effects, stillbirth and abortion due to haemorrhages, vacuolation of the cerebrum and meningoencephalitis [36,37]. Detection of BTV infection relies on both active surveillance, such as blood sampling and diagnostic tests; and passive surveillance like detection of clinical signs of infection by farmers. Infection with BTV, in particular BTV-8, is associated with decreased milk production and reduced fertility which can be an important indicator of infection when monitored [38,39] and could be widely used as another form of surveillance.

The nucleotide sequences of BTV isolates reflect their geographic origins [40] and most BTV genome segments can be divided into 'eastern' or 'western' topotypes [41,42], indicating that BTV has evolved with little genetic exchange between regions. This has allowed them to acquire point mutations and clear regional differences which may affect vaccine efficacy. Topotypes and serotypes are different, with BTV from the same serotype belonging to a different topotype. For example segment 2 of BTV can contain

74-81% amino acid identity and belong to the same serotype, while the same topotype will be 93-100% identical [23].

All BTV serotypes except BTV-18, 21, 23, 25, 26 and 27 have been isolated from Africa [43] and specific serotypes present in the USA, Australia, the Middle East and South East Asia. However, the distribution of BTV is changing and poses a threat to Europe as an emerging animal pathogen. The expansion of BTV northward into areas where the usual vector, *C. imicola*, is absent has been assisted by novel vector species such as *C. obsoletus* [44] and *C. pulicaris* [45]. It was in 1998 that BTV-9 first demonstrated an emergence into southern and eastern Europe, a region outside the normal habitat of the main vector *C. imicola*. BTV-9 was first identified in Greek islands off the Anatolian coast and in 2001 had reached Kosovo [46]. Following this in Greece BTV-4 and 16 incursions were detected in 1999 and BTV-1 was detected in 2001. It is thought that BTV-1, 9 and 16 infections were due to animal movements along the 'Eurasian ruminant street', similarly to other livestock diseases like foot-and-mouth disease [47]. Also in 2000, BTV-2 was detected in Tunisia, before spreading to Algeria, Morocco, Corsica, Sardinia, Sicily and Italy. It has been proposed that this spread of BTV-2 from sub-Saharan Africa to North Africa and Southern Europe was caused by the illegal movement of cattle, as shown by foot-and-mouth disease [48].

The BTV-8 serotype was responsible for a widespread outbreak. It was first detected in 2006 in the Netherlands and subsequently isolated in the Belgium, Germany, France and Luxembourg [49]. BTV-8 overwintered and in 2007 was confirmed in Germany [50]. New cases were found in Denmark, Switzerland, the Czech Republic and the UK [51–54].

Also in 2006, BTV-1 was reported in Morocco, Tunisia and Algeria [55–57], before spreading to Spain, Portugal and France in 2007-2008 [58–60]. A third serotype (BTV-6) was also present in Europe during 2008. It was first identified in the Netherlands and subsequently in Germany [61,62]. The BTV-6 strain caused less severe clinical signs and appeared to be very closely associated with the live attenuated vaccine strain of South Africa. Another outbreak closely related to an established live attenuated vaccine strain occurred in 2009 with BTV-11 detected in Belgium [63]. These outbreaks demonstrated that the live attenuated vaccine strains can circulate in a naïve animal population and cause clinical disease which is a concern for European vaccine strategies. New serotypes have also been detected in northern Europe. BTV-25 was originally isolated in Switzerland and BTV-27 from France [9]. The control measures for BTV outbreaks include: restriction of animal movement, vector control through the application of insecticides, slaughter of infected animals, and vaccination [64]. Preventative immunization against BTV is the most practical and effective control measure to combat infection. Presently, attenuated vaccines are used in several countries including South Africa and the USA. Attenuated live vaccines generally produce a higher and longer degree of protective immunity, compared to inactivated vaccines [65]. EU countries have historically used attenuated vaccines, but have recently moved to inactivated vaccines, favouring their relative safety. The major concerns of live attenuated vaccines are that they might not be sufficiently attenuated; mutate and revert to virulence when exposed to a large population, can show re-assortment with wild BTV strains [66], and that they do not inhibit post vaccination viremia [67]. Attenuated live vaccines can also have side effects such as: an increase in temperature, lameness,

oedema, hyperaemia and a decrease in milk production [68] - making them an unattractive option. Inactivated vaccines are not ideal either due to batch-to-batch variation; adverse reactions [69].

The concerns of classical live attenuated and inactivated vaccines; coupled with the current vaccines serotype specificity and the inability to differentiate infected from vaccinated animals (DIVA) [70], has resulted in the necessity to develop new generation vaccines. New-generation vaccines like subunit vaccines and virus-like particle (VLP) vaccines can be employed for DIVA because identifiable differences to wild-type virus can be designed into the vaccine and used for surveillance. Recombinant vaccines contain protein antigens which are produced from heterologous expression systems and closely mimic natural infection. These vaccines contain no genetic material and can generate cross-protection against multiple BTV serotypes. This is a good potential vaccine because often more than one serotype can be circulating within a population[71] and while conventional vaccines can be multivalent, the generation of recombinant vaccines can be very quick and easily scalable for an epidemic.

The development of a reverse genetics system for BTV [72] has led to the next generation of vaccines. Disabled infectious single cycle (DISC) vaccines replicate only once in a normal cell due to a mutation within an essential region. The mutant virus is incapable of producing infectious virions unless it is rescued in a complementary cell line that produces the defective protein *in trans*. The single replication cycle is sufficient to trigger a neutralising antibody response that protects vaccinated animals from challenge[73]. Sheep have been immunised in studies and each produced an

immune response and were protected against a virus challenge, showing proof of concept for DISC vaccine strains[73]. It is, however, possible that a DISC vaccine stain could re-assort with a wild type strain in the host animal and generate a fully infectious virus.

1.3 Bluetongue Virus Structure and Proteins

BTV is a large and structurally complex virus which contains 10 double stranded RNA segments [74], encapsidated within an icosahedral triple shelled virus particle which is found as both a whole particle, diameter of ~880 Å [75], and cores from which the outer capsid has been removed [76,77]. BTV possesses 4 major structural proteins (VP2, VP3, VP5 and VP7), 3 minor proteins (VP1, VP4 and VP6) (Figure 1) and 4 non-structural proteins (NS1, NS2, NS3/NS3A and NS4) [78] encoded by the 10 dsRNA segments.

The reconstitution of virus particles using baculovirus expressed structural proteins of BTV enabled the study of both virus and core structure. Core-like particles (CLPs) were shown to be similar to authentic BTV cores with regards to size, appearance, arrangement of VP3 to VP7, and the predominance of VP7 on the surface of the particles [79] (Figure 1.2. A & B). VLPs expressed the two major core proteins VP3 and VP7 of BTV and the outer capsid proteins VP2 and VP5 to synthesize non-infectious, double-shelled, virus-like particles [80] (Figure 1.2. C & D).

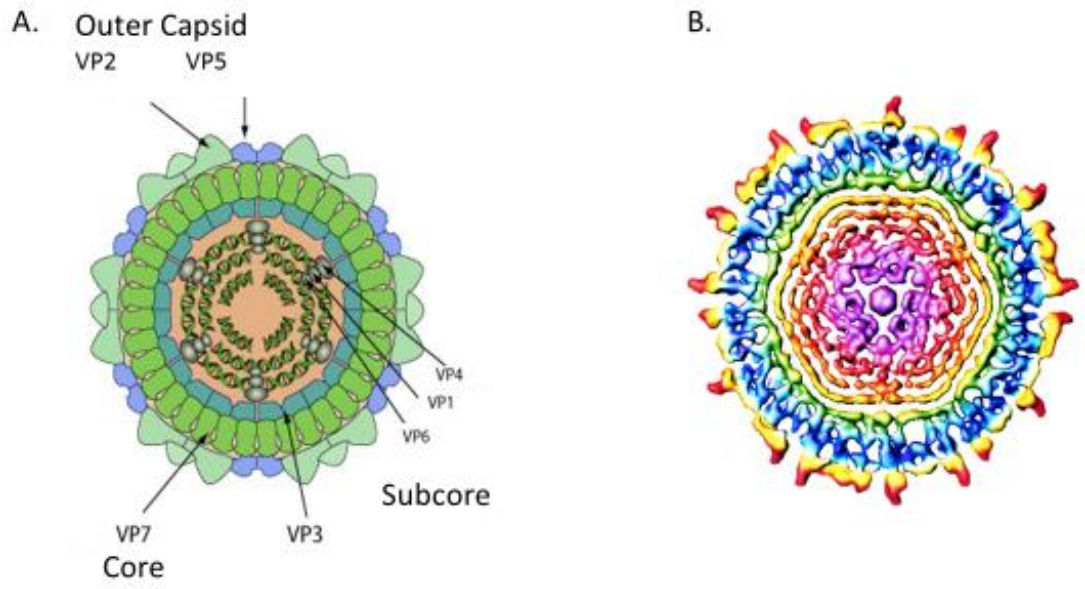

Figure 1.1. Cross-section of BTV.
A, Schematic layout of a cross-section of BTV. The virus is composed of three layers: the inner subcore of VP3 proteins, associated with VP1, VP4 and VP6 (minor structural proteins) and containing the 10 dsRNA segments, the core of VP7 proteins which stabilise the subcore; and outer capsid of VP2 and VP5 trimers which covers the core. Adapted Orbivirus diagram (www.expasy.com). **B,** Radial distribution of density cross section of BTV. Subcore = pink (RNA, VP1 and VP4) and green (VP3). Core = blue (VP7). Outer capsid = yellow (VP5) and red (VP2). Nason *et al*. 2004 [75].

Minor enzymatic proteins VP1 and VP4 were expressed by recombinant baculoviruses. Both proteins were encapsidated with core-like particles (CLPs), which indicated that the proteins were associated with subcore particles, particularly VP3 [81].

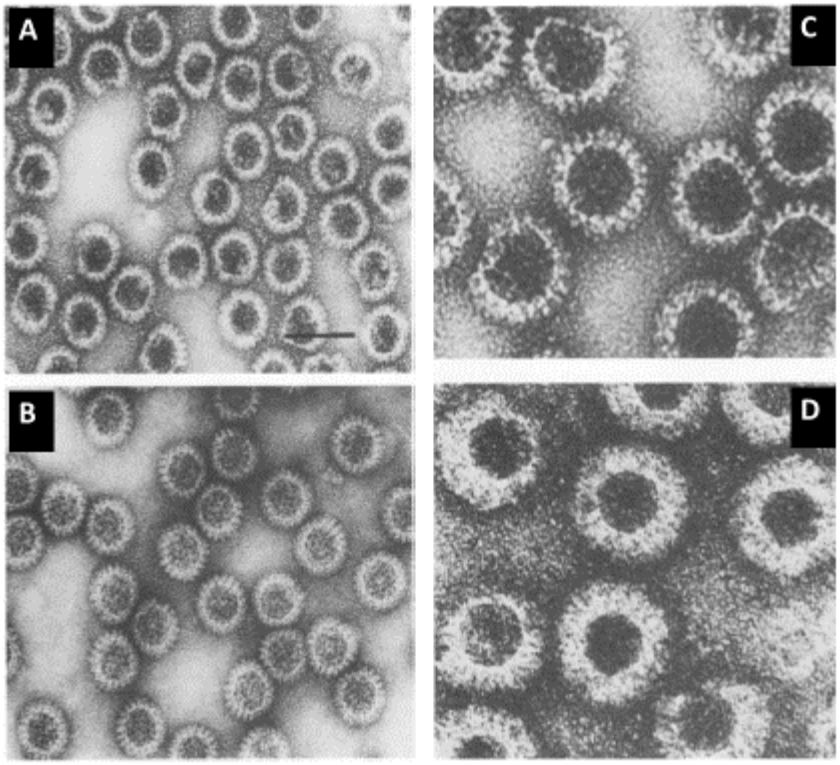

Figure 1.2. Electron micrographs of WT and Baculovirus expressed BTV particles
A, CLPs of baculovirus expressed VP3 and VP7 shown in panel compared with authentic BTV core particles in panel **B**. Bar, 100 nm. Adapted from French, Roy. 1990 [79]. **C,** CLPs of baculovirus expressed VP3 and VP7**. D,** Double shelled VLPS containing baculovirus expressed VP2, VP3, VP5 and VP7. Magnification x30, 000 Adapted from French, et al. 1990 [80].

1.3.1 Outer capsid

BTV, like the other members of Reoviridae: Rotavirus, Reovirus and Aquareovirus [82], has three concentric capsid layers. The outer layer is composed of the triskelion VP2 and the globular VP5 is similar to another Orbivirus, Broadhaven virus [83]. The outermost layer of BTV is comprised of 180 copies (60 trimers) of VP2 protein (110kDa) and 360 copies (120 trimers) of VP5 protein (60kDa)[84]. VP2 is a spike protein, three monomers of VP2 assemble as a triskelion structure with a propeller-like shape which

ends in three exposed tip domains (Figure 1.3. B,1), arranged around a central hub domain. (Figure 1.3. B,2).

VP2 is the most environmentally exposed BTV protein and because of this a high selective pressure is enforced upon VP2 by the host immune response. Sequencing data has demonstrated that VP2 is highly variable and falls into 26 distinct serotypes [8] with specific sequence variations exhibiting geographical origins or topotypes [25,85]. Some regions of VP2 display higher sequence variation which suggests specific regions of VP2 are under a higher selection pressure [86]. It has been speculated that these regions could comprise the highly exposed tip domains. VP2 alone has been shown to produce a neutralising antibody response which can protect an animal against BTV infection[87].

VP2 acts as a receptor binding protein; it attaches the virus to the mammalian cell surface through interactions with an as yet unknown glycoprotein [88] and sialic acid. Electron cryo-microscopy (cryo-EM) of the VP2 structure reveals structural features that facilitate this activity [89]. The hub domain (Figure 1.3. B,2) exhibits a galectin-like fold shared with that of the sialic acid binding domain VP8 in Rotavirus, which has been demonstrated to bind sialic acid [90] in a domain similar to the β-sandwich fold seen in the galectins family of sugar binding proteins [91]. BTV entry into the mammalian cell is via the clathrin mediated endocytotic pathway; entry into acidic endosomes is essential for effective virus infection [92]. There is however, evidence that the majority of BTV-1 entry into mammalian cells is clathrin and cholesterol-independent [93] and could be via micropinocytosis like HIV[94], KSHV [95]and Adenovirus type-3 [96].

VP5 is a globular, membrane permeablisation protein which lays slightly more internally than VP2 (Figure 1B) and mediates virus release from the endosome to the cytoplasm where virus replication and assembly take place[97]. Low pH changes VP5 conformation and allows for a fusion-like action between the endosome and the outer capsid, facilitating core release[98]. It has been postulated that VP2 may inhibit VP5 [89] by partially blocking the trimers [75]. VP2 may undergo a conformational change due to receptor interaction and endosome acidity, inducing or allowing VP5 permeablisation activity. It has been shown that removal of both VP2 and VP5 to release the BTV core is needed for virus replication into the cytoplasm[76]. Interestingly, VP2 and VP5 were shown by immunopercipitation to interact with each other minimally and with extensive interactions with VP7 [75]. VP2 interacts with the core layer on the fivefold axes of the T=13 lattice of VP7, occluding the Type I channels located there. VP5 interacts with VP7 above the Type II and III channels - effectively sealing the virus.

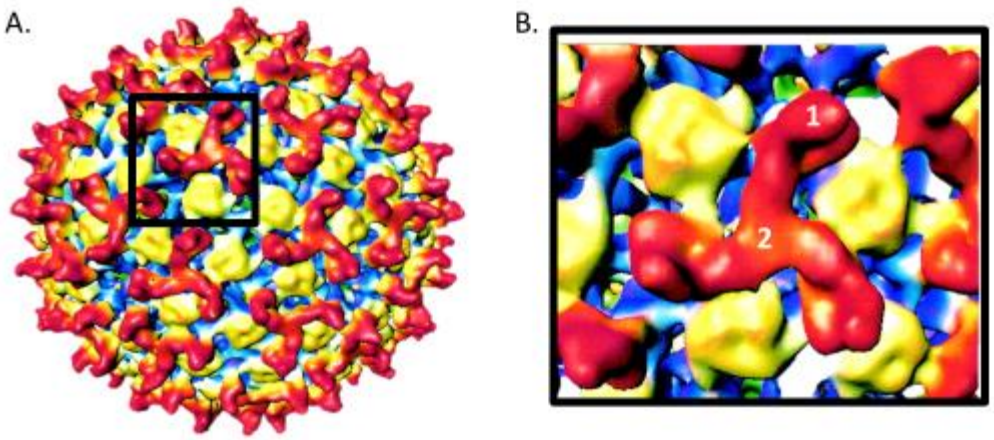

Figure 1.3. BTV outer capsid.
A, Electron cryomicroscopy (cryo-EM) reconstruction of a mature BTV particle. The structure is radially color-coded as in Figure 1B; yellow, VP5 and red, VP2. **B,** Close-up of the outer capsid structure showing the VP2 triskelion propellers of are shown in red with three tip domains (1) and a central hub domain (2). The VP5 globular domains are shown in yellow. Adapted from Nason *et al*. 2004 [75].

1.3.2 Core and subcore.

Most spherical viruses including BTV have some degree of icosahedral symmetry. An icosahedron has twenty faces with 5, 3 and 2 planes of rotational symmetry. There are five-fold axes of symmetry through the vertices (or apexes) of which there are twelve, ten 3-fold axes of symmetry though each face of the icosahedron and fifteen two-fold axes of symmetry passing through the edges. The shell is made of repeating subunits of viral protein, with the number of protein subunits placed in non-equivalent

positions determining the T-number; this has been derived from the 'quasi-equivalence theory' [99].

The core is made up of two concentric shells and has a diameter of 700 Å [100]. The core, composed of 780 copies (260 trimers) of VP7 (38.5 kDa), is arranged on a T = 13 icosahedral lattice [101] and is located between 260 Å to 345 Å from the centre of the core [102], and the subcore of 120 copies VP3 (103kDa) is arranged on a T = 2 icosahedral lattice as decamers [103] which is located between 230 to 260 Å from the centre of the core [102].

The VP7 trimers are described by the five copies of VP7 trimers found in each icosahedral lattice designated P, Q, R, S and T [102]. The P trimer is located closest to the icosahedral fivefold axis with alphabetical labelling according to their order, proceeding away from the fivefold axis towards the S trimer adjoining the icosahedral twofold axis and finally the T trimer located on the icosahedral threefold axis (Figure 1.4. A). The VP7 trimers are arranged to allow channels at all the five- and three-fold positions.

VP3 (T2) (103 kDa) has two folding patterns (VP3A and VP3B) (Figure 1.4, B outlined in Yellow) which form 'flower-like' decamers (Figure 1.4. B outlined in white), 12 decamers of equal numbers of both VP3A and VP3B 'zip' together in order to form a closed shell with small pores for extruding the ssRNA during translation[103]. VP7 is anchored onto the surface of the VP3 layer resulting in a very stable protein shell to shield the dsRNA genome from the cytoplasm.

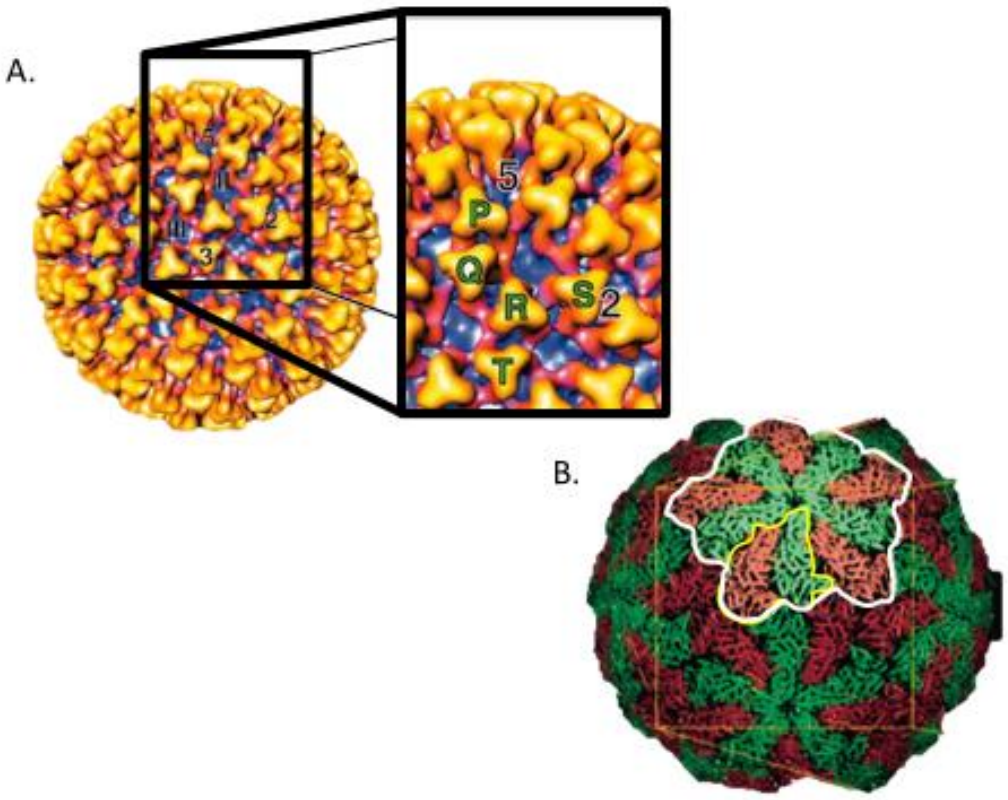

Figure 1.4. BTV core and subcore.
A, The 23 Å cryo-EM reconstruction of the core of BTV. Surface representation of the core showing the trimers of VP7 (yellow-red), and the sub-core VP3 (purple) below. 2, 3 and 5 denote the icosahedral symmetry; II and III denote the position of class II and class III channels. Enlarged portion highlighting the P, Q, R, S and T VP7 trimer positions. Adapted from Grimes *et al*. 1997 [102]. **B**, The 3.5 Å resolution X-ray crystallography structure of the subcore of BTV. The two forms of VP3 identified as, VP3A (green) and VP3B (red). These form a dimer (outlined in yellow) which associates to form a decamer (outlined in white), twelve of which compose the subcore. Adapted from Grimes *et al*.1998 [103].

The inner core contains 12 transcription complexes (comprised of VP1, VP4 and VP6) and 10 dsRNA segments. The transcriptase complex transcribes full length mRNA copies of the dsRNA genome and extrudes them from the cores surface[74]. X-ray crystallography[103] and Cryo-EM [75,101,102] have shown that channels penetrate through

the core and subcore to allow the release of mRNA at 10 of the 12 icosahedral vertices. Directly under the subcore at these vertices, reside the transcription complexes (Figure 1.5)

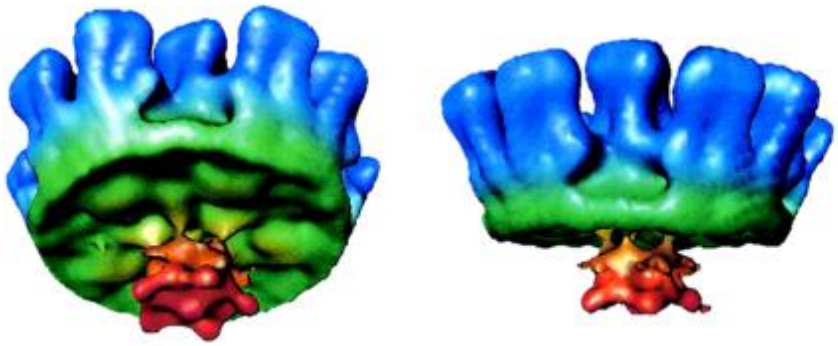

Figure 1.5. Cryo-EM structures of recombinant CLPs and the locations of the transcription complexes.
Transcription complexes = pink/red (VP1 and VP4), subcore = green (VP3), core = blue (VP7). Inside view of the CLP reconstruction with VP3, VP7, VP1, and VP4. A transcription complex (red) attached to the inside surface of VP3 (green) is found at all the fivefold vertices. Nason *et al*. 2004 [75].

VP1 is the largest BTV protein at 150kDa. By using a recombinant VP1, it was demonstrated that the protein acts as a RNA dependant RNA polymerase (RdRp) and thus able to catalyse RNA replication within the core [104,105,74]. This is unlike Rotavirus which requires both VP1 and VP2 [106]. Also of interest is the degree of specificity VP1

displays. VP1 can generate dsRNA from BTV and Rotavirus ssRNA transcripts but not non-viral transcripts unless 5' and 3' terminal sequences are added [107]. This suggests that a common secondary structure is found among Reoviruses which is necessary for RdRp replication.

VP4 is a 76kDa protein. Recombinant baculovirus expression of this protein established that VP4 is solely sufficient to generate the cap structures on ssRNA [108]. The capability of BTV VP4 to be the sole cap forming protein is similar to that found in Rotavirus VP3 [109], but unlike other viruses such as Vaccinia [110] where capping is reliant on a complex of proteins to carry out the different catalytic steps. BTV VP4 produces a cap 1 structure, similar to other Reoviruses [111], and thus demonstrates RNA triphosphatase, guanylyltransferase, guanine-N7-methyltransferase, and nucleoside-2'-O-methyltransferase [112,113]

VP6 (36kDa) is a helicase with ATPase activity [114,115] and both ssRNA and dsRNA binding [116]. These features are necessary for the unwinding of the dsRNA prior to the synthesis of the ssRNA by the polymerase, within the core. VP6 can form ring-like hexamers [114], similar to the other hexameric helicases such as the Papillomavirus DNA helicase E1 [117] and the *E. coli* ATP-dependent helicase rho [118]. Further investigation into VP6 using the BTV RG system to generate a VP6 deficient virus has shown that it is essential for replication [73], supporting its role in genome packing.

1.3.3 Genome

The BTV genome consists of ten dsRNA segments, S1 – S10. These vary in size from 3944 base pairs (bp) (BTV1 S1)[119] to 822 bp (BTV1 S10) [120]. Each segment codes for a

single protein except for S9 which encodes for VP6 and NS4 through different reading frames [121,122] and S10 which codes NS3 and NS3A [123] through different translation start sites [124]. The segments also have conserved sequences in the 5' (GUUAAA) and 3' (CACUUAC) UTR [125]. The length of the 3' UTR differs between the 10 segments of BTV, but is highly conserved among the same segments of different serotypes.

Each mRNA possess a 5' cap 1 structure and lack polyadenylation at their 3' terminus [108]. Transcripts are released from the core particle into the host cell cytoplasm where they act as templates both for translation of virus proteins and for the synthesis of negative strand RNA to generate genomic dsRNAs [123,126,127].

1.3.4 Non-structural proteins

BTV produces 4 non-structural proteins during infection; NS1, NS2, NS3/NS3A and NS4, of which NS1 (64kDa) is the most highly produced [128] during BTV infection and was shown to be the sole component of viral tubules through recombinant expression [129]. The tubules consist of coils of NS1 dimers which form a helical lattice 523 Å in diameter [130]. Originally the function of NS1 was thought to be involved in morphogenesis and the movement of progeny viruses to the cell membrane [131–133]. More recently however, NS1 has demonstrated the ability to promote the expression of BTV proteins - effectively acting as a positive regulator for translation [134]. The exact role of the tubules formed by NS1 is still unknown. Tubules and viral inclusion bodies (VIBs) are classic signs of BTV infection[135].

NS3 is the smallest BTV protein at 25 kDa. It is the only membrane protein of BTV [136] and has two forms NS3 (229 aa) and NS3A (216 aa) due to two initiation codons [124].

The interaction of NS3 with both the outer capsid proteins VP2 [137] and VP5 [138], as well as lipid raft domains [139] (which are associated with assembly of enveloped viruses like HIV [140], Ebola [141] and Measles [142]), suggests that NS3 brings the outer capsid proteins and the cores together for assembly into mature virions. NS3 has a role in BTV budding from insect cells [143] whilst egress from mammalian infected cells is largely through cell lysis, producing extensive cytopathic effect (CPE) [144], some particles are also released non-lytically through the plasma membrane using NS3 and the cellular trafficking protein S100A10/P11[145,146].

Bioinformatics had suggested that Segment 9 encoded another gene due to an overlapping open reading frame [147], this was recently shown to produce the NS4 protein[122]. The exact function of NS4 is still unknown although it has been shown that early in infection NS4 forms aggregates in the cytoplasm and nucleus while late in infection it associates with the cell membrane [121].

1.4 NS2

VIBs are large, perinuclear, granular structures [148,149] where viral replication and core assembly occur [148,150,151] (Figure 1.6). They are mainly formed of NS2 which produced in large quantities in BTV infected cells from as early as 2-4 hours post infection, with the largest amounts being produced between 12-20 hours [128,148]. Electron micrographs and immunogold labelling have shown that NS2 is associated with the VIBs and not with the virions themselves[152]. NS2 (42kDa) is encoded by segment 8 of the BTV genome and is essential for replication in mammalian cells [153].

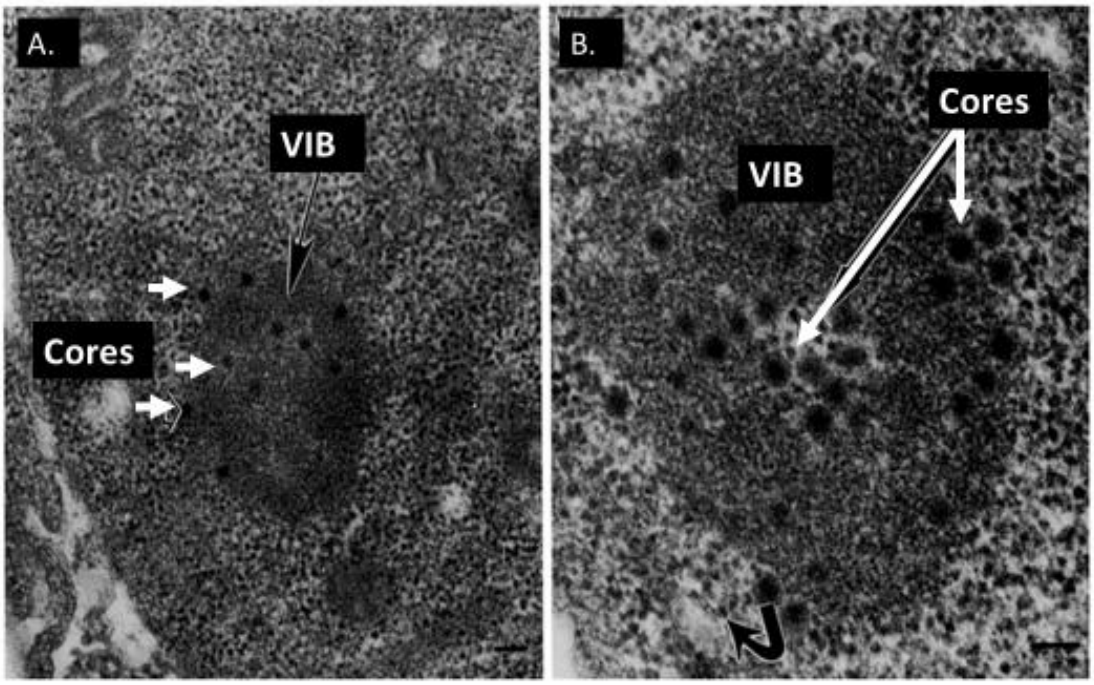

Figure 1.6. Transmission electron micrographs (TEMs) illustrating VIBs.
A, BTV infected mammalian cell showing a VIB (Black arrow) and BTV cores (White arrows). **B,** Close-up of a VIB late in infection. Curved clack arrow represents virus particles at the periphery of the VIB, possibly during release. All bars represent 100nm. Adapted from Brookes *et al,* 1993 [148].

Many recombinant expression systems have been used to express and study NS2 properties including bacterial [154], mammalian [150] and insect cells through baculovirus expression. The expression of NS2 alone using a baculovirus system results in the formation of inclusion bodies like those found in BTV infected mammalian cells [155]. This suggests that the NS2 protein is the minimal component for inclusion body formation. VIBs within BTV infected cells are also associated with ssRNA and viral proteins (VP1,

VP3, VP4, VP6 and VP7)[135,152,156,157]. The NS2 protein has several characteristics, the functions and domains of which are still not fully understood.

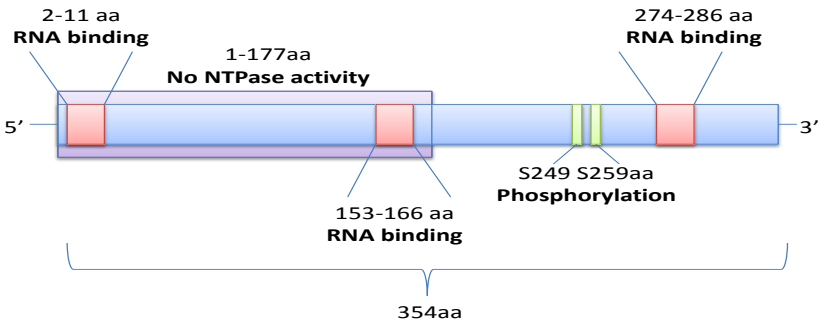

Figure 1.7. Schematic diagram of the putative functional domains of NS2.
NS2 is 354aa in length. Fillmore *et al*. 2002 [158], identified three regions which reduced ssRNA binding (shaded in red). Modrof *et al*. 2005 [151], determined that the Serines at 249 and 259 were phosphorylated (shaded in green). Mumtsidu *et al*. 2007 [159], demonstrated that a mutant lacking the N-terminal 177aa (shaded in purple) was still able to hydrolyse NTP's.

1.4.1 NS2 ssRNA binding

NS2 exhibits ssRNA binding activity. The VIBs in infected cells are able to recruit ssRNAs and co-localise with both core and subcore proteins, although VP7 recruitment was mediated by VP3 expression [150]. Non-specific ssRNA binding was initially suggested [155,160] ,but more recently NS2 has been shown to preferentially bind to BTV-RNA [156,161]. All BTV segments share conserved sequences in the 5' and 3' UTR (GUUAAA and

CACUUAC, respectively) [125]. It was originally thought that these sequences would be involved in RNA recruitment by NS2; deletion experiments however, showed that transcripts without these features had the same affinity for NS2 as wild type (WT) transcripts by Electrophoretic Mobility Shift Assay (EMSA) [162]. The lack of sequence specificity for binding to NS2 suggested that a secondary structure was necessary. A stem-loop structure on BTV segment 10 was identified as the recognised region of binding rather than a particular RNA sequence [161]. Other segments were subsequently investigated and unique secondary structures to each were found to bind to NS2 [156]

Through a series of deletion experiments Fillmore *et al* [158] identified three regions within NS2 which when removed impeded ssRNA binding (Figure 1.7). The ability to select and bind BTV mRNA segments is consistent with the idea that NS2 plays a key role in the assembly of progeny virions.

1.4.2 NS2 phosphorylation

Many viral proteins have the ability to be phosphorylated; the number of non-structural proteins with this ability is, however, far smaller. NS2 is the only phosphorylated BTV protein. Phosphorylation occurs at the serine residues S_{249} and S_{259} [163] (Figure 1.7). NS2 is phosphorylated in both BTV infected mammalian cells [160] and when expressed by recombinant baculovirus in insect cells[155]. Additionally, Modrof *et al* [151], showed that insect and mammalian expressed NS2 is phosphorylated at the same amino acids, serine residues 249 and 259 (Figure 1.7). Casein kinase 2 (CK2) has been identified as the cellular kinase which causes the phosphorylation of NS2[151].

A relationship between phosphorylation and ssRNA binding was previously suggested[161], however Modrof *et al* [151] showed that non-phosphorylated NS2 mutants still demonstrated specific RNA binding equal to that seen in WT BTV NS2. Phosphorylation of NS2 is essential for the formation of NS2-NS2 multimers and thus VIBs. The formation of inclusion bodies was impaired in unphosphorylated NS2 mutant $S_{249}A$ $S_{259}A$ [151].

1.4.3 NS2 NTPase activity

Bacterially expressed NS2 has the ability to hydrolyse the α, β and γ phosphodiester bonds of nucleotide triphosphates (NTPs) to nucleotide monophosphates (NMPs) [154], the process is dependent on divalent ions Ca^{2+}, Mg^{2+} and Mn^{2+} [164]. The energy produced is used during energy requiring processes such as BTV genome packaging and transport [165], or the unwinding of RNA loop structures[166]. The functional domains responsible for the NTPase activity are unknown, although it is presumed not to be within the first 177aa of NS2 (Figure 1.7) because a mutant protein missing this portion was still able to hydrolyse NTPs [159].

1.4.4 NS2 Structure and Multimerisation

NS2 exists in heterogeneous oligomeric states. When purified from recombinant baculovirus infected cells which were treated with RNase A, NS2 was detected as ~7S multimers [167]. These results are similar to a later study which found 8-10S multimers with RNase treatment and larger 18 and 22S multimers without RNase treatment [154] . An 8–10S multimer of NS2 has a molecular mass of between 140 and 250 kDa and

would assemble to form 6 ± 2 subunits. This is dissimilar to the findings from the X-ray crystallography obtained structure of the N-terminal domain of NS2, which indicated that the full-length protein could assemble as multimers of 10–11 subunits [168]

High-resolution structural information is difficult to obtain for the BTV NS1 and NS2 proteins because of their predisposition to form higher oligomers of variable size. The crystal structure of the N-terminal region of NS2 (8-160 aa) has been determined to a 2.4Å resolution and exhibits extensive monomer-monomer interactions, indicative of its ability to assemble into large complexes [169]. The asymmetric unit forms a dimer which stacks to form a spiralling helix. It has been suggested that RNA may bind within the inner channel (76.7 Å) along with the C-terminal of NS2, stabilising the oligomerisation. At 76.7 Å, the interior channel may have an insufficient volume to contain both the C-terminal domains of each of the monomers and RNA (Figure 1.8. A).

The structure of the C-terminal domain (178–354 aa) of NS2 has been reported by small-angle X-ray scattering measurements (SAXS) and size exclusion chromatography to form a dimer in solution [159] (Figure 1.8. B), 12 nm by 3nm. A full length model of NS2 was created upon the assumption that the C-terminal domain must reside inside the ring-like structure formed by the N-terminal domain and that the conformation of the domains would not change significantly in the full-length protein (Figure 1.8. C). These are a speculative, but reasonable hypotheses, considering the model matches the diameter of the central hole observed in the EM images at 25 Å. The external diameter of the proposed full-length model (100 (± 10) Å) differs slightly from the EM images (120 Å). In this model the putative RNA binding domains would be between the outer

ring formed by the N-terminal domain and the inner ring formed by the C-terminal domain, suggesting that RNA would lay between the two domains, as with rotavirus NSP2[170].

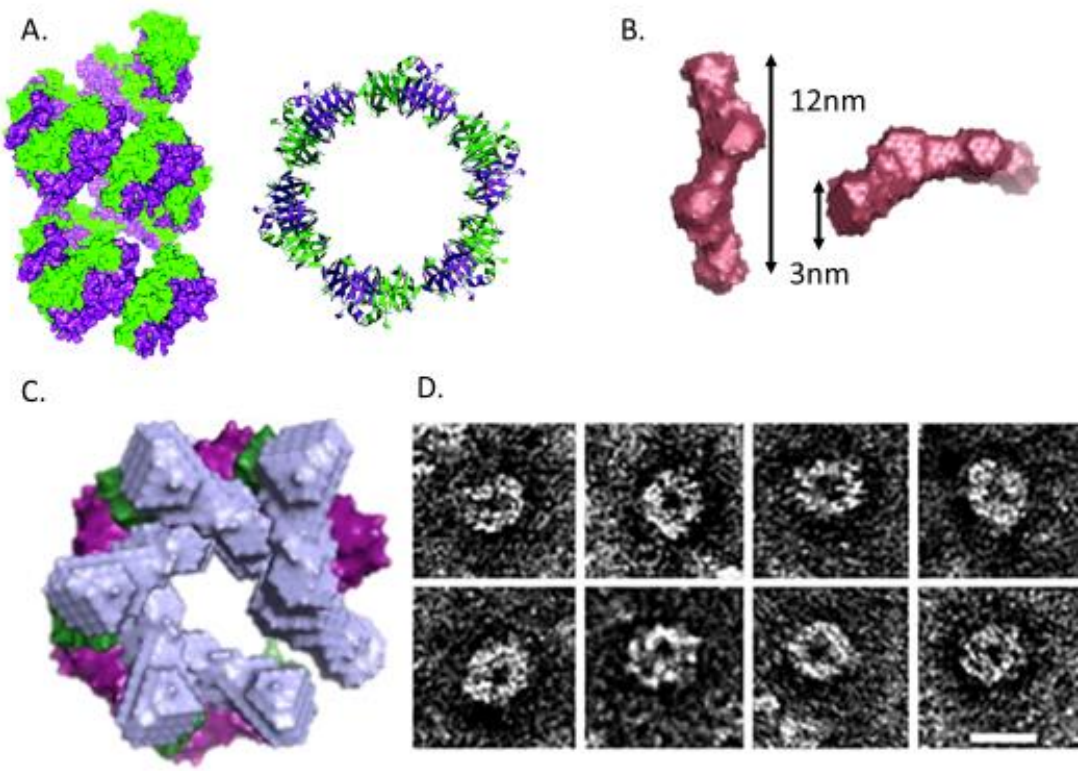

Figure 1.8. NS2 structure.
A, X-ray structure of the NS2 N-terminal domain (residues 8–160). A spiralling dimer (Green and Purple) in two different orientations. Diameter ~100 Å. Adapted from Butan *et al,* 2004 [169]. **B,** Model of the NS2 C-terminal dimer obtained by DAMMIN, in two different orientations. Adapted from Mumtsidu *et al,* 2007 [159]. **C,** The hypothesised structure of a decamer of full-length NS2. External diameter of 120 Å, internal diameter25 Å. Adapted from Mumtsidu *et al,* 2007. **D,** Electron micrographs of full-length NS2 ring-like structures with a diameter of 100 (± 10) Å and internal diameter 25 (± 10) Å. (scale bar 100 Å). Adapted from Mumtsidu *et al,* 2007.

Interestingly, VIB proteins from other members of the *Reoviridae* family; P9-1 Rice Black Streak Dwarf Virus (RBSDV) [171] and NSP2 Rotavirus [172], show low sequence

homology but form multimers in ring-like structures and bind RNA. These structures however, are octomers and form closed rather than helical rings.

1.4.5 NS2 homologues in the *Reoviridae* family

The *Reoviridae* family express non-structural proteins with a similar function to NS2, although there is very little sequence homology. In rotaviruses the functions of NS2 are undertaken by two proteins, NSP2 [173] and NSP5, whereas in reoviruses the σNS and μNS have these functions [174].

Like BTV NS2, complexes of NSP2/NSP5 and σNS/μNS are associated with ssRNAs during virus replication [175,176] to form VIBs [177] , specifically NSP2 [173] and σNS [178] and form multimers. NSP2 is octameric [172] whereas σNS is trimeric to hexameric [178], similar to NS2 which in the absence of RNA is proposed to form a hexamer (± 2 subunits) [167] or a decamer [168] .

BTV NS2 and Rotavirus NSP2 are able to hydrolyse NTPs to NMPs [154,164,173], but while NS2 can cleave α, β and γ phosphodiester bonds, rotavirus is only able to cleave the γ phosphodiester bond [154,173]. NSP2s is autophosphorylated due to the cleavage of the γ-phosphate from NTP but NS2 is phosphorylated by cellular kinase 2 [151] at the serine residues S_{249} and S_{259} [163]. σNS is not phosphorylated nor contains NTPase activity [178]. μNS does contain NTPase activity when associated with reovirus cores [179] and has an affinity for ssRNA [180]. σNS requires μNS for the formation of VIBs [181], in a comparable way to NSP2 requiring NSP5 [182].

1.5 BTV replication

The development of experimental systems such as reverse genetics, cell free *in vitro* assembly and tagged viruses have revolutionised the study of BTV replication and assembly. The BTV reverse genetics (RG) system has allowed specific mutations to be introduced into the exact copy clone of the gene [183]: enabling the role of proteins, and even individual amino acids, to be studied *in vivo* during replication. The generation of a cell-free assembly (CFA) system has enabled the reconstitution of subcore and core particles of BTV. This has enabled investigation into the assembly pathway of ssRNA and structural proteins into immature BTV particles [184]. Briefly, each core protein (VP1, VP4, VP6, VP3 and VP7) was synthesised *in vitro* as well as all 10 *in vitro* synthesised T7 derived transcripts [72] - due to the inherent assembly of BTV, infectious virus was produced. Recently, a tagged virus was generated which has facilitated the live cell imaging of BTV during replication for the first time [185]. These developments mean that BTV replication is the most well understood of the entire Orbivirus genus.

BTV replication in mammalian cells can be divided into virus entry, cell attachment, virus uncoating, ssRNA release from the core and genome replication, assembly, maturation and egress. BTV replication in mammalian cells is initiated by attachment to an as yet unknown cell surface glycoprotein [88] and sialic acid [89] (Figure 1.9. 1). BTV enters cells immediately after adsorption [185] through a clathrin-dependent endocytic pathway [92] (Figure 1.9. 2). This process was further examined by the tagged virus, which indicated that VP2 is shed from the virus in the early endosome and that VP5 is still present in the late endosome [185]. Due to the acidic conditions in the endosome,

VP5 undergoes pH-dependent conformational changes and is removed from the virus [92,98]. This releases the transcriptionally active cores into the cytoplasm [76] (Figure 1.9. 3).

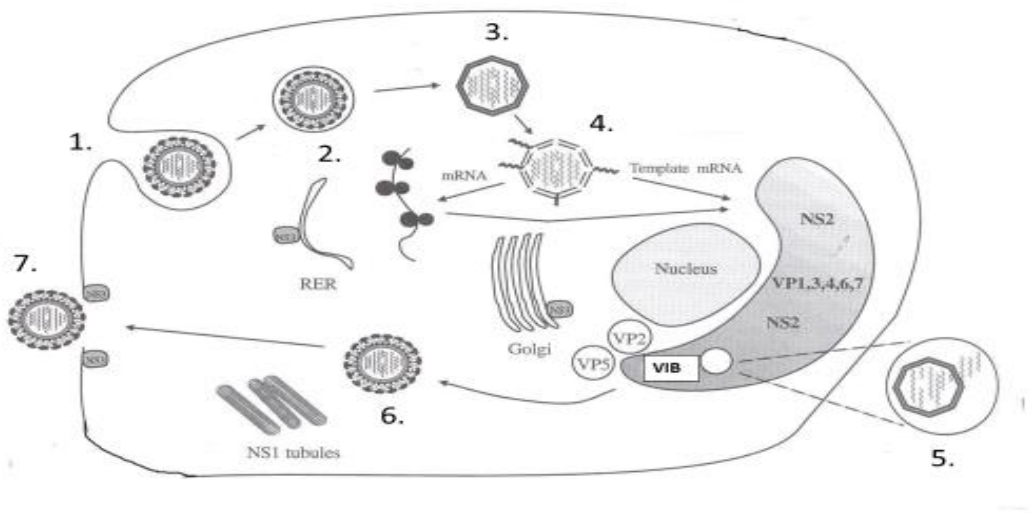

Figure 1.9. Diagram of BTV replication in mammalian cells.
1, BTV cellular attachment to an unknown glycoprotein receptor and sialic acid. **2,** Virus entry to cells through endocytosis. **3,** Acidic conditions cause the uncoating of the BTV core and release from the endosome. **4,** The core is transcriptionally active and extrudes ssRNAs which are used as templates for viral proteins and dsRNA segments. **5,** Assembly of progeny BTV cores within the VIBs. **6,** Release of the core from the VIBs and maturation with the addition of the VP2 and VP5 outer layer. **7,** Lytic and non-lytic virus egress. Diagram adapted from Fields Virology (3rd Ed), chapter 56, pg 1724.

The two major structural proteins of the core, VP3 and VP7, contain channels [102] through which NTPs can enter [186,187]. Within the core, NTPs are used to transcribe ssRNA from the dsRNA genome, by the VP1 polymerase and VP6 helicase. The newly synthesised ssRNAs are capped by VP4 and extruded through the channels located at the 12 vertices of the core [186] (Figure 1.9, 4).

These ssRNA molecules act as mRNA templates for both the synthesis of viral proteins and genomic dsRNA segments for progeny virions. NS1 enhances translation of BTV ssRNAs [134] but was shown by both the RG system and the CFA system to be a non-essential component of primary replication [153,184]. Assembly of BTV cores takes place within VIBs in the cytoplasm, with NS2 selectively recruiting BTV ssRNA and core proteins [150] (Figure 1.9, 5). The CFA system showed that the transcription complex (VP1, VP4 and VP6) and the ssRNAs assemble first and this is then encapsulated within VP3 to form the subcore. However, the addition of VP7 was shown to be necessary to form stable cores [184]. These cores were protected from RNase degradation by VP7 which plugs the largest pores in the VP3 layer [103], while retaining the channels needed for a transcriptionally active core. The ssRNA within the newly formed progeny cores are synthesised into the dsRNA segments of BTV [105].

Interestingly, the RG system demonstrated that NS2 is an essential component of the primary replication stage during *in vivo* BTV infection [153], while the CFA system revealed that NS2 is not essential for assembly of the core components *in vitro.* The essential nature of NS2 during *in vivo* replication was suggested to be due to its role as a concentrator of progeny virus components [153]. This was due to its ability to bind ssRNAs and the VIBs being associated with viral proteins (VP1, VP3, VP4, VP6 and VP7).

VP6 has been shown to be essential for *in vivo* replication by the RG system [73]. The complete role of VP6 during replication is unknown, but it has been demonstrated to be active early in infection [188], and may act as an RNA translocator during primary replicase complex assembly [153].

The cores are released from the VIBs and acquire the outer capsid of VP2 [137] and VP5 [138] with the aid of NS3/NS3A to form mature virions (Figure 1.9. 6). The majority of progeny BTV is released through cell lysis, with a small portion released non-lytically through budding using NS3/NS3A [143,189] (Figure 1.9. 7).

1.6 Reverse genetics

The BTV reverse genetics (RG) system, developed in our laboratory, allows specific mutations to be introduced into the exact copy clone of the gene, enabling the role of individual amino acids and structure to be studied. The ability to introduce specific mutations into the genome and study the phenotype of the recovered virus has transformed the study of some viruses, but not all viruses are agreeable to this technique. Positive sense ssRNA (+ssRNA) viruses were amongst the first to be studied using a reverse genetics system [190]. Poliovirus has a 7.5 kilo base pair (kb) infectious +ssRNA genome [191] which replicates its genome via a negative sense RNA (-ssRNA) intermediate template by RdRp (also called 3Dpol)[192]. A full length –ssRNA of the poliovirus genome was generated *in vitro* by bacteriophage SP6 DNA dependent RNA polymerase (DdRp) from a cloned cDNA template, which was in turn used as a template for the poliovirus RdRp. The resulting +ssRNA of the poliovirus genome were infectious when transfected into HeLa cells [193]. This was a major advance in the investigation of RNA viruses since site-directed mutagenesis of RNA to produce defined substitutions directly is not possible, but manipulation of DNA using recombinant techniques is well established; this is then reintroduced into viable

viruses [194]. This was followed by negative sense ssRNA viruses such as Rabies [195] and Measles [196], and segmented negative sense RNA viruses like bunyaviruses [197].

Using a RG system for BTV, it is possible to rescue an infectious virus from BTV ssRNA transcripts. The process involves the transfection of mammalian cells with a full complement of BTV core derived ssRNA, which are able to generate infective Bluetongue virus within the cell[183]. This method was further developed to include the manipulation of BTV at the sequence level. *In vitro* production of plasmid derived T7 ssRNA transcripts have been used in isolation or with core derived transcripts to produce infectious BTV [72]. The plasmids were designed so that the transcripts are under the control of the T7 promoter and contained a restriction site in order to form the exact 3' end. This is a very powerful system which allows the recovery of mutants from a known genetic background, without having to screen for wild-type virus and allows specific mutations to be engineered into the gene, enabling the role of individual amino acids to be studied. Additionally, the use of complementary cell lines has allowed the recovery of replication defective mutants [73,189], through the supply of the defective protein *in trans*.

This method has been further optimized with the addition of a two-stage transfection. The first transfection contains plasmid DNA of the primary replication complex (VP1, VP3, VP4, VP6, NS1 and NS2) [188], this is followed by the second transfection of all 10 plasmid derived T7 ssRNA transcripts.

1.7 The Baculovirus expression system

The *Baculoviridae* family is a large and varied group with over 1000 members, most of which infect arthropods. These viruses have a large double stranded, circular DNA genome of 88-153 kb. The family has two genera: *nucleopolyhedroviruses* (NPV) and *granuloviruses* (GV) [198].

The largest sub-group of baculoviruses are the NPV which have been extensively studied, especially the *Autographa californica* multicapsid nucleopolyhedrovirus (AcMNPV) [199,200], which is widely used for the expression of heterologous proteins [201]. There are four classes of baculovirus genes. The immediate early and late early genes induce viral gene expression at the beginning of infection; late genes can be transcribed by virus only transcriptional machinery. The very late genes code for proteins such as the polyhedrin or occlusion bodies which protect and package progeny viruses in the host nucleus [202].

For over 30 years [203], polyhedrin and p10 genes have been vital in the development and use of the baculovirus expression system. This is because they are transcribed through a strong promoter in the later stages of insect infection [204]. The polyhedrin and p10 proteins can account for up to 50% of total insect cell protein [205]. Most importantly, the polyhedrin and p10 proteins are not essential for survival in cell culture so a foreign gene can be inserted to replace them [203]

There are many advantages to baculovirus expression over other expression systems: polyhedrin and p10 have strong promoters which produce large quantities of protein,

these proteins are expressed very late in the virus life cycle (24 hours post infection) so cytotoxic proteins will not affect virus replication [200]. Foreign proteins will undergo eukaryotic post-translation processing such as phosphorylation, and disulphide bond formation, and will also be correctly folded. The baculovirus genomes can accommodate large inserts because of their large (~130kb AcMNPV) genome and they are safe to work with as they do not infect humans [206]. The baculovirus expression system can be propagated to high titres in insect cell suspension, which makes obtaining large amounts of recombinant virus relatively easy. Late and very late promoters are similar except that the very late elements have an additional downstream enhancer sequence which leads to hyper-transcription [207]. There have been constant improvements on the system to address the constraints of the initial baculovirus expression system. These fall into two general categories; transfer plasmid modifications and baculovirus genome modifications. Transfer plasmid modifications aimed to improve the identification of recombinant virus plaques through screening with a visual marker such as *E.coli* β-galactosidase [208]. They also aimed to assist recombinant protein expression. Parental genome modifications have been designed for many reasons but the initial aim was to improve the low recombination efficiency. Kitts and Possee 1990 [209], developed a recombinant baculovirus which contained a *Bsu*36I restriction site to linearize the baculovirus genome, and the linear forms were found to be 15 -150 fold less infectious than the native circular genome when transfected into *Spodoptera frugiperda* (Sf) cells . The linear baculovirus, when recombined with an appropriate transfer vector to restore circularisation and hence infectivity, generated a 10-fold higher number of positive recombinants compared to

the original circular AcMNPV genome. It is commonly used to aid co-transfection in insect cells and to reduce the number of parental progeny viruses produced. A second improvement was the mutation downstream of orf:1629 to produce a genetically unstable bacmid, rendering the genome non-infectious. Infectivity is only rescued once there is successful recombination with an appropriate transfer vector [210].

Chapter 2

Materials and methods

2.1 Cell lines and viruses

BSR cells (baby hamster kidney cell derived line) and BS8-S8 (baby hamster kidney cells constitutively expressing NS2) cells were maintained at 37°C in Dulbecco's modified Eagle's media (DMEM, Sigma, UK) containing 10% [v/v] Foetal Calf Serum (FCS) and 1x antibiotic/antimycotic (AA). BSR-S8 media contained an additional 75 µg/ml puromycin.

The BTV serotype 1 (BTV-1) was used as the wild-type control and as the basis for BTV NS2 mutants. Alignment of NS2 amino acid sequence was based on serotype. Information on accession numbers, serotype, location and collection date is shown in table 1. Appendix 1 contains the full Alignment of NS2 amino acid sequences.

Table 1. Information on the serotypes used in the NS2 amino acid alignment

GI and Accession Number	BTV Serotype	Collection Date	Location
gi|238821240|gb|ACR58465.1	1		South Africa
gi|557882471|gb|AEO19765.2	2		South Africa
gi|480327200|gb|AGJ83438.1	3		South Africa
gi|410443430|gb|AFV67789.1	4	1997	China
gi|480327240|gb|AGJ83458.1	5		South Africa
gi|480327260|gb|AGJ83468.1	6		South Africa
gi|480327280|gb|AGJ83478.1	7		South Africa
gi|410444351|gb|AFV68257.1	8		
gi|557882457|gb|AEO19789.2	9	2000	Italy
gi|385722006|gb|AFI73131.1	10	2004	India
gi|480327360|gb|AGJ83518.1	11		South Africa
gi|480327380|gb|AGJ83528.1	12		South Africa
gi|480327400|gb|AGJ83538.1	13		South Africa
gi|480327420|gb|AGJ83548.1	14		South Africa
gi|480327440|gb|AGJ83558.1	15		South Africa
gi|545290083|gb|AGW27499.1	16	2011	India

gi|480327480|gb|AGJ83578.1	17		South Africa
gi|480327500|gb|AGJ83588.1	18		South Africa
gi|480327520|gb|AGJ83598.1	19		South Africa
gi|389616810|gb|AFK91775.1	20	1977	Australia
gi|480327560|gb|AGJ83618.1	21		South Africa
gi|480327600|gb|AGJ83638.1	22		South Africa
gi|443411621|gb|AGC83568.1	23	1988	India
gi|480327640|gb|AGJ83658.1	24		South Africa
gi|210076696|gb|ACJ06706.1	25	2008	Switzerland
gi|355346214|gb|AER60537.1	26	2010	Kuwait

All baculovirus work was performed in the *Autographa californica* multicapsid nucleopolyhedrovirus (*Ac*MNPV). Bacmid (KO:1629) contained a mutation at the 1629 polyhedrin locus. Recombinant baculoviruses were propagated by infection of monolayer cultures of *Spodoptera frugiperda* cells *Sf*9 [203] and *Sf*21 [211] cells at 28°C in Insect express media (Lonza, Biowhittaker) supplemented with 1x AA or TC-100 media (Lonza, Biowhittaker) 8% FCS and 1x AA respectively, and maintained as previously described [212].

All plasmids (pAcYM1, pAcYM1-H/GST, pAcYM1-H/GST NS2 and pUc19-T7 S1-S10) were kindly donated by the Roy laboratory. Plasmids were purified from transformed DH5α *E.coli* cells grown in Luria-Bertani (LB) broth and appropriate antibiotic at 200 rpm, or on a solid LB-agar media (1.5% [w/v] agar) at 37°C. In-Fusion cloning (ClonTech) was performed in Steller competent cells (ClonTech). The media was sterilised by autoclaving (121°C, 20lb/in^2 for 20 min). Glycerol stocks of bacteria were made by mixing bacterial culture and sterile glycerol to a 1:1 ratio and stored at -80°C. All incubation was performed in an Infors AG CH-4104 incubator.

2.1.1 Preparation of chemically competent cells for plasmid amplification

DH5α *E. coli* cells were used for propagation of plasmid vectors. Briefly, a 1:50 dilution of a 37°C overnight culture of DH5α cells grown in LB was made using fresh broth and grown to an OD of 0.35-0.6 at A_{550} measure on an Ultraspec 1000 (Amersham Pharmacia biotech) spectrophotometer. All further steps were performed on ice or at 4°C. After 15 min incubation the culture was then centrifuged at 3000 rpm in an Allegra 21R centrifuge (Beckman Coulter) for 10 min. The pellet was resuspended in 1/3 the original volume of ice-cold RF1 (100mM KCl, 50mM $MnCl_2$, 30mM KAc, 10Mm $CaCl_2$ and 15% [v/v] glycerol), incubated for 15 min and centrifuged as stated above. The pellet was then resuspended in 1/12 the original volume of ice-cold RF2 (10mM MOPS pH6.8, 10mM KCl, 7.5mM $CaCl_2$ and 15% [v/v] glycerol) and incubated for a final 15 min. Aliquots of 100-200µl were flash frozen using a dry ice/ethanol slurry and stored at -80°C.

2.1.2 Purification of plasmid and bacmid DNA

All plasmid and bacmid DNA was purified using either the alkaline lysis midi prep method as outlined in Sambrook [213] or by commercial kit. The following changes were made to the Sambrook method. Briefly, room temperature solution I (5mM Tris HCl pH7.5, 2 mg/ml RNaseA), II (1% [w/v] SDS, 0.8% [w/v] NaOH) and III (29.5% [v/v] glacial acetic acid, pH 4.8 potassium acetate) were added sequentially at equal quantities to the pellet of an overnight growth to fully lyse the cells and form a white precipitate. After centrifugation the plasmid was extracted from the supernatant by phenol:chloroform:isoamyl alcohol (25:24:1, PCI) followed by precipitation with

isopropanol and ethanol. Briefly, an equal volume of PCI was added to the supernatant and centrifuged, the aqueous phase was collected and an equal volume of chloroform added and centrifuged. The aqueous phase was added to an equal volume of isopropanol and placed at 4°C to improve DNA yield, then centrifuged at 14,000 rpm for 20 min. The pellet was resuspended in 70% ethanol, centrifuged twice, resuspended in TE buffer (100mM Tris HCl pH 7.5, 10mM EDTA) and stored at -20°C. The same procedure was used to purify bacmid DNA, but greater care was taken to prevent shearing. All centrifugation was performed at 3000 rpm and the purified stock was stored at 4°C.

Plasmids for recombination and transformation were purified with the PureLink plasmid midiprep kit (Invitrogen) or the Wizard gel and PCR clean up kit (Promega), these were used to manufacturer's instructions. The only modification to the protocol was the placement of the sample at -20°C after the addition of isopropanol to improve DNA yield. All centrifuge steps were performed using an Allegra 21R (Beckman Coulter). All plasmids underwent restriction digestion using an appropriate enzyme to verify presence of the insert before any experimental work. The reaction contained 1x enzyme specific buffer, purified plasmid DNA, 5U enzyme per µg DNA and dH_2O to final volume. Reactions were digested for 2 hours and products detected by gel electrophoresis on a 1% [w/v] TBE (89 mM Tris, 89 mM boric acid, 2 mM EDTA) agarose gel with 1 µg/ml ethidium bromide at 110 V for 30 min.

2.2 Generation of mutant BTV

2.2.1 Amplification and sequencing of DNA fragments by PCR

Polymerase Chain Reaction (PCR) was used to amplify DNA fragments using specific primers to amplify coding regions of BTV (Table 1). Primers were designed using Integrated DNA Technologies web software and ordered from Sigma (Poole, UK).

PCR was routinely performed using the proofreading Kappa HiFi polymerase (Kappa Biosystems, UK). The reactions contained 1x Kappa HiFi reaction buffer, 0.2 mM dNTPs, 15 pmol/µl specific forward and reverse primers (Table 1), 0.02 U Kappa HiFi polymerase and template DNA. Reactions were carried out in a Verti 96 well thermocycler (Applied Biosystems)

Sanger sequencing was performed by Source BioScience (London, UK). The complete sequence of the NS2 coding region was compiled using Bio-edit software and confirmed as BTV Segment 8 with appropriate mutations through nucleotide Blast (NCBI). Products were detected by gel electrophoresis on a 1% [w/v] TBE agarose gel with 1 µg/ml ethidium bromide at 110 V for 30 min

Table 2. Primers

Oligonucleotide Name	Sequence (5'-3')	Components
BTV-1 S8 T7 *Bam*HI F	CGGGATCCTAATACGACTCACTATAGTTAAAAAATC CTTGAGTCA	BamHI T7 Promoter
BTV-1 S8 *Bsm*BI/ *Bam*HI/*Rsr*II R	CATGGGATCCGGACCGTCTCCGTAAGTGTAAAACAT TCACATTTT	BamHI BsmBI RsrII
BTV-1 NS2 *Bam*H1 F	CGGGATCCGTAAATCATGGAGCAAAAGCAACGTAG ATTTACTA	BamHI PH promoter

BTV NS2.N BamH1 F	CGGGATCCTAAATCATGGCCCAAGCGCAAGCTGCTTTTACTA	*Bam*HI PH promoter
BTV-1 S8 627R	CCAGCAGATTGGAGAAGCTG	
BTV-1 S8 530F	GAGAATCAGCGCCACGGC	
BTV-S8.N HaeIII F Mutation Primer	GTTAAAAAATCCTTGAGTCATGGCCCAAGCGCAAGCTGCTTTTACTAAAAACATTTTTG	S8.N mutations
BTV-S8.N HaeIII R Mutation Primer	CAAAAATGTTTTTAGTAAAAGCAGCTTGCGCTTGGGCCATGACTCAAGGATTTTTTAAC	S8.N mutations
BTV-S8.M SacII F Mutation Primer	CGATGTTCGTGAACTGCGGCAAAAGATCGCAAATGCAGCAGCATCAGCGCCGCGGCTTCAAGTTCAAAGC	S8.M mutations
BTV-S8.M SacII R Mutation Primer	GCTTTGAACTTGAAGCCGCGGCGCTGATGCTGCTGCATTTGCGATCTTTTGCCGCAGTTCACGAACATCG	S8.M mutations
BTV-S8.C PvuII F Mutation Primer	GAGAAGGTTGCAAAGCAGATTGCATTAGCAGCTGCAGCGTTCATGAGTCTATCAAGCGCTATGC	S8.C mutations
BTV-S8.C PvuII R Mutation Primer	GCATAGCGCTTAGTAGACTCATGAACGCTGCAGCTGCTAATGCAATCTGCTTTGCAACCTTCTC	S8.C mutations
In-Fusion F Primer	GAAAACTTGTACTTTCAAGGATCCATGGAGCAAAAGCAA	*Bam*HI
In-Fusion S8.N F Primer	GAAAACTTGTACTTTCAAGGATCCATGGCCCAAGCGCAA	*Bam*HI S8.N mutations
In-Fusion R Primer	ATAAATGTACTAATAACCGGATCCGTAAGTGTAAAACAT	*Bam*HI

Table 3. Typical thermocycler conditions used for the amplification of target DNA.

Stage	Step	Temperature (°C)	Duration (min:s)	Cycles
1	initial denaturation	98	2:00	1
2	denaturation	98	0:20	35
	annealing	55-70	0:15	
	extension	72	0:30	

3	final extension	72	7:00	1
4	hold	15	10:00	

2.2.2 Site-directed mutagenesis, restriction digest of parental plasmid and transformation

Forward and reverse mutagenesis primers were designed to be complementary to each other and contain the mutations (pUc19T7S8.N, pUc19T7S8.M and pUc19T7S8.C) to be inserted and at least 15 flanking bases identical to the parental sequence to ensure annealing [214]. Primers were designed using Intergrated DNA Technologies web software and ordered from Sigma (Poole, UK). PCR reaction was as above, as were conditions, except for extension time which was extended to 3 min to allow for extension to proceed around the whole plasmid. Products were detected by gel electrophoresis on a 1% [w/v] TBE agarose gel with 1 µg/ml ethidium bromide at 110 V for 30 min

The parental plasmid pUc19T7S8 was restriction digested with *Dpn*I in 1xTango buffer (Fermentas, UK) for 1 hour at 37 °C to eliminate parental plasmid DNA and increase the recovery of mutant plasmid. *Dpn*I was deactivated by a 20 min incubation at 80°C. PCR products were purified using a commercial kit prior to transformation into chemically competent *E. coli* DH5α (section 2.1.1) by heat-shock. Competent cells (50 µl) were incubated on ice for 30 min, heat-shocked at 42°C for 30 s and further incubated on ice for 2 min. 300 µl of LB was added and the transformation reaction was incubated at 37°C for 45 min to allow the *E. coli* to recover. Transformed cells were plated onto LB agar containing 100 µg/ml ampicillin.

2.2.3 Selection, screening and sequence analysis of recombinant *E.coli*

Initial selection of DH5α containing the inserted plasmid was by ampicillin resistance. Screening of colonies was performed either by restriction digestion (Section 2.1.2) using an appropriate enzyme, or through a colony PCR method. Colony PCR was as section 2.2.1, but the template DNA was provided by transformed DH5α colonies and specific primers amplify a region of the plasmid if a successful transformation has occurred. Following this, selected colonies were grown in 5 ml LB broth containing 100 µg/ml ampicillin at 37°C for at least 16 hours. Plasmids were purified by alkaline miniprep method described in section 2.1.2.

Positive constructs were sequenced using specific forward primer (BTV-1 S8 T7 *Bam*HI F), internal (BTV-1 S8 627R and BTV-1 S8 530F) and reverse (BTV-1 S8 *Bsm*BI/ *Bam*HI/*Rsr*II R) to ensure the exact insertion of the mutations. Full length sequencing was performed by Source Bioscience (London, UK). The complete sequence of the coding region was compiled using Chromas software and confirmed as BTV-1 S8 with the designed mutations through nucleotide Blast (NCBI).

2.2.4 Generation of RNA transcripts

Previously within the lab 10 cDNA plasmid clones were generated each containing one of the 10 BTV-1 genome segments (pUc19 T7 S1- S10), a T7 promoter and a restriction site to give the correct 3' end when transcribed into RNA [72]. RiboMAX (Promega) (RNA polymerase, recombinant RNasin® ribonuclease inhibitor and recombinant inorganic pyrophosphatase) was used for uncapped RNA production through the T7 promoter

[215]. The reaction (10 µl) contained 100 mM rNTPs, 1x RiboMAX buffer (HEPES, pH 7.5), 2µg template DNA (pUc19 T7 S1- S10, restriction digested and highly purified in RNase free conditions), 10U T7 RNA polymerase, 10U RNasin RNase inhibitor (Promega), 0.1 % DEPC-treated H_2O and was incubated for 3 hours at 37°C before the addition of 0.5U RNase-free DNaseI to digest the template DNA and a further 15 min incubation. The reaction volume was increased to 70 µl with 10mM Tris-HCl pH8 and added to an equal volume of PCI, mixed and centrifuged. The aqueous layer was added to an equal volume of chloroform, mixed and centrifuged again. Illustra MicroSpin G-25 columns (GE Healthcare Life Sciences) were used as manufacturer's instructions to remove any remaining free NTPs from the product.

The RNA transcripts were precipitated with isopropanol and ethanol. An equal volume of isopropanol, 1/10 volumes of 3M Na acetate pH5.2 and 0.5 µl Glycogen were added to the transcripts and placed at 4°C to improve RNA yield, then centrifuged at 14,000 rpm for 20 min. The pellet was resuspended in 70% ethanol, centrifuged twice, and allowed to air-dry in a fume hood before being resuspended in 10 µl DNase-free RNase-free H_2O and stored at -80 °C.

Transcripts were detected on MOPS denaturing agarose gels (1% agarose, 1x MOPS, 0.1% DEPC-treated H_2O, 2M formaldehyde) in a 1x MOPS running buffer to assess the size, integrity and quantity of RNA transcripts. 1X MOPS was diluted with DEPC-treated H_2O from a 10x MOPS stock (400 mM MOPS pH7, 100 mM sodium acetate, 10 mM EDTA pH8). 0.5 µl RNA samples or 1µl RNA Marker (Promega) was added to 5 µl 2X

RNA loading dye (Thermo Scientific), heated for 2 min at 75°C and placed on ice before being loaded onto the gel and run at 80 V for 1 hour.

2.2.5 Reverse genetics system: recovery of mutant BTV

The BTV reverse genetics system (RG) allowed the recovery mutant viruses with specific mutations engineered into the genome, enabling the role of individual amino acids and structure to be studied. This system includes a two stage transfection: the primary transfection containing plasmid DNA of the primary replication complex (pCAG PBTV1VP1, pCAG PBTV1VP3, pCAG PBTV1VP4, pCAG PBTV1VP6, pCAG PBTV1NS1 and pCAG PBTV1NS2) [153,188]; and a secondary transfection containing all 10 BTV plasmid derived RNA transcripts, including the mutant segment 8 (Figure 2.1).

The primary DNA transfection reaction contained 120 ng of each plasmid and 2.5 µL (per µg DNA) lipofectamine 2000 (Invitrogen), both plasmid DNA and transfection reagent were diluted 1:1 in OptiMEM (Gibco) before being combined and incubated at room temperature for 20 min. BSR cells were grown to ~70% confluence and washed with DMEM serum-free media before the addition of the transfection reaction.

18 hours after the primary transfection was the secondary transfection. The reaction contained 120 ng of each of the 10 RNA transcripts and 2.5 µL (per µg RNA) lipofectamine 2000 (Invitrogen), both diluted 1:1 in OptiMEM (Gibco) before being combined and incubated at room temperature for 20 min. The cells were washed with DMEM serum free media, the transcription reaction added and then moved to the Category 3 laboratory. Cytopathic effect (CPE) was monitored for 72 hours.

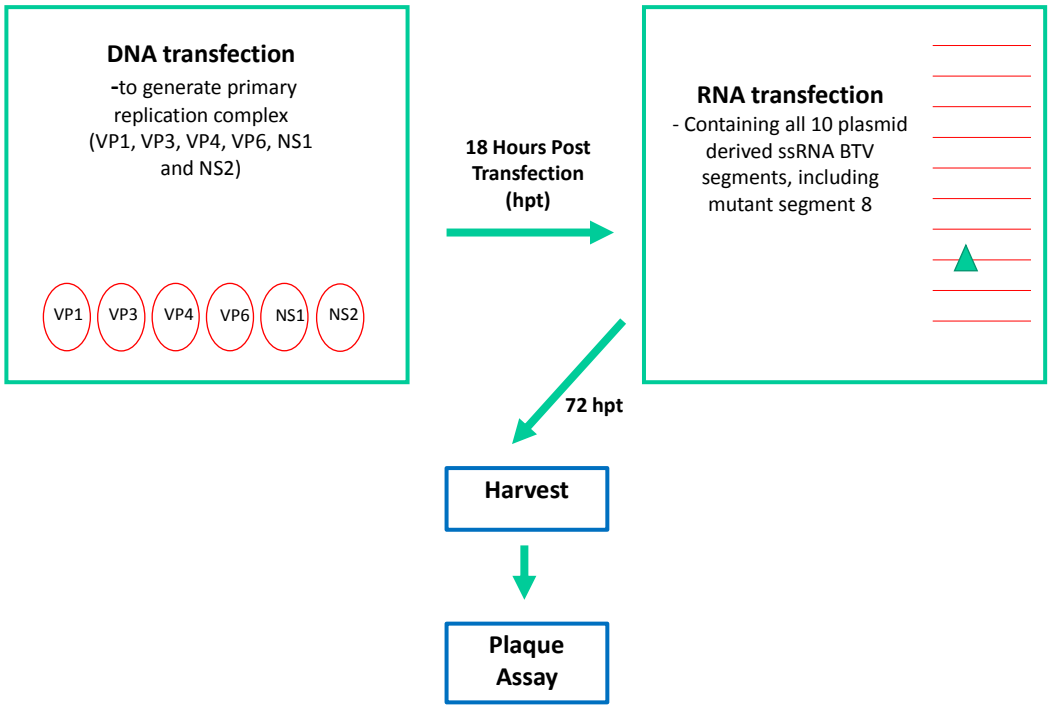

Figure 2.1. Diagram of the reverse genetics system used for the generation of BTV mutants.

2.3 Bluetongue Virus amplification

All experiments containing live BTV were carried out in the containment level 3 laboratory in compliance with Defra guidelines. The virus was propagated in BSR or BSR-S8 complementary cells. Briefly, confluent monolayers of BSR or BSR-S8 cells were washed in DMEM (no serum). A low MOI of BTV-1 was diluted in media without serum and added to the cells. The virus was adsorbed for 1 hour on a rocking platform and then the media replaced with DMEM (2% FCS, 1x AA). Virus was harvested and stored at 4°C once 100% CPE was achieved.

2.4 Plaque Assays

Plaque assays were performed for determining virus titre or generating clonal virus stocks. 6-well plates were seeded with BSR or BSR-S8 cells and infected with 1 ml of ten-fold virus dilutions ($1x10^{-1}$ - $1x10^{-6}$). After 1 hour absorption the monolayers were overlaid with sterile 3% low melting temperature agarose diluted 1:1 in 2x MEM supplemented with 8% [v/v] FSC, 2x AA and 2x Glutamine and incubated for 72 hours. Plates were either fixed with 4% paraformaldehyde for 3 hours prior to removal from the containment laboratory and plaques identified by crystal violet staining (0.2% [v/v] crystal violet, 20% [v/v] ethanol); or stained with Neutral Red (Sigma) (1:5 autoclaved 1x PBS (Oxoid)) to visualise the plaques for harvesting clonal stocks.

2.5 dsRNA purification and visualisation

The genomic pattern of segmented RNA was analysed using TRIzol (Life Technologies) for RNA isolation, a method based on guanidinium thiocyanate, phenol and chloroform extraction [216,217]. Briefly, 750 µl of TRIzol was used to re-suspend harvested and pelleted BSR or BSR-S8 cells infected with virus. Once the sample was deactivated by incubation for 10 min at room temperature), it was removed from the containment laboratory and mixed well with 1/10 volume chloroform. TRIzol contains phenol which when mixed with chloroform, increases yield [218], and also guanidine isothiocyanate which denatures protein. Centrifugation for 10 min at 14,000 rpm forms an aqueous layer which was harvested and added to an equal volume of isopropanol. After incubation for 20 min on ice the RNA was pelleted (14,000 rpm, 10 min) and

resuspended in 70 % ethanol (repeated twice). The pellet was resuspended in DEPC-treated H_2O and LiCl (final concentration 2M) and incubated overnight at 4°C to precipitate the ssRNA. The dsRNA remains in the supernatant was harvested by centrifugation (14,000 rpm, 5 min) and added to an equal volume of isopropanol before a 20 min incubation on ice and a subsequent centrifugation (14,000 rpm, 5 min) to pellet the precipitated dsRNA. The resulting pellet was resuspended in 5 µl DEPC H_2O

DsRNA was detected on a 9% non-denaturing PAGE to analyse the quality and quantity of dsRNA produced. Electrophoresis was performed with a Tris-Glycine running buffer [219].The gel was run at 170 V for 4 hours with 1.5 µl dsRNA sample in 6 µl of loading buffer and stained with ethidium bromide (0.5 µg/ml). All the above steps were performed under RNase free conditions to maintain RNA integrity.

2.6 RT-PCR

Reverse transcription was used to generate a cDNA copy of viral segment 8. The primary mix contained 2 pmol/µl of each forward primer BTV-1 S8 T7 *Bam*H1 and reverse primer BTV-1 S8 *Bsm*BI/*Bam*HI/*Rsm*II (Table 1), 0.25 µl RNasin Plus and 4 µl dsRNA. The secondary mix: 1x RT buffer (Fermentas), 0.8 µl RNasin Plus, 1U reverse transcriptase Revertase (Fermentas), 10mM dNTPs; was added after initial denaturation (95˚C) and cooling to the annealing temperature (55 ˚C). The mix was incubated (90 minutes, 55 ˚C) and then heated (85 ˚C) for inactivation.

Polymerase chain reaction (PCR) was used to amplify the cDNA produced from the Reverse transcription reaction. See section 2.2.1 for details.

2.7 Characterisation of mutant BTV

2.7.1 Virus growth at different time points

Confluent monolayers of BSR or BSR-S8 cells grown in 6 well plates were infected with wild-type BTV or mutant BTV at an MOI 1. At 0, 8, 16, 24, 36, 48, 72 and 96 hours post infection (hpi), both cells and supernatant were harvested and stored at 4°C to determine virus titre by plaque assay. Alternately, cells were pelleted and lysed in 1x cracking buffer (50 mM Tris HCl pH6.8, 2% SDS, 10% glycerol, 1% β-mercaptoethanol, 12.5 mM EDTA and 0.02 % bromophenol blue) prior to removal from the containment laboratory. Lysate samples were analysed on an SDS-PAGE and transferred to a nitrocellulose membrane for Western immno blotting using Trans-blot Turbo semi-dry blotter (Bio Rad).

2.7.2 BTV protein profile in infected cells

Viral proteins were detected by Western blotting using specific antibodies. The nitrocellulose membranes were blocked in 5% skimmed milk-PBST buffer (1x PBS, 0.25% Tween20) and incubated for 1 hour with the primary antibodies (Rabbit anti-NS1 antibody [1:5000], Rabbit anti-VP5 antibody [1:3000], Guinea pig anti-NS2 antibody [1:3000] or Mouse anti-Actin antibody [1:5000] diluted in 5% skimmed milk PBST) on a rotating platform. Membranes were washed for 5 min with PBST three times to remove excess of the primary antibodies. As secondary antibody Alkaline

phosphate conjugated anti-primary antibody was diluted 1:5000 with 5% skimmed milk PBST, incubated on a rotating platform for 2 hours. After extensive washing protein bands were detected with BCIP/NBT alkaline phosphatase substrate (Sigma-Aldrich)

2.7.3 Immunofluroesence and Confocal microscopy

Standard protocols were used as described previously [137]. Briefly, BSR cells were grown to 100% confluency on 13mm glass cover slips. The cells were washed and infected at an MOI 10 as section 2.3. 24 hpi the infected cells were fixed with 4% paraformaldehyde and removed from the containment laboratory. Dual staining was performed with primary antibodies (guinea pig α BTV-1 VP7 [1:100] and rabbit α BTV-10 NS2 [1:100]) and secondary antibodies (TriTC - rabbit [1:1000], Alexa 488 - guinea pig [1:1000] nuclear staining Hoechst [1:2000]). The slides were examined using a Zeiss Axiovert 200M laser scanning microscope and the images were acquired using Velocity confocal software.

2.8 Generation of recombinant baculovirus expressing mutant BTV proteins

2.8.1 In-Fusion cloning of mutant BTV NS2 into pAcYM1-H/GST

The In-Fusion cloning system (ClonTech) is a PCR based system which allows the insertion of any PCR fragment or gene (20 bp to 15 kb), directionally into a linearized vector in a single reaction. This system is free from the need to clone into restriction

sites and established on the In-Fusion enzyme's ability to create single-stranded regions at the 5' and 3' ends of the PCR insert and linearized vector, creating complementary regions on the insert and vector DNA which anneal through base pairing without the need for a ligase.

Previously within the Roy laboratory In-Fusion cloning was used to generate pAcYM1-H/GST- NS2, a pAcYM1 plasmid containing BTV-1 S8 coding region with 5' His and GST tags connected by a short flexible linker. Figure 2.2 shows an outline of the In-Fusion cloning method. The primers (In-Fusion F Primer and In-Fusion R Primer) were also used to generate appropriate 5' and 3' pAcYM1 homologous ends onto BTV-1 S8.M and BTV-1 S8.C, with a new 5' primer (In-Fusion S8.N F Primer) designed for BTV-1 S8.N which would not interfere with the mutations at the 5' end. PCR was used as section 2.2.1 with a small modification: 30 pmol specific forward and reverse primers were used and pUc19T7S8, pUc19T7S8.N, pUc19T7S8.M and pUc19T7S8.C as template DNA. The products were detected by ethidium bromide staining (section 2.2.1) and purified with the Wizard gel and PCR clean-up kit (section 2.1.2).

Plasmid pAcYM1-H/GST was purified by alkali lysis as section 2.1.2, fully linearized by restriction digest with *Bam*HI and further purified by Wizard gel and PCR clean-up kit (section 2.1.2). This was quantified by ND-1000 Nanodrop. A ratio of 2:1 linearized pAcYM1-H/GST vector to insert was used for ligation. The amount of insert required for ligation of 100 ng of vector was calculated with this equation:

$$\frac{\text{ng of vector} \times \text{Kb of insert}}{\text{Kb of vector}} \times \text{ratio of vector to insert} = \text{ng of insert needed}$$

The ligation reaction (10 µl) contained 100ng linear vector, 50ng insert and 1U In-Fusion enzyme was incubated at 50 °C for 15 min and placed on ice for 5 min before being transformed into Steller competent cells (ClonTech) by heat-shock (Section 2.2.2). Selection, screening and sequencing of positive *E. coil* colonies containing the plasmid and insert was performed as section 2.2.3.

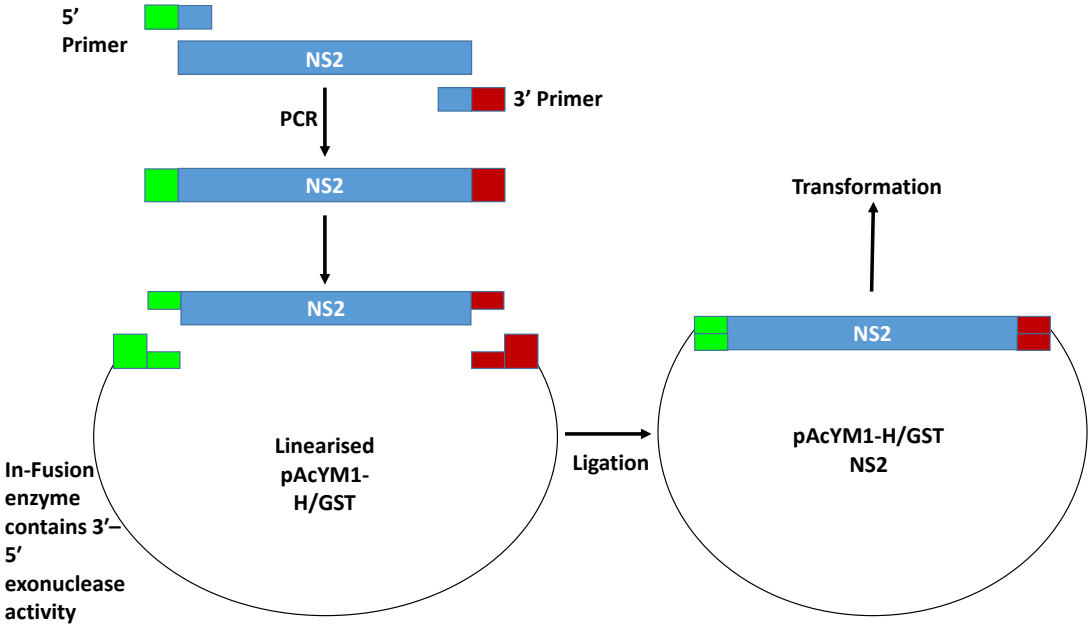

Figure 2.2. Diagram of the In-Fusion cloning of NS2 into pAcYM1-H/GST.

2.8.2 Transfection of Bacmid and pAcYMI-H/GST NS2 WT and mutants

The WT and mutant BTV-1 NS2 expression must be validated prior to *in vitro* characterisation of the effects of the mutations on ssRNA binding. To achieve this, Bacmid KO:1629 DNA was purified and digested by *Bsu*36I restriction enzyme for 2

hours at 37°C to linearize the DNA. The reaction consisted of 1x NEB buffer 3; purified bacmid DNA (section 2.1.2); *Bsu*36I (NEB) 5U per µg bacmid DNA.

*Sf*9 cells (0.6 x10^6 cells) were seeded onto 12-well plates and transfected with the *Bsu*36I linearized AcMNPV KO:1629, transfer vector pAcYM1-H/GST containing either WT or mutant BTV S8 and X-tremeGENE 9 (Roche) according to manufacturer's protocol. 250 ng pAcYM1-H/GSTS8 plasmid, 200 ng *Bsu*36I linearized AcMNPV KO:1629 and 1.5 µl transfection reagent with 50 µl OptiMEM (Gibco) used to dilute both the plasmid/bacmid mixture and the transfection reagent. These separate reactions were mixed together and incubate for 15 min at room temperature. The *Sf*9 cells were washed with Insect Express (no serum) and the transfection reaction was added to them and incubated for 2 hours at room temperature on a rotating platform to ensure an even transfection.

To ensure transfection and recombination efficiency AcMNPV KO:1629 was also transfected with pRN43-GFP as above to produce a positive control indicating successful recombination by green florescent protein expression which can be identified by U.V microscopy.

2.8.3 Clonal selection of WT and mutant BTV-1 NS2 expressing baculovirus.

To select clonal populations for expression of NS2, plaque assays were performed. 6 well plates were seeded with *Sf*9 cells (1x10^6 cells), washed with serum-free Insect Express (Lonza, Biowhittaker) and infected with 1 ml of ten-fold virus dilutions (1x10^1 - 1x10^6), incubated for 2 hours. The cell monolayers were overlaid with sterile 3% low melting temperature agarose diluted 1:1 in Insect Express (Lonza, Biowhittaker)

containing 5% [v/v] FSC and incubated for 72 hours. Plaques were identified through addition of 1 ml Neutral Red (Sigma) diluted 1:5 in filter sterilised 1x PBS (Oxoid) to the agarose overlay, incubated for 2-3 hours, aspirated and the plates were inverted.

Putative recombinant plaques were removed as agarose plugs with sterile glass pipettes and individually used to infect fresh *Sf*21 monolayers ($1x10^6$ cells). The putative recombinant virus underwent three rounds of virus amplification to increase virus titre and obtain virus stocks. Briefly, 6 well plates were seeded with *Sf*21 or *Sf*9 cells ($1x10^6$ cells) and infected with 250 µl virus supernatant added drop wise. TC100 media or Insect Express (Lonza, Biowhittaker) was added to 2 ml and incubated for 72 hours; this was repeated three times.

2.8.4 Recombinant protein production

To validate baculovirus NS2 protein production, monolayers were infected with 500 µl of virus stocks and incubated at 28°C for 72 hours. Cells were harvested, pelleted and resuspended 1x cracking buffer (section 2.7.1). The cell lysate samples were loaded on 10% SDS-PAGE [220] and electrophoresed at 200 V for 50 min. To visualise the protein bands, gels were either stained with Coomassie brilliant blue (1 % [w/v] Coomassie Brilliant Blue, 7% [v/v] glacial acetic acid, 12% [v/v] methanol) and de-stained (7% [v/v] glacial acetic acid, 12% [v/v] methanol) or transferred to a nitrocellulose membrane for Western immno blotting using a Trans-blot Turbo semi-dry blotter (Bio Rad) as described in section 2.7.2.

2.8.5 Protein purification by ion exchange chromatography

*Sf*9 cells (2x 10^6) were infected with recombinant baculoviruses as described previously and 72 hpi the culture was transferred to 50ml falcon tubes and centrifuged (4000 rpm, 15 min 4 °C) to form a pellet containing cells expressing recombinant protein and a supernatant containing baculovirus for further infections. The pellet was resuspended (1/10 culture volume) in NS2 lysis buffer (20 mM Tris-HCl pH8, 1 mM EDTA, 0.5% Triton X-100) and 1:100 Protease Inhibitor Cocktail V (Sigma-Aldrich) before being transferred to a chilled dounce homogeniser for 20 strokes. The cell debris was pelleted by a 14,000 rpm, 15 min centrifugation and the supernatant transferred to a fresh tube. 20 µg RNaseA per ml of supernatant was added and incubated at 4 °C for at least 16 hours.

The supernatant was clarified through a 5 µm syringe filter and applied to a 5 ml HiTrap Q HP anion exchange column (GE Healthcare) within an ÄKTA purifier (GE Healthcare), equilibrated and washed with NS2 buffer (20 mM Tris-HCl pH8, 1 mM EDTA). The elution buffer (1M NaCl, 20 mM Tris-HCl pH8, 1 mM EDTA) was added to the column as a gradient from 1-100%. Five ml elution fractions were collected from the sample binding (F1), column washing (F2 and F3) and elution (F4-13). Fractions were analysed by 10% SDS-PAGE and detected with Coomassie brilliant blue staining. Fractions containing NS2 were stored at 4 °C.

2.8.6 Protein purification with His/GST tags

As section 2.7.6, *Sf*9 cells (2x 10^6) were infected with recombinant baculoviruses and incubated at 28 °C for 72 hours before being harvested, dounce homogenised and RNaseA treated overnight with 10 units of 25µg/ml stock (Thermo Scientific). 1 ml Ni-NTA agarose beads (GE Healthcare) were washed in 10 bead volumes NS2 -10 buffer (20 mM Tris-HCl pH8, 1 mM EDTA, 10 mM Imidazole) and pelleted by centrifugation (14,000 rpm, 5 min). The supernatant containing NS2 was added to the beads and allowed to bind through the polyhistidine-tag (2 hours, 4 °C) on a rolling platform. The NS2 bound beads were pelleted (14,000 rpm, 5 min) and the unbound protein supernatant discarded before the sample was washed twice with 20 volumes of NS2 -20 buffer (20 mM Tris-HCl pH8, 1 mM EDTA, 20 mM Imidazole). The NS2 bound Ni beads in a final wash of 20 volumes of NS2 -20 buffer was applied to a syringe column and allowed to drain by gravity to produce a packed NS2-Ni bead bed. NS2 was eluted from the Ni beads with 15 volumes of NS2 -350 buffer (20 mM Tris-HCl pH8, 1 mM EDTA, 350 mM Imidazole), which drained by gravity and the NS2 eluate collected and stored on ice until needed.

For further purification, 400 µl of GST beads (GE Healthcare) were washed in 10 bead volumes of NS2 -10 buffer before being made into a 50% slurry and added to the NS2 eluate. This was bound for 1 hour at room temperature on a rotating platform. The beads were then pelleted by centrifugation (1,000 rpm, 5 min) and the unbound supernatant discarded. The beads were washed in 20 bead volumes of NS2 -10 buffer and pelleted (1,000 rpm, 5 min) and the bound NS2-GST beads made into a 50 % slurry

with NS2 -10 buffer and transferred to a 1.5 ml Eppendorf tube. 500 µL of GST elution buffer (NS2 buffer, 20 mM Glutathione, 1 mM DTT pH 8) was added to the NS2-GST beads and incubated for 15 min at room temperature before pelleting the beads (1,000 rpm, 5 min) and collecting the NS2 eluate. This was repeated twice to produce 1 ml of NS2 elute to which AcTEV protease (Sigma) was added and incubated over night at 4 °C to cleave the purification tags.

Ni-NTA beads were washed with NS2 buffer (Section 2.8.5), applied to a syringe column and allowed to drain by gravity to produce a packed Ni bead bed, to which the cleaved NS2 was added. The purified NS2 eluate was collected while the cleaved tags remained bound to the beads. Two or three further NS2 fractions were produced by washing the beads with NS2 buffer to collect all remaining NS2. Fractions were analysed by 10% SDS gels and detected with Coomassie brilliant blue staining. Fractions containing NS2 were stored at 4 °C.

2.8.7 Protein quantification

All purified NS2 fractions were pooled and added to Amicon Ultra 10K centrifugation devices (Merck), used to manufacturer's instructions, for either concentration or desalting. Briefly, 500 µl of NS2 sample was added to an assembled Amicon Ultra device and centrifuged at 14,000 x g for 15 min. The flow through was discarded and the concentrated NS2 solute is either recovered by inversion into a clean micro-centrifuge tube and spun for 1,000 x g for 2 min (for concentration), or diluted in the NS2 buffer and then recovered as above (for desalting).

Bradford assays [221] were used as a rapid and accurate method for quantification of NS2 protein samples. A series of known bovine serum albumin (BSA) standards were diluted in H_2O and Bradford solution (Bio Rad) and analysed in triplicate on a Nanodrop spectrophotometer to form a calibration curve. The absorbance of dilutions of NS2 was plotted on the calibration curve and used to quantify the protein present.

2.9 Characterisation of recombinant wild-type and mutant NS2

2.9.1 Electrophoretic Mobility Shift Assay (EMSA)

In order to analyse the ability of the mutant NS2 proteins to bind ssRNA, 0.5 µg radiolabeled BTV segment 7 was used in this electrophoretic mobility shift assay to visualise the difference in migration of unbound RNA and NS2 bound RNA. Transcripts were generated with RiboMAX (Promega) as section 2.2.4, but the reaction mix contained 25 mM UTP/GTP/ATP and 50 µCi α^{32}P CTP and was performed in compliance with the LSHTM radioactivity guidelines. The EMSA reaction (20 µl) contained purified NS2 in increasing concentrations (1, 5, 10 and 15 µg or 1, 15, 20, 25 µg), 1x EMSA buffer (2mM $MgCl_2$, 60 mM KCl, 150 mM NaCl, 20 mM Hepes pH 7.5, 1 mM EDTA, 1 mM DTT, 20% glycerol, 10U RNasin Plus RNase inhibitor (Promega)), radiolabeled BTV segment 7. The RNA only control and the NS2 only control replaced the NS2 and RNA, respectively, with H_2O.

These reactions were allowed to bind for 30 min at 4 °C before the addition of 10 µl ssRNA loading buffer. 15 µl of sample was analysed on 1% agarose gels in TBE buffer for 1 hour at 80 V. Gels were then dried on a 583 Gel Dryer (Bio Rad) and exposed to a

phosphor screen. Radiation was detected by a Typhoon trio fluorescence scanner (Amersham Biosciences) and analysed by ImageJ software.

2.9.2 Sedimentation Assay

Purified NS2 with and without the addition of 1 µg S10 ssRNA, and protein standards (bovine serum albumin [monomer 66 kDa, 4.5 S and dimer 132 kDa, 6.7 S] and catalase [250 kDa, 11.3 S]) were added to 12ml 5-20 % (w/v) sucrose gradients and centrifuged in a Optima L-90K ultracentrifuge (Beckman Coulter) at 35,000 rpm, 10 °C for 16 hours in a SW40 Ti rotor [154]. 1 ml fractions were collected and analysed on 10 % SDS-PAGE. The protein standards were detected by Coomassie blue staining and the NS2 fractions transferred to a nitrocellulose membrane for Western immuno blotting using a semi-dry blotter and NS2 specific primary antibodies (Section 2.6.2). The membranes were scanned and quantified by LI-COR Image Studio Lite software. The red, green and blue signals generated from each fraction were used to form an average signal, which was plotted on and compared.

Chapter 3

In vivo and *in vitro* investigation into the N-terminal RNA binding domain of BTV NS2

3.1 Introduction

BTV NS2 (42kDa) forms the VIBs, which are the sites of core assembly. NS2 is the only phosphorylated BTV protein, has NTPase activity and binds BTV ssRNA (Section 1.4). NS2 is predicted to form a doughnut-shaped multimer with a diameter of 100 (± 10) Å [159]. Many doughnut-shaped protein complexes are involved in RNA metabolism and thus have the ability to bind RNA. These include the *S. solfataricus* exosome [222], *S. antibioticus* PNPase [223], *E. coli* RraA [224,225], *A. fulgidus* Sm [226], *M. thermoautotrophicum* Lsm [227], rotavirus NSP2 [172] and *X. laevis* Ro60 [228].

Some of the doughnut-shaped RNA-binding proteins, such as the exosome and PNPase are proposed to have RNA binding domains located on the inside of the doughnut [229]. Others, such as the Sm protein, bind RNA on the surface of the doughnut [230]. Rotavirus NSP2 forms a doughnut shaped octamer with a central hole that is lined by neutral residues. These were originally thought to be involved with RNA binding. Recent cryo-EM studies showed that this hole is not used for RNA-binding, but instead provides a protective environment for newly synthesized dsRNAs [170]. NSP2 RNA binding domains are located in the inner ring between the N-terminal and the C-terminal. It is believed that the central hole in the NS2 structures are also unimportant for RNA binding because the residues shown to be important for RNA binding are situated at the interface between the N and C-terminal domains, like NSP2 [159].

The N-terminal of NS2 (1–92 aa) was originally thought to be solely required for RNA binding, which was subsequently narrowed to the first 8 amino acids, specifically three charged amino acids; K_4, R_6 and R_7 [231]. Current literature however, suggests the NS2

contains three ssRNA binding domains: 2–11 aa, 153–166aa and 274–286 aa [158] and stressed the importance of a triple mutant (BTV-17 $NS2_{2\text{-}11/153\text{-}166/274\text{-}286}$) being necessary for the complete cessation of RNA binding. Differences in the activity of the individual binding domains were also reported. A singly expressed recombinant deletion mutant of BTV-17 $NS2_{2\text{-}11}$ [158], indicated here as the dashed box in Figure 3.1, was expressed in *E. coli*, purified and used in non-BTV specific ssRNA EMSAs. The EMSAs showed that $NS2_{2\text{-}11}$ was less able to bind non-specific ssRNA compared to WT NS2. A less important role for the 2–11 aa binding domain was described with double deletion mutants BTV-17 $NS2_{2\text{-}11/153\text{-}166}$ and BTV-17 $NS2_{2\text{-}11/274\text{-}286}$ showing a greater affinity for RNA than the BTV-17 $NS2_{153\text{-}166/274\text{-}286}$ mutant.

The 2–11 aa region contains 3 positively charged amino acids (K_4, R_6 and R_7), which were shown to have a significant role in RNA binding. [231]. Arginine and lysine have previously been shown to be required for RNA binding in both influenza A NS1 and the SH2 domain of the *Src* oncoprotein [232,233]. Within the 2–11 aa region is the negatively charged E_2, which similarly to the lysine and arginines, is hydrophilic but was shown to not be involved in RNA binding of NS2 [231]. A second lysine (K_{10}) is also located within this region. It has a disputed role in RNA binding because it has been both discounted [231] and implicated [158] in RNA binding

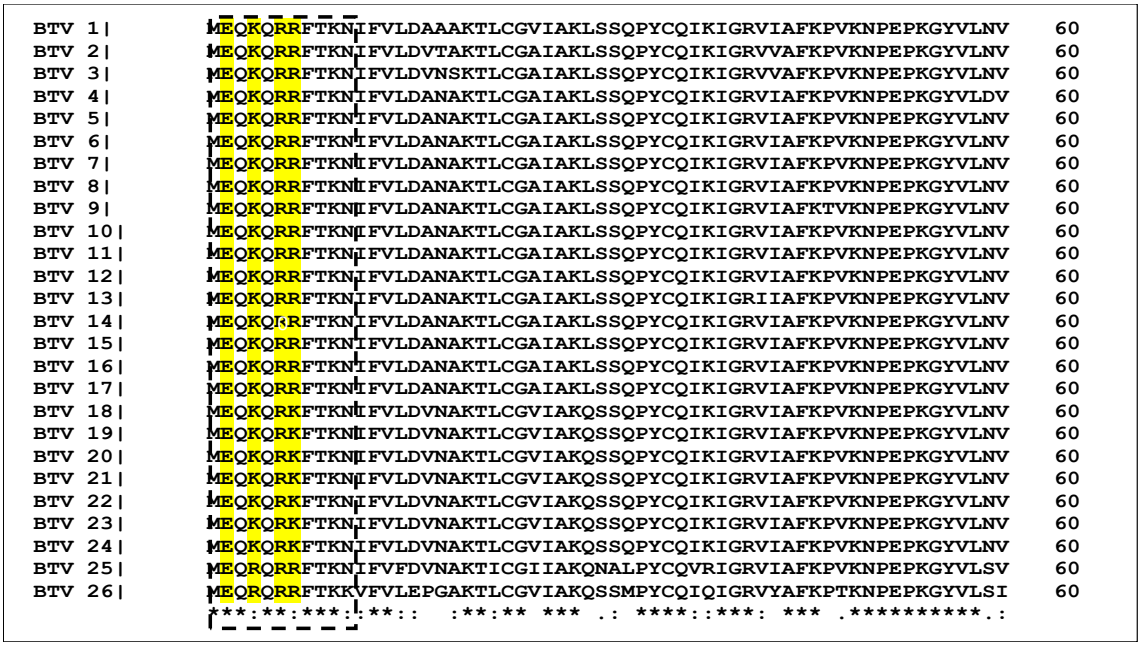

Figure 3.1. Clustal alignment of BTV 1- 26 NS2 amino acid sequences.
Sequences from each of the 26 serotypes were aligned using Clustal Omega (http://www.ebi.ac.uk/Tools/msa/clustalo). Dashed box indicates the putative N-terminal binding region 2aa – 11aa. Amino acids highlighted in yellow are the conserved, charged amino acids chosen for mutation to disrupt RNA binding. An asterisk indicates positions which have a fully conserved residue. A colon indicates conservation between groups of strongly similar properties. A full-stop indicates conservation between groups of weakly similar properties. Appendix 1 contains the full Alignment of NS2 amino acid sequences

Previous RNA binding studies involving NS2 have been performed *in vitro* using recombinant NS2 mutants. Consequently, the relevance of NS2 amino terminal domain, specifically residues K_4, R_6 and R_7 during virus replication *in vivo* was not known. In order to study the importance of the 2–11 aa RNA binding domain of BTV NS2 in context of a virus infection, this putative RNa binding domain was mutated and the BTV reverse genetics (RG) system utilised, to generate mutants containing specifically designed nucleotide changes. The mutations examined *in vivo* were also investigated *in vitro* through the recombinant baculovirus expression of NS2 containing

the same mutations. This dual characterisation of the 2–11 aa RNA binding domain is novel and has generated the most complete data on the importance of the domain. Most importantly, the *in vivo* and *in vitro* investigation in this chapter has given a unique insight into the important role RNA, and RNA binding, plays in BTV replication.

3.2 Results

3.2.1 Design and construction of BTV-1 S8.N mutants

When designing mutations it is necessary to consider whether the amino acids are conserved among all serotypes because variable amino acids are less likely to have an important role. Generally, NS2 is highly conserved among all serotypes of BTV, as illustrated in Figure 3.1, which shows a partial alignment of NS2 sequences from each of the 26 serotypes. There was variation at amino acids 4 and 7, with both shown as either a lysine or an arginine. These changes are between amino acids which are strongly similar and both likely to be involved in RNA binding, as such they were considered candidates for mutation.

The charged residues E_2, K_4, R_6 and R_7, in the putative N-terminal RNA binding region (Figure 3.1. Dashed box) were designed to be substituted for alanine because it is a small, neutral amino acid. These substitutions were unlikely to greatly change the overall structure, whilst still being a significant enough to impede RNA binding and allow the investigation of RNA binding. Mutations only to the positive amino acids likely to bind RNA would create a negatively charged region which would repel RNA and not just disrupt the activity.

Using the RG system for BTV, a mutant virus with substitutions in the N-terminal RNA binding domain was generated. Previously within the lab, 10 pUC19 plasmids (pUC19 T7 S1-S10) were produced for use in the RG system. Each plasmid contained a T7 promoter, an exact DNA copy of one of the ten BTV RNA segments, and a restriction site to generate the correct 3' end. Site directed mutagenesis was performed on pUC19 T7 S8 using forward mutation primer BTV-S8.N *Hae*III F and reverse mutation primer BTV-S8.N *Hae*III R. These primers were designed to substitute alanines for the charged residues at E_2, K_4, R_6 and R_7. A silent *Hae*III restriction site was also inserted into these primers for further selection of positive mutants (Figure 3.3. A).

*Dpn*I was used to digest the parental plasmid DNA, before plasmid purification and transformation into DH5α chemically competent cells. Colonies were initially screened through ampicillin resistance conferred by the pUc19 plasmid.

Positive colonies were further screened by *Hae*III restriction digestion and analysed by gel electrophoresis (Figure 3.2. A). The six colonies screened seemed to contain the extra *Hae*III restriction site (Figure 3.2. A, Lanes 3-8) but the differences in the resulting banding patterns were not as clear as expected (Figure 3.2. A, dashed arrows).

To confirm that the colonies were positive for pUC19 T7 S8.N, colony PCR was performed on colonies 3 to 6, using forward primer BTV-1 S8 T7 *Bam*HI F and reverse primer BTV-1 S8 *Bsm*BI/*Bam*HI/*Rsr*II R to indicate which colonies contained the S8 insert. Positive amplification was shown by one band, visible by gel electrophoresis at the expected size of 1,100 bp. All of the four colonies selected contained Segment 8 (Figure 3.2. B, Lanes 4-7).

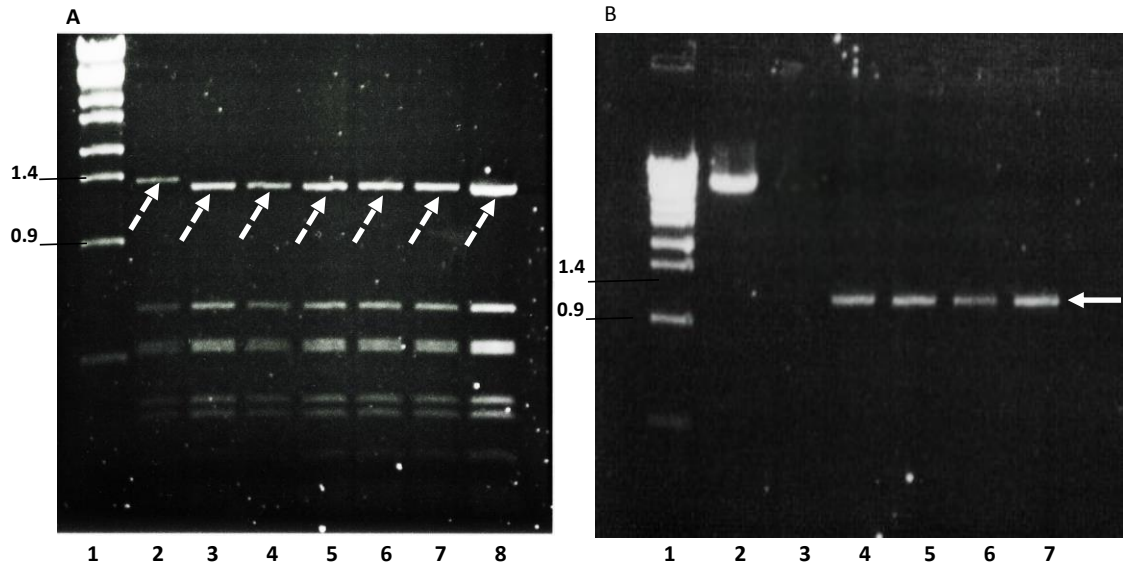

Figure 3.2. Restriction digest and colony PCR of pUC19 T7 S8.N DH5α.
DH5α *E. coli* colonies were screened for pUC19 T7 S8.N initially by *Hae*III restriction digestion and then by colony PCR. Both were detected on a 1% agarose gel containing ethidium bromide. **A,** *Hae*III restriction digestion of DH5α *E. coli* colony pDNA. Lane 1, *Sty*I digested λ DNA ladder. Lane 2, pUC19 T7 S8 control. Lanes 3-8, putative pUC19 T7 S8.N containing DH5α *E. coli* colonies 1-6. Dashed white arrows show differences between pUC19 T7 S8 control (top) and positive pUC19 T7 S8.N clones (Bottom). Size marker shown in Kb. **B,** colony PCR products of S8 amplification. Lane 1, *Styl* digested λ DNA ladder. Lanes 2, pUC19 T7 S8 control. Lane 3, H_2O control. Lanes 4-7, colony PCR product from DH5α *E. coli* colonies 3-6. Solid white arrow indicates approximately 1.1Kb. Size marker shown in Kb.

To confirm the presence of the mutation, pUC19 T7 S8.N was purified and sent for sequencing (Figure 3.3. B). The results were compiled by Bio-edit software and BlastN confirmed as BTV S8. Alignments of pUC19 T7 S8.N with BTV-1 published data revealed the expected alanine substitutions at residues E_2 K_4 R_6 R_7**,** consistent with the designed mutations (Figure 3.3. C).

Figure 3.3. Confirmation of S8.N mutations in pUC19 T7 S8.
A, Forward mutation primer of BTV1 S8.N containing a silent *Hae*III site (underlined)**,** mutations highlighted in yellow, start site highlighted in green. **B,** Partial chromatogram sequence pUC19 T7 S8.N, sites of expected mutations underlined. **C,** Partial sequence of Pubmed alignment pUC19 T7 S8.N and the published BTV-1 NS2 sequence. Resulting amino acid differences are indicated.

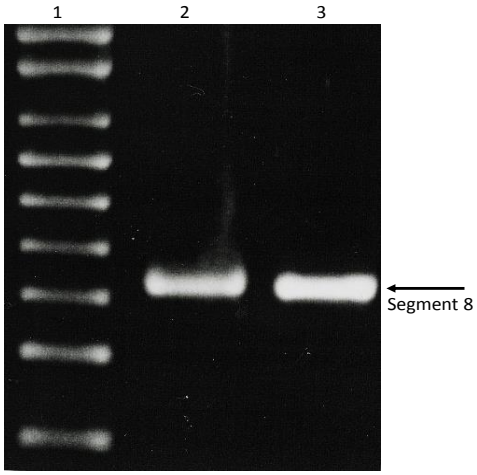

Figure 3.4. Segment 8 ssRNA transcripts.
BTV ssRNA transcripts were generated and detected on denaturing agarose gels. Lane 1, 1µl Promega RNA marker. Lane 2, ssRNA transcripts from pUC19 T7 S8.N. Lane 3, ssRNA transcripts from pUC19 T7 S8. Arrow indicates expected S8 band.

For the generation of mutant virus by reverse genetics, BSR cells were first transfected with 6 plasmids (encoding VP1, VP3, VP4, VP6, NS1 and NS2) to form the primary replication complex. These cells were subsequently transfected a second time at 18 hours post transfection (hpt), with all 10 RNA transcripts including S8.N, which was shown to be indistinguishable from WT S8 when analysed a on denaturing agarose gel (Figure 3.4. A). The transcripts were uncapped because of the prior formation of the primary replication complex which is able to cap BTV ssRNAs. Three days post second transfection, cells and supernatant were harvested.

The BSR-S8 complimentary cell line was previously made within the lab. It was analysed often by 10% SDS-PAGE and western immuno blot using NS2 specific antibodies to confirm the continued expression of NS2 (Figure 3.4. B).

The putatively recovered mutant viruses were used to infect both BSR cells and BSR-S8 cells in a plaque assay. Plaques were only visible in the BSR-S8 cells and from this 6 were picked (BTV-1 S8.N 1-6). No cytopathic effect (CPE) was visible in BSR cells at 72 hours post infection (hpi). Virus stocks were generated by infection of BSR-S8 complementary cells which produce NS2 *in trans*. All clones exhibited CPE and once 100% CPE was observed, stocks were harvested and virus titre obtained through plaque assays. These stocks were used throughout and re-made frequently to maintain a high virus titre.

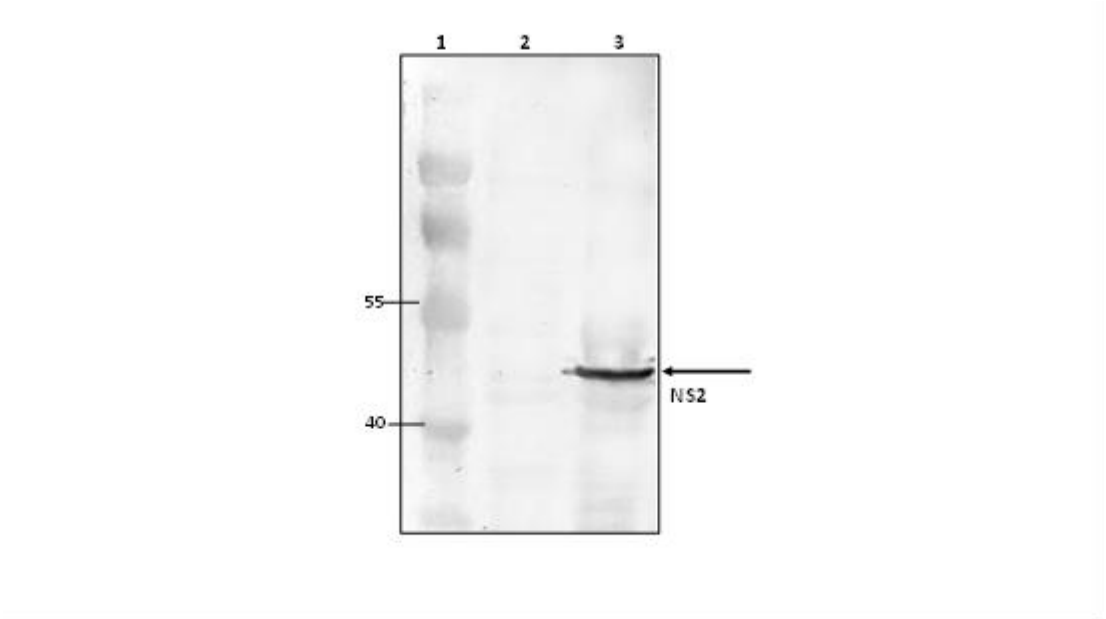

Figure 3.4 B. Confirmation through western immuno blot of NS2 producing BSR cells. Whole cell lysates of BSR-S8 complimentary cells were routinely analysed for NS2 production. Proteins separated by 10% SDS-PAGE and detected by western immune blot Lane 1, PageRuler Prestained Protein ladder (Thermo Scientific). Lane 2, BSR cell lysate control. Lane 3, BSR-S8 cell lysate. Arrow indicates expected NS2 band (46 kDa). Size marker shown in kDa.

3.2.2 Confirmation of S8.N mutations

Following recovery of the putative BTV-1 S8.N mutant viruses (1- 6) from BSR-S8 cells, the presence of virus and the validation of the inserted mutations were performed. Analysis of the pattern of genomic dsRNA of BTV S8.N and the comparison of WT S8 confirmed the recovery of virus from the RG system. The genomic dsRNAs of the mutant viruses were extracted and analysed by native page electrophoresis, which showed all 10 genomic segments from BTV S8.N (Figure 3.5. A, Lanes 3-7) and WT BTV (Lane 1).

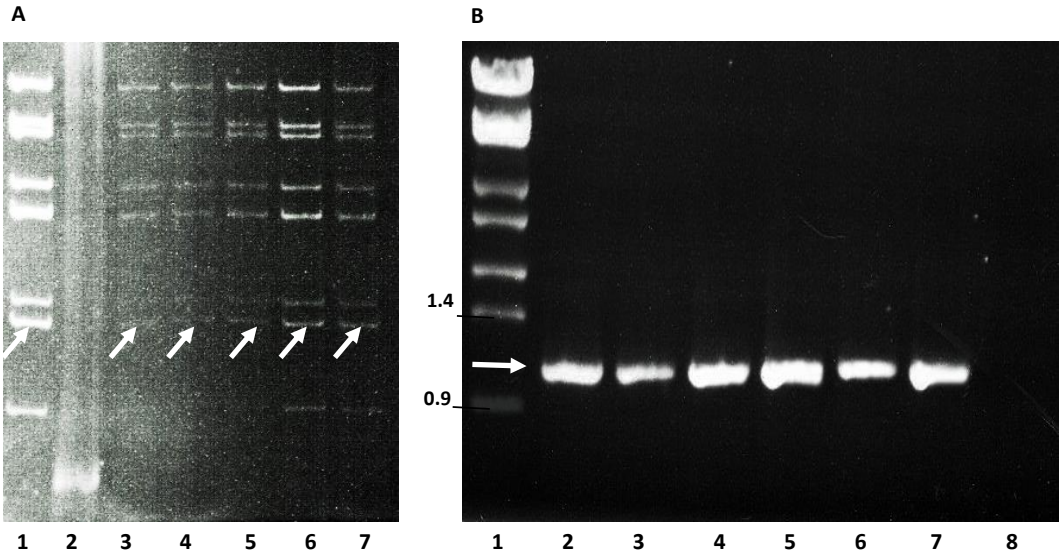

Figure 3.5. dsRNA purification and Reverse Transcriptase Polymerase Chain Reaction (RT-PCR) of BTV-1 S8.N.
A, dsRNA purification of BTV-1 S8.N from infected BSR-S8 cells analysed on a 9% non-denaturing polyacrylamide gel stained with ethidium bromide. Lane 1, BTV-1 dsRNA used as a marker. Lanes 2-7, BTV-1 S8.N 1-6, respectively. White arrows indicate migration of segment 8. **B,** RT-PCR products of BTV-1 S8.N detected on a 1% agarose gels by ethidium bromide. Lane 1, *Sty*I digested λ DNA ladder. Lanes 2-6, BTV-1 S8.N clones 2-6. Lane 7, RT-PCR control of WT BTV-1 dsRNA. Lane 8, H_2O control. White arrows indicate approximately 1,100bp. Size marker shown in Kb. Clone 2 was used in further work.

Both mutant and WT S8 migrate to the same position and are indistinguishable from each other. Lane 2 of Figure 3.5 showed no dsRNA from BTV-1 S8.N virus 1. As CPE was observed from BSR-S8 cell infection it is plausible to assume that the dsRNA was lost during purification or contaminated by RNases.

The detection of dsRNA bands identical to those found in WT BTV indicated that virus was present. Following this, the correct insertion of the mutations was confirmed. Specific primers (BTV-1 S8 T7 *Bam*HI F and BTV-1 S8 *Bsm*BI/*Bam*HI/*Rsr*II R) were used

to amplify the full-length S8 by reverse transcriptase PCR (RT-PCR). Firstly, a cDNA copy of the dsRNA S8 was generated by reverse transcription, then the product was amplified by PCR using the same primers to generate a product for sequencing. The RT-PCR generated the expected S8 band at ~1,100 bp when analysed by gel electrophoresis (Figure 3.5. B).

An RT-PCR amplification of WT BTV-1 S8 was used as a positive control and demonstrated a corresponding band of ~1,100 bp (Figure 3.5. B, Lane 7). No amplification was detected in the negative control which contained H_2O instead of dsRNA template for the RT-PCR (Figure 3.5. B, Lane 8). The amplified S8 band of clone 2 was excised, purified and sent for sequencing to confirm the mutation in the recovered BTV RNA.

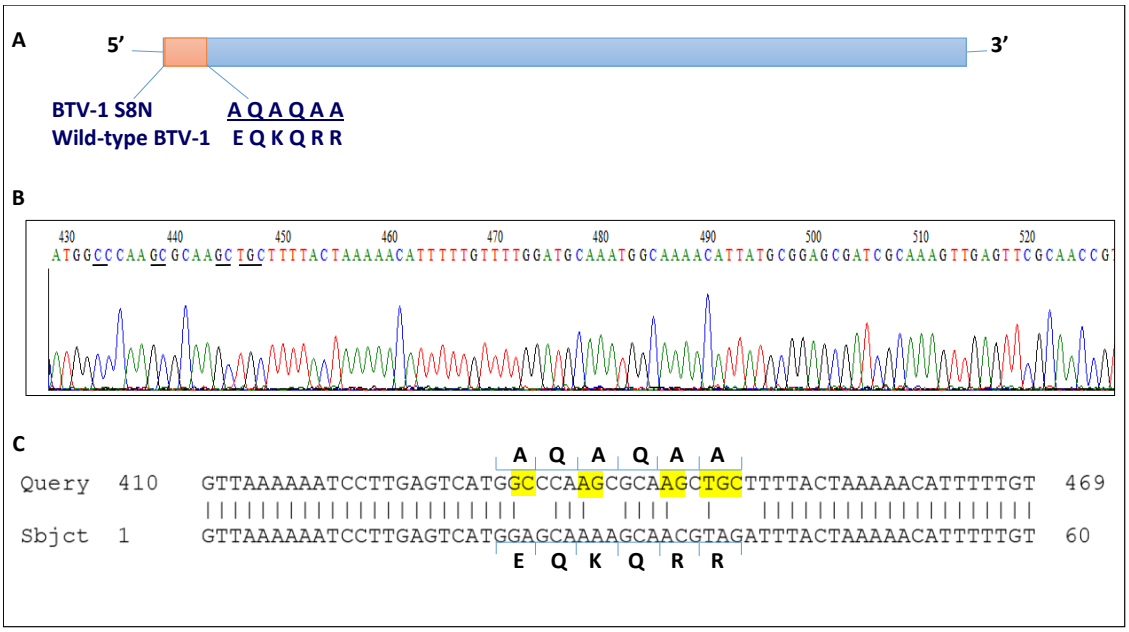

Figure 3.6. Confirmation of mutations in BTV -1 S8.N.
A, Schematic diagram of NS2 showing the wild-type amino acid sequence of BTV-1 (accession number detailed in Table 1)and the designed mutations to disrupt ssRNA binding. **B,** Partial chromatogram sequence of BTV -1 S8.N sites of expected mutations

underlined. **C,** Partial sequence of Pubmed alignment of BTV -1 S8.N and the published BTV-1 NS2 sequence. Sequence differences highlighted in yellow and the resulting amino acids indicated.

The presence of the specific mutations were confirmed through sequencing of the RT-PCR product of BTV-1 S8.N virus 1. The results were compiled by Bio-edit software and BlastN used to form alignments. BTV S8.N virus 1 (Figure 3.6) aligned with BTV-1 published data revealed the expected alanine substitutions at residues E_2 K_4 R_6 R_7**,** consistent with the designed mutations. The mutant was subsequently referred to as BTV-1 S8.N.

3.3 BTV S8.N characterisation

3.3.1 Plaque formation of the BTV S8.N mutant in BSR cells

The mutant virus was first characterised by its capacity to form plaques in BSR cells and BSR-S8 complimentary cells. However, no plaques were formed from infection of BSR cells at 72 hpi (Figure 3.7.B). The WT virus in the same cells formed large distinct plaques consistent with those usually produced by WT BTV-1. (Figure 3.7.C). In contrast, the complementary cell line (BSR-S8) infected with BTV S8.N showed a WT-like plaque phenotype (Figure 3.7.A). The plaques formed from WT BTV-1 in the complementary cell demonstrated no change in plaque phenotype compared to those seen in BTV-1 BSR plaques (Figure 3.7.D). This observation indicated that the mutation introduced in S8 had a significant effect on virus growth in BSR cells but when functional NS2 is supplied *in trans* the virus growth returned to normal.

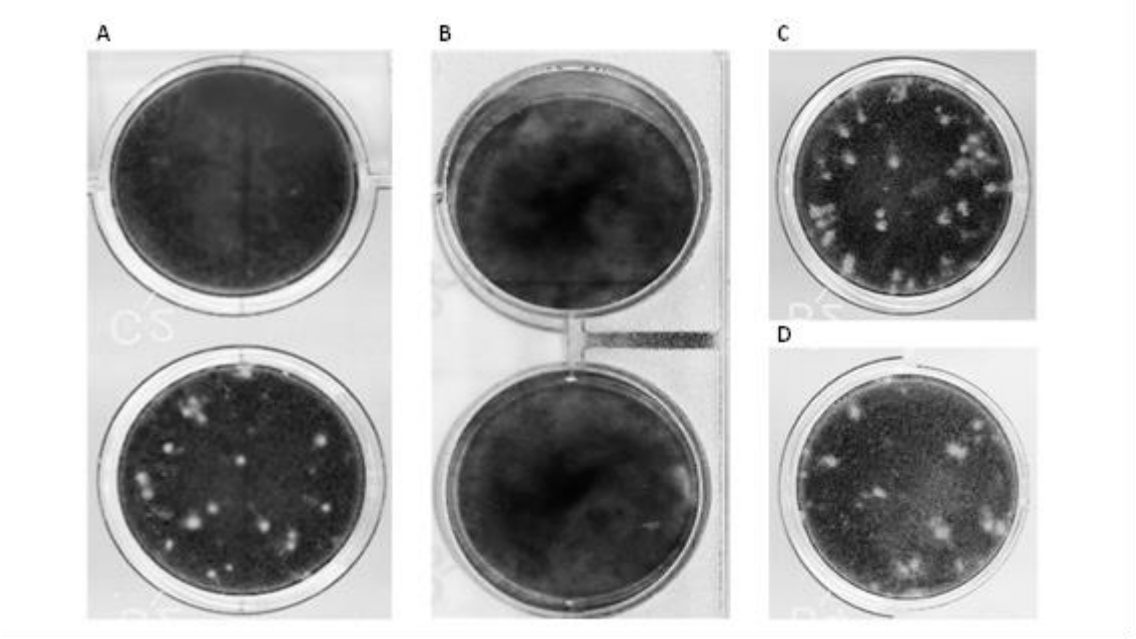

Figure 3.7. Examples of the plaques formed by WT BTV-1 and BTV-1 S8.N in BSR and BSR-S8 cells.
BSR or BSR-S8 complementary cells were infected with virus and fixed 3 days post infection and stained with crystal violet. **A,** BTV-1 S8.N plaques formed in BSR-S8 complementary cells (lower well) and a non-infected control (top well). **B,** BTV-1 S8.N plaques formed in BSR cells (lower well) and a non-infected control (top well). **C,** WT BTV-1 plaques formed in BSR cells. **D,** WT BTV-1 plaques formed in BSR-S8 cells.

3.3.2 Growth kinetics of BTV S8.N in BSR cells

The lack of plaque formation of BTV-1 S8.N in BSR cells indicated that further study of the mutant viruses' growth was necessary to fully understand the growth kinetics of the virus. Both BSR and BSR-S8 complementary cells were infected with BTV S8.N at MOI 1. Cells and supernatant were harvested at 0, 8, 16, 24, 36, 48, 72 and 96 hpi. Virus growth was assessed through plaque assay in the cell type they were harvested from. This experiment was performed in triplicate and the average virus titre used to plot the growth curve (Figure3.8). As a comparison control wild-type virus growth in

both BSR and BSR-S8 was also analysed. A 95% confidence interval (95% CI) was used to indicate the degree of variation the averages were likely to show [234]. There is a 5% (0.05) chance that the true average is outside of the limits. A greater than 25% overlap in intervals can indicate that the averages are not significantly different [235,236].

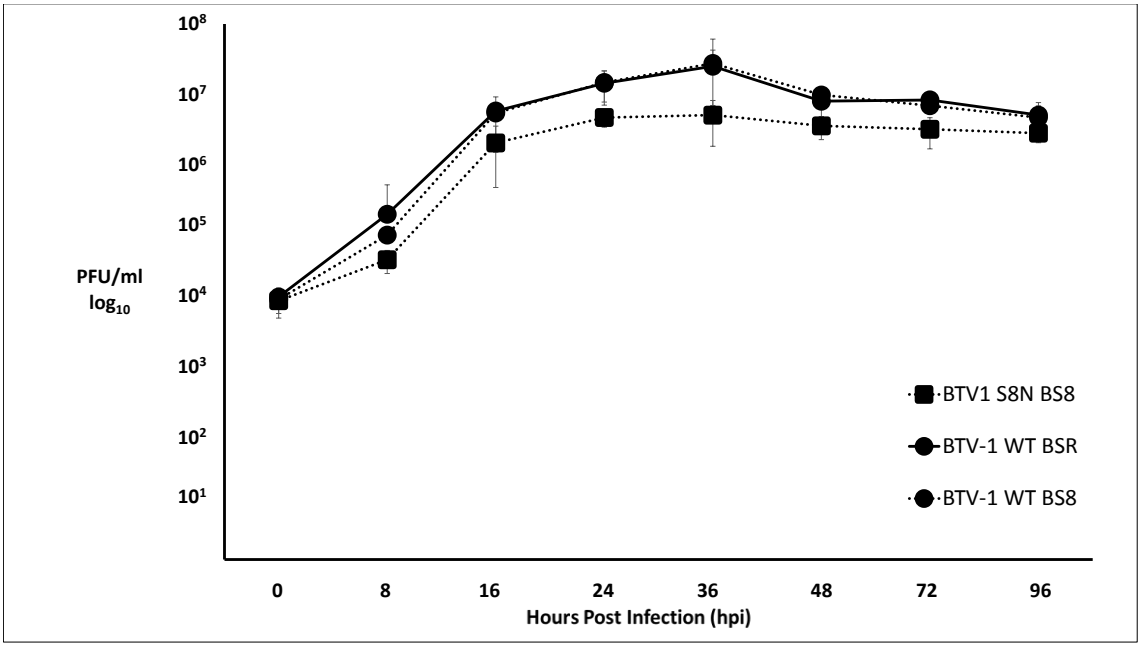

Figure 3.8. BTV-1 S8.N growth curve BSR-S8 cell line.
Mammalian BSR-S8 cells were infected at MOI 1 and harvested at the indicated times. Viral titre was determined by plaque assay (in triplicate) and the averages plotted on a logarithmic scale. BSR and BSR-S8 cells infected with wild-type BTV was used as a comparison control. Error bars indicate 95% confidence intervals (95% C.I)

BSR cells infected with BTV-1 S8.N demonstrated no visible plaques which indicated that the inserted mutations were lethal and confirmed previous reports that NS2 is essential for BTV replication. BTV-1 S8.N growth in the complimentary cell line (Figure 3.8. Square) was shown to be similar to WT growth but to a reduced titre. The <25% overlap in confidence intervals between WT (BSR and BSR-S8) and mutant demonstrated that this reduction in titre is statistically significant. The mutant

displayed an increase in growth up to 36 hpi with a maximum titre of 4.3 x10^6, a 0.8 log difference compared to WT maximum titres in the BSR cell line (2.3 x10^7) and the BSR-S8 cell line (2.5 x10^7). The growth decreased after 36 hpi, similarly to WT. The largest increase in BTV-1 S8.N growth rate was seen at 16 hpi with a 1.8 log increase (Figure 3.9. Square).

WT BTV growth in BSR cells demonstrated an increase in virus titre up to 36 hpi (Figure 3.8. Circle, solid line), with the greatest increase of growth rate at 16 hpi with a 1.3 log increase. Virus growth decreased after 36 hpi which is comparable with published data [73]. WT growth in BSR-S8 cells was similar to WT with the greatest titre at 36 hpi (Figure 3.8. Circle, dotted line), and with the greatest increase in growth rate shown at 16 hours with a 1.7 log increase. It displayed an increase in growth up to 36 hpi, followed by a decrease at comparable levels to that seen BSR cells. Maximum BTV titre is slightly higher in BSR-S8 cells with an average at 36 hpi of 2.5 x10^7, compared to the average at 36 hpi in BSR cells of 2.3 x10^7, but this difference was not statistically significant. The reduction in BTV-1 S8.N growth compared to WT may have been due to competition between the functional NS2 supplied by the complimentary cell line and the defective NS2.N protein of the mutant.

To further investigate the lethality of the BTV-1 S8.N mutation, protein expression was investigated. Cell lysate samples of BTV-1 WT or BTV-1 S8.N infected BSR cells were harvested at the time points indicated in the growth curves, and protein synthesis analysed in triplicate. Samples were resolved by 10% SDS-PAGE, transferred to a nitrocellulose membrane and western immuno blotted using specific antibodies

against a cellular protein (anti-actin), a virus structural protein (anti-VP5) and virus non-structural proteins (anti-NS1 and anti-NS2). Actin (42kDa) is a cellular protein used as a control to eliminate variation in overall protein load.

VP5, NS1 and NS2 of BTV-1 S8.N were not detected from infected cells by western immuno blot while the actin control resulted in clear bands at the expected size and at a similar intensity the WT actin control (data not shown). This indicated that the cell harvesting and protein detection were not contributing factors to the absence of viral protein. Non-structural proteins NS1 and NS2 were detected at 16 and 8 hpi, respectively from WT infected cells and remained constant until 96 hpi. BTV WT structural protein VP5 was detected at 16 hpi, and expressed at a constant level until 96 hpi (Figure 4.7). The successful detection of WT virus proteins confirmed the specificity of the antibodies used in the western immuno blot, and indicated that antibody specificity was not the cause of the absence of mutant virus protein. The lack of detectable mutant virus protein production further confirmed the lethality of the N-terminal mutation.

3.3.3 Effect of the S8.N mutation on VIB formation in BSR cells

Virus inclusion bodies are predominantly composed of NS2 and are the sites of virus core assembly, therefore the effect of the S8.N mutation on the formation of the VIBs was investigated using Immuno Fluorescence Assay (IFA). BSR cells were infected with an MOI 10 of either WT or BTV S8.N and fixed 24 hpi. Dual staining was performed using anti–NS2 antibodies to show VIB formation and anti-VP7 antibodies as a

confirmation of viral infection when visualised by confocal microscopy. A visual analysis of WT BTV demonstrated distinct, punctuate structures of NS2 (VIBs) typical of BTV infection [150,151] (Figure 3.10).

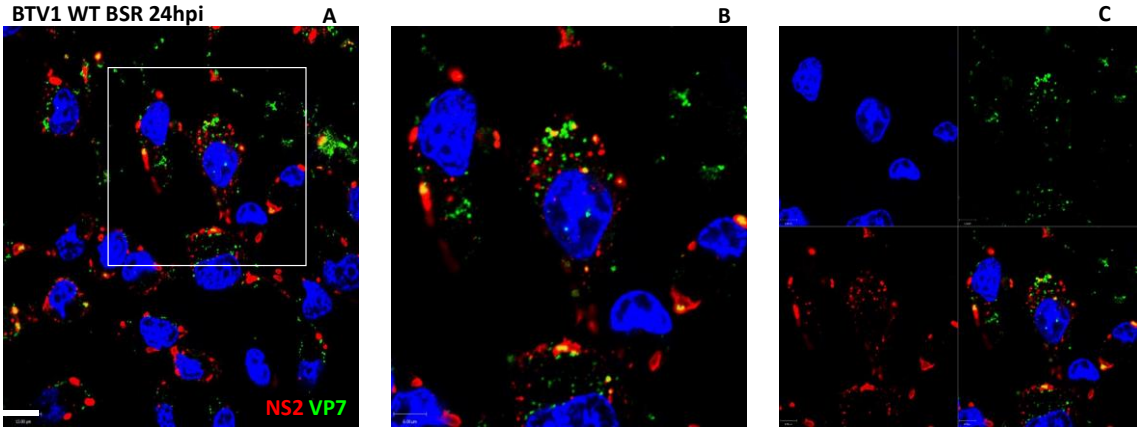

Figure 3.10. Immunofluorescence assay of BTV-1 WT at 24 hpi.
Dual staining for NS2 and VP7. BSR cells were fixed 24 hours post infection and protein fluorescence investigated by confocal microscopy. Primary antibodies, Guinea pig anti-VP7 and Rabbit anti-NS2; Secondary antibodies Guinea pig α Alexa 488, Rabbit α TritC and Hoechst nuclear staining. **A,** Image obtained by a x100 lens. **B,** Section of image at x2 magnification. **C,** Three split laser channels and merged image. White scale shows 10µm.

In comparison, visual assessment of BTV S8.N showed two different VIB phenotypes. In the first, infected BSR cells showed smaller and fewer VIBs which maintained a punctuate structure (Figure 3.11. 1A). The second observed phenotype was a diffuse grouping of NS2 protein (Figure 3.11. 2A). Both phenotypes showed less co-localisation with VP7 than WT BTV-1. Following this, quantification of the images was undertaken to generate more robust and comparable data. The NS2 signal generated by the

secondary antibody in each field of view obtained by the x100 lens was quantified by Volocity software.

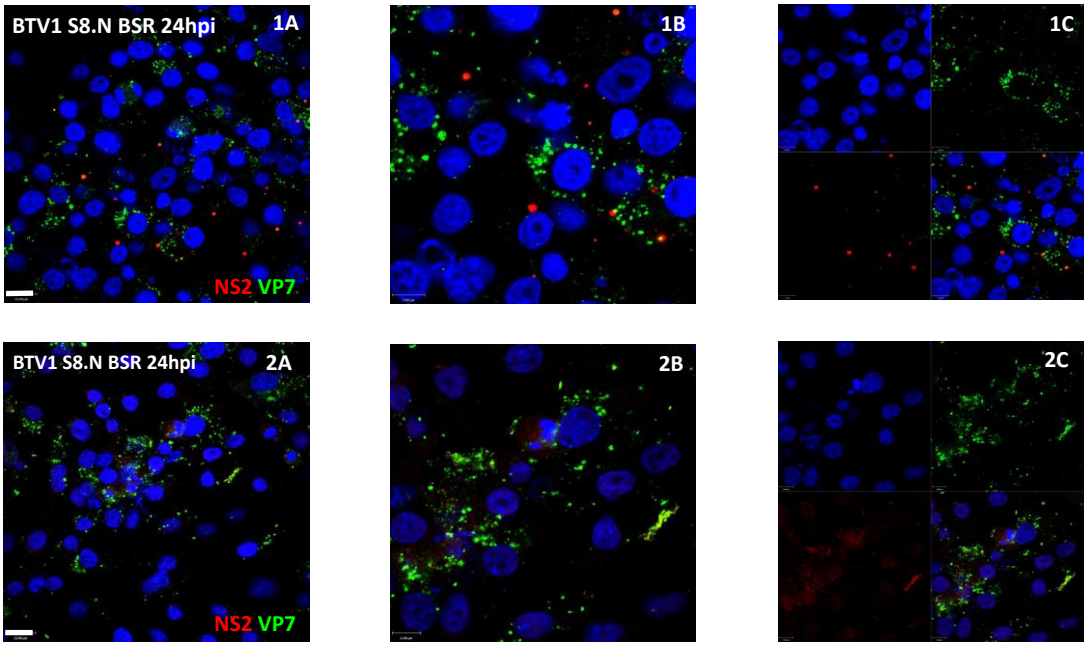

Figure 3.11. Immunofluorescence assay of BTV-1 S8.N at 24 hpi in normal BSR cells. Dual staining for NS2 and VP7. BSR cells were fixed 24 hours post infection and protein fluorescence investigated by confocal microscopy. Primary antibodies, Guinea pig anti-VP7 and Rabbit anti-NS2; Secondary antibodies Guinea pig α Alexa 488, Rabbit α TritC and Hoechst nuclear staining. Two examples shown. **A,** images obtained by an x100 lens. **B,** image at x2 magnification. **C,** three split laser channels and merged image.

Ten fields of view typical of both WT BTV-1 and BTV-1 S8.N infections in BSR cells were compared. The data generated supported of the visual assessment of the IFA. BTV-1 S8.N produced ~82% fewer and ~43% smaller VIBs. WT BTV-1 produced an average of 257 VIB in the BSR cells visible per field of view while BTV-1 S8.N generated 45.3 (Figure 3.12). Not only is the mean size of VIBs smaller for BTV-1 S8.N (0.78 μm^2) compared to BTV-1 (1.38 μm^2) (Figure 3.12), but the average maximum size of BTV-1 S8.N inclusion body (4.36 μm^2) was also smaller than WT (19.66 μm^2) (Figure 3.13). The

minimum VIB size between BTV-1 S8.N was estimated to be comparable to WT BTV-1 at 0.11 µm^2 and 0.12 µm^2, respectively (Figure 3.13).

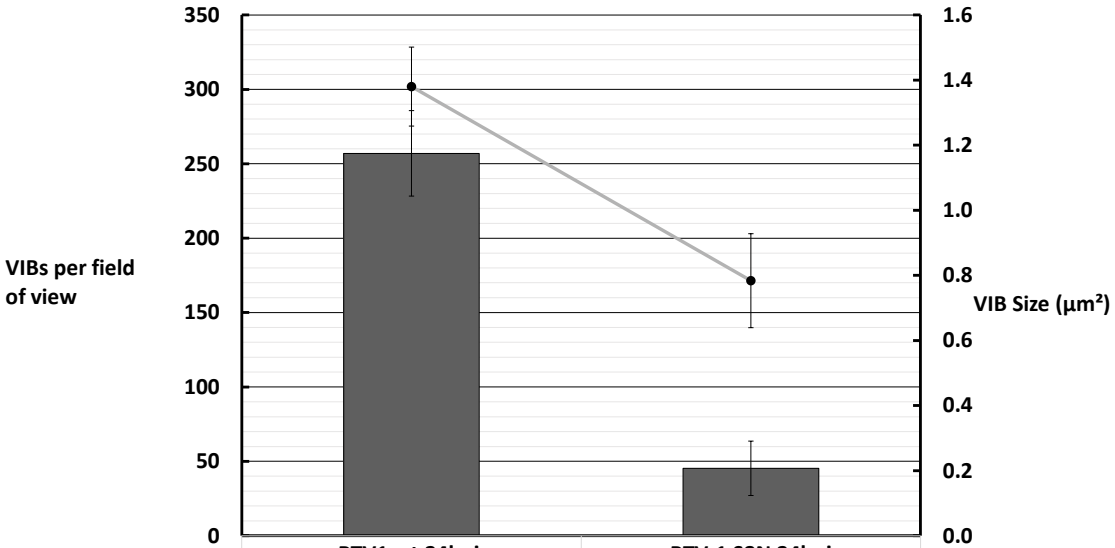

	BTV1 wt 24hpi	BTV-1 S8N 24hpi
Number of VIBs	257.00	45.33
VIB Size (µm²) mean	1.38	0.78

Figure 3.12. Average number and size of VIBs produced by both WT BTV-1 and BTV-1 S8.N during BSR cell infection.

Data were quantified using Volocity software from confocal images of BSR cells infected with MOI 10 of virus and fixed at 24 hpi. Data shown are the averages of ten standard fields of view at x100 magnification. 95% confidence intervals (95% C.I) shown.

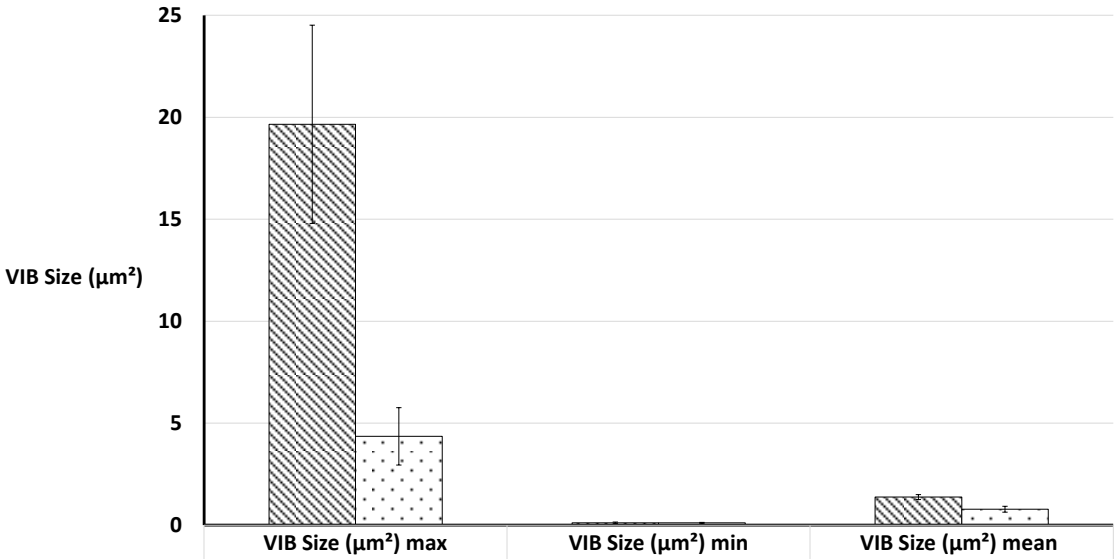

	VIB Size (µm²) max	VIB Size (µm²) min	VIB Size (µm²) mean
BTV1 wt 24hpi	19.66	0.12	1.38
BTV-1 S8N 24hpi	4.36	0.11	0.78

Figure 3.13. Average maximum, minimum and mean size of VIBs produced by both WT BTV-1 and BTV-1 S8.N during BSR cell infection.
Data were quantified using Volocity software as Figure 3.12. (95% C.I).

The 95% confidence intervals showed that the difference in minimum VIB size was not significant. Whereas, all the other data generated showed that the mutant VIBs differed significantly for WT (<25% CI overlap).

BTV-1 S8.N stocks were maintained in the complimentary cell line and then characterised in a relevant cell, which had the potential for functional NS2 carry-over. If this was demonstrated here, the NS2 would be expected to form VIBs of a similar size to WT VIB. This was not shown, validating the mutant VIB data. The detection of VP7 in the mutant confirmed that protein production early in infection is not disturbed.

3.4 *In vitro* characterisation of recombinantly expressed NS2.N

Although, the *in vivo* data established that the S8.N mutation was lethal and abolished virus replication in normal BSR cells , the question remains whether this phenotype was due to abrogation of RNA binding or if the NS2 structure was altered by the introduction of the mutations. Due to this, it was necessary to characterise the protein on its own, by the generation of a recombinant protein.

Fillmore *et al* 2002, used an *E. coli* based expression system to generate recombinant protein for non-specific RNA binding analysis. Although the expression of proteins in *E.*

coli is a quick, easy and cost effective method of expression it is not optimal for the study of BTV proteins. This is because they will not have the post-translational modifications which are found on proteins generated by eukaryotic cells. A baculovirus expression system was chosen due to the reliability of successful recombination, proper protein folding, post-translational modifications and high levels of protein production. This was particularly important for NS2, which is a phosphorylated protein.

3.4.1 Construction and confirmation of transfer vector pAcYM1-H/GST NS2.N

Within the lab, a pAcYM1 baculovirus transfer vector was modified to contain two protein purification tags (polyhistidine and GST). Also inserted into the plasmid was BTV-1 S8, which resulted in the generation of pAcYM1-H/GST NS2. This new transfer vector enabled the quick purification of WT NS2 through binding, washing and elution from Ni beads and anti-GST beads, using the tags which were located at the 5' connected via a short flexible linker.

Using an In-Fusion cloning method, PCR and specific primers (In-Fusion S8.N F Primer and In-Fusion R) were used to generate 15 bp 5' and 3' complementary regions to pAcYM1-H/GST plasmid, on the S8.N insert. The In-Fusion enzyme created single stranded over-hangs in the 15 bp homologous regions generated by the PCR primers and allowed insertion into the linearized pAcYM1-H/GST vector. PAcYM1-H/GST NS2.N was then transformed into chemically competent Stellar *E. coli* and grown on LB plates containing ampicillin.

Initial selection of Stellar cells containing the pAcYM1-H/GST NS2.N plasmid was by ampicillin resistance conferred by pAcYM1-H/GST. Further screening was performed

by colony PCR using a GST forward primer and internal reverse primer BTV-1 S8 627 R to indicate which colonies contained the S8 insert and the 5' GST tag. Positive transformation was shown by one band, detected by gel electrophoresis at the expected size of 1,400 bp. All of the five colonies selected contained the expected band.

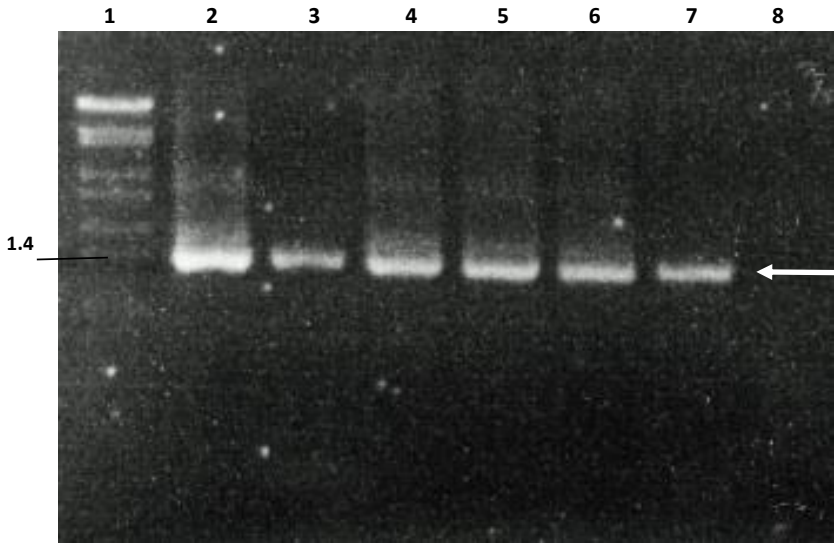

Figure 3.14. Colony PCR for selection of clones containing pAcYM1-H/GST NS2.N. Stellar *E. coli (*HST08 strain) colonies containing pAcYM1-H/GST NS2.N were identified through the amplification of a region of the plasmid between the GST primer and internal S8 primer, detected on a 1% agarose gel containing ethidium bromide. Lane 1, *Styl* digested λ DNA ladder. Lanes 2-6, PCR product from Stellar *E. coli* colonies. Lane 7, positive PCR control of pAcYM1-H/GST NS2. Lane 8, H_2O control. Arrow indicates approximately 1.4 Kb. Size markers shown in Kb.

PAcYM1-H/GST NS2.N colony 1 (Figure 3.14. Lane 2) was chosen for sequencing and future work. The full-length sequencing results were compiled by Chromas software and were BlastN confirmed as BTV-1 S8.N full length coding region. Alignment with

PubMed published data of BTV-1 revealed no deletions insertions or frame shifts which would affect protein production (Data no shown).

3.4.2 Generation of recombinant virus expressing NS2.N

To promote homologous recombination, non-infectious bacmid KO:1629 DNA was digested with *Bsu*36I to linearize the genome. The pAcYM1-H/GST NS2.N colony 1, identified above, was successfully transfected with the linearized bacmid using X-treamgene 9 to produce AcMNPV YM1-H/GST NS2.N recombinant virus. A GFP containing plasmid (pRN43-GFP) was transfected with bacmid KO:1629 DNA as a positive control to visually indicate a possible successful transfection. AcMNPV KO:1629 baculovirus transfected with pRN43-GFP was identified by fluorescent microscopy and successful recombination was recognised as the production of green florescent protein within cells (Figure 3.15. A and B).

To confirm that the GFP signal was due to recombination and not due to background levels; a negative control of linearized non-infectious AcMNPV KO:1629 with no GFP insert was also transfected and resulted in no florescence detection (Figure 3.15. C & D). Confirming that successful recombination of AcMNPV KO:1629 with pRN43-GFP was achieved.

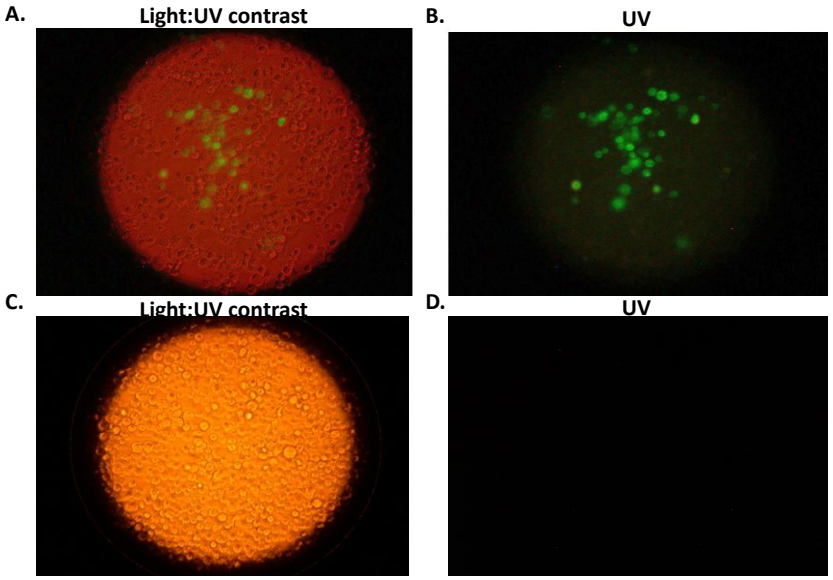

Figure 3.15. Green florescent protein (GFP) produced from *Sf9* insect cells infected with recombinant AcMNPV pRN43-GFP.
GFP was used as a control to indicate infection of a cell with recombined plasmid and baculovirus; from this an estimation of the recombination of pAcYM1-H/GST NS2.N with baculovirus could be determined. **A,** GFP florescence from AcMNPV pRN43-GFP infected insect cells under light:U.V contrast. **B,** GFP florescence from AcMNPV pRN43-GFP infected insect cells under U.V light. **C,** GFP florescence of linearized bacmid control under light:U.V contrast. **D,** GFP florescence of linearized bacmid control U.V light. (100x magnification)

3.4.3 Selection and purification of NS2.N

Successful recombination of AcMNPV RN43-GFP strongly suggested that an AcMNPV YM1-H/GST NS2.N recombinant virus had been generated. This was supported by visible CPE in *Sf*9 infected cells. Harvested AcMNPV YM1-H/GST NS2.N potentially contained a mixed population of recombinant virus, therefore plaque assays were performed to select clonal viruses and to validate expression of NS2.N. Three putative

recombinant plaques were picked and underwent three rounds of virus amplification to increase virus titre and generate stocks.

Expression of BTV-1 NS2.N was analysed from low passage viruses. Cells infected with the three putative recombinant viruses were harvested 72 hpi, the proteins present were analysed by SDS-PAGE and the gel was stained using Coomassie Brilliant (Figure 3.16. A). Expression of His/GST tagged NS2.N would result in a band at 65 kDa, which was present in all three of the AcMNPV YM1-H/GST NS2.N clones analysed (Figure 3.16. A, lanes 3-5). A positive control of a cell lysate of *Sf*9 cells infected with the lab generated AcMNPV YM1-H/GST NS2 also produced a large protein band at the expected size of 65 kDa (Figure 3.16. A, lane 2).

NS2 is a 42 kDa protein but migrates on SDS-PAGE gels to ~47 kDa. A band is visible between 40 and 55 kDa (Figure 3.16. Solid arrow.), suggesting the recombinant baculovirus produced some NS2 which had lost the His/GST tag or has been degraded in such a way to remove it. The Coomassie stained gel clearly demonstrated all of the viruses produced a protein of the expected size to contain His/GST tagged NS2.N, and produced far less of the untagged NS2.N. Virus 1 was chosen for future work due to a balance between the high levels of the tagged NS2.N and a weaker band of untagged protein (Figure 3.16. A, lane 3).

Subsequently, a purification of AcMNPV YM1-H/GST NS2.N virus 1 using Ni and GST beads was performed. Fifty ml of *Sf*9 cells were infected and harvested 72 hpi by centrifugation to separate the cell pellet. Samples of each purification step were separated by 10 % SDS-PAGE and detected by Coomassie blue (Figure 3.16. B). The

final NS2.N elution (Figure 3.16. B, lane 8) did not produce any purified His/GST tagged NS2.N.

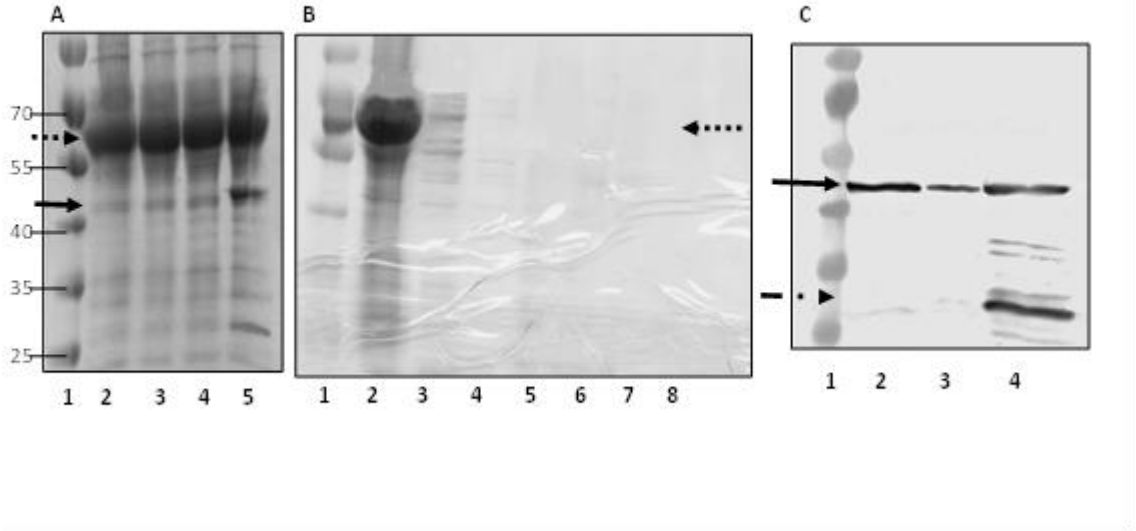

Figure 3.16. Expression and purification of NS2.N.
A, Cell lysates of *Sf9* cells infected with plaque picked AcMNPV YM1-H/GST NS2.N viruses. Proteins separated by 10 %SDS-PAGE and detected with Coomassie Blue. Lane 1, Page Ruler Prestained Protein ladder (Thermo Scientific). Lane 2, AcMNPV YM1-H/GST NS2 positive control. Lanes 3 -5, AcMNPV YM1-H/GST NS2.N viruses 1-3, respectively. **B,** Trial purification of the NS2 produced by AcMNPV YM1-H/GST NS2.N virus 1 using Ni and GST beads. Samples taken at points during purification were analysed by 10 %SDS-PAGE and detected with Coomassie Blue. Lane 1, Protein ladder. Lane 2, cell supernatant of *Sf9* cells infected with AcMNPV YM1-H/GST NS2.N after dounce homogenisation. Lane 3, unbound protein supernatant from Ni bead binding. Lane 4, unbound protein following two washes of NS2-20 buffer. Lane 5, Protein eluted from Ni beads. Lane 6, unbound protein supernatant from GST bead binding. Lane 7, unbound protein following two washes of NS2-10 buffer. Lane 8, Protein eluted from GST beads. **C,** Cell lysates of *Sf9* cells infected with AcMNPV YM1-H/GST NS2.N clones. Proteins were separated by 10 % SDS-PAGE and transferred to a nitrocellulose membrane for visualisation using western immuno blot and guinea pig anti-NS2 antibody (1:3000). Lane 1, Protein ladder. Lanes 2-4, AcMNPV YM1- S8.N clones 1-3, respectively. Bands at 42 kDa (solid black arrow) were identified as NS2. Dotted arrow indicates His/GST tagged NS2.N. Dash/dot arrow indicated the most dominant non 42 kDa NS2 at ~26 kDa. Size marker shown in kDa.

Due to the failure of Ni and GST beads to purify NS2.N, protein production was further investigated. Early passages of the viruses (pn 2) were used to infect *Sf9* cells and harvested 72 hpi. The proteins present were separated by SDS-PAGE and transferred to a nitrocellulose membrane for Western analysis using BTV NS2 specific primary antibody (Figure 3.16. C). Of the 3 recombinant viruses investigated, none produced His/GST tagged NS2.N which would have been identified by a band at 65 kDa. All viruses however, generated a strong NS2 specific band at 46 kDa, the correct size for untagged NS2.N (Figure 3.16. C, Solid arrow). Some degradation products were detected in recombinant virus 3 but, overall, large amounts of NS2.N was clearly identified in each virus.

Although AcMNPV YM1 S8.N viruses did not contain the His and GST tags to facilitate purification, NS2.N was highly produced. Other purification methods were available and were applied. Virus 1 was selected for further work due to the large amounts on NS2.N produced and the lack of visible degradation products (Figure 3.16. C, Lane 2). AcMNPV YM1 S8.N VIRUS ONW1 was subsequently referred to as AcMNPV YM1 S8.N.

A ion exchange chromatography purification method was undertaken as previously described [156,161,237]. *Sf*9 cells were infected with AcMNPV YM1 S8.N and harvested 72 hpi by centrifugation to generate a pellet, which contained the NS2.N protein. The pellet was washed with NS2 buffer and resuspended in NS2 lysis buffer. The supernatant containing the soluble NS2.N was bound to an anion exchange column (Figure 3.17. A, F1), washed (F2-F3) and eluted (F4-F13) from the column with increasing concentrations of NaCl-NS2 elution buffer.

All of the fractions were collected, the proteins were separated by 10% SDS PAGE and detected with Coomassie brilliant blue staining (Figure 3.17). Successfully purified NS2.N was expected to be exhibited as a single band at 46kDa. Fraction 13 contained the largest concentration of NS2.N and while there were some non-specific bands, NS2.N was by far the dominant protein.

Fraction 13 contained ~400mM sodium chloride from the elution buffer used to elute proteins from the column (Figure 3.17. A). The sample was desalted (Figure 3.17. B, DS) and concentrated (Figure 3.17. B, Conc) to remove the sodium chloride. The resulting NS2.N protein was highly pure. A single protein band was detected at ~25 kDa; this band was also present in Figure 3.16. C (dash/dot arrow) which due to the specific nature of the NS2 antibody used to for detection suggested it was likely to be degraded NS2. Protein quantification was performed by Bradford assays and even at 3µg/µl displayed here, NS2.N did not form aggregates.

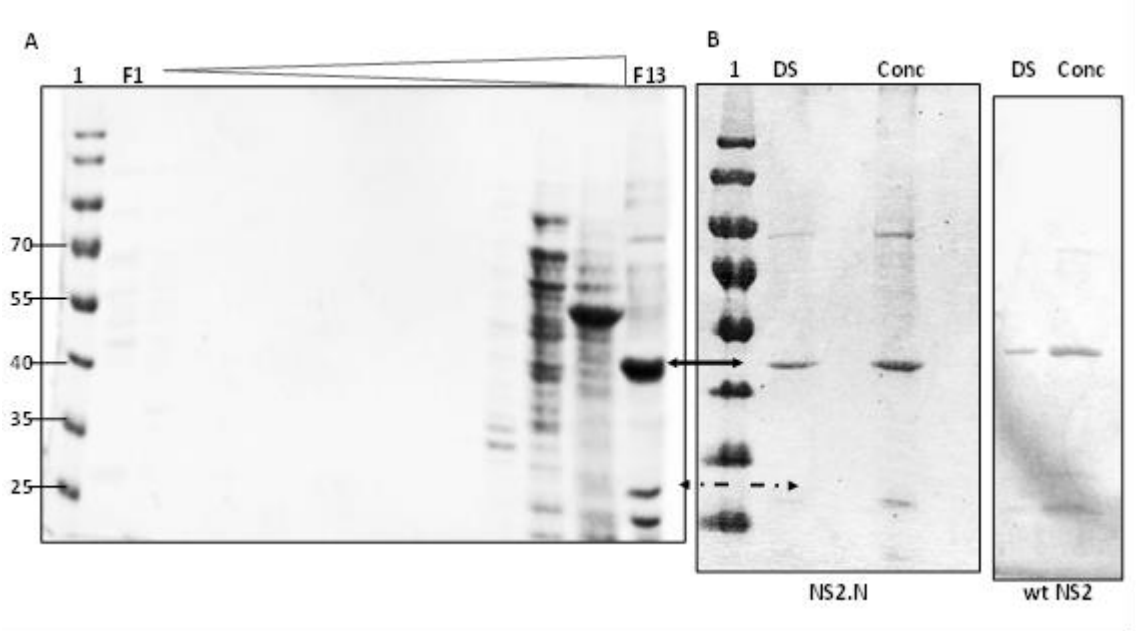

Figure 3.17. Ion exchange chromatography purification, desalting and concentration of NS2.N.

A, Fractions collected from ion exchange chromatography of AcMNPV YM1- S8.N infected *Sf9* cell lysate. Collected fractions were separated by 10 %SDS-PAGE and detected with Coomassie Blue. Lane 1, Page Ruler Prestained Protein ladder (Thermo Scientific). F1- F13, the first 13 fractions collected. Sample binding (F1), washing (F2 and F3) and elution (F4-13). Bands at 42 kDa were identified as NS2.N. **B,** Desalting and concentration was performed on NS2.N fraction 13 and purified WT NS2 from AcBTV10 S8. The resulting samples were separated by 10% SDS-PAGE and detected with Coomassie Blue. Lane 1, Protein ladder. DS, desalted sample. Conc, concentrated sample after desalting. Bands at 42 kDa (solid black arrow) were identified as NS2. Dash/dot arrow indicates an additional, non 42 kDa NS2 protein band at ~26 kDa. Size marker shown as kDa.

As a positive control AcBTV10 S8, already available in the lab, was used. *Sf*9 cells were infected with AcBTV10 S8. NS2 was subsequently purified, desalted, concentrated and detected by SDS-PAGE as for NS2.N (Figure 3.17 B). WT NS2 was highly purified but demonstrated the same degradation product as NS2.N.

Since the mutant NS2.N protein was soluble and eluted in same fraction as WT, this suggested that the overall structure was very similar to WT and that the mutations did not greatly altered it.

3.4.4 ssRNA binding activity of NS2.N mutant protein

WT NS2 and NS2.N were expressed and purified for use in characterisation assays. To determine if the mutation in the N-terminal of NS2 had any effect on BTV ssRNA binding activity, electrophoretic mobility shift assays (EMSAs) were undertaken. EMSAs have been extensively used with NS2 to show the ability of NS2 to bind ssRNA [160] and also BTV ssRNA specificity [161]. EMSA is based on the principle that protein and nucleic acid complexes migrate slower than the unbound ssRNA when under electrophoretic

conditions. Therefore, by analysing the differences between the smaller and faster unbound protein or nucleic acid, and the larger, and therefore slower, migrating, bound protein-nucleic acid complexes, conclusions can be reached about the interactions between proteins and nucleic acids [238].

The EMSAs were used to detect the BTV ssRNA binding capability of WT NS2 and NS2.N. Radiolabeled BTV segment 7 ssRNA was chosen for examining this activity [239]. Transcripts (ssRNA) were generated in the presence of 50 µCi α^{32}P CTP, purified and added to the EMSA buffer. Purified WT NS2 and NS2.N were diluted to specific concentrations in DEPC H_2O, mixed with the RNA and allowed to bind for 30 minutes to form the protein-ssRNA complexes. The positive and the negative controls replaced the NS2 and RNA, respectively, with H_2O. NS2-RNA complexes were analysed by an agarose gel to detect if ssRNA was retarded by NS2 protein. Gels were then dried and followed by autoradiography. A successful shift of ^{32}P ssRNA was identified by a band visible at a higher position than the RNA only control (Figure 3.18, A & B. Lane 1).

The initial EMSA did not show any NS2.N-ssRNA complexes at 15 µg of NS2.N (Figure 3.18. B), while 15 µg of WT NS2 was sufficient to shift the ssRNA to a bound position (Figure 3.18. A). Due to this, the RNA binding ability of NS2.N was further investigated with EMAS containing up to 25 µg of NS2 or NS2.N (Figure 3.19).

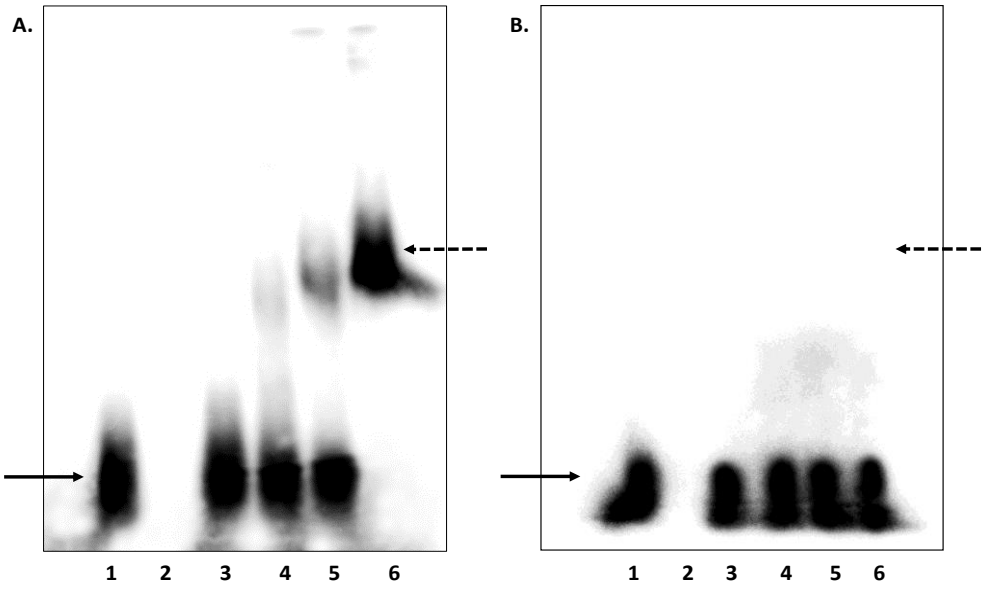

Figure 3.18. EMSA of WT NS2 and NS2.N (1-15 µg).
Radiolabeled BTV segment 7 T7 derived ssRNA was bound to NS2 or NS2.N and analysed on a 1 % agarose gel. This was dried and identified on a Typhoon variable mode imager. **A**, EMSA of ssRNA and WT NS2. Lane 1, ssRNA only control. Lane 2, NS2 only control. Lanes 3-6, RNA and 1, 5, 10 and 15 µg NS2, respectively. **B**, EMSA of ssRNA and NS2.N. Lane 1, ssRNA only control. Lane 2, NS2.N only control (15 µg). Lanes 3-6, RNA and 1, 5, 10 and 15 µg NS2.N, respectively. Solid black arrows indicate unbound RNA. Dashed black arrows signify RNA-NS2 complexes.

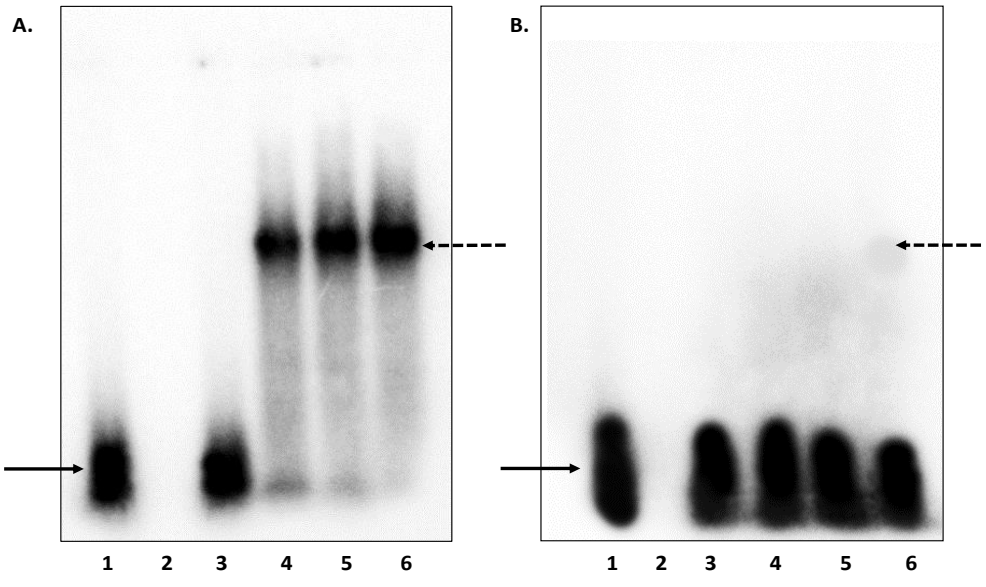

Figure 3.19. EMSA of WT NS2 and NS2.N (1-25 µg).
Radiolabeled BTV segment 7 T7 derived ssRNA was bound to NS2 or NS2.N and analysed on a 1 % agarose gel. This was dried and identified on a typhoon variable

mode imager. **A,** EMSA of ssRNA and WT NS2. Lane 1, ssRNA only control. Lane 2, NS2 only control. Lanes 3-6, RNA and 1, 15, 20 and 25 µg NS2, respectively. **B,** EMSA of ssRNA and NS2.N. Lane 1, RNA only control. Lane 2, NS2.N only control (25 µg). Lanes 3-6, RNA and 1, 15, 20 and 25 µg NS2.N, respectively. Solid black arrows indicate unbound RNA. Dashed black arrows signify RNA-NS2 complexes.

The images (Figure 3.19) were quantified using ImageJ software. Lanes on the image were marked and the total lane signal used to indicate 100% RNA signal. The distribution of signal within these lanes as either bound or unbound RNA was identified by plotting the area of each signal peak and demonstrated as a percentage of the total RNA signal (Figure 3.20).

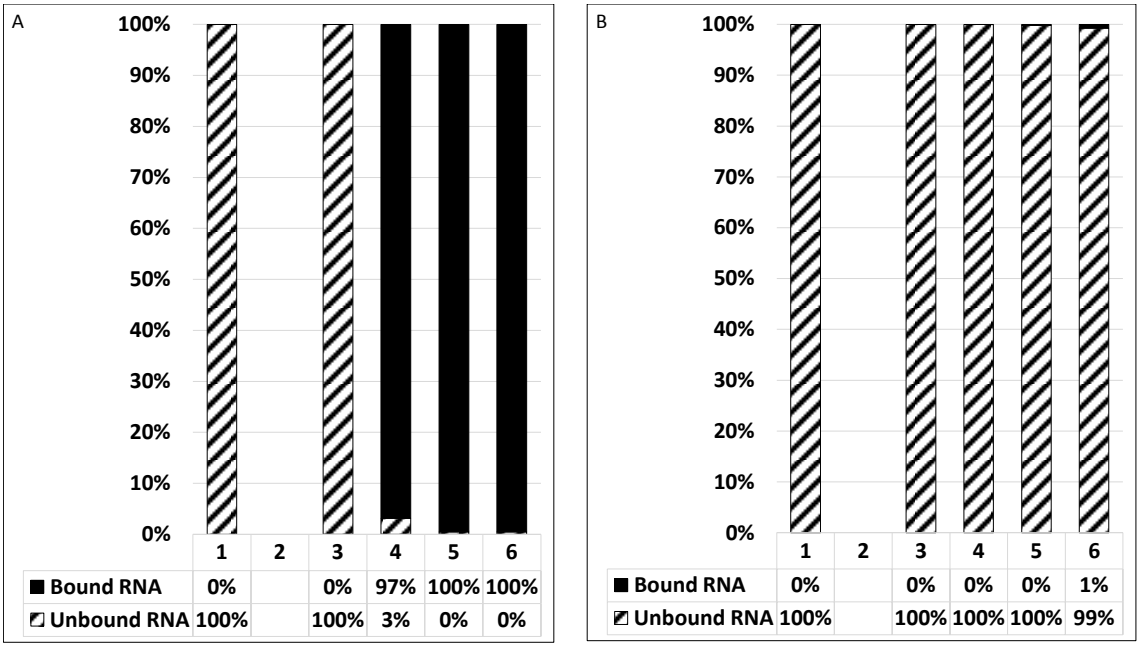

Figure 3.20. Quantification of WT NS2 and NS2.N EMSA.
EMSA images were quantified using ImageJ software. Total lane signal was considered as 100% RNA signal. The distribution of signal as bound or unbound to NS2 was identified by plotting the pixels. **A,** EMSA of WT NS2 and RNA. Lane 1, RNA only control. Lane 2, NS2 only control. Lanes 3-6, RNA and 1, 15, 20 and 25 µg NS2, respectively. **B,** EMSA of NS2.N and RNA. Lane 1, RNA only control. Lane 2, NS2.N only control. Lanes 3-6, RNA and 1, 5, 10 and 15 µg NS2.N, respectively.

When both WT and mutant NS2 were incubated with S7 ssRNAs in increasing concentrations (1-25 µg), it was clear that the mutant protein was unable to bind ssRNA (Figure 3.18 & 3.19. B). Although, the quantification of the gel measured a 1% binding, a visual analysis of the gel demonstrated no binding. This suggested a degree of error within the quantification. WT NS2 exhibited a gradual increase of RNA binding up to 15 µg NS2 where 97% of the ssRNA was bound (Figure 3.19. B Lane 4). Subsequently, 20 and 25 µg WT NS2 also show 100% in the bound position.

3.4.5 NS2.N oligomerisation in the presence and absence of ssRNA

NS2 has been shown to require RNA as an initiator of oligomerisation or as supporting scaffold [151]. This was further investigated with the N-terminal RNA binding mutant generated in this chapter, which was shown to have had the ability to bind BTV ssRNA abrogated.

As previously described [154], sucrose gradients (5-20%) were generated and 50 µg of diluted NS2 added the top. The samples were sedimented through ultracentrifugation and 1 ml fractions taken from the top of the gradient. These were then separated by 10% SDS-PAGE and initially identified by Coomassie staining but this was not sensitive enough to detect the diluted NS2, therefore the complexes were detected by western immuno blot using NS2 specific antibodies (1:3000). This experiment was performed with both WT NS2 (Figure 3.21) and NS2.N (Figure 3.22). During the protein purification process RNase A was added; in order to analyse the largest multimeric forms of NS2 reported previously, 1µg BTV-1 S10 ssRNA was added the NS2 before sedimentation.

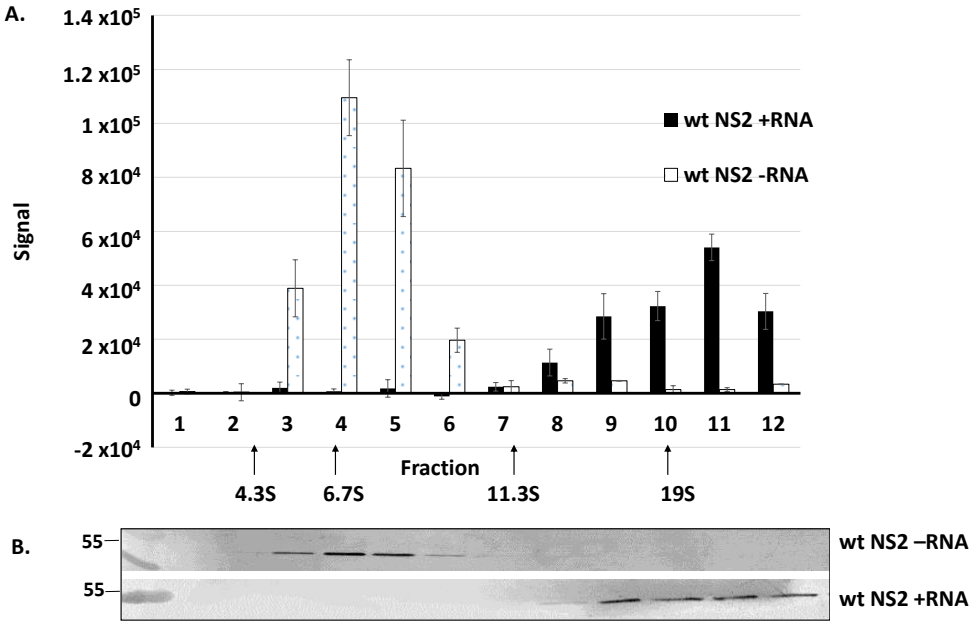

Figure 3.21. Oligomerisation assay of WT NS2 in the presence and absence of ssRNA. Purified NS2 was incubated for 30 minutes with RNA before sedimentation through a 5-20% sucrose gradient. The twelve fractions collected were separated on 10 % SDS-PAGE and analysed by western immuno blot using an anti-NS2 antibody (1:3000). These membranes were scanned and quantified by LI-COR Image Studio Lite software. The Red, Green and Blue signals for each fraction used to form an average signal. **A,** A graph showing NS2 present in each fraction, with and without the addition of RNA (95% C.I). **B,** western immuno blot images used for analysis. NS2 Bands identified at 42 kDa. Size marker shown in kDa.

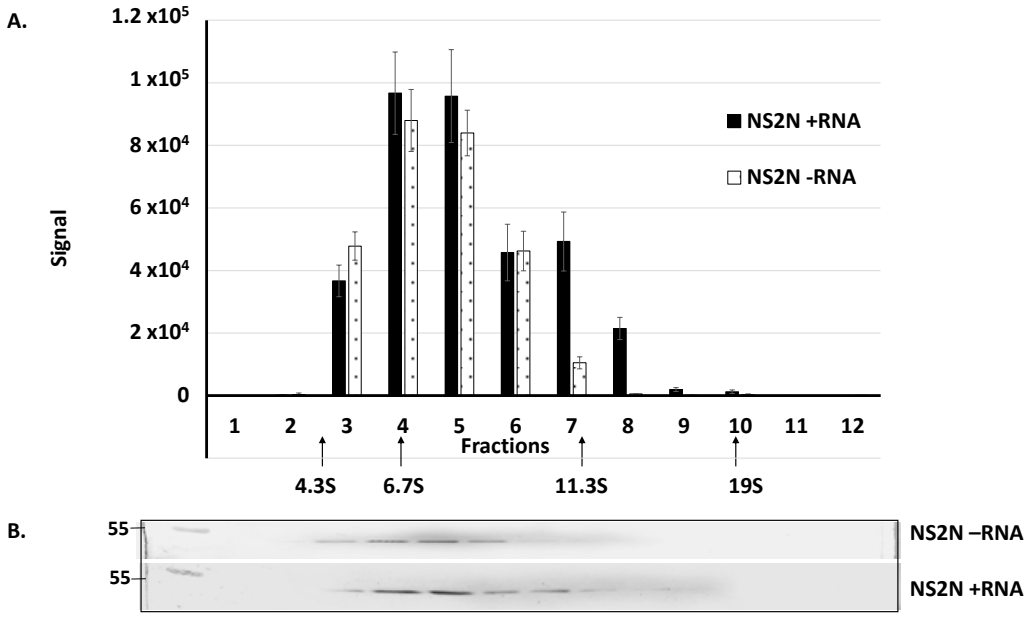

Figure 3.22. Oligomerisation assay of NS2.N in the presence and absence of ssRNA.

The twelve fractions from the oligomerisation assay were separated on 10 % SDS-PAGE and transferred to a nitrocellulose membrane as described in Figure 3.21. **A,** A graph showing NS2.N present in each the gradient fractions, with and without the addition of RNA (95% C.I). **B,** western immuno blot images used for analysis. NS2 Bands identified at 47 kDa.

NS2.N primarily formed 7S to 8S complexes (Figure 3.22. F4 – F5) in the absence of RNA, which equates to 4 to 5 copies of 42 kDa forming the most stable multimer of NS2. This was similar to WT NS2 which formed predominantly 7S complexes (Figure 3.21. F4) in the absence of RNA, with the second largest band at 8S. This relates to 4 to 5 copies of 42 kDa forming the most stable multimer of NS2. The data showed that the overall structure of NS2.N is very similar to WT, which validated that the mutations did not greatly change the general structure of the protein. The addition of 1µg BTV-1 S10 ssRNA formed a wider range of NS2.N complexes detected from fractions 3 to 7, which contain 6 - 12S complexes (Figure 3.22). The NS2.N complexes were predominantly identified in fractions 4 and 5 (7 – 8S) which was equivalent to NS2.N without RNA. Some larger complexes were generated by the addition of RNA which were not present in samples without RNA (Figure 3.22. F7). Although, these ~12S complexes were at a far lower intensity than the smaller 7 – 8S structures, the 95% confidence intervals demonstrated that these differences are statistically significant. This was very dissimilar to WT NS2 which with the addition of ssRNA, was mostly found in fractions 9 to 12, containing 18-22S complexes (Figure 3.21), with the strongest signal from fraction 11 indicating predominantly 20–22S complexes. This indicated that the NS2.N mutant was unable to bind the RNA, which was shown to be essential for the formation of the large NS2 homomultimers.

3.5 Discussion

The experiments in this chapter were undertaken to investigate the NS2 ssRNA binding domain between residues 2 - 11 [158]. The recently developed BTV reverse genetics system enabled a BTV-1 mutant to be generated with specific mutations designed to disrupt BTV ssRNA binding in this region and allowed the first *in vivo* study of BTV NS2 ssRNA binding. An *in vitro* study of the NS2 mutant was also performed to confirm that the mutations had not greatly affected the overall structure of the protein but had affected NS2-ssRNA binding ability. The *in vitro* characterisation was used to support and confirm the findings of the *in vivo* study.

The doughnut shaped proposed structure of NS2 is based on the merging of the high resolution N-terminal structure and the lower resolution C-terminal structure. The N-terminal structure (8-160 aa) does not include the first 7 amino acids, where the putative N-terminal RNA binding domain is located. Also not included in the full-length structure is the 160-178 aa region which contains the middle binding domain. The full-length structure also assumed that the N-terminal and C-terminal structures will not be altered when expressed together. If the full-length structure is correct three RNA binding domains are located in a groove between the N and C-terminal domains like rotavirus NSP2 [159], but does not indicate which sites have specific BTV ssRNA binding ability.

The BTV-1 S8.N mutant generated by the reverse genetics system was confirmed to contain the designed alanine substitutions and characterised to explore the effects of the mutations. Initial plaque assays of BTV-1 S8.N showed no plaque formation in BSR

cells when identified at 72 hpi. However, when BTV-1 S8.N was grown in the complementary cell line BSR-S8, the plaque phenotype resembled WT BTV-1 plaques of both BSR and BSR-S8 infections. This was due to the mutation in the NS2 protein because plaque formation was visually similar to a WT-like phenotype when a functional version of the NS2 protein was supplied *in trans* with the complementary cell line.

Plaque formation is an indication of virus growth, because of this the growth kinetics were further investigated with a time course of virus growth and protein production. The BTV-1 S8.N mutant was confirmed to be lethal by the lack of plaque formation. BTV-1 S8.N growth in the complimentary cell line was comparable to WT BTV due to the presence of functional NS2, but still demonstrated statistically significant reduced titres when compared to WT.

To investigate further the lethality of the mutation, protein samples were taken. Both structural (VP5) and non-structural (NS1, NS2) proteins were investigated but not detected from BTV-1 S8.N infected BSR cells. The actin controls of both WT and mutant infected cells displayed similar bands which indicated that the absence of mutant viral proteins was not due to any technical errors. This data confirmed that at some point during replication, the inserted mutations in the N-terminal RNA binding domain of NS2 have caused a lethal defect. This mutant only replicated when functional NS2 was supplied by the complimentary cell line.

As the S8.N mutation had been shown to be lethal during BSR infection, an immuno fluorescence assay was undertaken to visualise and analyse the VIBs produced by both

WT and BTV-1 S8.N. VIBs were examined because they are predominantly composed of NS2 and are the sites of immature progeny virus assembly. The images showed WT BTV-1 and BTV-1 S8.N infection of BSR cells through the labelling and fluorescence of viral structural protein VP7, while labelling of NS2 visualised VIBs.

The apparent disagreement between the failure to detect BTV-1 S8.N proteins by western immune blot and the ability to detect them by immuno fluorescence can be explained when considering the MOI's used in each infection. An MOI I was used for the protein production analysis by western blot while and MOI 10 was used for the immuno fluorescence assay. Given the very high infection used in the immuno fluorescence assay, the VP7 could be left from the initial infection.

WT BTV-1 formed VIBs comparable to those previously published [150]. BTV VIBs are often described as having a perinuclear location late in infection[133,148,152], similar to rotavirus viroplasms [240,241] and reovirus inclusion bodies [242,243]. BTV, rotavirus and reovirus have been depicted forming many inclusion bodies early in infection which merge later in infection and attain the perinuclear location. The data presented here however displayed WT and BTV-1 S8.N VIBs throughout the cytoplasm. This is most clearly demonstrated in Figure 3.11. 1C, where the split channels show BTV-1 S8.N VIBs dispersed all through the cytoplasm.

BTV-1 S8.N formed VIBs but these were smaller than WT VIBs and fewer in number despite the high MOI used for infection of both viruses. The mutant is likely to still recruit the core proteins and, perhaps, non-specific ssRNAs to form these structures. NS2.N was also occasionally shown to not form distinct, punctate VIB structures.

Instead a diffuse staining of NS2 was observed which, as VIBs are the sites of assembly, could account for the impairment in growth.

These initial findings were generated by a visual inspection of the images, which led to formal image quantification. WT BTV-1 infection of BSR cells produced an average of 257 VIBs per frame with an average size of 1.38 μm^2. Under the same conditions BTV-1 S8.N produced an average of 45 VIBs per frame with an average size of 0.78 μm^2. Both the 95% confidence intervals and P-value showed that this was a statistically significant ($p<0.05$) 82% reduction in total number of VIBs and 43% reduction in VIB size. Previous characterisation of BTV VIBs [148] showed that the average size of VIB was 1.1 μm^2 at 24 hpi, which was between the average size of BTV-1 S8.N VIBs and BTV-1 VIBs. Both investigations used the same MOI 10 but Brookes *et al* 1993 used SVP cells derived from porcine stable (PS) cells [244] while this analysis used BSR cells. Also, this analysis measured 1542 BTV-1 VIBs and 272 BTV-1 S8.N VIBs, while Brookes *et al* 1993 only measured on 48 structures. The previous study used electron micrographs to measure the VIBs. The samples were fixed and stained which would have altered the size of the VIBs.

The mean maximum size of VIB varied greatly; both within the same virus infection type, as shown by the large upper and lower confidence levels; and between WT BTV-1 and BTV-1 S8.N, with BTV-1 S8.N average VIB size of 4.36 μm^2 and BTV-1 average VIB size of 19.66 μm^2. These differences were shown to be statistically significant ($p<0.05$) by both the 95% CI and P-value. Conversely, the mean minimum size for both WT BTV-1 and BTV-1 S8.N VIB was very similar at 0.12 μm^2 and 0.11 μm^2, respectively. The

difference was shown not to be statistically significant ($p<0.05$) by the >25% overlapping 95% CI and a P-value of 0.22. This might represent the minimal structure detectable or the minimal structure of a VIB.

BTV VIBs are similar to rotavirus viroplasms, in so far as the size, location and number are dynamic and change throughout infection [148,240]. A greater number of inclusion bodes are seen early in infection, which then fuse to form fewer but larger bodies over time. The work described here was a characterisation of VIB size and number at a specific time post infection and as such is limited. It is unable to explain if the differences in WT and BTV-1 S8.N VIBs were just a delay, as with the virus growth, and would fuse to form larger VIBs later in infection or a true depiction of phenotype throughout infection.

All the *in vivo* characterisation of BTV-1 S8.N showed that the designed mutations effect virus growth and VIB formation. The growth was completely impaired and lethal in BSR cells. This could be due to the differences seen in the VIBs, which are the sites of virus assembly. Sometimes BTV-1 S8.N displayed a diffuse staining of NS2 rather than a punctuate VIB. When VIBs were formed, they were smaller and far fewer, which could be a limiting factor in replication. A disruption in inclusion body formation affecting virus replication has previously been shown with rotavirus viroplasms and thiazolide drugs [245]. Treatment with the drugs reduced the size and number of viroplasms per cell, decreasing the dsRNA formation and resulted in an overall reduction in rotavirus replication. This mutation has the possibility to form a disabled infectious single cycle

(DISC) vaccine strain vaccine because it was only able to replicate when a functional copy of the NS2 protein is supplied *in trans*, like the VP6 vaccine candidate [73].

The *in vivo* data clearly showed that the mutations affected virus replication and VIB formation but not if this was due to any changes in s structure rather than due to a change in a single functional domain. *In vitro* investigation of the N-terminal RNA binding domain mutant would also generate data on the actual effect on RNA binding or NS2 oligomerisation, which is thought to require RNA to act either an initiator or as a supporting scaffold [151] for the larger oligomeric forms reported. This was investigated *in vitro* with the generation of a recombinant baculovirus expressing NS2 with the same mutations as BTV-1 S8.N.

The transfer plasmid pAcYM1-H/GST NS2.N was generated by an In-Fusion cloning method, which at a 15 min incubation at 50° C was quicker than using a traditional ligase enzyme, was not limited to insertion into restriction sites and was 100% successful with all of the colonies tested containing the insert.

However, the recombinant construct lost the purification tag, possibly due to its large size or repeats in the flexible region between the tag and the NS2 protein. The strong band at 65 kDa, originally identified as tagged NS2.N, was most likely baculovirus protein GP64 which is an envelope fusion protein [246] produced to high levels during infection and has a size of 65 kDa[247]. Nevertheless, it was still possible to purify the mutant protein, allowing characterisation despite some degradation product.

A protein band was seen at ~25 kDa; this band was also present in the earlier western blot which due to the specific nature of the NS2 antibody used suggested it was likely

to be a protein degradation product, despite the use of protease inhibitors during the purification process. The C-terminal domain of NS2 has previously been shown to degrade rapidly at 4 °C, both with and without a protease inhibitor, to produce a major degradation product of 25 kDa and smaller fragments [159]. Even at highly purified 3µg/µl quantities, WT NS2 and NS2.N did not form aggregates. This was unlike the previously reported attempts of NS2 purification prior to investigation into NS2 oligomerisation and structure, which stated that full-length protein concentrations higher than 2 µg/µl formed aggregates and prevented future work [159].

When purified WT and mutant NS2 was investigated for their specific BTV ssRNA binding ability, it was clear that the mutant protein lost this functional capacity in contrast to that of WT, which exhibited concentration dependent, specific ssRNA binding. The mutant completely failed even at the highest concentrations of protein used. Therefore it was concluded that the inability of BTV ssRNA binding most likely perturbed the core assembly and virus replication.

Neither 1 µg NS2.N nor WT NS2 was found to bind any BTV ssRNA. Given the binding of WT protein to ssRNA at larger quantities, it is probable that 1 µg NS2 could still bind ssRNAs but at insufficient amounts to be detected. This is despite the use of radioactive labelling being used for detection due to its high sensitivity [239].

It has been suggested that oligomerisation of NS2 is triggered by the binding of RNA [151]. In order to investigate this, the oligomerisation of both RNA binding mutant NS2.N and WT NS2 in the presence and absence of RNA was examined by sedimentation analysis.

WT NS2 was predominantly detected in fraction 4 (7S complexes) which equates to ~6 copies of 42 kDa NS2 complexes. NS2 was also present in large amounts in fraction 5 (~8S). This strongly supported the previous reports of a 7S complex comprised of 6 copies of 42 kDa baculovirus expressed NS2 [167], and partially supports the published 8-10S complexes of 6 (+/-2) copies of bacterially expressed NS2 [154]. This is maintained throughout the *Reoviridae* family with NS2 homologs, such as African horsesickness Virus (AHSV) NS2 and Epizoonotic haemorrhagic disease virus (EHDV) NS2 also forming 7S minimal complexes [167].

The addition of BTV S10 ssRNA was shown to form larger WT NS2 complexes found in fractions 9–12, forming 18–22S complexes of NS2. This is a verification of previously published work which found that BTV-1 NS2 form a variety of larger complexes in the presence of RNA [154], as does Reovirus functional homologue σNS, which forms 13–19S complexes [248]. The strongest signal indicated in this work was from fraction 11 indicating predominantly 20–22S complexes which aligns closer to the findings of Huismans *et* al 1987 [160].

NS2.N was predominantly detected in fractions 4 and 5 which equates to 7-8S complexes, but NS2 was also present in fractions 3 and 6 (5-10S). This was similar to the NS2 complexes formed by WT NS2 above and the previously published work [154,167]. The addition of RNA was shown to form a wide range of NS2.N complexes found in fractions 3–7 (5–12S). The quantification of the gels showed that these complexes were predominantly seen in fractions 4 and 5 (7–8s) which is identical to NS2.N

without RNA. More complexes are generated in fraction 7 by the addition of RNA than without RNA but these were at a far lower intensity than the smaller complexes.

While the work undertaken here has not clarified if the oligomerisation of NS2 is triggered by the binding of RNA or if it is a scaffold to support larger structures, it has shown that the binding of RNA resulted in larger NS2 complexes. It was shown that WT NS2 forms 7-10S complexes in the absence of RNA and 18-22S complexes in the presence of RNA, similar to published work. This is in contrast with an NS2.N, which has a severely diminished RNA binding ability and so forms the same complexes in the absence and presence of RNA.

It has been suggested that 8–10S (140–152 kDa) would consist of 6 (+/-2) units of NS2 [154], which is contradictory to the proposed structure of NS2 which indicated that the full-length protein could assemble as multimers of 10–11 subunits to form ring-like structures [168]. It is somewhat similar, however, to VIB proteins from other members of the *Reoviridae* family. P9-1 Rice Black Streak Dwarf Virus (RBSDV) [171] and NSP2 Rotavirus [172] have low sequence homology but form octamers in ring-like structures, as NS2 is reported to do. These structures however, are octamers which form closed rings. Also somewhat similar is Rift Valley Fever Virus (RVFV) which contains a hexameric ring-shaped nucleoprotein (N) with the ability to bind RNA [249]. This is a component of the ribonucleoprotein complex rather than VIB formation as with NS2, but both are important in virus replication.

The *in vitro* characterisation of NS2.N showed that the designed mutations severely compromised the proteins ability to bind RNA compared to WT NS2 with 20 µg NS2.N

unable to bind any RNA while 20 µg WT NS2 was sufficient to bind 100 %, resulting in a complete shift of all RNA to a bound position. NS2.N oligomerisation was similar to WT NS2 in the absence of RNA but the mutations and the impaired binding of RNA resulted in no difference in complexes formed in the presence of RNA, with the greatest amount of NS2.N forming 7–8S complexes with and without RNA. When analysed with the *in vivo* characterisation of BTV-1 S8.N, which showed that the BTV-1 S8.N mutations were lethal to growth in BSR cells and had a significant effect on VIB formation, it is clear that the N-terminal RNA binding domain is essential in BTV replication and that binding of RNA is important in the formation of VIBs and, in general, the efficient replication of the virus.

Chapter 4

In vivo and *in vitro* investigation into the Middle RNA binding domain of BTV NS2

4.1 Introduction

BTV VIBs are the sites of virus assembly and are predominantly composed of NS2 (42kDa). NS2 has NTPase activity, it is the only phosphorylated BTV protein, and preferentially binds BTV ssRNA [156,161]. NS2 also demonstrated non-specific RNA binding [155,160].

Initial investigations into the locations of the RNA binding domains focused on the N-terminal 1–92 aa and the C-terminal 227–357 aa, but not the central 133 aa between 93–226 aa of NS2 [231]. The C-terminal was reported not be required for RNA binding while the N-terminal, in particular residues 4, 6 and 7, were necessary for RNA binding. Subsequent results have indicated three NS2 ssRNA binding domains, one between residues 153-166 [158] which is indicated here in Figure 4.1. (Dashed box).This putative middle binding domain is highly charged. It contains 9 positively or negatively charged amino acids (D_{154}, R_{156}, E_{157}, R_{159}, K_{161}, K_{162}, E_{164}, R_{165} and E_{166}).

Recombinant WT BTV-17 NS2 and deletion mutant BTV-17 $NS2_{153-166}$ were expressed in *E. coli*, purified and used in non-BTV specific ssRNA EMSAs [158]. This showed that $NS2_{153-166}$ was less able to bind non-specific ssRNA compared to WT NS2, but of the 3 domains identified (2-11, 153-166 and 274-286) this deletion mutant retained the largest affinity for the RNA. Interestingly, despite single mutation $NS2_{153-166}$ showing the greatest affinity, the double deletion mutant BTV-17 $NS2_{153-166/274-286}$ demonstrated a lower affinity for non-specific RNA than both BTV-17 $NS2_{2-11/153-166}$ and BTV-17 $NS2_{2-11/274-286}$ [158]. This demonstrated that there may be interaction between domains.

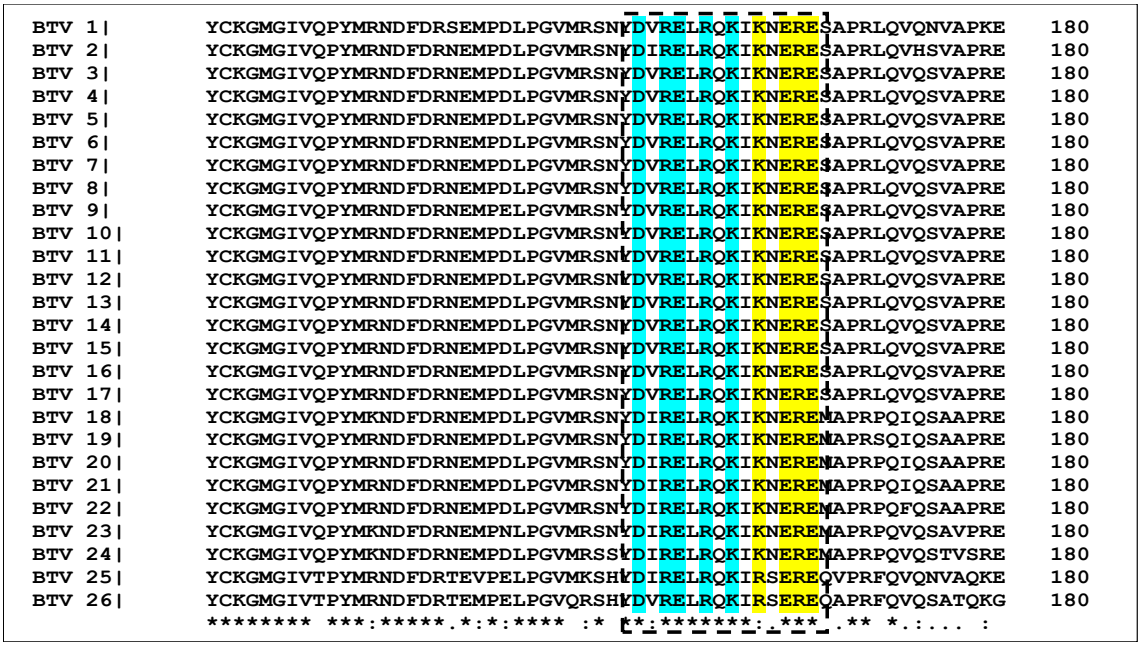

Figure 4.1. Clustal alignment of BTV 1- 26 NS2 amino acid sequences.
Sequences from each of the 26 serotypes were aligned using Clustal Omega (http://www.ebi.ac.uk/Tools/msa/clustalo). Dashed box indicates the putative N-terminal binding region 153-166 aa. Amino acids highlighted in yellow are the conserved, charged amino acids chosen for mutation to disrupt RNA binding. Amino acids highlighted in blue are charged amino acids not chosen for mutation. An asterisk indicates positions which have a fully conserved residue. A colon indicates conservation between groups of strongly similar properties. A full-stop indicates conservation between groups of weakly similar properties. Appendix 1 contains the full Alignment of NS2 amino acid sequences

Previous work identified an RNA binding domain at 153-166 aa [158], but the relevance of this domain *in vivo* during virus replication was unknown because all studies were performed *in vitro* using recombinant NS2 mutants. In this chapter the 153-166 aa RNA binding domain of BTV NS2 was investigated *in vivo* for the first time, with mutations specifically designed to alter the charged residues identified as involved in the binding of RNA. This was only possible due to the development of a reverse genetics system. This system has allowed the generation of BTV mutants containing specifically

designed nucleotide changes. The mutations examined *in vivo* were also investigated *in vitro* through the recombinant baculovirus expression of NS2 containing the same mutations. This dual characterisation of the 153-166 aa RNA binding domain is novel and has generated the most complete data on the importance of the domain. Most importantly, the *in vivo* and *in vitro* investigations in this chapter has given a unique insight into the important role NS2-ssRNA binding plays in BTV replication.

4.2 Results

4.2.1 Design and confirmation of **S8.M** mutations

All of the charged residues were possible targets in the investigation of the RNA binding site. All charged amino acids were not targeted however, due to the large number of nucleotide changes needed to generate the mutant.

NS2 is highly conserved in this region, apart from serotypes 25 and 26, which show a larger degree of variation. Figure 4.1 shows a partial alignment of NS2 sequences from each of the 26 serotypes. It is because of this, that the charged amino acids D_{154}, R_{156} and E_{157} were disregarded as possible sites of mutation due to their proximity to amino acid I_{155} which varies between BTV-1 and all other serotypes shown. Amino acids R_{159} and K_{161} were discounted in favour of K_{162} E_{164} R_{165} E_{166} because of their less clustered nature. The most significant variation within the middle RNA binding domain is the exchange of N_{163} for a weakly similar serine. Also variable is K_{162} for the strongly similar arginine, both have previously been shown to be required for RNA binding [232,233]. The

K_{162} and N_{163} variation was only shown in serotypes 25 and 26 which was considered acceptable because generally these serotypes vary more from the other 24.

The RG system for BTV was previously used to generate a mutant virus with alanine substitutions to the middle RNA binding domain (K_{162}A E_{164}A R_{165}A E_{166}A). The substitution of alanine to replace the charged residues was hypothesised to disrupt the interaction with the ssRNA and affect virus replication. Alanine was chosen as the substitution amino acid because it is a small, neutral amino acid unlikely to greatly change the overall structure, whilst still achieving a significant change to alter activity of this functional region.

Two BTV-1 S8.M mutant viruses were previously designed and recovered by a member of lab (virus 12 and virus 17). For this thesis, the viruses were validated to confirm the correct insertion of the designed mutations and characterised. Virus stocks were generated by infections at an MOI 1 of BSR cells and BSR-S8 complementary cells. Once 100% CPE was reached, stocks were harvested and virus titre obtained by plaque assays. These stocks were used throughout and re-made frequently to maintain a high virus titre. The BSR-S8 complementary cell line was frequently analysed for the production of NS2 (Figure 3.4. B), which can be reduced or lost over time despite the use of an antibody to select for NS2 producing cells.

Analysis of the pattern of genomic dsRNA of BTV S8.M and the comparison of wild-type S8 was used to confirm the presence of BTV. Mutant viruses 12 and 17 were harvested and the genomic dsRNA extracted and analysed by native page electrophoresis, which showed all 10 genomic segments from BTV S8.N (Figure 4.2. A,

Lanes 2 &3) and wild-type BTV (Lane 1). Both mutant and wild-type S8 migrated to the same position and were indistinguishable from each other. The detection of dsRNA bands, like those found in WT BTV, indicated that virus was recovered, but did not verify that the viruses contain the designed mutations.

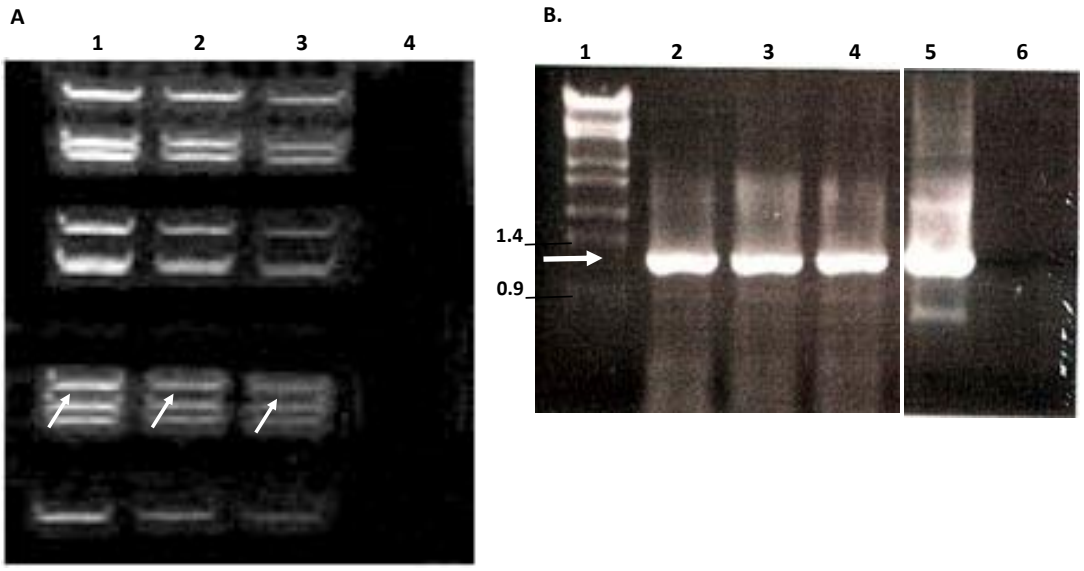

Figure 4.2. Genomic dsRNA purification and RT-PCR of BTV-1 S8.M.
A, dsRNA purification from infected BSR cells infected with BTV-1 S8.M analysed on a 9% non-denaturing polyacrylamide gel stained with ethidium bromide. Lane 1, BTV-1 dsRNA used as a marker. Lanes 2 & 3, BTV-1 S8.M clones 17 and 12, respectively. White arrows represent migration of segment 8. **B,** RT-PCR of BTV-1 S8.M detected on a 1% agarose gels by ethidium bromide. Lane 1, *Sty*I digested λ DNA ladder. Lanes 2 & 3, BTV-1 S8.M clones 17 and 12. Lane 3, PCR only control of amplified S8 from pUC19 T7 S8. Lane 5, RT-PCR control of WT BTV-1 dsRNA. Lane 6, H_2O control. White arrows indicate approximately 1,100 bp, the expected size for Segment 8. Size marker shown in Kb.

Specific primers (BTV-1 S8 T7 *Bam*HI F and BTV-1 S8 *Bsm*BI/*Bam*HI/*Rsr*II R) were used to amplify the full-length S8 by reverse transcriptase PCR (RT-PCR). Firstly, a cDNA copy of the dsRNA S8 was generated by reverse transcription. This was then amplified by

PCR using the same primers, which then generated a product for sequencing. One band in each lane (Figure 4.2. B, Lane 3 and 4) was visible by gel electrophoresis at the expected size of ~1,100 bp. A plasmid containing a cloned S8 (pUC19 T7 S8) was used as PCR control (Figure 4.2. B, Lane 5) and showed a corresponding band also at ~1,100bp. No amplification was detected in the negative control (Figure 4.2. B, Lane 6). The amplified segment was excised, purified and sent for sequencing commercially.

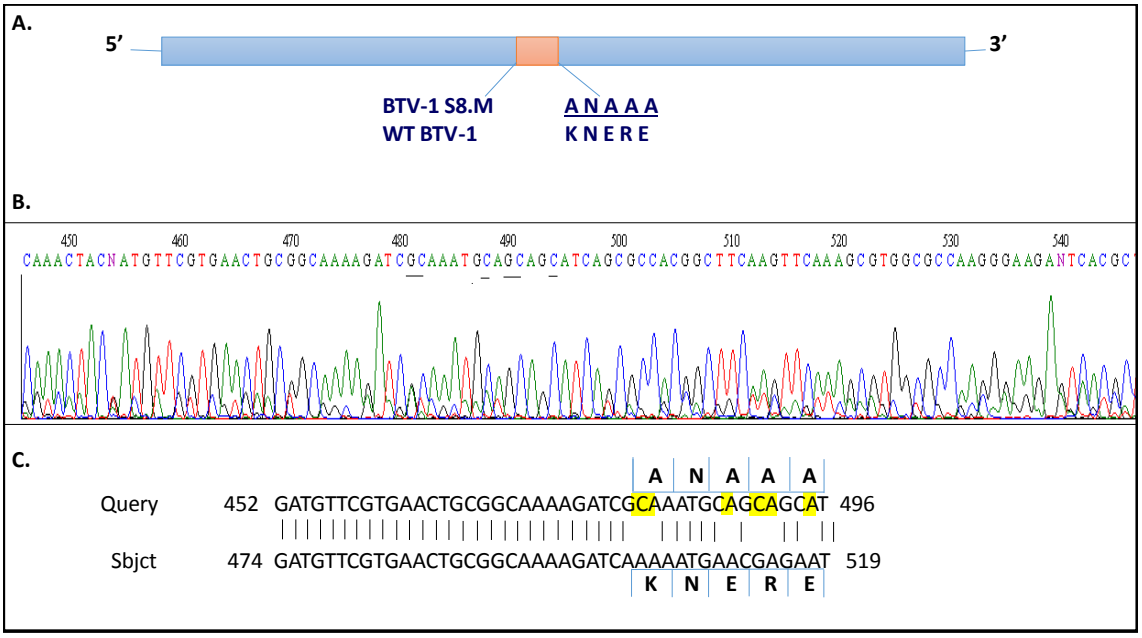

Figure 4.3. Confirmation of mutations in BTV-1 S8.M.
A, Schematic diagram of NS2 demonstrating the WT BTV-1 amino acid sequence and the designed mutations to disrupt ssRNA binding (BTV-1 S8.M). **B)** Partial chromatogram sequence of BTV-1 S8.M, sites of expected mutations underlined. **C)** Partial sequence of PubMed alignment of BTV-1 S8.M and the published BTV-1 NS2 sequence. Sequence differences highlighted in yellow and the resulting amino acids indicated.

The presence of the specific mutation in BTV -1 S8.M clone 17 was confirmed through sequencing of the RT-PCR product. The results were compiled by Bio-edit software and BlastN confirmed as BTV S8. Alignments of BTV -1 S8.M (Figure 4.3. C) with BTV-1

published data revealed the expected alanine substitutions at residues K_{162} E_{164} R_{165} E_{166}**,** consistent with the designed mutations. BTV -1 S8.M clone 17 was subsequently referred to as BTV -1 S8.M and used for all investigations.

4.3 BTV-1 S8.M characterisation

4.3.1 Plaque formation of the BTV S8.M mutant in BSR cells

The BTV -1 S8.M mutant virus was initially characterised by its ability to form plaques in both BSR and BSR-S8 complementary cells. Differences between BTV -1 S8.M and wild-type plaques were observed in BSR cells. The mutant formed smaller plaques in BSR cells (Figure 4.4. B), while the WT virus in the same cells formed larger plaques consistent with those usually produced by WT BTV-1. (Figure 4.4. C).

BTV -1 S8.M in the complementary cell line (BSR-S8), however, demonstrated a WT-like plaque phenotype (Figure 4.4. A). The plaques formed from WT BTV-1 in the complementary cell exhibited no change in plaque phenotype compared to those seen in WT BTV-1 BSR plaques (Figure 4.4. D). This observation indicated that the middle RNA binding domain mutation introduced into S8 had some effect on virus growth in BSR cells and the recovered virus was attenuated. When functional NS2 is supplied *in trans* the virus growth returned to normal, supporting the assumption that the change is due to the inserted mutations.

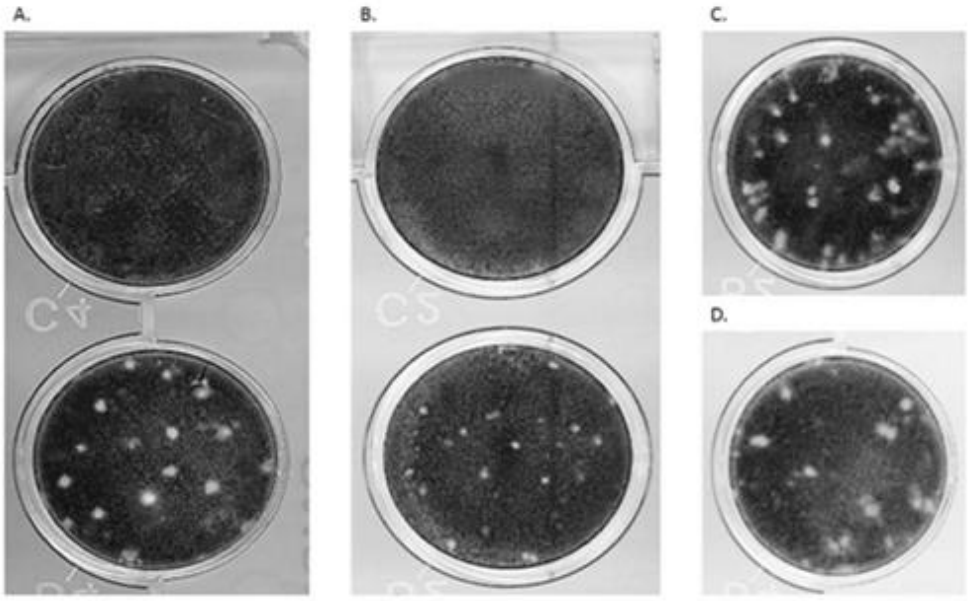

Figure 4.4. Examples of the plaques formed by WT BTV-1 and BTV-1 S8.M in BSR and BSR-S8 cells.
BSR or BSR-S8 complementary cells were infected with virus, fixed 3 days post infection and stained with crystal violet. **A,** BTV-1 S8.M plaques formed in BSR-S8 complementary cells (lower well) and a non-infected control (top well). **B,** BTV-1 S8.M plaques formed in BSR cells (lower well) and negative control non-infected cells (top well). **C,** WT BTV-1 plaques formed in BSR cells. D, WT BTV-1 plaques formed in BSR-S8 cells.

4.3.2 Growth kinetics of the BTV S8.M mutant in BSR cells

Since the mutant virus exhibited much smaller plaques it was subjected to further investigation. Both BSR and BSR-S8 complementary cells were therefore infected with BTV -1 S8.M at an MOI 1. Cells and supernatant were harvested at 0, 8, 16, 24, 36, 48, 72 and 96 hpi. Virus growth was assessed through plaque assay in the cell types they were previously grown in. This experiment was performed in triplicate and the average virus titre used to plot the growth curve (Figure 4.5). A 95% confidence interval (95%

CI) was used to assess statistical significance. As a comparison control WT BTV-1 growth in BSR and BSR-S8 cells was also analysed.

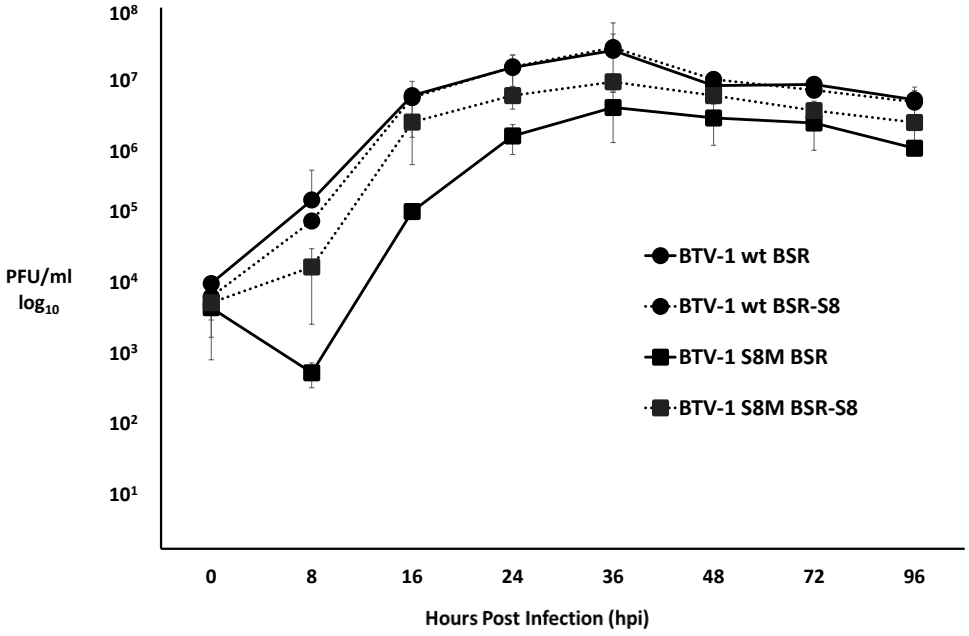

Figure 4.5. BTV-1 S8.M growth curves in BSR and BSR-S8 cell line.
Mammalian BSR or BSR-S8 cells were infected at MOI 1 and harvested at the indicated times. Viral titre was determined by plaque assay (in triplicate) and the averages plotted on a logarithmic scale. BSR and BSR-S8 cells infected with wild-type BTV were used as controls. (95% C.I).

WT BTV growth in BSR cells demonstrated an increase in virus titre up to 36 hpi (Figure 4.5. Circle, solid line), with the greatest increase of growth rate shown at 16 hpi as shown by a 1.4 log increase in titre. Virus growth decreased after 36 hpi, which was comparable with published data [73]. WT growth in BSR-S8 cells was similar to WT, with the greatest titre at 36 hpi (Figure 4.5. Circle, dotted line) and the greatest increase in growth rate also shown at 16 hours with a 1.7 log increase. This was followed by a decrease at in titre at comparable levels to that seen BSR cells. Maximum BTV titre was slightly higher in BSR-S8 cells with an average at 36 hpi of 2.5 $x10^7$, compared to the

average at 36 hpi in BSR cells of 2 x10^7. Any minor variation between WT growth in the different cell lines was shown not statistically significant due to >25% overlap in confidence intervals (C.I). BTV -1 S8.M in normal BSR cells showed a reduction in virus titre at 8 hpi compared to initial infection (Figure 4.5. Square, solid line). An increase in virus titre was then visible up to 36 hpi, with the largest increase of growth rate at 16 hpi, a 2.5 log increase in titre. This was followed by a decrease in virus titre between 36 and 96 hpi. BTV-1 S8.M never reached the highest titres of WT BTV with a maximum titre of 3.3 x10^6, a statistically significant 0.9 log reduction.

After the initial delay BTV -1 S8.M growth in BSR-S8 cells was more similar to WT growth (Figure 4.5. Square, dotted line). It displayed an increase in growth up to 36 hpi (8 x10^6) at comparable levels to WT in the BSR cell line (2 x10^7) and the BSR-S8 cell line (2.5 x10^7), and a growth decrease after 36 hpi. The fastest rate of growth was demonstrated at 16 hpi with a 2 log increase in titre. Generally, any variation of BTV -1 S8.M growth in BSR-S8 cells was not statistically significant from WT as shown by the >25% overlap in CI. Apart from at 8 hpi which demonstrated a statistically significant, 0.6 - 1 log reduction.

To characterise the virus growth further, BSR cells were infected with BTV -1 S8.M at MOI 1 and harvested at the time points indicated. Cell lysate samples were taken in triplicate and the protein synthesis analysed. Samples were resolved by 10% SDS-PAGE, transferred to a nitrocellulose membrane and western immuno blotted using specific antibodies against a cellular protein (anti-actin), a virus structural protein (anti-

VP3) and virus non-structural proteins (anti-NS1 and anti-NS2). Actin (42kDa) is a cellular protein used as a control to eliminate variation in overall protein load.

Western immuno blotting was performed with the antibodies indicated in Figure 4.6. Western immuno blot analysis demonstrated that the BTV -1 S8.M produced NS2 which was recognised by a specific anti-BTV-10 NS2 and indistinguishable in size to wild-type BTV NS2. Although NS2 is a 42kDa protein, it runs on an SDS-PAGE gel to about 46kDa [154,162].

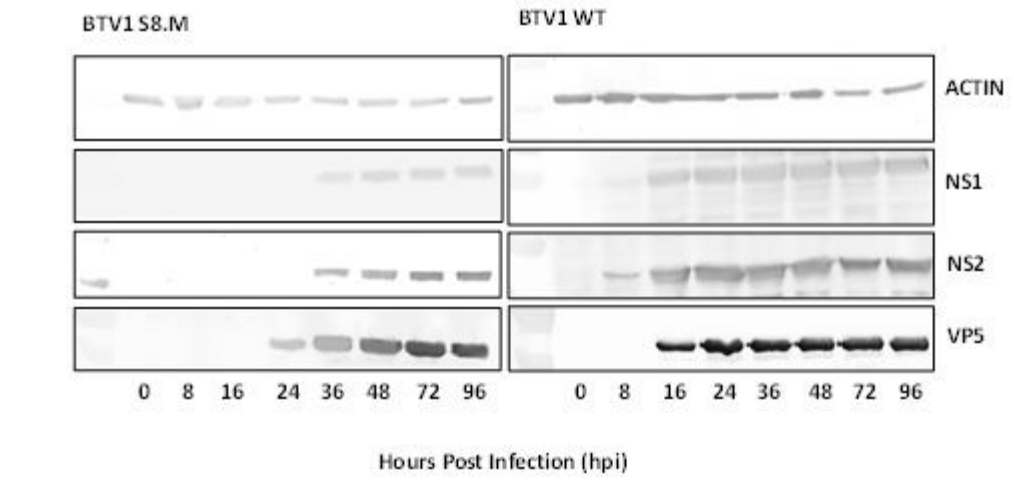

Figure 4.6. Analysis of BTV-1 S8.M proteins during BSR cell infection.
Proteins harvested at indicated time points, separated on a 10 % SDS-PAGE and transferred to a nitrocellulose membrane for visualisation using western immuno blot. Rabbit anti-NS1 antibody (1:5000) detected bands at 64 kDa. Guinea pig anti-NS2 antibody (1:3000) detected bands at 42 kDa. Guinea pig anti-VP5 antibody (1:3000) detected bands at 59 kDa. Ladder used was Page Ruler Prestained Protein ladder (Thermo Scientific). Protein load control was indicated by Mouse anti-Actin antibody (1:5000) (42 kDa).

Visual analysis of the western immuno blots of viral protein demonstrated that BTV1 S8.M first expressed non-structural proteins NS1 and NS2 at a high enough level to be detected between 24 and 36 hpi (Figure 4.6) and showed a slight increase until 96 hpi. BTV S8.M structural protein VP5 was shown at 24 hpi, with an increase in production until 96 hpi. BTV-1 WT non-structural proteins NS1 and NS2 were detected at 16 and 8 hpi, respectively (Figure 4.6), and expressed until 96 hpi. NS2 can be identified in cells from as early as 2-4 hpi [128], but those time points were not analysed here. BTV-1 WT structural protein VP5 was shown at 16 hpi, and was expressed at a seemingly constant level until 96 hpi. Cellular protein actin was used as a protein loading control; the constant levels show that the same amount of protein was added to each well. Visual analysis of the western immuno blot protein expression images (Figure 4.6) produces data of limited value; therefore the images were quantified with LI-COR Image Studio Lite to generate more detailed description of protein expression at each of the time points. The signal intensities from the red, green and blue signal channels were averaged and normalised to the actin load control (Figures 4.7, 4.8 & 4.9).

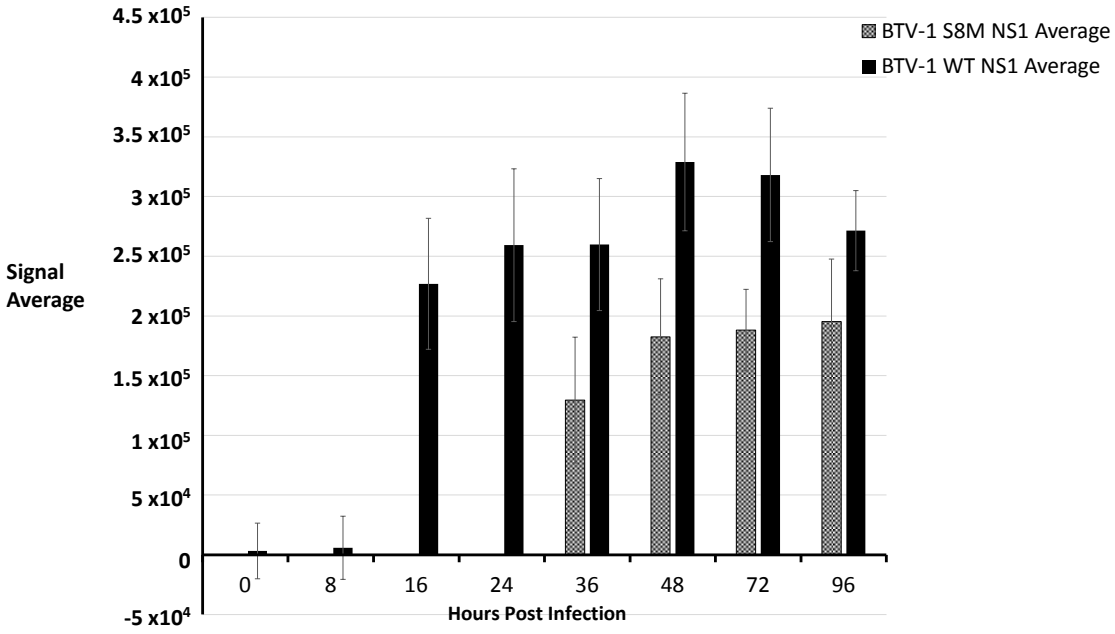

Figure 4.7. NS1 protein expression of BTV-1 WT and BTV-1 S8.M in BSR cells over time.

The western immuno blot protein expression images for BTV-1 WT and BTV-1 S8.M (Figure 4.6) were quantified with LI-COR Image Studio Lite and the colour channel signals for each time point used to form a three channel signal average. NS1 was normalised to the respective actin loading control and plotted. (95% C.I).

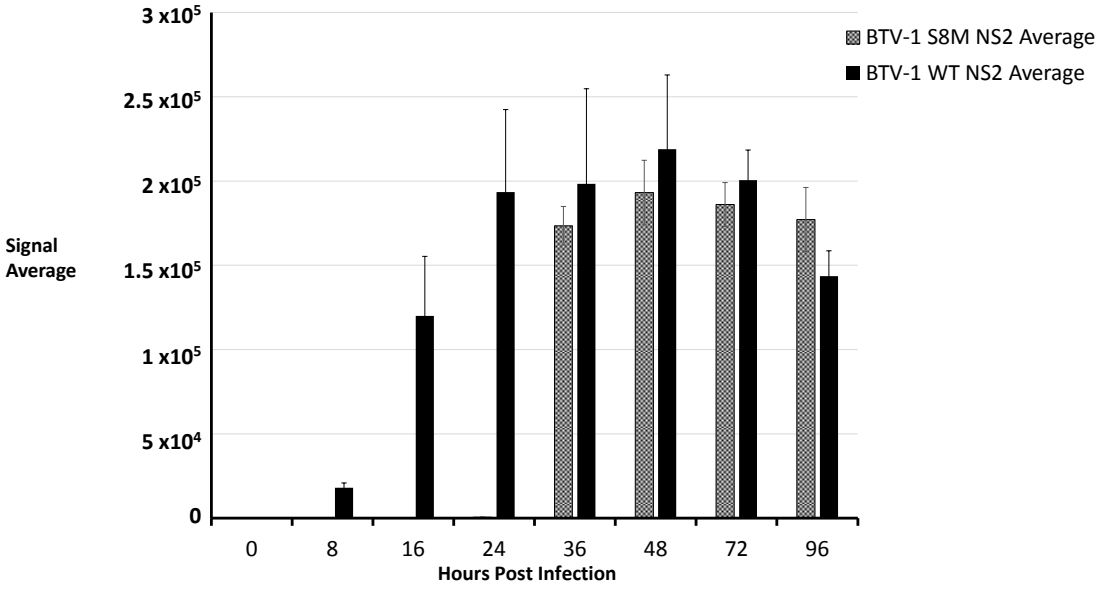

Figure 4.8. NS2 protein expression of BTV-1 WT and BTV-1 S8.M in BSR cells over time.

The western immuno blot protein expression images for BTV-1 WT and BTV-1 S8.M (Figure 4.6) were quantified as described in Figure 4.8. NS2 was normalised to the respective actin loading control and plotted. (95% C.I).

Quantification of NS1 expression of both BTV-1 WT and BTV-1 S8.M (Figure 4.7) displayed that BTV-1 S8.M had a delayed NS1 expression at detectable levels from 16 hpi as shown by WT BTV-1, to 36 hpi. Expression increased up to 46 hpi and plateaued. This was dissimilar to WT NS1 production which increased up to 72 hpi and then decreased. BTV-1 S8.M NS1 maximum expression (96 hpi) shows a 40% reduction compared to WT NS1 maximum expression (48 hpi).

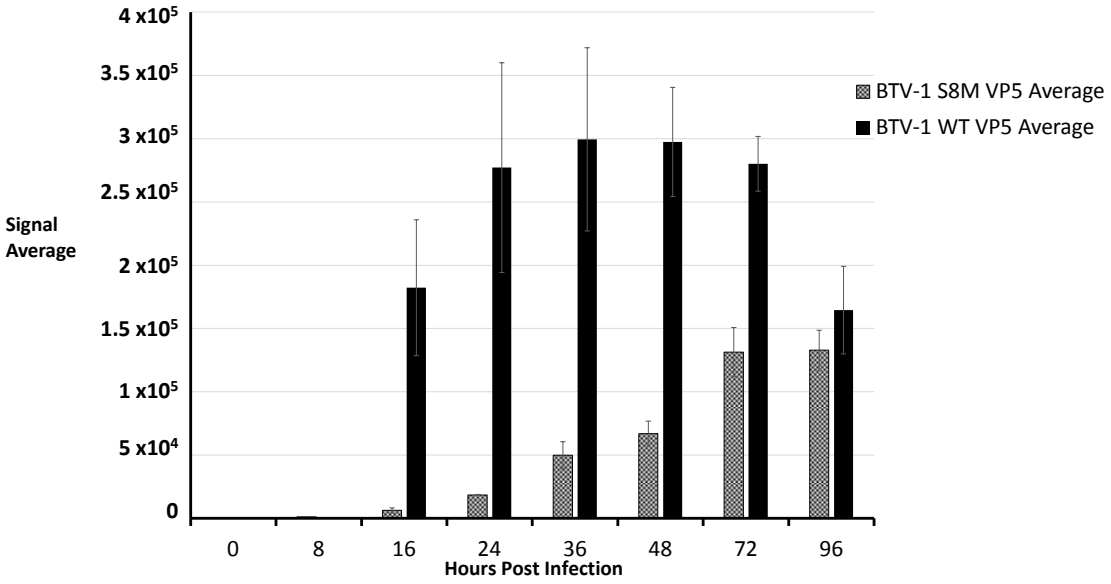

Figure 4.9. VP5 protein expression of BTV-1 WT and BTV-1 S8.M in BSR cells over time.
The western immuno blot protein expression images for BTV-1 WT and BTV-1 S8.M (Figure 4.6) were quantified as described in Figure 4.8. VP5 was normalised to the respective actin loading control and plotted. (95% C.I).

Detectable BTV-1 S8.M NS2 production was delayed when compared to WT NS2 expression (Figure 4.8), with BTV-1 S8.M NS2 detected at 36 hpi rather than 8 hpi for BTV-1. NS2 expression peaks at 48 hpi for both WT and BTV-1 S8.M and is followed by a reduction in NS2 levels to 96 hpi. Maximum NS2 production of BTV-1 S8.M showed an 11.7% reduction compared to the maximum production in WT.

BTV-1 S8.M VP5 was detectable at 16 hpi (Figure 4.9) which was the same time point as WT VP5 but BTV-1 S8.M VP5 displayed a 97% reduction compared to WT. BTV-1 S8.M VP5 increases up to 72 hpi and plateaued while WT VP5 increased up to 36 hpi and then decreases. Maximum BTV-1 S8.M VP5 expression is at 96 hpi and demonstrates a 55.6% reduction compared to maximum WT VP5 expression.

Overall, mutant non-structural protein production was delayed by at least 20 hours and the amount generated is reduced compared to WT. Structural protein VP5 was detected at the same time point as WT but at a greatly reduced level.

4.3.3 Effect of the S8.M mutation on VIB formation in BSR cells

One of the characteristic signs of BTV-1 infection are virus inclusion bodies (VIBs) composed of NS2. The effect of the mutation in S8 on the formation of the VIBs was therefore investigated using Immuno Fluorescence Assay (IFA) and visualised by confocal microscopy (Figure 4.10). Dual staining was performed using anti–NS2 antibodies to show VIB formation and anti-VP7 antibodies as a confirmation of viral infection. Both wild-type and BTV S8.M infected BSR cells show high levels of VP7, which reflects the MOI 10 that was used to infect cells and gives a clear indication that both samples were infected with replicating virus.

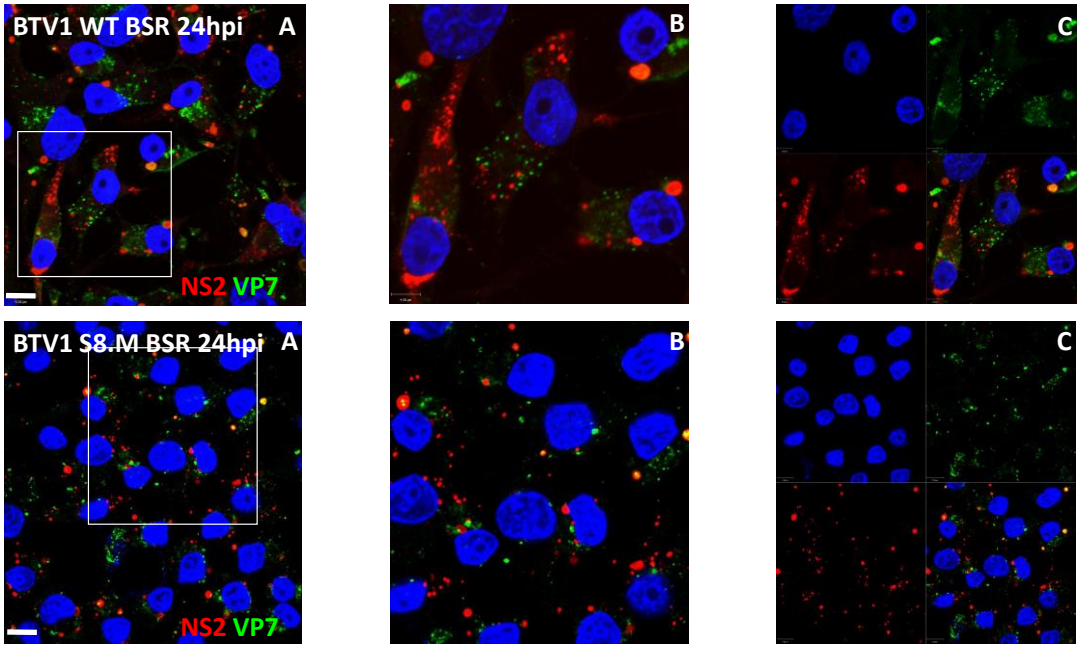

Figure 4.10. Immunofluorescence assay of BTV-1 WT and BTV-1 S8.M infection at 24 h in normal BSR cells.
Dual staining for NS2 and VP7. BSR cells were fixed 24 hours post infection and protein expression investigated by confocal microscopy. Primary antibodies, Guinea pig anti-VP7 and Rabbit anti-NS2; Secondary antibodies Guinea pig α Alexa 488, Rabbit α TritC and Hoechst nuclear staining. **A,** Images obtained by an x100 lens. **B,** Detailed section of image in A at x2 magnification. **C,** Split laser channels and merged image. White scale shows 10 µm.

A visual analysis of BTV S8.M infected BSR cells show smaller and fewer VIBs (Figure 4.10. A). In comparison, WT BTV demonstrates distinct, punctuate structures of NS2 (VIBs) typical of BTV infection [150,151].

The NS2 signal generated by the secondary antibody in each field of view obtained by the x100 lens (Figure 4.10) was quantified by Volocity software. Ten fields of view typical of both WT BTV-1 and BTV-1 S8.M infections in BSR cells were compared, and in support of the visual assessment of the IFA, BTV-1 S8.M produced ~66% fewer detectable VIBs. Of those VIBs produced during infection, BTV-1 S8.M produced ~25% smaller VIBs. WT BTV-1 produced an average of 257 VIBs in the BSR cells visible at x100 magnification while BTV-1 S8.M generated ~88 VIBs (Figure 4.11). Not only was the

mean size of VIBs much smaller for BTV-1 S8.M (1.05 μm^2) compared to BTV-1 (1.38 μm^2) (Figure 4.11 & Figure 4.12), but the maximum size of inclusion body of BTV-1 S8.M (7.48 μm^2) was also smaller than WT (19.66 μm^2) (Figure 4.12). The minimum VIB size between BTV-1 S8.M was comparable to WT BTV-1, at 0.13 μm^2 and 0.12 μm^2, respectively.

The 95% confidence intervals showed that the difference in minimum VIB size was not significant. Whereas, all the other data generated showed that the mutant VIBs differed significantly for WT.

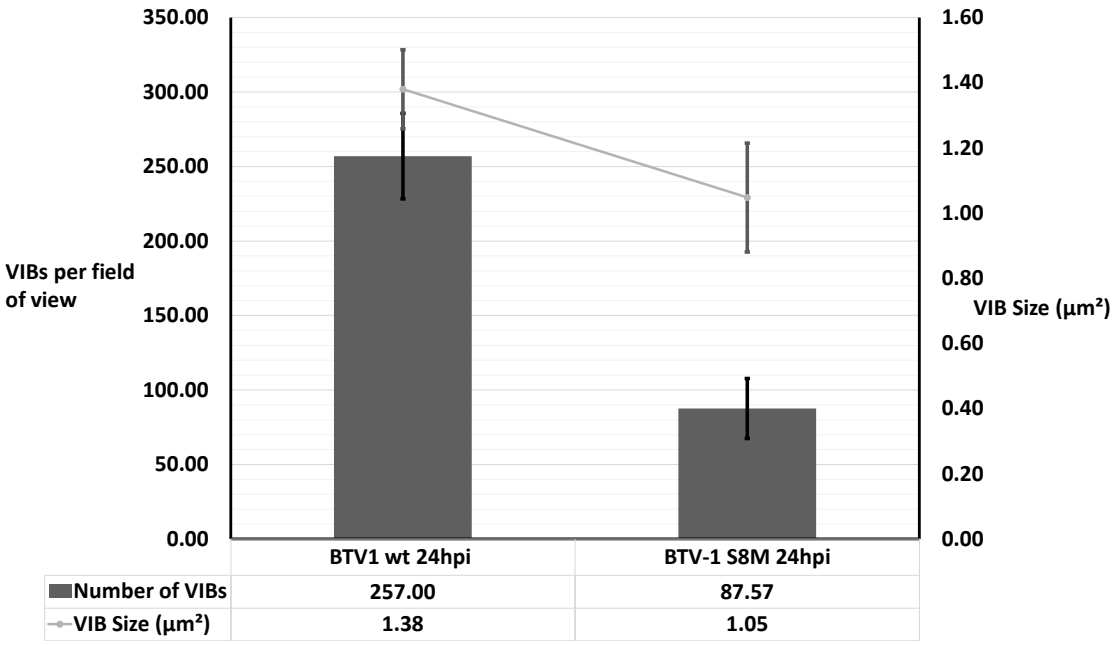

Figure 4.11. Average number and size of VIBs produced by both WT BTV-1 and BTV-1 S8.M during BSR cell infection.
Data were quantified using Volocity from confocal images of BSR cells infected with MOI 10 of virus and fixed at 24 hpi. Data shown are the mean of ten standard fields of view at x100 magnification. (95% C.I).

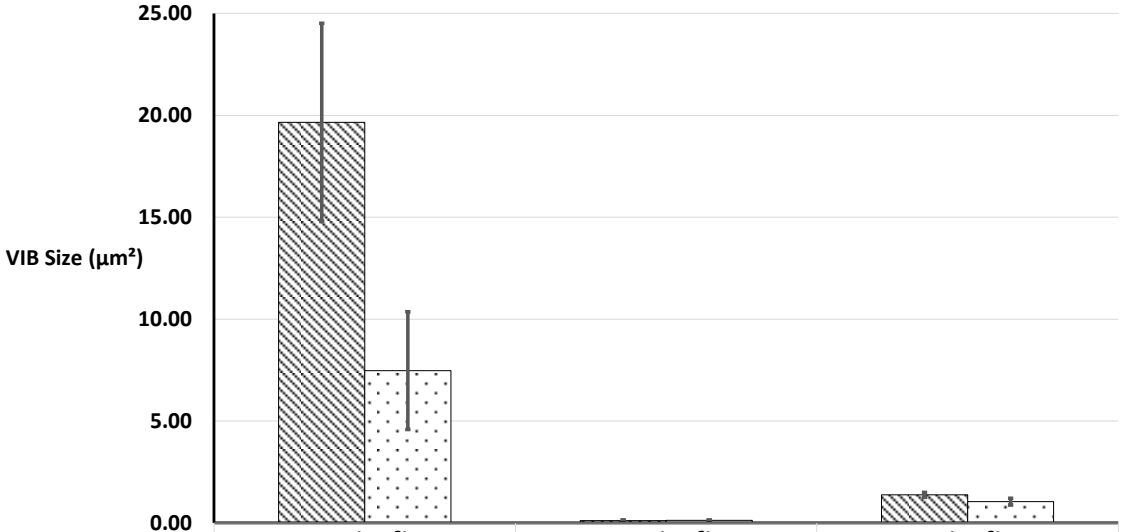

	VIB Size (µm²) max	VIB Size (µm²) min	VIB Size (µm²) mean
BTV1 wt 24hpi	19.66	0.12	1.38
BTV-1 S8M 24hpi	7.48	0.13	1.05

Figure 4.12. Graph of average maximum, minimum and mean size of VIBs produced by both WT BTV-1 and BTV-1 S8.M during BSR cell infection.
Data were quantified using Volocity as in Figure 4.11.

4.4 *In vitro* characterisation of recombinantly expressed NS2.M

The *in vivo* data established that the S8.M mutation had a significant effect on VIB formation and virus growth in BSR cells. In order to confirm this was because of a functional deficiency, due to the mutations in the RNA binding domain, rather than a harmful change in the overall protein structure; a recombinant baculovirus expressing the mutant protein was generated.

4.4.1 Construction and confirmation of transfer vector pAcYM1-H/GST NS2.M

The baculovirus expression system and transfer plasmid which was used to generate NS2.N, was used for the generation of NS2.M.

Using In-Fusion cloning, specific primers (In-Fusion F Primer and In-Fusion R) were used to generate 5' and 3' complementary regions to the pAcYM1-H/GST plasmid, on the S8.M insert. The In-Fusion enzyme generated single stranded over-hangs in the 15 bp homologous regions created by the PCR primers and allowed insertion into the linearized pAcYM1-H/GST vector. PAcYM1-H/GST NS2.M was then transformed into chemically competent Stellar *E. coli* and grown on LB plates containing ampicillin.

Initial selection of Stellar cells containing the pAcYM1-H/GST NS2.M plasmid was by ampicillin resistance conferred by the plasmid. Further screening was performed by colony PCR using forward primer BTV-1 S8 T7 *Bam*HI F and reverse primer BTV-1 S8 *Bsm*BI/*Bam*HI/*Rsr*II R to indicate which colonies contained the S8 insert. Positive amplification, shown by one band at the expected size of 1,100 bp, was detected by gel electrophoresis. All of the ten colonies selected contained Segment 8 (Figure 4.13).

PAcYM1-H/GST NS2.M colony 1 (Figure 4.13, Lane 2) construct was confirmed through sequencing. The full-length sequencing results were compiled by Chromas software and were BlastN confirmed as BTV-1 S8.M full length coding region. Alignment with PubMed published data revealed no deletions, insertions, or frame shifts which would affect protein production (Data not shown).

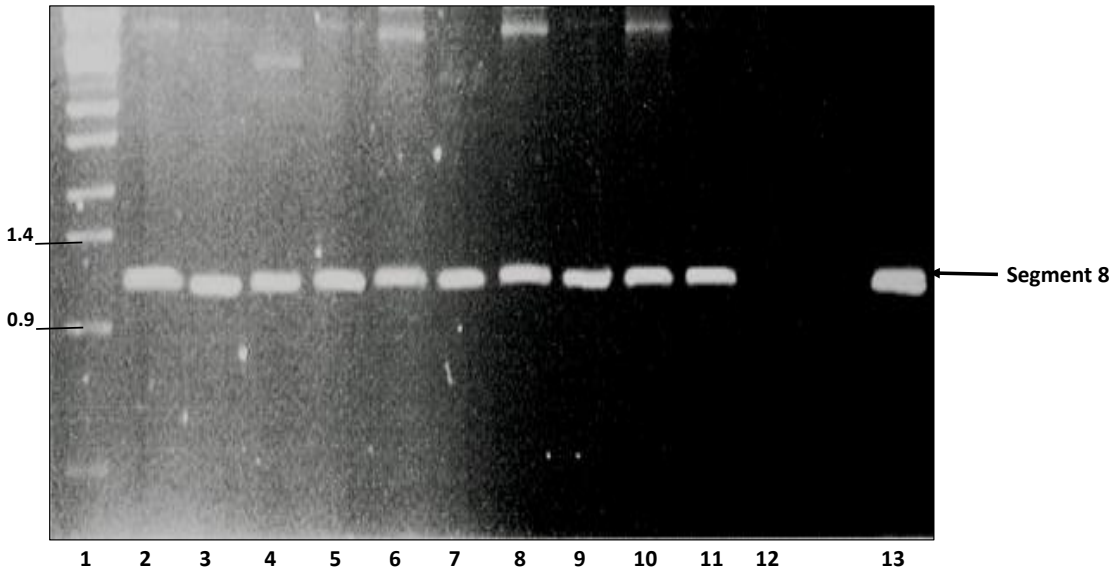

Figure 4.13. Colony PCR for selection of colonies containing pAcYM1-H/GST NS2.M. Stellar *E. coli (*HST08 strain) colonies containing pAcYM1-H/GST NS2.M were identified by the amplification of S8 and detected on a 1% agarose gel containing ethidium bromide. Lane 1, *StyI* digested λ DNA ladder. Lanes 2-11, colony PCR product from Stellar *E. coli* colonies. Lane 12, H_2O control. Lane 13, positive PCR control of pUC19 T7 S8. Arrow indicates segment 8 at approximately 1.1 Kb. Size markers shown in Kb.

4.4.2 Generation of recombinant virus expressing NS2.M

To promote homologous recombination, non-infectious bacmid KO:1629 DNA was digested with *Bsu*36I to linearize the genome. The pAcYM1-H/GST NS2.M 1, identified above, was successfully transfected with the linearized bacmid using X-treamgene 9 to produce AcMNPV YM1-H/GST NS2.M recombinant virus. A positive transfection control was performed in parallel to visually indicate successful transfection. AcMNPV KO:1629 baculovirus transfected with pRN43-GFP was identified by fluorescent microscopy, and successful recombination was recognised by the production of green

florescent protein within cells (Figure 3.14. A & B). No background florescence was detected (Figure 3.14 C & D).

4.4.3 Expression and purification of NS2.M

Successful recombination of AcMNPV RN43-GFP strongly implied that an AcMNPV YM1-H/GST NS2.M recombinant virus had also been generated; this was supported by visible CPE in infected *Sf*9 cells compared to uninfected cells. Harvested AcMNPV YM1-H/GST NS2.M potentially contained a mixed population of recombinant virus. Plaque assays were performed to select clonal viruses and to validate expression of NS2.M. Three putative recombinant plaques were picked and underwent three rounds of virus amplification to increase virus titre and form stocks.

Expression of BTV-1 NS2.M was analysed from low passage viruses. Cells infected with the three putative recombinant viruses were harvested 72 hours post infection and the proteins present were separated according to size by SDS-PAGE. The gel was stained using Coomassie Brilliant blue to visualise the protein (Figure 4.14. A). Expression of His/GST tagged NS2.M would result in a band at 65 kDa, which WAS present in all three of the viruses analysed (Figure 4.14, A. Lanes 3 -5) and positive control (Figure 4.14. A, Lane 2). AcMNPV YM1-H/GST NS2.M virus 1 was chosen for future work (Figure 4.14. A, lane 3) and was subsequently referred to as AcMNPV YM1-H/GST NS2.M.

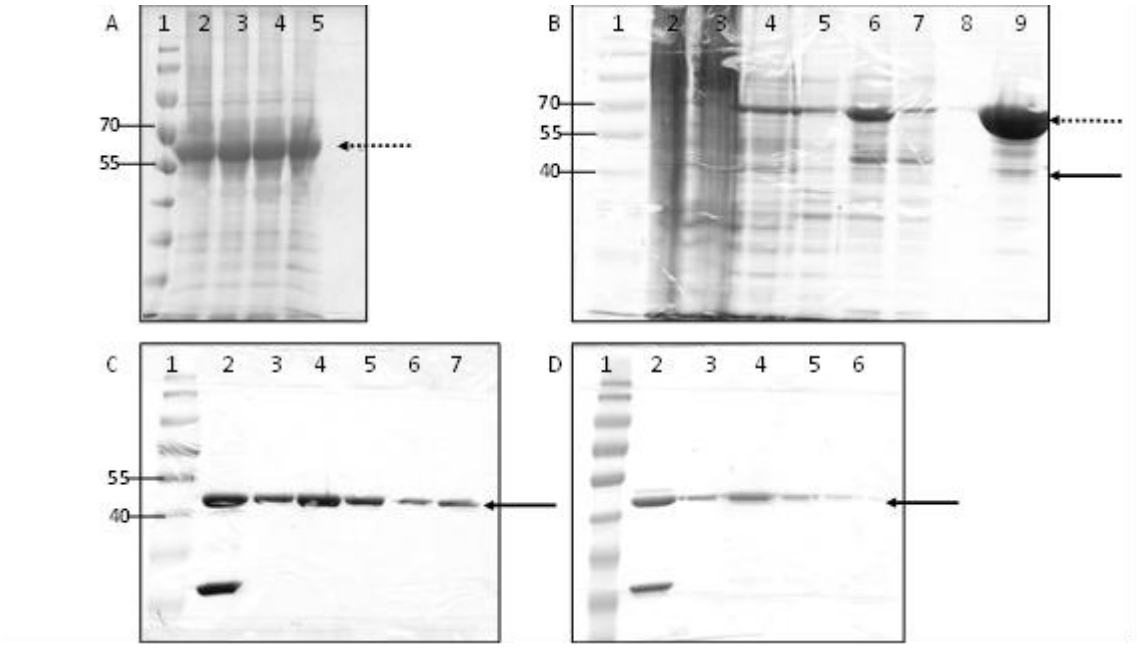

Figure 4.14. Expression and purification of NS2.M.
A, Cell lysates of *Sf9* cells infected with AcMNPV YM1-H/GST NS2.M clones. Proteins separated on a 10% SDS-PAGE and detected with Coomassie Blue. Lane 1, protein ladder. Lanes 2, AcMNPV YM1-H/GST NS2 positive control. Lanes 3 -5, AcMNPV YM1-H/GST NS2.M clones 1-3, respectively. **B,** Purification of NS2.M using Ni and GST beads. Samples taken at points during purification were analysed by 10% SDS-PAGE and detected with Coomassie Blue. Lane 1, protein ladder. Lane 2, whole cell lysate of *Sf9* cells infected with AcMNPV YM1-H/GST NS2.M. Lane 3, supernatant after dounce homogenisation. Lane 4, unbound protein supernatant from Ni bead binding. Lane 5, unbound protein following two washes of NS2-20 buffer. Lane 6, Protein eluted from Ni beads. Lane 7, unbound protein supernatant from GST bead binding. Lane 8, unbound protein following two washes of NS2-10 buffer. Lane 9, Protein eluted from GST beads. **C,** Purification NS2.M after overnight AcTEV protease cleavage. Lane 1, protein ladder. Lane 2, protein after overnight AcTEV protease cleavage. Lane 3 – 7, 1 ml elutions of cleaved NS2.M. **D,** Purification of WT NS2 after overnight AcTEV protease cleavage. Lane 1, protein ladder. Lane 2, protein after overnight AcTEV protease cleavage. Lane 3 – 7, 1 ml elutions of cleaved WT NS2. Bands at 42 kDa (solid black arrow) were identified as NS2. Bands at ~65 kDa (dotted black arrow) were identified as H/GST tagged NS2. Size marker shown in kDa.

Purification of NS2.M using Ni and GST beads was performed. *Sf*9 cells were infected with AcMNPV YM1-H/GST NS2.M and harvested at 72 hpi (Figure 4.14. B, Lane 2), dounce homogenised (Figure 4.14. B, Lane 3) and RNaseA treated overnight. The RNA

free protein was bound to Ni-NTA agarose beads for 2 hours and the unbound protein supernatant discarded (Figure 4.14. B, Lane 4) before the sample was washed twice in 20 bead volumes NS2 -20 buffer (Figure 4.14. B, Lane 5). NS2 was eluted from the Ni beads with 15 volumes of NS2 -350 buffer (Figure 4.14. B, Lane 6). This was bound for 1 hour to GST beads and the unbound protein supernatant discarded (Figure 4.14. B, Lane 7). The beads were washed in 20 bead volumes of NS2 -10 buffer (Figure 4.14. B, Lane 8). The GST elution buffer was added to the NS2-GST beads and the NS2 eluate retained (Figure 4.14. B, Lane 9). AcTEV protease was added and incubated overnight at 4 °C to cleave the purification tags (Figure 4.14. C, Lane 2). The sample was added to Ni-NTA beads and washed with NS2 buffer. The purified NS2 eluate was collected while the cleaved tags remained bound to the beads (Figure 4.14. C, Lanes 3–7). Samples of each purification step were analysed by 10% SDS-PAGE and detected by Coomassie blue (Figure 4.14. B & C). The gel profiles exhibited the presence of highly purified (>3 µg/µl) NS2.M since a single protein band at 46 kDa was detected.

Recombinant baculovirus AcMNPV YM1-H/GST NS2 was previously generated within the lab and was used as a control. *Sf*9 cells were infected with recombinant baculovirus expressing NS2 protein, purified and followed by detection by SDS-PAGE as for NS2.M (Figure 4.14. D), which demonstrated WT NS2 was highly purified. Both purified NS2 and NS2.M were further verified by western immuno blot using specific anti-BTV-10 NS2 antibody (results not shown).

4.4.4 ssRNA binding activity of NS2.M mutant protein

WT NS2 and NS2.M were produced and purified for use in assays to generate *in vitro* data to support the *in vivo* findings of the effects the mutations have on the NS2 proteins ssRNA binding ability. Electrophoretic mobility shift assays (EMSAs) have been extensively used with NS2 to show not only the ability of NS2 to bind ssRNA [160], but also BTV ssRNA specificity [161].

The EMSAs were used to detect specific BTV ssRNA binding of WT NS2 and compare it with NS2.M. Radiolabeled BTV segment 7 was used to demonstrate the difference in ssRNA migration. Transcripts (ssRNA) were generated with 50 µCi α^{32}P CTP, purified and added to the EMSA buffer. Purified WT NS2 and NS2.M were diluted to specific concentrations in DEPC H_2O, mixed with the RNA and allowed to bind for 30 minutes. The positive and the negative controls replaced the NS2 and ssRNA, respectively, with H_2O. NS2-RNA samples were loaded on an agarose gel and electrophoresed, resulting in separation of the large NS2-RNA complexes from the smaller free RNA. Gels were then dried and analysed. A successful shift and thus RNA-NS2 binding was visually identified by a band visible at a higher position than the RNA only control (Figure 4.15. A & B. Lane 1 Solid arrow).

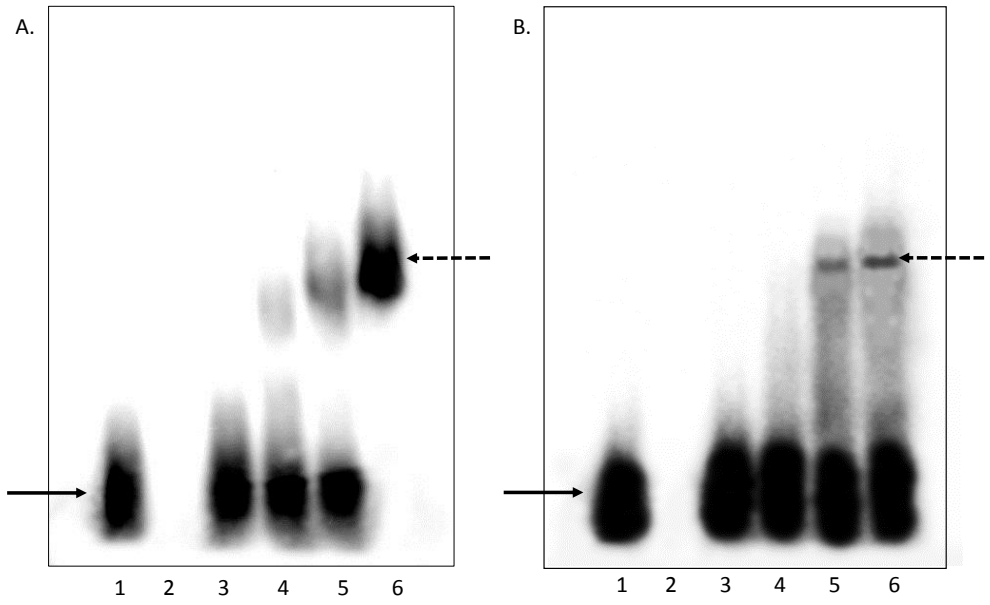

Figure 4.15. EMSA of WT NS2 and NS2.M.
Radiolabeled T7-derived ssRNA BTV segment 7 was bound to NS2 or NS2.M and run on a 1% agarose gel. This was dried and identified by autoradiography on a Typhoon Variable Mode Imager. **A,** EMSA of RNA and WT NS2. Lane 1, RNA only control. Lane 2, NS2 only control. Lanes 3-6, RNA and 1, 5, 10 and 15 µg NS2, respectively. **B,** EMSA of RNA and NS2.M. Lane 1, RNA only control. Lane 2, NS2.M only control. Lanes 3-6, RNA and 1, 5, 10 and 15 µg NS2.M, respectively. Solid black arrows indicate unbound RNA. Dashed black arrows signify RNA-NS2 complexes.

The images (Figure 4.15) were quantified using ImageJ software. Lanes on the image were marked and the total lane signal used to indicate 100% RNA signal. The distribution of signal within these lanes as either bound or unbound RNA was identified by plotting the area of each signal peak (Figure 4.16) and demonstrated as a percentage of the total RNA signal.

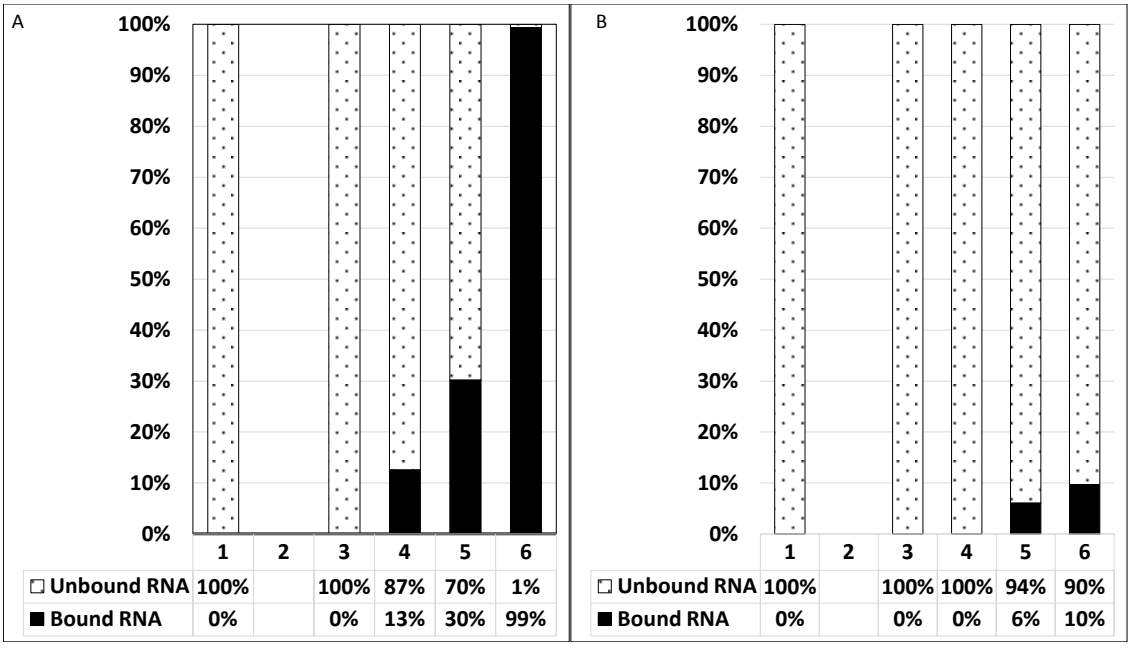

Figure 4.16. Quantification of WT NS2 and NS2.M EMSA.
EMSA images were quantified using ImageJ software. Lanes on the image were quantified and the total lane signal used to indicate 100% RNA signal. The distribution of signal as bound or unbound to NS2 was identified by plotting the pixels. **A,** EMSA of WT NS2 and ssRNA. Lane 1, RNA only control. Lane 2, NS2 only control. Lanes 3-6, RNA and 1, 5, 10 and 15 µg NS2, respectively. **B,** EMSA of NS2.M and ssRNA. Lane 1, RNA only control. Lane 2, NS2.M only control. Lanes 3-6, RNA and 1, 5, 10 and 15 µg NS2.M, respectively

The EMSA of RNA and NS2.M (Figure 4.15 & 4.16. B) demonstrated no shifting with 1 µg of NS2.M (Lane 3) which is identical to the EMSA of RNA and 1 µg of WT NS2 (Figure 4.15 & 4.16. A, Lane 3), this analysis was supported by the quantification of the gels, with 100% of the signal as unbound RNA.

WT NS2 (Figure 4.15 & 4.16. A) demonstrated a protein concentration dependent increase in BTV specific ssRNA binding up to 15 µg (Lane 6) which resulted in a complete shift of ssRNA to the bound position. The NS2.M mutant (Figure 4.15 & 4.16. B) also demonstrated a protein dependent increase in BTV specific ssRNA binding,

however, this binding ability was greatly reduced. Unlike 15 µg WT NS2, 15 µg NS2.M did not have the binding ability to completely bind of all the RNA; instead it bound 10% of the RNA (Lane 6).

4.4.5 NS2.M oligomerisation in the presence and absence of RNA

NS2.M has shown a greatly reduced ability to bind RNA, which was hypothesised to have an effect on structure because the binding of RNA has been shown to necessary for the formation of larger oligomeric forms [151]. Whether the diminished RNA binding ability of NS2.M perturbs oligomerisation of the protein was investigated by examining the sedimentation of the structures formed in the presence and absence of RNA.

Previously, NS2 purified from mammalian cells infected with BTV was reported to form 22S complexes in the presence of RNA [160]. Baculovirus expressed NS2 was later found to form multimers of ~7S when RNA was removed by RNase treatment. Later work [154] demonstrated that bacterially expressed NS2 formed complexes which sedimented to 18-22S, which was at least a 650kDa multimer; relating to ~15+ subunits of 42kDa NS2. Removal of the associated RNA resulted in NS2 that sedimented to 8-10S, indicating that the purified NS2 was bound to bacterial RNA. An 8-10S multimer has a mass of ~140-250 kDa, which relates to 6 (+/- 2) subunits of 42kDa NS2 [154].

Sucrose gradients (5-20%) were generated and 50 µg of diluted NS2 added to the top of the gradient. The samples were sedimented through ultracentrifugation and 1 ml fractions taken, which were then separated by 10% SDS-PAGE. Initially, Coomassie staining on the SDS-PAGE gels was attempted to identify the bands but this was not

sensitive enough to detect the diluted NS2. The complexes were thus detected by western immuno blot using NS2 specific antibodies (1:3000).

This experiment was performed with both WT NS2 (Figure 3.21) and NS2.M (Figure 4.17). During the purification process of NS2, RNase A was added so in order to analyse the largest multimeric forms of NS2 seen in other work, 1µg BTV-1 S10 RNA was added the NS2 before sedimentation.

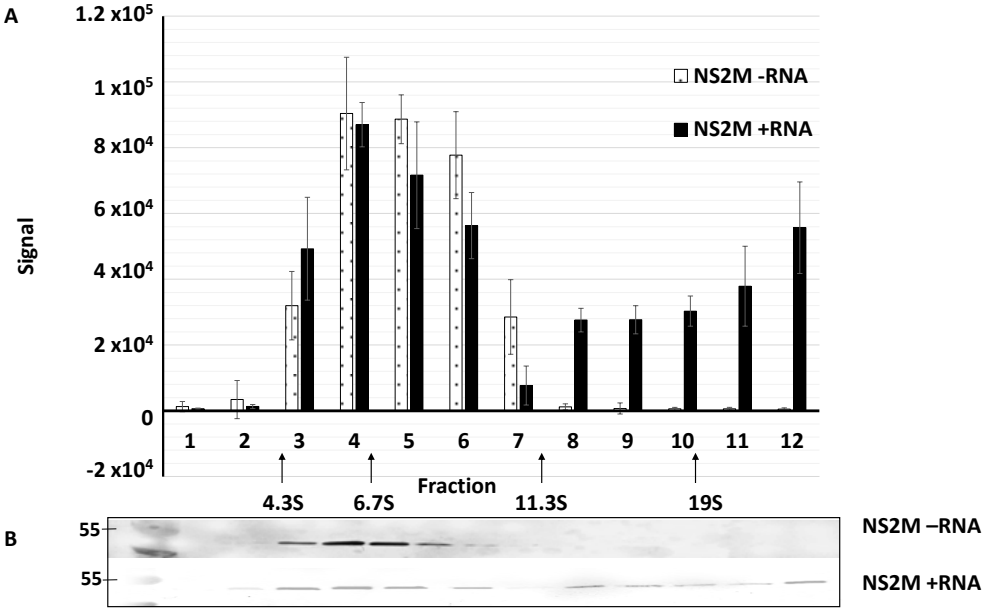

Figure 4.17. Oligomerisation assay of NS2.M in the presence and absence of RNA. The twelve fractions from the oligomerisation assay were separated on 10% SDS-PAGE and transferred to a nitrocellulose membrane for visualisation using western immuno blot and guinea pig anti-NS2 antibody (1:3000). These membranes were analysed with LI-COR Image Studio Lite and the red, green and blue signals for each fraction used to form an average signal. **A,** a graph showing NS2.M present in each gradient fraction, with and without the addition of RNA. (95% confidence intervals shown. **B,** western immuno blot images used for analysis. NS2 Bands identified at 42 kDa.

NS2.M primarily formed 6S to 10S complexes (Figure 4.17. F4 – F6) in the absence of RNA, which equates to 4 to 6 copies of 42 kDa NS2 forming the most stable multimer

of NS2. This was similar to WT NS2 which formed predominantly 7S complexes (Figure 3.21) in the absence of RNA, with the second largest band at 8S. This relates to 4 to 5 copies of 42 kDa forming the most stable multimer of NS2

The addition of RNA formed a wide range of NS2.M complexes detected in fractions 3 to 12, which contained 6-22S complexes (Figure 4.17). The largest proportion of NS2.M complexes were observed between fractions 3 and 6 (6–10S), similar to the structure size seen without RNA. Some larger complexes were also generated with the addition of RNA but these were at a much lower intensity than the smaller structures. This was very dissimilar to WT NS2, which, with the addition of RNA, was mostly found in fractions 9 to 12, containing 18-22S complexes (Figure 3.21), with the strongest signal from fraction 11 indicating predominantly 20–22S complexes. This indicated that NS2.M was able to bind a proportion of the RNA which was lower than WT, data which mirrors the EMSA. It was also shown that the binding of RNA was needed for the formation of the large NS2 homomultimers.

4.5 Discussion

The experiments in this chapter were undertaken to investigate the NS2 ssRNA binding domain between residues 153-166 [158]. This is the first *in vivo* investigation of BTV NS2 ssRNA binding sites by direct mutagenesis in replicating viral genes. The specific mutations were designed to disrupt RNA binding of the middle binding domain. A study of the NS2 mutant *in vitro* was also performed to confirm that the middle domain mutations had not greatly affected the overall structure of the protein and to analyse the precise effect the mutation had on RNA binding. The *in vitro* characterisation complemented and supported the findings of the *in vivo* study. Current NS2 structural data does not include the full-length structure of NS2 and lacks the first 7 amino acids and the 160-178 aa region which contains the middle binding domain. The full-length structure assumes that the N-terminal and C-terminal structures are not altered when expressed together. If the structure is correct then the 3 putative RNA binding domains are similar to rotavirus NSP2 [159] and located in a groove between the N and C-terminals.

A mutant virus with alanine substitutions in the putative middle RNA binding domain (BTV-1 S8.M) was previously generated by the Roy lab using the reverse genetics system. In this chapter the BTV-1 S8.M mutant was confirmed to contain the designed mutations and characterised to explore the effects of the mutations. Initial plaque assays of BTV-1 S8.M demonstrated a distinct mutant plaque phenotype in BSR cells, which was smaller than those generated by WT BTV-1 when both infections were fixed and detected at 72 hpi. However, when BTV-1 S8.M was grown in the complementary

cell line BSR-S8, the mutant plaque phenotype reverted to a WT BTV-1 plaque phenotype. It strongly suggested that the mutation in the NS2 protein has caused the growth deficiency because plaque formation is returned to a WT-like phenotype when a functional version of the NS2 protein is supplied *in trans* with the complementary cell line.

The growth kinetics of the mutant virus were further investigated in parallel with the WT virus. The growth curves showed that BTV-1 S8.M titre in BSR cells initially decreased before increasing to a maximum tire of 3.3 x 10^6 at 36 hpi which could be due to an extended eclipse period. A 95% CI was used to indicate that this continued difference was statistically significant [235,236]; each time point exhibited a <25% overlap in CI. It has previously been published that the titre of WT BTV infection of BSR cells decreases at 2 hpi compared to initial infection [73]. 2 hpi was not analysed in this study but it could be presumed that the decrease in BTV-1 S8.M titre was an extension of the initial decrease demonstrated by WT BTV. This delay in virus growth affected the overall growth of BTV-1 S8.M with the maximum titre demonstrating a 0.9 log difference compared the WT BTV BSR cell control (36 hpi, 2 x10^7) or WT BTV BSR-S8 cell control (36 hpi 2.5 x10^7). The reduction in BTV-1 S8.M maximum titre may be due to external factors. BSR cells were infected at almost 100% confluence so at 48 hours post infection the cells will be overgrown, not replicating as efficiently and so potentially limiting the replication of BTV-1 S8.M.

As indicated by the plaque phenotype, BTV-1 S8.M growth in BSR-S8 cells was returned to statistically similar levels (>25% overlap of 95% CI) as WT BTV, although still not

exhibiting as high a maximum titre. This was due to the presence of functional NS2 supplied by the complementary cell line. The only data point which was statistically significant (<25% overlap in 95% CI) was 8 hpi, which exhibited a 0.6-1 log difference compared to WT. The data suggested that the mutation had generated a highly attenuated virus.

To further characterise BTV-1 S8.M *in vivo*, protein samples were taken in parallel to the growth curve. No significant protein production deficiencies were detected in comparison to the lysate from wild-type infected cells, similar to that which was reported previously [73]. Differences in protein production were detected between time points, a reflection of the delayed growth of the virus which was observed in the growth curve. The western blot analysis showed that BTV-1 S8.M was recognised by a specific anti-BTV-10 NS2 antibody and was indistinguishable in size and antigenicity to wild-type BTV. NS2 protein was detected higher than the 42kDa published because it is phosphorylated and forms multimers; both of which are factors which can contribute to the actual band size differing from that predicted [154,162].

Remarkably, after the initial reduction in growth rate and resulting loss of virus titre, the highest increase in rate of growth was shown by BTV-1 S8.M in BSR cells at 16 hpi with a 2.5 log increase in titre; compared to a 2 log increase of BTV-1 S8.M in BSR-S8 cells, a 1.7 log increase of WT BTV in BSR-S8 cells and a 1.5 log increase of WT BTV in BSR cells. This implied that the mutation in BTV-1 S8.M did not adversely affect the rate of growth but instead, given NS2s role in the concentration of viral components during assembly [153], retarded the assembly of progeny virus. Over time the mutation is

overcome which then allows assembly at the high rates shown due to the accumulation of component parts.

VIBs, primarily composed of NS2, are a characteristic signs of BTV infection and the sites of immature progeny virus assembly. As the S8.M mutation had been shown to delay virus growth and reduce the overall titre, an immuno fluorescence assay was undertaken to visualise and analyse the VIBs produced during infection and show if the mutant BTV-1 S8.M formed different VIBs compared to WT. BTV-1 formed VIBs comparable to those previously published [150]. BTV VIBs are often described as having a perinuclear location late in infection[133,148,152], similar to rotavirus viroplasms [240,241] and reovirus inclusion bodies [242,243]. The data presented here however displayed WT and BTV-1 S8.M VIBs throughout the cytoplasm. This is mostly clearly demonstrated in Figure 4.10. C, where the split channels show VIBs dispersed all through the cytoplasm. BTV-1 S8.M formed VIBs which seemed smaller than WT VIBs and fewer in number despite an MIO 10 being used for infection of both viruses.

These initial findings were generated by a visual inspection of the images, which resulted in formal image quantification. WT BTV-1 infection of BSR cells at MOI 10 produced an average of 257 VIBs per frame with an average size of 1.38 μm^2. Under the same conditions BTV-1 S8.M produced an average of 88 VIBs per frame with an average size of 1.05 μm^2. Both the 95% CI and a T-test generated P-value showed that this was a statistically significant ($p<0.05$) ~66 % reduction in total number of VIBs and a ~25 % reduction in average VIB size. Previous characterisation of BTV VIBs [148] showed that the average size of VIB was 1.1 μm^2 at 24 hpi, which was closer to the mutant BTV-

1 S8.M VIBs than WT. Both investigations used the same MOI but Brookes *et al* 1993 infected SVP cells derived from porcine stable (PS) cells [244], while this analysis used BSR cells. Also, this analysis measured 1542 BTV-1 VIBs and 272 BTV-1 S8.M VIBs, while Brookes *et al* 1993 only measured on 48 structures.

The minimum average size for both WT BTV-1 and BTV-1 S8.M VIB was very similar at 0.12 μm^2 and 0.13 μm^2, respectively. The difference was shown not to be statistically significant ($p>0.05$) by the overlapping 95% confidence intervals and a P-value of 0.46. This might represent the minimal structure detectable or the minimal structure of a VIB. The average maximum size of VIB varied greatly within the same virus infection type, as shown by the large upper and lower confidence levels, and between WT BTV-1 and mutant, with the BTV-1 S8.M average VIB size of 7.48 μm^2 and BTV-1 average VIB size of 19.66 μm^2. This was shown by 95% CI and P-value to be statistically significant difference ($p<0.05$).

VIBs are similar to viroplasms, in so far as the size, location and number is dynamic [148,240]. The work described here was a characterisation of VIB size and number at a specific time post infection and as such was unable to clarify if the differences in WT and BTV-1 S8.M VIBs were just a delay or a true depiction of phenotype throughout infection. If this was a true depiction of phenotype it would suggest that RNA binding is important for VIB formation because the impaired RNA binding of the mutant resulted in VIBs which were smaller and fewer in number than those of WT.

All the *in vivo* characterisation of BTV-1 S8.M showed that the designed mutations effected virus growth and VIB formation. The growth was retarded early in infection

and displayed a lower maximum virus titre, but the mutation did not adversely affect the rate of virus replication or virus protein synthesis. This delay in virus assembly but not production of component parts could be due to the differences seen in the VIBs, which are the sites of virus assembly. Due to this, fewer and smaller VIBs could be a limiting factor early in replication or directly related to impairment in RNA binding. Like thiazolide drugs were shown to do with rotavirus viroplasms [245].

The *in vivo* data clearly showed that the mutations affected virus replication and VIB formation but did not conclusively demonstrate that this was because the mutations in the middle RNA binding region were affecting NS2s ability to bind RNA. It could be due to the mutations causing the structure or oligomerisation of NS2 to change so significantly that it was unable to bind RNA. NS2 oligomerisation is thought to require RNA to act either an initiator or as a supporting scaffold for the larger oligomeric form, and as such was of interest. This was investigated *in vitro* with the generation of a recombinant baculovirus expressing NS2 with the same mutations as BTV-1 S8.M.

The transfer plasmid pAcYM1-H/GST NS2.M was generated by an In-Fusion cloning method which was quicker than using a traditional ligase enzyme, not limited to insertion into restriction sites and was 100% successful with all 10 colonies investigated containing pAcYM1-H/GST NS2.M. Recombinant expressed protein was successfully purified with Ni and GST beads to produce highly pure NS2.M. It was necessary to remove the purification tags so that they would not interfere with future assays. The AcTEV protease was added and incubated overnight at 4 °C to cleave the purification tags between the glutamine and glycine of the protease recognition

sequence (EDLYFQG). The C-terminal domain of NS2 has previously been shown to degrade rapidly at 4 °C and form aggregates [159]. Samples of NS2.M were purified in the presence of protease inhibitor cocktail V and no degradation was detected. Even at highly purified >3µg/µl quantities, WT NS2 and NS2.M did not form aggregates. The purified NS2.M was soluble, which was an indication that the inserted mutations had not altered the overall protein structure and so differences between could be attributed to a functional impairment rather than structural one.

EMSA was used to investigate BTV specific ssRNA binding. WT NS2 demonstrated a protein concentration dependent increase in BTV specific ssRNA binding up to 15 µg which was sufficient to completely shift of ssRNA to the bound position. The NS2.M mutant also demonstrated a protein dependent increase in BTV specific ssRNA binding. This binding ability was greatly reduced compared to WT with 15 µg NS2.M able to shift 10% of the RNA, whilst WT binds 99%. This data indicated that the inserted mutations in the middle RNA binding domain of NS2 resulted in a significant impairment in BTV specific ssRNA binding activity.

The oligomerisation of NS2.M and WT NS2 in the presence and absence of RNA was examined by sedimentation analysis in order to investigate if oligomerisation of NS2 was triggered by the binding of RNA [151]. NS2.M was predominantly detected in fraction 5 which equates to ~8S complexes, but also present in large amounts in fractions 4-10 (7-10S) which relates to 6 (+/-2) copies of NS2. This was similar to the NS2 complexes formed in this investigation by WT NS2 and previously published work on BTV NS2 [154,167]. It is also similar to the NS2 proteins of African horsesickness virus (AHSV) and

epizoonotic haemorrhagic disease virus (EHDV) NS2 [167]. The addition of RNA was shown to form a wide range of NS2.M complexes. These were detected in fractions 3–12 (6–22S). The quantification of the gels showed that these complexes fall into two groups: the largest group of complexes fall within 6–10S, typical of unbound NS2; and a second, smaller group of complexes in the 18–22S range, which was similar to the complexes formed when WT NS2 was bound to RNA and of published work [154].

The reduction in the ability of NS2.M to bind RNA seen in the EMSAs above, is illustrated here by the formation of a few 18–22S complexes and resulted in the remaining NS2.M retaining the smaller, unbound oligomeric 7–10S form of 6 (+/-2) copies of NS2. The separation of NS2 complexes into two different oligomeric forms has previously been caused by the limiting of RNA from which the NS2 can bind to [160]. This suggested that the binding of RNA was a limiting factor of the formation of the larger oligomeric complexes. The work undertaken did not elucidate if the oligomerisation of NS2 was triggered by the binding of RNA. It did demonstrate however, that the addition of RNA resulted in larger NS2 complexes. It was shown that the NS2.M mutant, which has impaired RNA binding ability, formed normal 7-10S complexes in the absence of RNA and far fewer of the 18-22S complexes in the presence of RNA, with the remaining NS2.M retaining 7–10S form.

The *in vitro* characterisation of NS2.M revealed that the mutations severely impaired RNA binding as it was designed to do. 15 µg NS2.M was able to bind 10 % of the RNA while 15 µg WT NS2 was sufficient to bind 99 % of the RNA resulting in a complete shift of all RNA to a bound position. NS2.M oligomerisation was similar to WT NS2 in the

absence of RNA but the mutations and the impaired binding of RNA resulted in the formation of few of the larger 18–22S complexes in the presence of RNA, with the greatest amount of NS2.M forming 7–10S complexes without RNA. When analysed with the *in vivo* characterisation of BTV-1 S8.M, which showed that the BTV-1 S8.M mutations delayed and reduced virus growth and VIB formation, it was clear that the middle RNA binding domain is important in BTV replication and that the binding of RNA in general is important in the efficient replication of the virus. Most importantly the delay in virus assembly and growth but with an increased rate of growth suggested that the RNA binding mutation in BTV-1 S8.M affected NS2s role in the concentration of viral components during assembly [153]. Later in infection, the component viral structural proteins and RNA have accumulated within the cell so when the mutation is overcome and assembly occurs, it does so at the increased rates shown for this mutant.

Chapter 5

In vivo and *in vitro* investigation into the C-terminal RNA binding domain of BTV NS2

5.1 Introduction

The N-terminal of NS2 (1–92 aa) was originally thought to be required for RNA binding, but not the C-terminal (227–357 aa) [231]. Current literature, however, suggests that in addition to the N and M domains, there is a third RNA binding region in the C-terminal between amino acids 274-286 [158] which is shown in Figure 5.1 (Dashed box). The 274-286 aa region contains 8 charged amino acids (E_{274}, K_{275}, K_{278}, K_{281}, K_{283}, D_{284}, R_{285} and E_{286}).

Recombinant WT BTV-17 NS2 and deletion mutant BTV-17 $NS2_{274-286}$ were expressed in *E. coli*, purified and used in non-BTV specific ssRNA EMSAs, which showed that $NS2_{274-286}$ was less able to bind ssRNA compared to WT NS2. Double deletion mutants to these RNA binding domains (BTV-17 $NS2_{2-11/153-166}$, BTV-17 $NS2_{2-11/274-286}$ and BTV-17 $NS2_{153-166/274-286}$) demonstrated that there may be interaction between domains [158].

Although previous work has identified an RNA binding domain at 274-286 aa [158], the relevance of this domain *in vivo* during virus replication was not investigated. All studies were performed *in vitro* using recombinant NS2 mutants. In this chapter the C-terminal 274-286 aa RNA binding domain of BTV NS2 was investigated *in vivo* with mutations specifically designed alter the charged residues identified as involved in the binding of RNA. Similar to the studies undertaken with the N and M domains, the RG system was used to recover mutant virus with specifically designed nucleotide changes. The mutations examined *in vivo* were also investigated *in vitro* through the recombinant baculovirus expression of NS2 containing the same mutations.

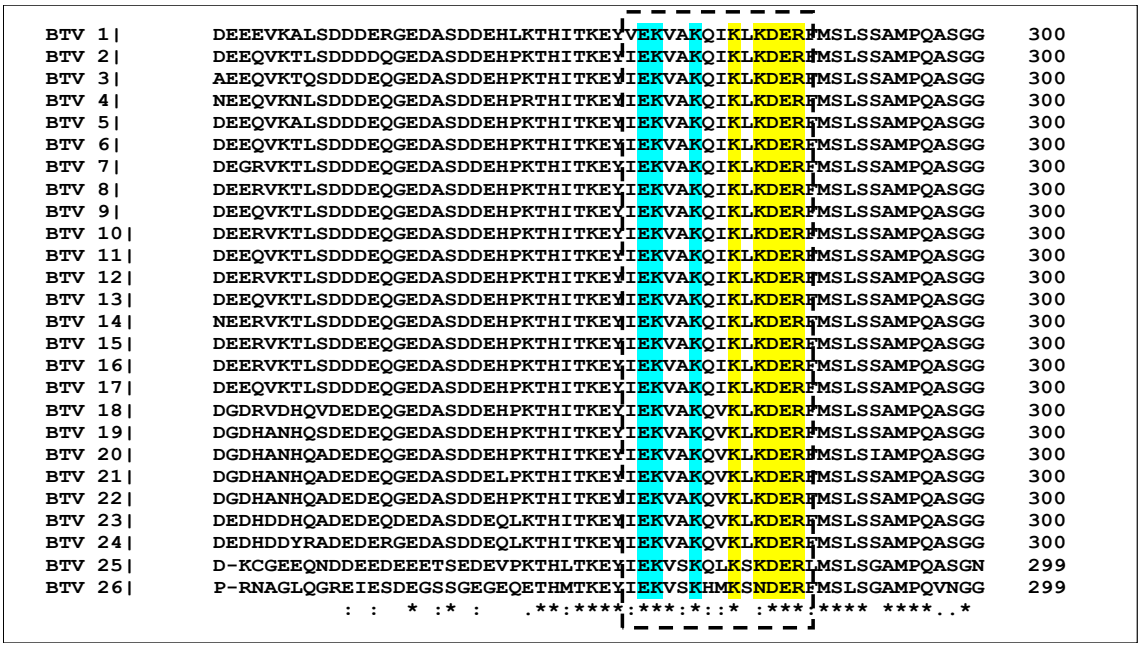

Figure 5.1. Clustal alignment of BTV 1- 26 NS2 amino acid sequences.
Sequences from each of the 26 serotypes were aligned using Clustal Omega (http://www.ebi.ac.uk/Tools/msa/clustalo). Dashed box indicates the putative C-terminal binding region 274aa – 286aa. Amino acids highlighted in yellow are the conserved, charged amino acids chosen for mutation to disrupt RNA binding. Amino acids highlighted in blue are charged amino acids not chosen for mutation. An asterisk indicates positions which have a fully conserved residue. A colon indicates conservation between groups of strongly similar properties. A full-stop indicates conservation between groups of weakly similar properties. Appendix 1 contains the full Alignment of NS2 amino acid sequences

5.2 Results

5.2.1 Design and construction of BTV-1 S8.C mutants

NS2 is highly conserved amongst all but BTV serotypes 25 and 26, as illustrated in Figure 5.1 which shows a partial alignment of NS2 sequences from all of the 26 serotypes of NS2. Amino acids E_{274} and K_{275} were omitted from the mutation design in favour of K_{281}, K_{283}, D_{284}, R_{285} and E_{286} because they are located near the BTV-1 variable amino acid V_{273}. K_{278} was also discounted due to its less clustered nature with the other charged amino acids. The most significant variation within the C-terminal RNA binding domain is the hydrophobic L_{282} which is exchanged for a polar hydrophilic serine in serotypes 25 and 26. This was considered acceptable because generally serotypes 25 and 26 vary more from the other serotypes. Arginine and lysine, which are present in this region, have been shown to be required for RNA binding [232,233]. It has also been reported that the DRYG region of eukaryotic initiation factor t eIF4 is rich in aspartic acid and arginine; acts as an intermediary between mRNA and eukaryotic initiation factor 4B and as such may have the ability to bind RNA [250]. Both aspartic acid and arginine are also found clustered in the C-terminal RNA binding domain.

Using the RG system for BTV, mutant viruses with substitutions in the C-terminal RNA binding domain (K_{281}, K_{283}, D_{284}, R_{285} and E_{286}) were generated. The substitution of alanine to replace the charged residues was expected to disrupt the interaction with the ssRNA and affect BTV replication whilst still retaining the overall protein structure.

As with the generation of the N-terminal and middle domain mutants, site directed mutagenesis was performed on pUC19 T7 S8 using forward mutation primer BTV-S8.C *Pvu*II F and reverse mutation primer BTV-S8.C *Pvu*II R. These primers contained the alanine substitutions and a silent *Pvu*II restriction site for further selection of positive mutants (Figure 5.3. A). DpnI was used to digest the parental plasmid DNA, before plasmid purification and transformation with DH5α chemically competent cells.

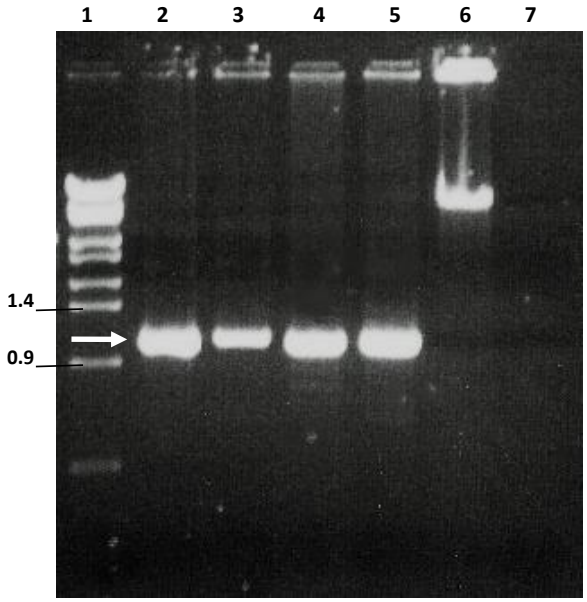

Figure 5.2. Colony PCR of pUC19 T7 S8.C DH5α.
Putative DH5α *E. coli* colonies containing pUC19 T7 S8.C were identified by the amplification of S8 and detected on a 1% agarose gel containing ethidium bromide. Lane 1, *Sty*I digested λ DNA ladder. Lanes 2-5, colony PCR product from DH5α *E. coli* colonies. Lane 6, pUC19 T7 S8 control. Lane 7, H_2O control. Solid white arrow indicates approximately 1.1Kb. Size marker shown in Kb

Although a silent *Pvu*II restriction site was part of the mutation, it was not used for screening due to time constraints. Positive colonies were selected by ampicillin resistance and colony PCR, using forward primer BTV-1 S8 T7 *Bam*HI F and reverse

primer BTV-1 S8 *Bsm*BI/*Bam*HI/*Rsr*II R. Positive amplification was shown by one band, identified by gel electrophoresis at the expected size of 1,100 bp. All of the four colonies selected contained Segment 8 (Figure 5.2. Lanes 2-5) therefore sequencing was performed to confirm the presence of the mutations. The four positive colonies were purified by Wizard PCR clean up and sent for sequencing (Figure 5.3.B). The results were compiled by Bio-edit software and BlastN confirmed as BTV S8. Alignments of pUC19 T7 S8.C with BTV-1 published data revealed the expected alanine substitutions at residues K_{281} A_{283} D_{284} R_{285} E_{286}, consistent with the designed mutations (Figure 5.3. C).

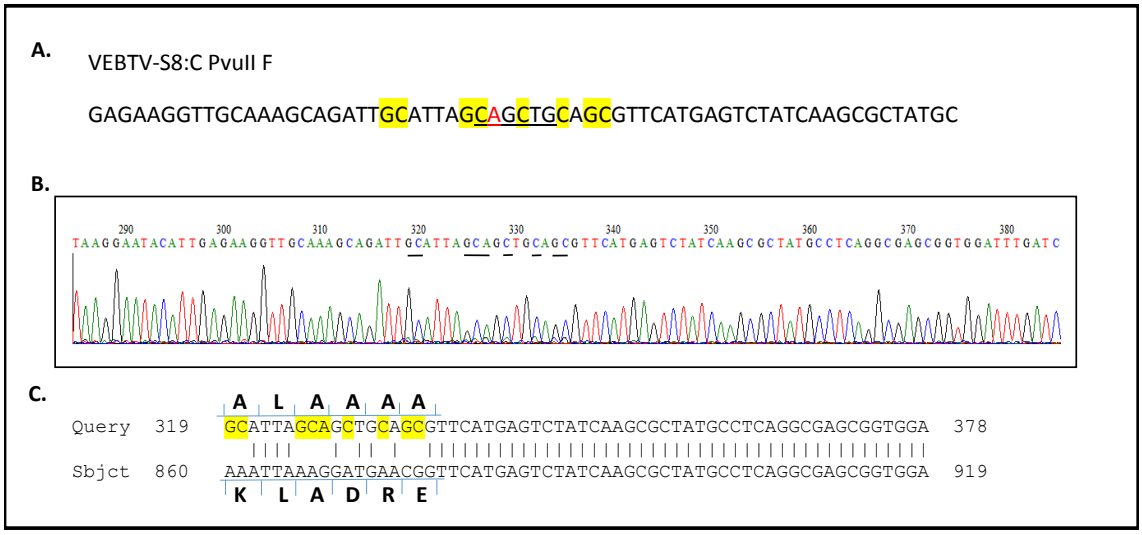

Figure 5.3. Confirmation of S8.C mutations in pUC19 T7 S8.
A, Sequence of the Forward mutation primer of BTV1 S8.C containing a silent *Pvu*II restriction site (underlined)**,** mutations highlighted in yellow **B,** Partial chromatogram sequence pUC19 T7 S8.C, sites of expected mutations underlined. **C,** Partial sequence of PubMed alignment pUC19 T7 S8.C and the published BTV-1 NS2 sequence. Sequence differences highlighted in yellow and the resulting amino acids indicated.

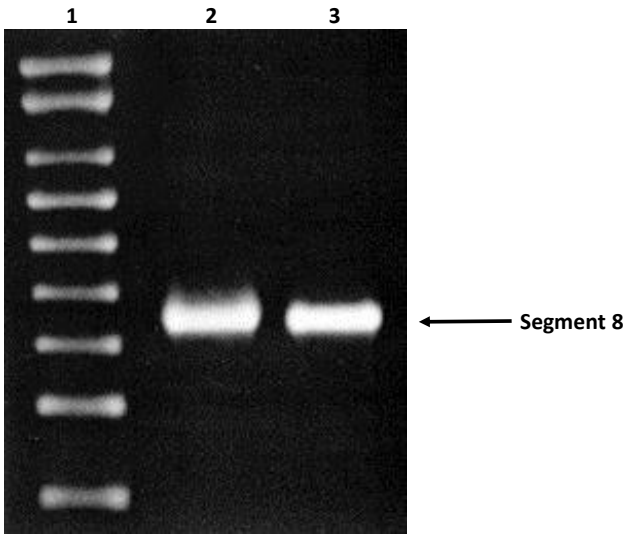

Figure 5.4. Segment 8 ssRNA transcripts.
SsRNA transcripts were generated and detected on denaturing agarose gels Lane 1, 1µl Promega RNA marker. Lane 2, ssRNA transcripts from pUC19 T7 S8.C. Lane 3, ssRNA transcripts from pUC19 T7 S8. Arrow indicates expected S8 band

To generate the mutant viruses, BSR cells were first transfected with 6 plasmids (encoding VP1, VP3, VP4, VP6, NS1 and NS2) to form the primary replication complex. These cells were subsequently transfected at 18 hpi with all 10 RNA transcripts including S8.C, which was shown to be indistinguishable from WT S8 when analysed on a denaturing agarose gel (Figure 5.4). Three days post second transfection the cells were harvested.

The putative mutant viruses were grown in BSR cells and the whole cell lysates used in a plaque assays. 6 plaques were picked to form BTV-1 S8.C viruses 1- 6. Stocks of these were generated by infections at an MOI 1 of BSR cells and BSR-S8 complementary cells which produce NS2 *in trans*. All viruses exhibited CPE and once 100% CPE was reached

stocks were harvested and virus titres obtained through plaque assays. These stocks were used throughout and re-made frequently to maintain a high virus titre. The BSR-S8 complimentary cell line was previously made within the lab. It was analysed often by 10% SDS-PAGE and western immuno blot using NS2 specific antibodies to confirm the continued expression of NS2 (Figure 3.4. B).

5.2.2 Confirmation of S8.C mutations

Following recovery of the putative BTV-1 S8.C viruses (1- 6) from BSR cells, the presence of virus and the validation of the inserted mutations was performed. Analysis of the pattern of genomic dsRNA of BTV S8.C and the comparison of WT S8 confirmed recovery of virus from the RG system. Viruses were harvested and the dsRNA extracted and analysed by electrophoresis on a 9% non-denaturing gel. The gel showed all 10 genomic segments from BTV S8.C (Figure 5.5. A, Lanes 2, 4-7) and WT BTV (Lane 1). Both mutant and WT S8 migrated to the same position and were indistinguishable from each other. Lane 3 showed little dsRNA from BTV-1 S8.C virus 5. As CPE was observed from both BSR and BSR-S8 cell infection it was plausible to assume that the dsRNA was lost during purification.

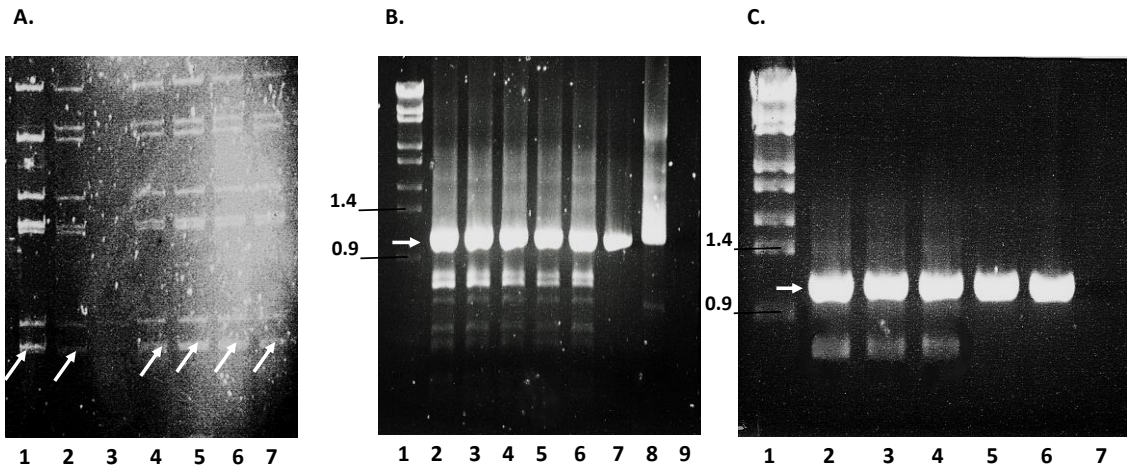

Figure 5.5. Genomic dsRNA purification and RT-PCR of BTV-1 S8.C.
A, dsRNA purification of BTV-1 S8.C from infected BSR cells analysed on a 9% non-denaturing PAGE stained with ethidium bromide. Lane 1, BTV-1 dsRNA used as a marker. Lanes 2-7, BTV-1 S8.C clones 6-1, respectively. White arrows represent migration of segment 8. **B,** RT-PCR of BTV-1 S8.C detected on a 1% agarose gels by ethidium bromide. Lane 1, *Styl* digested λ DNA ladder. Lanes 2-7, BTV-1 S8.C clones 1-4 and 6. Lane 7, PCR control of amplified S8 from pUC19 T7 S8. Lane 8, RT-PCR control of WT BTV-1 dsRNA. Lane 9, H_2O control. **C,** Optimised RT-PCR. Lane 1, *Styl* digested λDNA ladder. Lanes 2-4, BTV-1 S8.C clones 3, 4 and 6. Lane 5, PCR control of amplified S8 from pUC19 T7 S8. Lane 6, RT-PCR control of WT BTV-1 dsRNA. Lane 7, H_2O control. White arrows indicate approximately 1.1kb. Size markers shown in kb.

The identification of dsRNA bands, like those found in WT BTV, indicated that a replicating virus was recovered. Subsequently, the correct insertion of the designed mutations was confirmed. Specific primers (BTV-1 S8 T7 *Bam*HI F and BTV-1 S8 *Bsm*BI/*Bam*HI/*Rsr*II R) were used to amplify the full-length S8 by reverse transcriptase PCR (RT-PCR). Firstly, a cDNA copy of the dsRNA S8 was generated by reverse transcription. This was then amplified by PCR using the same primers to generate a product for sequencing. The initial RT-PCR generated many non-specific bands in

addition to the expected band at ~1100 bp (Figure 5.5. B), when detected by gel electrophoresis. The PCR reaction was optimised with a reduction in the amount of primers, dNTPs and cDNA template added, and the addition of $MgCl_2$. This succeeded in reducing the amount of non-specific amplification (Figure 5.5. C), whilst retaining a strong band at the correct size for S8 (~1100 bp). A small amount of non-specific product is still produced (Figure 5.5. C, lanes 2-6)A plasmid containing a cloned S8 (pUC19 T7 S8) was used as positive PCR control (Figure 5.5. B, Lane 7 & C, Lane 5). Similarly, the RT-PCR amplification of WT BTV-1 S8 was used as a positive RT-PCR control (Figure 5.5. B, Lane 8 & C, Lane 6). Both of these showed corresponding bands at ~1100bp. No amplification was detected in the negative control, which contained H_2O instead of dsRNA template for the RT-PCR (Figure 5.5. B, Lane 9 & C, Lane 7). The amplified S8 band (Figure 5.5. C, white arrows) was excised from the gel and underwent purification before being sequenced to confirm the mutation in the recovered BTV.

The presence of the specific mutations was confirmed through sequencing of the RT-PCR product of BTV-1 S8.C virus 6. The results were compiled by Bio-edit software and BlastN confirmed as BTV S8. Alignments of BTV S8.C 6 with BTV-1 published data revealed the expected alanine substitutions at residues K_{281} L_{282} A_{283} D_{284} R_{285} E_{286}, consistent with the designed mutations (Figure 5.6. C). BTV-1 S8.C virus 6 was subsequently referred to as BTV-1 S8.C.

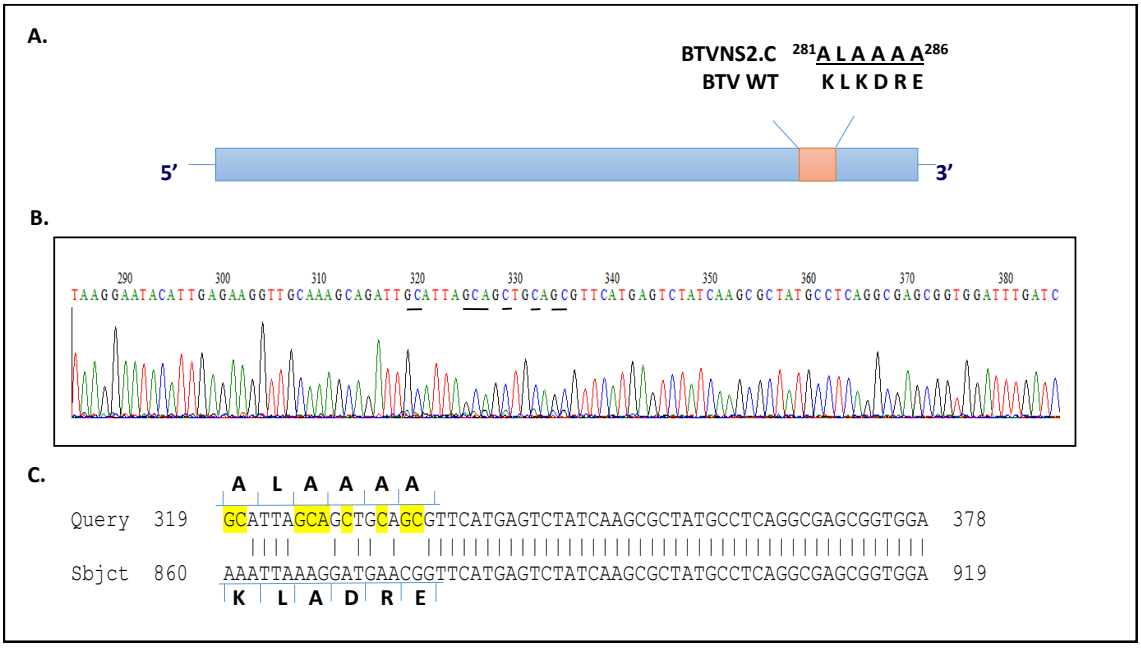

Fig 5.6. Confirmation of mutations in BTV-1 S8.C.
A, Schematic diagram of NS2 showing the wild-type amino acid sequence and the designed mutations to disrupt ssRNA binding. **B,** Partial chromatogram sequence of BTV-1 S8.C, sites of expected mutations underlined. **C,** Partial sequence of PubMed alignment of BTV-1 S8.C and the published BTV-1 S8 sequence. Sequence differences are highlighted in yellow and the resulting amino acids indicated.

5.3 BTV S8.C characterisation *in vivo*

5.3.1 Plaque formation of the BTV S8.C mutant in BSR cells

As the first step in BTV S8.C *in vivo* characterisation, plaque assays were performed in both BSR and BSR-S8 complementary cells to assess virus growth. Differences between BTV-1 S8.C and WT plaques were observed in BSR cells, which were similar to those generated by BTV S8.M. BTV S8.C formed smaller plaques in BSR cells (Figure 5.7. B), while the WT virus in the same cells formed larger plaques consistent with those usually produced by BTV-1. (Figure 5.7. C). In contrast, the complementary cell line

(BSR-S8) infected with BTV S8.C showed a WT-like plaque phenotype (Figure 5.7. A). The plaques formed from WT BTV-1 in the complementary cell demonstrated no change in plaque phenotype when compared to those seen in BTV-1 BSR plaques (Figure 5.7. D). This observation indicated that the mutation introduced in S8 had an effect on virus growth in BSR cells, but when functional NS2 is supplied *in trans* the virus growth returned to normal.

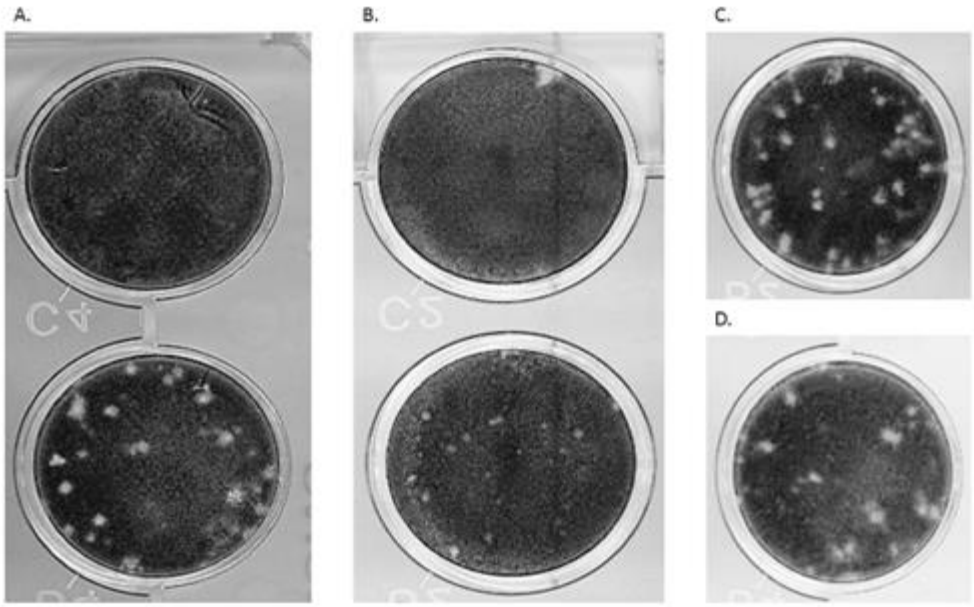

Figure 5.7. Examples of the plaques formed by WT BTV-1 and BTV-1 S8.C in BSR and BSR-S8 cells.
BSR or BSR-S8 complementary cells were infected with virus, fixed 3 days post infection and stained with crystal violet. **A,** BTV-1 S8.C plaques formed in BSR-S8 complementary cells (lower) and a non-infected control (top). **B,** BTV-1 S8.C plaques formed in BSR cells (lower) and negative control (top). **C,** WT BTV-1 plaques formed in BSR cells. **D,** WT BTV-1 plaques formed in BSR-S8 cells.

5.3.2 Growth kinetics of BTV S8.C in BSR cells

The differences demonstrated in plaque morphology between WT and mutant infected BSR cells indicated that a more in-depth study of the mutant viruses' growth was necessary to fully understand the growth kinetics of the virus. Both BSR and BSR-S8 complementary cells were infected with BTV S8.C at an MOI 1. Cells and supernatant were harvested at 0, 8, 16, 24, 36, 48, 72 and 96 hpi, and virus growth was assessed through plaque assay in the cell types they were previously grown in. This experiment was performed in triplicate to generate the average virus titre and 95% CI, which was plotted to form the growth curve (Figure 5.8). As a comparison control WT virus growth in both BSR and BSR-S8 was also analysed.

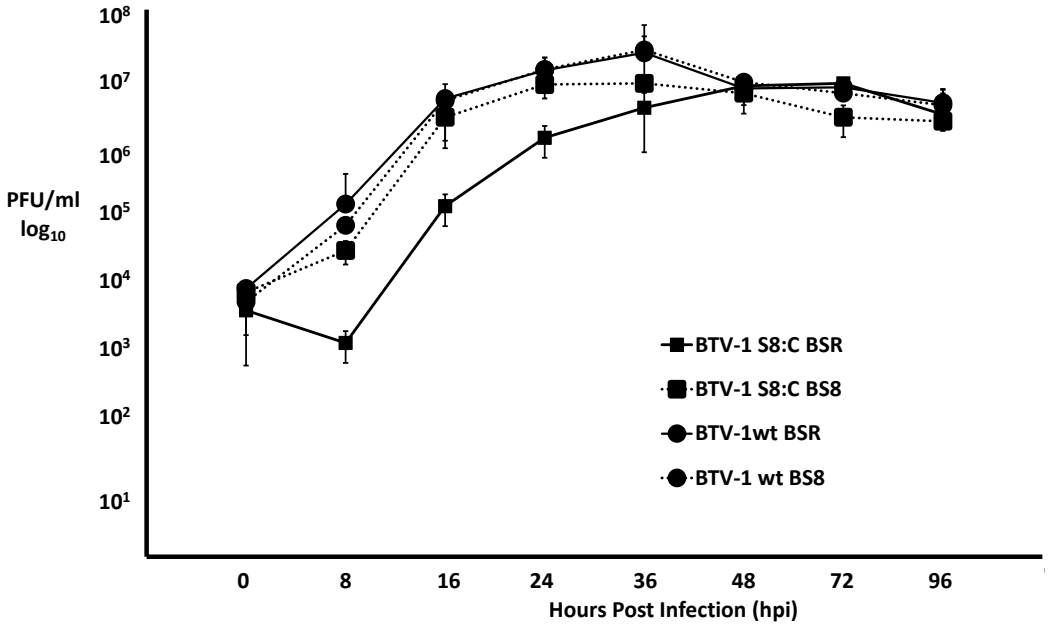

Figure 5.8. BTVS8.C growth curves in BSR and BSR-S8 cell line.
Mammalian BSR or BSR-S8 cells were infected at MOI 1 and harvested at the indicated times. Viral titre was determined by plaque assay (in triplicate) and the averages plotted on a logarithmic scale. BSR and BSR-S8 cells infected with wild-type BTV was used as a control. 95% confidence intervals shown (95% C.I).

WT BTV growth in BSR cells demonstrated an increase in virus titre up to 36 hpi (Figure 5.8. Circle, solid line), with the greatest increase in growth rate at 16 hpi (1.4 log increase). Virus growth decreased after 36 hpi which was comparable with published data [73]. WT growth in BSR-S8 cells was similar with the greatest titre at 36 hpi and the greatest increase in growth rate at 16 hours (1.7 log increase) (Figure 5.8. Circle, dotted line). Maximum BTV titre was slightly higher in BSR-S8 cells with an average at 36 hpi of 2.5 $x10^7$, compared to the average at 36 hpi in BSR cells of 2 $x10^7$ but this was not statistically significant (>25% overlap in 95% CI).

BTV-1 S8.C growth in normal BSR cells shows a reduction in virus titre at 8 hpi compared to initial infection (Figure 5.8. Square, solid line). An increase in virus titre was then visible up to 72 hpi, with the largest increase of growth shown at 16 hpi (2 log increase). BTV S8.C never reached the highest titres of WT BTV with a maximum titre of 8 $x10^6$. The differences in titre between the mutant and WT at 36 hpi was shown to be statistically significant (<25% overlap in 95% CI) 0.9 log difference. Similarly to BTV S8.M, BTV-1 S8.C displayed WT-like growth in BSR-S8 cells (Figure 5.8. Square, dotted line). It displayed an increase in growth up to 36 hpi (8.3 $x10^6$) at comparable but reduced levels when compared to WT in the BSR cell line (2 $x10^7$) and the BSR-S8 cell line (2.5 $x10^7$), which was followed by a growth decrease after 36 hpi. The largest increase in growth rate was at 16 hpi (1.9 log increase). The differences shown between BTV -1 S8.M growth in BSR-S8 cells was not statistically significant

from WT (>25% overlap in 95% CI), apart from at 8 hpi which demonstrated a statistically significant 0.4 – 0.7 log reduction.

As with the BTV-1 S8.N and BTV-1 S8.M mutants, the mutant was characterised further with the analysis of mutant protein synthesis of virus structural protein VP5 and non-structural proteins NS1 and NS2. Actin was used as a control to eliminate variation in overall protein load (Figure 5.9).

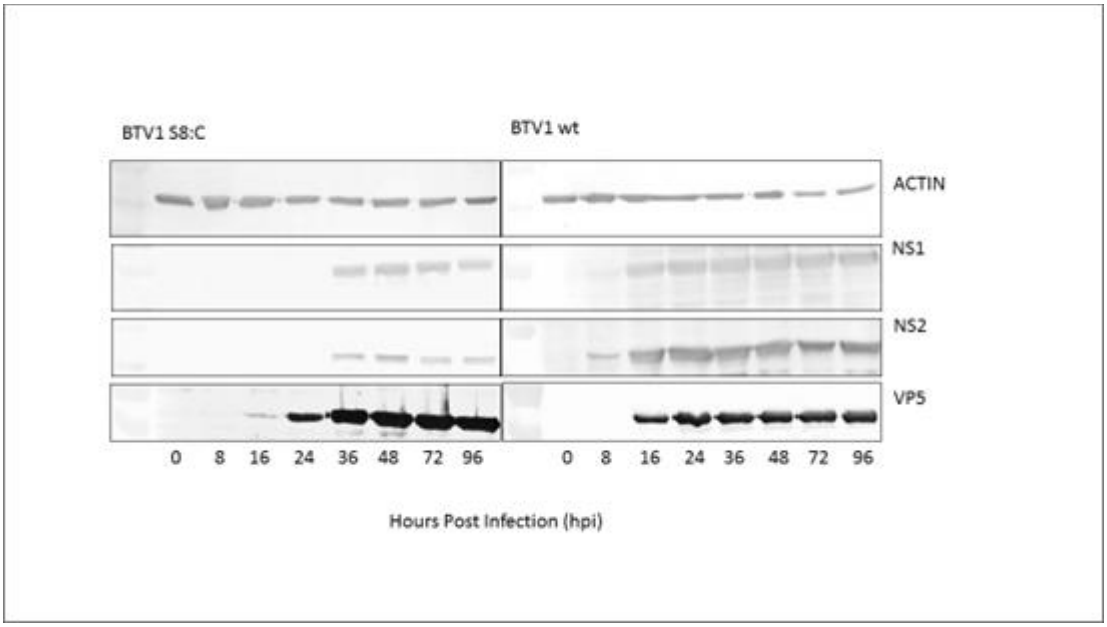

Figure 5.9. Analysis of BTVS8.C proteins during BSR cell infection.
Proteins harvested at indicated time points, separated on a 10% SDS-PAGE and transferred to a nitrocellulose membrane for visualisation using western immuno blot. Rabbit anti-NS1 antibody (1:5000) detected bands at 64 kDa. Guinea pig anti-NS2 antibody (1:3000) detected bands at 42 kDa. Guinea pig anti-VP5 antibody (1:3000) detected bands at 59 kDa. Ladder used was Page Ruler Prestained Protein ladder (Thermo Scientific). Protein load control was indicated by Mouse anti-Actin antibody (1:5000) (42 kDa).

Western blot analysis demonstrated that the BTV-1 S8.C produced NS2 which was recognised by a specific anti-BTV-10 NS2 and indistinguishable in size to WT BTV NS2.

BTV1 S8.C first expressed non-structural proteins NS1 and NS2 at a detectable level between 24 and 36 hpi (Figure 5.9), and the amount remained constant until 96 hpi. BTV S8.C structural protein VP5 was first detected at 16 hpi and demonstrated an increase in production until 36 hpi, after which the amount plateaued.

BTV-1 WT non-structural proteins NS1 and NS2 were detected at 16 and 8 hpi, respectively (Figure 5.9), and remained constant until 96 hpi. BTV WT structural protein VP5 was detected at 16 hpi, and was expressed at a constant level until 96 hpi. Cellular protein actin was used as a protein loading control; the constant levels indicated that the same amount of protein was added to each well.

Generally, when compared to WT BTV-1 protein production in BRS cells, BTV-1 S8.C displays a delay in protein production until 24-36 hpi. Following this the protein production was similar to that seen with WT.

The western blot protein expression images (Figure 5.9) were quantified with LI-COR Image Studio Lite. The mutant protein signal intensities from the light channels were averaged, normalised to the actin control and plotted against the corresponding WT protein (Figures 5.10, 5.11 & 5.12).

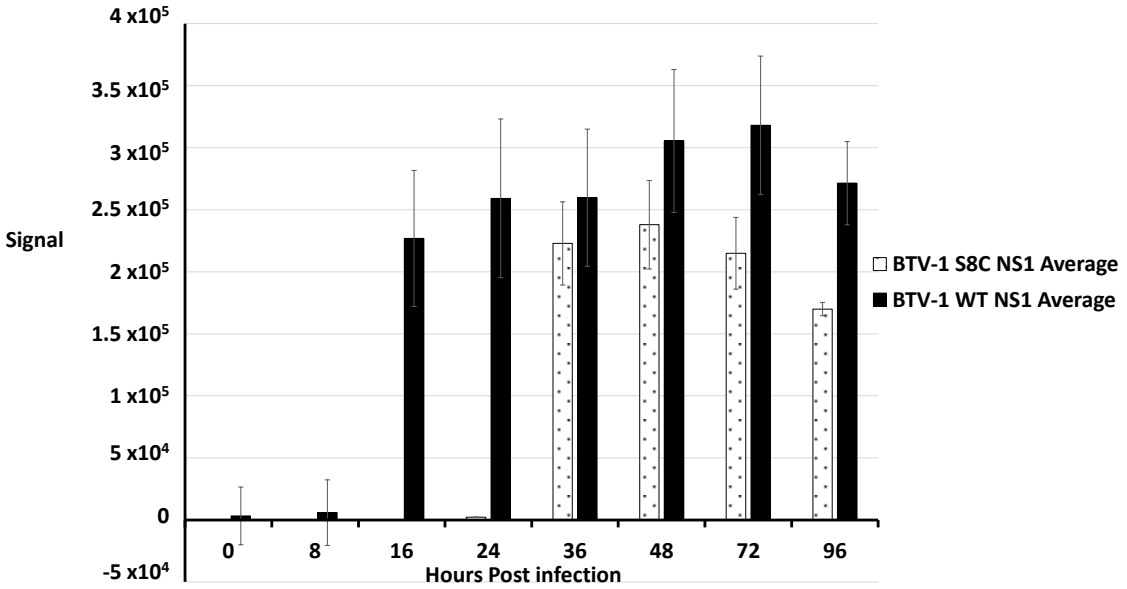

Figure 5.10 NS1 protein expression of BTV-1 WT and BTV-1 S8.C in BSR cells over time.
The western blot protein expression images for BTV-1 WT and BTV-1 S8.C (Figure 5.9) were quantified with LI-COR Image Studio Lite. NS1 was normalised to the respective actin loading control and plotted. (95% CI).

The NS1 signal seen at 0 hours (Figures 5.10) was possibly due to insufficient washing following the initial infection. This is because NS1 is a non-structural protein and is only produced by a replicating virus later in infection. For this reason, the earliest possible detection would be two hours post infection [128]. When compared to the western blot image (Figure 9), which did not have a detectable band at 0 hours, it suggested that this small signal was an artefact of the quantification. This was supported by the 95% confidence interval, which indicated that there was significant chance that the NS1 average seen at 0 and 8 hpi was artificial.

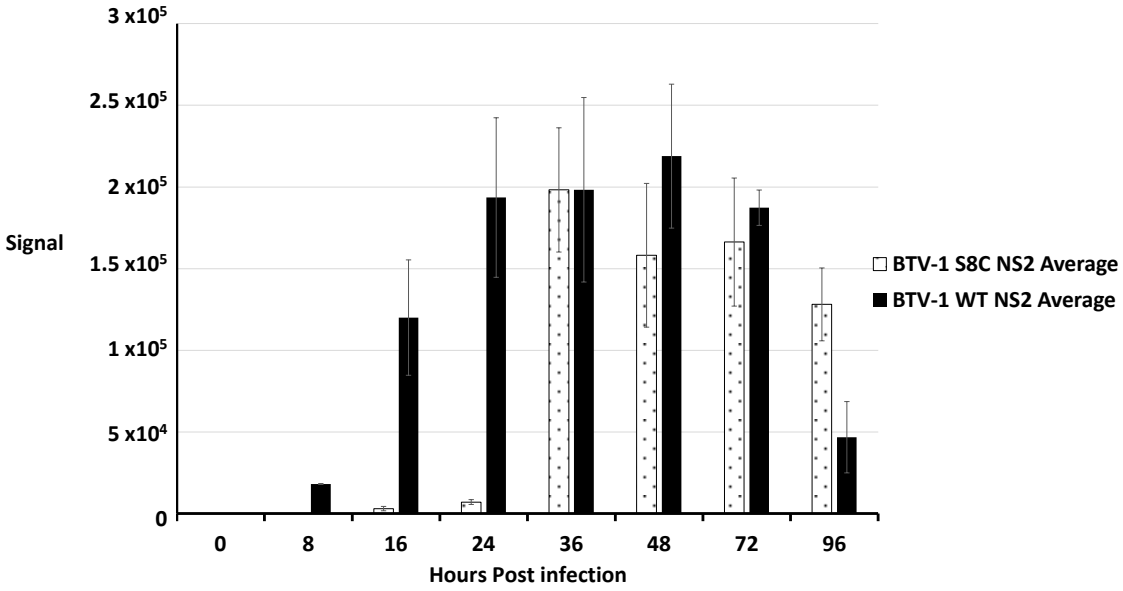

Figure 5.11. NS2 protein expression of BTV-1 WT and BTV-1 S8.C in BSR cells over time.

The western blot protein expression images for BTV-1 WT and BTV-1 S8.C (Figure 5.9) were quantified as described in Figure 5.10. NS2 was normalised to the respective actin loading control and plotted. (95% CI).

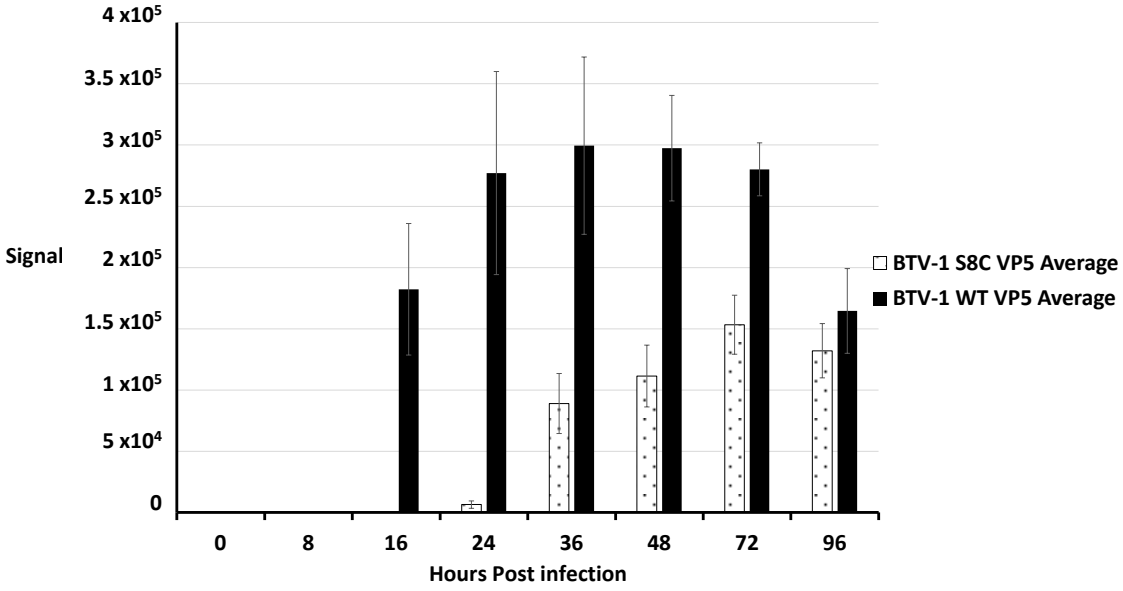

Figure 5.12. VP5 protein expression of BTV-1 WT and BTV-1 S8.C in BSR cells over time.

The western blot protein expression images for BTV-1 WT and BTV-1 S8.C (Figure 5.9) were quantified as described in Figure 5.10. VP5 was normalised to the respective actin loading control and plotted. (95% CI).

Quantification of NS1 expression (Figure 5.10) displayed that BTV-1 S8.C had a delayed NS1 expression compared to WT. WT BTV-1 first expressed NS1 at 16 hpi while BTV-1 S8.C expresses NS1 at 36 hpi. Maximum NS1 expression was seen at 46 hpi for BTV-1 S8.C. This was dissimilar to WT NS1 production which demonstrated a maximum expression at 72 hpi. Maximum NS1 production of BTV-1 S8.C showed a 27% reduction compared to the maximum NS1 production in WT.

Detectable BTV-1 S8.C NS2 production was delayed when compared to WT NS2 expression (Figure 5.11), with BTV-1 S8.C NS2 detected at 36 hpi rather than 8 hpi for WT BTV-1. NS2 expression peaked at 48 hpi for WT while BTV-1 S8.C NS2 expression was highest at 36 hpi and then decreased. Maximum NS2 production of BTV-1 S8.C showed a 9.4 % reduction compared to the maximum production in WT.

BTV-1 S8.C VP5 was detectable at 24 hpi (Figure 5.12) while WT VP5 was detected at 16 hpi. WT VP5 expression increased up to 24 hpi, plateaued until 72 hpi and then decreased at 96 hpi. BTV-1 S8.C VP5 expression, however, increased up to 72 hpi. Maximum BTV-1 S8.M VP5 expression demonstrated a 48% reduction compared to maximum WT VP5 expression. Overall, mutant non-structural protein production was delayed by at least 20 hours and the amount generated reduced compared to WT. Structural protein VP5 was detected at the same time point as WT but at a greatly reduced level.

5.3.3. Effect of the S8.C mutation on VIB formation in BSR cells

The effect of the mutation in S8 on the formation of VIBs was investigated using an Immuno Fluorescence Assay (IFA). Dual staining was performed at 24 hpi using anti–NS2 antibodies to show VIB formation and anti-VP7 antibodies as a confirmation of viral infection, which were visualised by confocal microscopy (Figure 5.13). Both WT and BTV S8.C infected BSR cells showed high levels of VP7, which reflected the MOI 10 that was used to infect cells and gives a clear indication that both samples were infected with replicating virus.

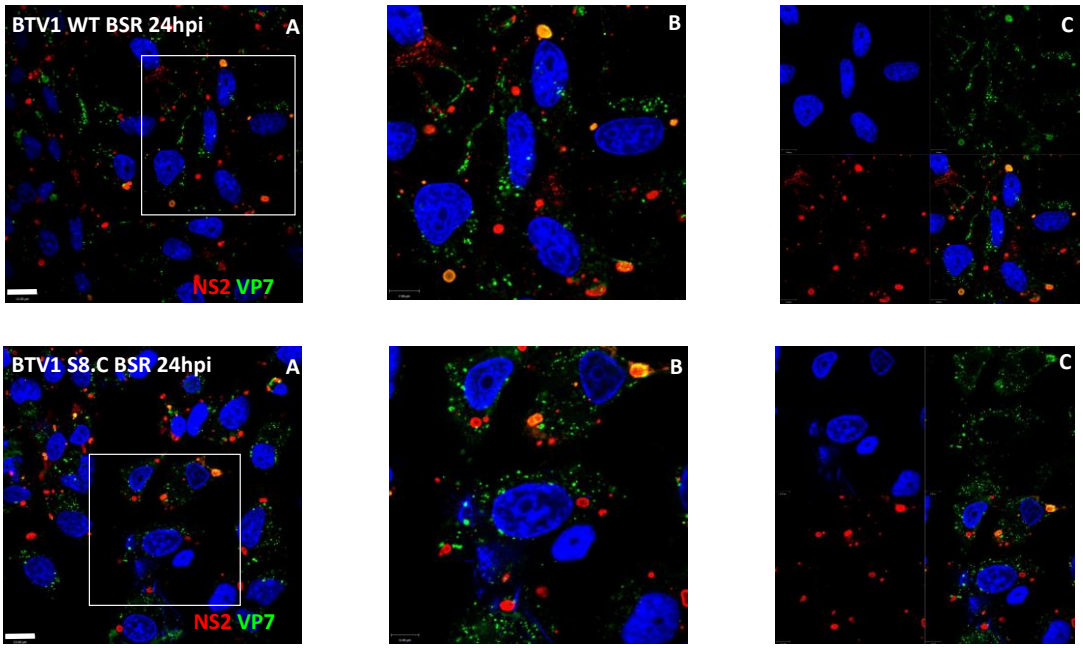

Figure 5.13. Immunofluorescence assay (IFA) of BTV-1 WT and BTV-1 S8.C at 24 hpi. Dual staining for NS2 and VP7. BSR cells were infected with BTV-1 WT (top panels) or BTV1 S8.C (lower panels) fixed 24 hpi and protein expression investigated by confocal microscopy. Primary antibodies, Guinea pig anti-VP7 and Rabbit anti-NS2; Secondary antibodies Guinea pig-Alexa 488, Rabbit-TritC and Hoechst nuclear staining (blue). **A,**

Images obtained by an x100 lens. **B,** Image at x2 magnification. **C,** Three laser channels and merged image. White scale shows 10 µm.

A visual analysis of BTV S8.C infected BSR cells show smaller and fewer VIBs (Figure 5.13), in comparison to WT BTV which demonstrated distinct, punctuate structures of NS2 (VIBs) typical of BTV infection [150,151].

The NS2 signal was quantified by Volocity software as with the BTV-1 S8.N mutant and the BTV-1 S8.M mutant. BTV-1 S8.C produced ~23% smaller and ~69 % fewer detectable VIB. WT BTV-1 produced an average of 257 VIBs in the BSR cells per field of view while BTV-1 S8.C generated ~78 VIBs (Figure 5.14). Not only was the mean size of VIBs smaller for BTV-1 S8.C (1.07 μm^2) compared to BTV-1 (1.38 μm^2) (Figure 5.14 & 5.15), but the maximum size of BTV-1 S8.C VIB (7.22 μm^2) was also smaller than WT (19.66 μm^2). The minimum VIB size between BTV-1 S8.C was comparable to WT BTV-1 at 0.13 μm^2 and 0.12 μm^2, respectively. (Figure 5.15).

The 95% CI demonstrated that that the difference in VIBs generated during mutant and WT infections were statistically significant. Due to the >25% overlap of 95% CI shown by the mean VIB size and minimum VIB size of mutant and WT, the P-value was analysed. The differences in minimum VIB size however were not significant (p-0.3). The mean VIB size for BTV-1 S8.C demonstrated some larger bodies which increased the 95% CI, but a statistically significant P-value ($p<0.05$) was still produced.

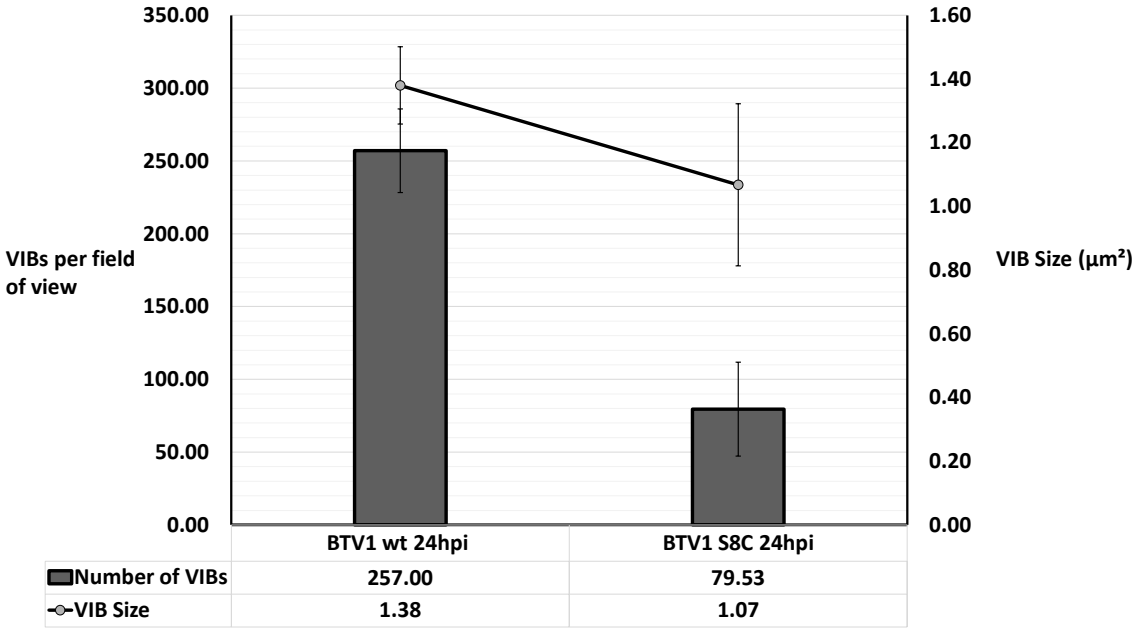

Figure 5.14. Graph of average number and size of VIBs produced by both WT BTV-1 and BTV-1 S8.Cduring BSR cell infection.
Data were quantified using Volocity from confocal images of BSR cells infected with MOI 10 of virus and fixed at 24 hpi. Data shown are the averages of ten standard fields of view at x100 magnification. (95% CI).

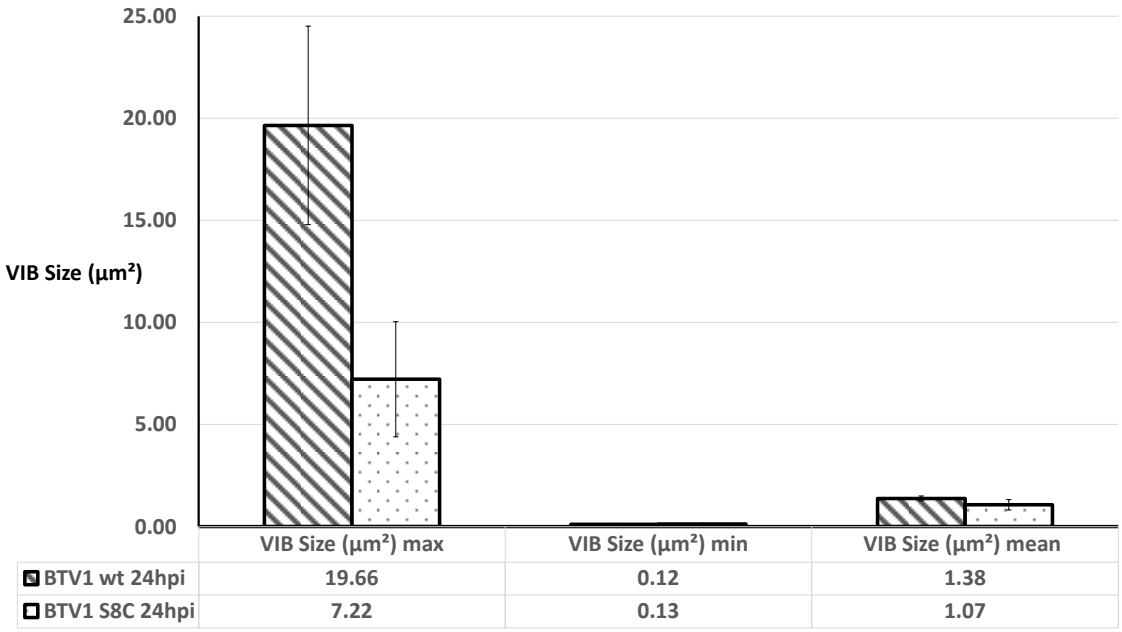

Figure 5.15. Graph of average maximum, minimum and mean size of VIBs produced by both WT BTV-1 and BTV-1 S8.Cduring BSR cell infection.
Data were quantified using Volocity, as Figure 5.16. (95% CI).

5.4 *In vitro* characterisation of recombinantly expressed NS2.C

The *in vivo* data established that the S8.C mutation effected virus growth and VIB formation in BSR cells. In order to confirm that this was due to a functional impairment in the binding of RNA, rather than an effect on the overall structure, recombinant NS2.N was generated and characterised.

5.4.1 Construction and confirmation of transfer vector pAcYM1-H/GST NS2.C

As described previously, an In-Fusion cloning method and specific primers (In-Fusion F Primer and In-Fusion R) were used to generate 5' and 3' 15 bp complementary regions on the S8.C insert to the pAcYM1-H/GST plasmid. The In-Fusion enzyme then allowed insertion into the linearized pAcYM1-H/GST vector. PAcYM1-H/GST NS2.C was then transformed into chemically competent Stellar *E. coli* and grown on LB plates containing ampicillin.

Screening was performed by ampicillin resistance and colony PCR, using forward primer BTV-1 S8 T7 *Bam*HI F and reverse primer BTV-1 S8 *Bsm*BI/*Bam*HI/*Rsr*II R to indicate which colonies contained the S8 insert. Positive amplification was shown by one band at the expected size of 1,100 bp which was detected by gel electrophoresis. All of the six colonies selected contained Segment 8 1 (Figure 5.16. Lane 2).

Colony 1 (Figure 5.16. Lane 2) was sent for sequencing and the full-length sequence results of were compiled by Chromas software and were BlastN confirmed as BTV-1 S8.C full-length coding region. Alignment with PubMed published data revealed no

deletions, insertions or frame shifts which would affect protein production (Data not shown).

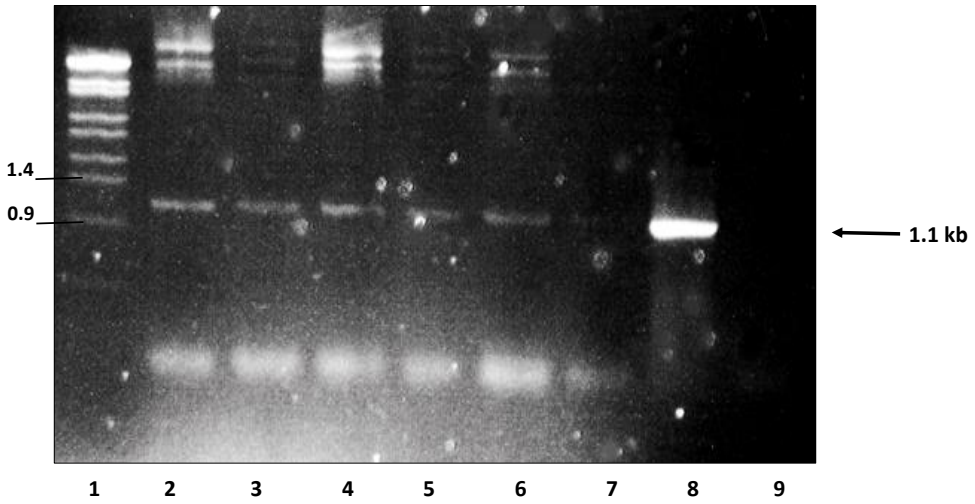

Figure 5.16. Colony PCR for selection of colonies containing pAcYM1-H/GST NS2.C. Stellar *E. coli (*HST08 strain) colonies containing pAcYM1-H/GST NS2.C were identified by the amplification of S8 and detected on a 1% agarose gel containing ethidium bromide. Lane 1, *Sty*I digested λ DNA ladder. Lanes 2-7, colony PCR product from Stellar *E. coli* clones. Lane 8, H_2O control. Lane 9, positive PCR control of pUC19 T7 S8. Arrow indicates segment 8 at approximately 1.1kb. Size markers shown in kb.

5.4.2 Generation of recombinant virus expressing NS2.C

To promote homologous recombination, non-infectious bacmid KO:1629 DNA was digested with *Bsu*36I to linearize the genome. Colony 1, identified above, was successfully transfected with the linearized bacmid using X-treamgene 9 and produced an AcMNPV YM1-H/GST NS2.C recombinant virus. This was visually indicated by the production of GFP in the parallel transfection of pRN43-GFP and bacmid KO:1629

(Figure 3.15. A and B). No background florescence was detected (Figure 3.15. C & D) which confirmed recombination of AcMNPV KO:1629 with pRN43-GFP.

Successful recombination of AcMNPV RN43-GFP indicated that AcMNPV YM1-H/GST NS2.C recombinant viruses had also been generated. This was supported by visible CPE of infected cells. Harvested AcMNPV YM1-H/GST NS2.C potentially contained a mixed population of recombinant virus. Plaque assays were therefore performed with virus harvested from infected cells to select clonal viruses and to validate expression of NS2.C. Four putative recombinant plaques were picked and underwent three rounds of virus amplification to increase virus titre.

Protein expression of the 4 AcMNPV YM1-H/GST NS2.C viruses were analysed. Cells were infected with the putative viruses, harvested 72 hpi and the proteins present separated according to size by SDS-PAGE. The gel was stained using Coomassie Brilliant blue to identify the protein (Figure 5.19). Expression of His/GST tagged NS2.C would result in a band at 65 kDa, which was present in all 4 of the putative AcMNPV YM1-H/GST NS2.C viruses analysed (Figure 5.19. A, lanes 2-5)

NS2 alone is a 42 kDa protein but migrates on SDS-PAGE to ~47 kDa and a band was clearly evident between 40 and 55 kDa (Figure 5.19. Solid arrow), which suggested the recombinant baculovirus produced some NS2 which did not contain the His/GST tag. The Coomassie stained gel clearly demonstrated all of the viruses produced a protein of the expected size to contain His/GST tagged NS2.C, and produced less of the untagged NS2.C. Plaque purified virus 1 was chosen for future work due to a balance

between a high production of the presumed tagged NS2.C and a weaker band of untagged protein (Figure 5.19. A, lane 2).

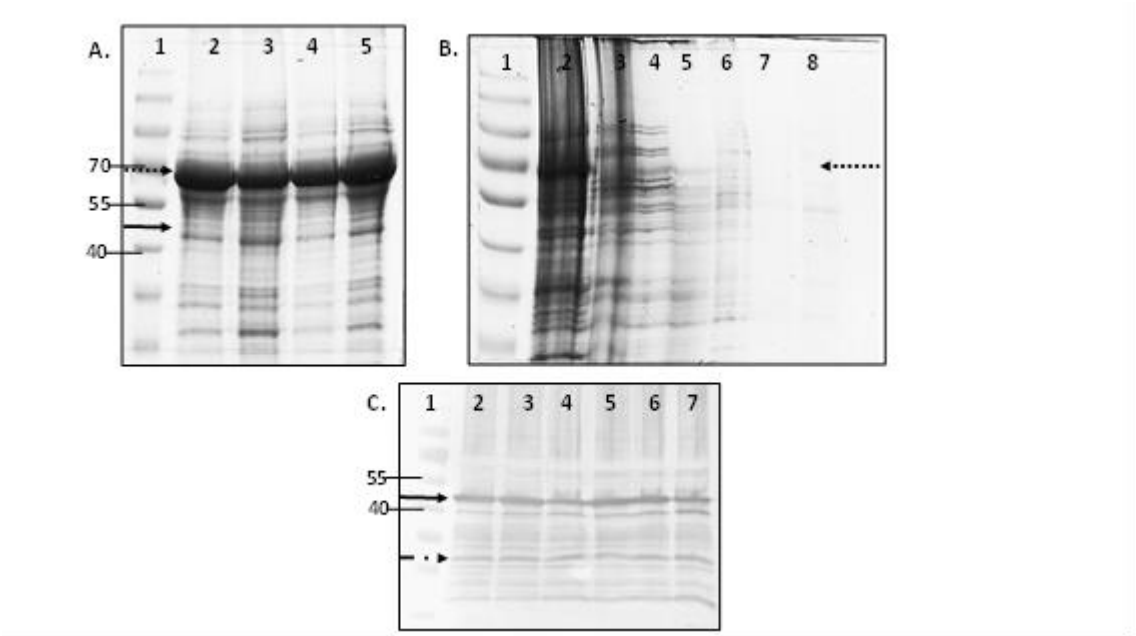

Figure 5.19. Expression and purification of NS2.C.
A, Cell lysates of *Sf9* cells infected with plaque purified AcMNPV YM1-H/GST NS2.C viruses. Proteins separated by 10 %SDS-PAGE and detected with Coomassie Blue. Lane 1, protein ladder. Lanes 2-5, AcMNPV YM1-H/GST NS2.C clones 1-4, respectively. **B,** Trial purification of AcMNPV YM1-H/GST NS2.C using Ni and GST beads. Samples taken at points during purification were analysed by 10% SDS-PAGE and detected with Coomassie Blue. Lane 1, protein ladder. Lane 2, cell supernatant of *Sf9* cells infected with AcMNPV YM1-H/GST NS2.C after dounce homogenisation. Lane 3, unbound protein supernatant from Ni bead binding. Lane 4, unbound protein following two washes of NS2-20 buffer. Lane 5, Protein eluted from Ni beads. Lane 6, unbound protein supernatant from GST bead binding. Lane 7, unbound protein following two washes of NS2-10 buffer. Lane 5, Protein eluted from GST beads. **C,** Cell lysates of *Sf9* cells infected with AcMNPV YM1-H/GST NS2.C clones. Proteins were separated on a 10 % SDS-PAGE and transferred to a nitrocellulose membrane for detection using western immuno blot and guinea pig anti-NS2 antibody (1:3000). Lane 1, protein ladder. Lanes 2-7, AcMNPV YM1-H/GST NS2.C clones 1-6, respectively. Dotted black arrow indicates expected migration of His/GST tagged NS2.C. Solid black arrow shows ~46 kDa, the expected size of NS2. Protein size marker shown in kDa.

A trial purification of AcMNPV YM1-H/GST NS2.C virus 1 using Ni and GST beads was performed. 50 ml of *Sf*9 cells were infected and harvested 72 hpi by centrifugation to form a pellet. Samples of each purification step were run by 10% SDS-PAGE and detected by Coomassie blue (Figure 5.19. B). The final NS2.C elution (Figure 5.19. B, Lane 8) did not produce any purified His/GST tagged NS2.C.

Due to the failure of Ni and GST beads to purify NS2.C, protein production was further investigated. Six new putative recombinant viruses (AcMNPV YM1-H/GST NS2.C viruses 1-6) were plaque purified from the original stocks and underwent three rounds of amplification. The cells were then harvested at 72 hpi and the proteins present separated by SDS-PAGE and transferred to a nitrocellulose membrane for Western immuno blotting using BTV NS2 specific primary antibody (Figure 5.19. C). Of the 6 clones investigated, none produced His/GST tagged NS2.C which would have been identified by a band at 65 kDa. All clones however, generated a strong NS2 specific band at 46 kDa, the correct size for untagged NS2.C (Figure 5.19. C, Solid arrow). Some non-specific bands were seen (Figure 5.19. C, Dash/dot arrow) but the majority of protein was NS2.C.

Although the 6 AcMNPV YM1 S8.C viruses did not contain the His and GST tags to facilitate purification, NS2.C was highly produced and there are other methods of purification which can be applied. A ion exchange chromatography purification method was selected because it had previously been used to purify NS2 [156,161,237]. *Sf*9 cells were infected with AcMNPV YM1 S8.C virus 1 and harvested 72 hpi by centrifugation to form a pellet. The pellet was washed once with NS2 buffer and

resuspended in NS2 lysis buffer. Cells were lysed with twenty strokes of a dounce homogenizer and the cell debris pelleted. The supernatant containing the soluble NS2.C was clarified and added to a 5 ml HiTrap Q HP anion exchange column. Proteins were bound (F1), washed (F2-F3) and eluted (F4-13) from the column with increasing concentrations of NaCl-NS2 elution buffer. All of the fractions were collected and analysed by 10% SDS and detected with Coomassie brilliant blue staining (Figure 5.20. A).

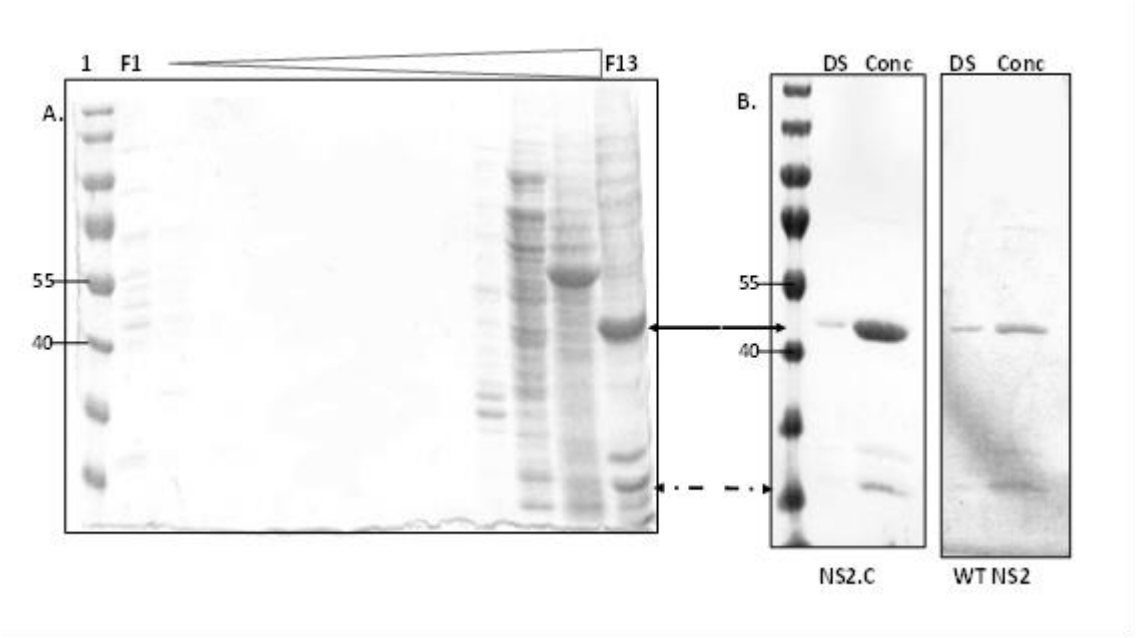

Figure 5.20. Ion exchange chromatography purification, desalting and concentration of NS2.C.
A, Fractions collected from purification of AcMNPV YM1-NS2.C infected *Sf9* cells. Collected fractions were separated on a 10% SDS-PAGE and detected with Coomassie Blue. Lane 1, protein Ladder. F1- F13, the first 13 fractions collected which showed sample binding (F1), washing (F2 and F3) and elution (F4-13). Bands at 46 kDa were identified as NS2.C. **B,** Desalting and concentration were performed on NS2.C fraction 13 and purified WT NS2 from AcBTV10 S8. The resulting samples were separated by 10% SDS-PAGE and detected with Coomassie Blue. DS, de-salted sample. Conc, concentrated sample after desalting. Bands at 46 kDa (solid black arrow) were identified as NS2. Protein size marker shown in kDa.

Successfully purified NS2.C was expected to form a single band at 46kDa. Fraction 13 contained the highest concentration of NS2.C and while there were some non-specific bands, NS2.C was by far the dominant protein.

Fraction 13 contained ~400mM sodium chloride from the elution buffer used to elute proteins off the column (Figure 5.20. A). If the salt was not removed it would interfere with any assays preformed using the purified protein. The sample was de-salted (Figure 5.20. B, DS) and concentrated (Figure 5.20. B, Conc) to remove the sodium chloride; the resulting NS2.C protein was highly pure (>3 µg/µl) (Figure 5.20. Solid arrow). A single protein band was shown at ~25 kDa. This band was also present in Figure 5.19. C (dash/dot arrow) which, due to the specific nature of the NS2 antibody used for visualisation, suggested it was a protein degradation product. No aggregates were observed.

WT NS2 was needed as a control for assays containing NS2.C. Recombinant baculovirus AcBTV10 S8 was previously generated within the lab. It was used to infect *Sf*9 cells, harvested, purified, de-salted and concentrated using the same method as NS2.C. This purified protein was detected by SDS-PAGE (Figure 5.20 B). WT NS2 was shown to be highly purified and demonstrated the same degradation products as NS2.C.

The generation of soluble mutant protein demonstrated that the overall protein structure was not greatly perturbed by the mutations added and so purified NS2.C was used in *in vitro* characterisation studies.

5.4.4 ssRNA binding activity of NS2.C mutant protein

WT NS2 and NS2.C were produced and purified for use in assays to generate *in vitro* data. The aim was to support the *in vivo* findings by characterising the effects the mutations have on the NS2 proteins ssRNA binding ability. EMSAs were used to detect RNA binding to WT NS2 and NS2.C. Radiolabeled BTV segment 7 was used to detect the difference in ssRNA migration. Purified WT NS2 and NS2.C were diluted to specific concentrations in DEPC H_2O, mixed with the RNA and allowed to bind for 30 minutes. The resulting NS2-RNA complexes were loaded and run on an agarose gel causing separation of the large NS2-RNA complexes, from the smaller free RNA. Gels were then dried and analysed. A successful shift and thus RNA-NS2 binding was identified by a band visible at a higher position than the RNA only control in the autoradiography gels (Figure 5.21, A & B. Lane 1).

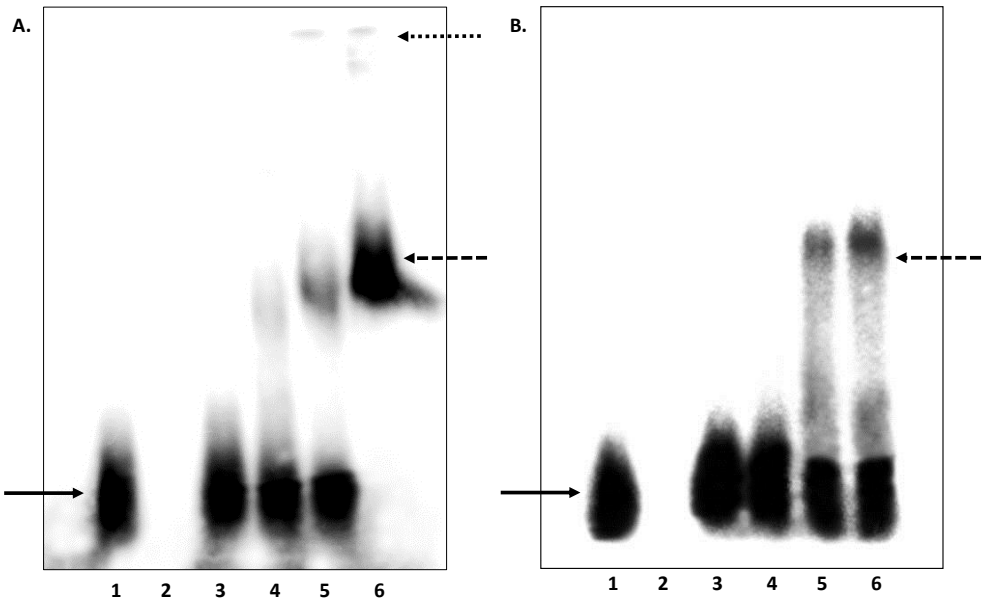

Figure 5.21. EMSA of WT NS2 and NS2.C.

Radiolabeled T7-derived ssRNA BTV segment 7 was bound to NS2 or NS2.C and run on a 1% agarose gel. **A,** EMSA of RNA and WT NS2. Lane 1, RNA only control. Lane 2, NS2 only control. Lanes 3-6, RNA and 1, 5, 10 and 15 µg NS2, respectively. **B,** EMSA of RNA and NS2.C. Lane 1, RNA only control. Lane 2, NS2.C only control. Lanes 3-6, RNA and 1, 5, 10 and 15 µg NS2.C, respectively. Solid black arrows indicate unbound RNA. Dashed black arrows signify RNA-NS2 complexes.

The images (Figure 5.21) were quantified using ImageJ software. Lanes on the image were marked and the total lane signal used to indicate 100% RNA signal. The distribution of signal within these lanes as either bound or unbound RNA was identified by plotting the area of each signal peak and calculated as a percentage of the total RNA signal.

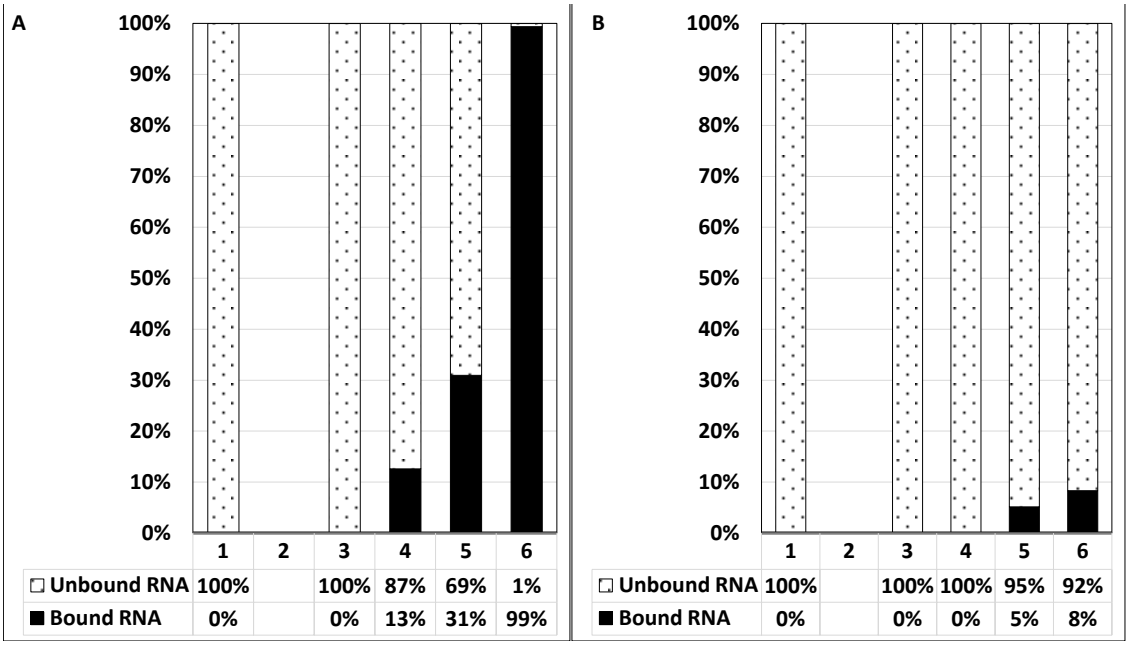

Figure 5.22. Quantification of WT NS2 and NS2.CEMSA.
EMSA images were quantified using ImageJ software. Total lane signal used to indicate 100 % RNA signal. **A,** EMSA of WT NS2 and RNA. Lane 1, RNA only control. Lane 2, NS2 only control. Lanes 3-6, RNA and 1, 5, 10 and 15 µg NS2, respectively. **B,** EMSA of NS2.C and RNA. Lane 1, RNA only control. Lane 2, NS2.C only control. Lanes 3-6, RNA and 1, 5, 10 and 15 µg NS2.C, respectively.

The BTV specific ssRNA binding demonstrated by NS2.C was very similar to that shown by NS2.M. The EMSA of SSRNA and NS2.C (Figure 5.21 & 5.22. B) demonstrated no shifting with 1 µg of NS2.C (Lane 3), identical to the EMSA of RNA and 1 µg of WT NS2 (Figure 5.21 & 5.22. A, Lane 3).

WT NS2 (Figure 5.21 & 5.22. A) demonstrated a protein concentration dependent increase in BTV specific ssRNA binding up to 15 µg (Lane 6) which resulted in a complete shift of ssRNA to the bound position. The NS2.C mutant also demonstrated a protein dependent increase in BTV specific ssRNA binding (Figure 5.21 & 5.22. B.). This binding was, however, greatly reduced compared to WT. 15 µg NS2.Mwas able to bind 9% of the ssRNA, whereas WT was able to bind 99% at the same concentration.

5.4.5 NS2.C oligomerisation in the presence and absence of RNA

The effect C-terminal RNA binding mutation on NS2 oligomerisation was investigated similarly to that undertaken with the NS2.N and NS2.M mutants. 5-20% sucrose gradients were generated and 50 µg of NS2 added to them. The samples were sedimented through and detected as previously described. It was performed with both WT NS2 (Figure 3.21) and NS2.C (Figure 5.23). During the purification process RNase A was added to eliminate all non-specific RNAs. To determine if the multimers could form in the presence of BTV ssRNA, 1µg BTV-1 S10 RNA was incubated with NS2 prior to sedimentation.

NS2.C formed predominantly 7S to 8S complexes (Figure 5.23. F4 – F5) in the absence of RNA, which equates to 4 to 6 copies of 42 kDA forming the most stable multimer of NS2. This was the same as WT NS2 without RNA Figure 3.21. F4 – F5). The addition of

RNA formed a wide range of NS2.C complexes seen from fractions 3 to 12, which contained 6 - 22S. The largest proportion of NS2.C complexes were demonstrated at between fractions 3 and 6 (6 – 10S) which was similar to the structure size seen without RNA. Some larger complexes were also generated with the addition of RNA but these were at much lower intensities than the smaller structures. RNA was essential for the formation of large NS2 complexes. NS2.C had impaired RNA binding ability which resulted in a reduction in the formation of large homomultimers.

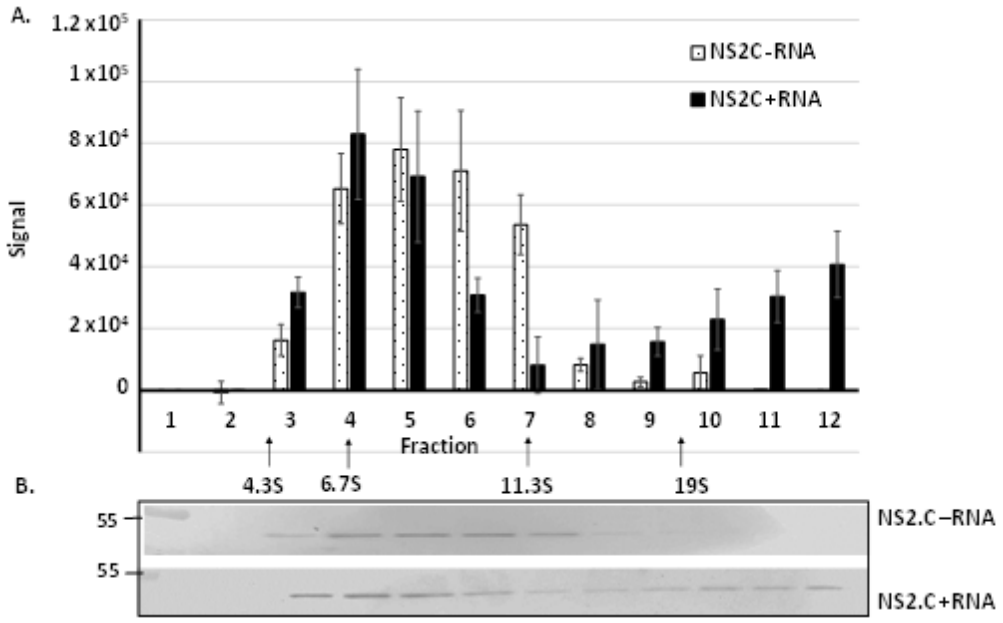

Figure 5.23. Oligomerisation assay of NS2.C in the presence and absence of RNA.
The twelve fractions from the oligomerisation assay were separated by 10% SDS-PAGE and transferred to a nitrocellulose membrane for visualisation using western immuno blot and guinea pig anti-NS2 antibody (1:3000). These membranes were analysed and quantified as described in Figure 5.24. **A,** a graph showing NS2.C present in each the gradient fractions, with and without the addition of RNA (95% CI). **B,** western immuno blot images used for analysis. NS2 Bands detected at 42 kDa

5.5 Discussion

The experiments in this chapter were undertaken to investigate the NS2 ssRNA binding domain between residues 274 - 286 [158]. The RG system was used to generate a BTV-1 mutant with specific mutations designed to disrupt RNA binding in this region for analysis *in vivo*. An *in vitro* study of the NS2 mutant was also performed to confirm that the mutations had not greatly affected the overall structure of the protein and to analyse the precise effect the mutation had on RNA binding and oligomerisation. The *in vitro* characterisation was used to support and explain the findings of the *in vivo* study.

The BTV-1 S8.C mutant generated by the RG system was confirmed to contain the designed mutations and characterised *in vivo* to explore the effects of the mutation on virus replication. Initial plaque assays of BTV-1 S8.C showed a distinct mutant plaque phenotype in BSR cells, which was smaller than those generated by WT BTV-1 when both infections were fixed and detected at 72 hpi. However, when BTV-1 S8.C was grown in the complementary cell line BSR-S8, the plaque phenotype reverted to a WT plaque phenotype. The reduction in plaque size was proposed to be due to the mutation in the NS2 protein because plaque formation was returned to a WT-like phenotype when a functional version of the NS2 protein is supplied *in trans* with the complementary cell line. The growth kinetics were further investigated with a time course of virus growth and protein production. The growth curves showed that BTV-1 S8.C titre in BSR cells initially decreases, potentially due to an extended eclipse period, before increasing to a maximum average tire of 8.3×10^6 at 72 hpi, and decreasing by

92 hpi. 2 hpi was not analysed here, but has been assumed that the initial decrease in BTV-1 S8.C was an extension of this eclipse period [73]. This delay in virus growth, and virus titre, was continued throughout the time course with BTV-1 S8.C growth increase demonstrated up to 72 hpi compared to 36 hpi for WT BTV. Furthermore, BTV-1 S8.C never reached the maximum titre seen in the WT BTV BSR cell control (36 hpi, 2 $x10^7$) nor the WT BTV BSR-S8 cell control (36 hpi 2.5 $x10^7$). The reduction in BTV-1 S8.C maximum titre may be due to infecting the cells at almost 100% confluence. At 72 hours post infection the cells will be overgrown and not replicating as efficiently which would limit replication. As shown with BTV-1 S8.M, BTV-1 S8.C growth in BSR-S8 cells was returned to similar levels as WT BTV due to the presence of functional NS2 supplied by the complementary cells.

To further characterise BTV-1 S8.C *in vivo*, protein samples were taken in parallel to the growth curve. Both structural (VP5), and non-structural (NS1, NS2) proteins, were detected in the cell lysates of BSR cells infected with mutant and WT viruses. No major differences in overall protein production were detected in comparison to the lysate from WT infected cells, similar to that which was reported previously [73]. Differences in protein production between time points, reflecting the growth of the virus were observed. The western blot analysis also showed that BTV-1 S8.C was recognised by a specific anti-BTV-10 NS2 antibody and was indistinguishable in size and antigenicity to WT BTV. Remarkably, after the initial negative growth rate and resulting loss of virus titre, the highest increase in rate of growth is shown by BTV-1 S8.C (BSR cells at 16 hpi) with a 2 log increase in titre; compared to BTV-1 S8.C in BSR-S8 cells at 16 hpi which exhibited a 1.9 log increase, BTV-1 in BSR-S8 cells at 16 hpi with a 1.7 log increase, and

BTV-1 in BSR cells at 16 hpi which shows a 1.4 log increase. This implied that the mutation in BTV-1 S8.C did not adversely affect the rate of growth, but instead retard the assembly of progeny virus.

As the S8.C mutation had been shown to delay virus growth and reduce the overall titre, an immuno fluorescence assay was undertaken to visualise and analyse the VIBs produced. BTV-1 formed VIBs comparable to those previously published [150] but without the perinuclear location which they are described as having [133,148,152]. This is most clearly demonstrated in Figure 5.14. C, which demonstrated that VIBs were dispersed throughout the cytoplasm. Image quantification was performed which demonstrated WT BTV-1 infection of BSR cells produced an average of 257 VIBs per frame with an average size of 1.38 μm^2. Under the same conditions BTV-1 S8.C produced an average of 79.5 VIBs per frame with an average size of 1.07 μm^2. This was shown by 95% CI and P-value to be a statistical significant 69% reduction in total number of VIBs and a 23% reduction in VIB size. Previous characterisation of BTV VIBs [148] showed that the average size of VIB was 1.1 μm^2 at 24 hpi, which is closer to the mutant BTV-1 S8.C VIBs than WT. This analysis measured 1542 BTV-1 VIBs and 769 BTV-1 S8.C VIBs, while Brookes *et al* 1993 only measured 48.

The minimum size for both WT and BTV-1 S8.C VIBs was very similar at 0.12 μm^2 and 0.13 μm^2, respectively. This was a statistically insignificant difference (>25% CI overlap and $p>0.05$) and might represent the minimal structure detectable or the minimal structure of a VIB. Conversely, the maximum size of VIB varied greatly between WT and BTV-1 S8.C, with a BTV-1 S8.C average VIB size of 7.22 μm^2 and WT average VIB size

of 19.66 μm^2. VIBs are similar to rotavirus viroplasms, in so far as the size, location and number is dynamic and changes throughout infection [148,240]. The work described here was a characterisation of VIB size and number at a specific time post infection; so could not explain if the differences in WT and BTV-1 S8.C VIBs were just a delay, or a true depiction of phenotype throughout infection.

All the *in vivo* characterisation of BTV-1 S8.C showed that the designed mutations affected virus growth and VIB formation. The growth is retarded early in infection and results in a 36 hour delay in maximum virus titre compared to WT, but does not adversely affect the rate of virus replication or virus protein synthesis. This delay in virus assembly, but not production of component parts, could be due to the differences seen in the VIBs as they are the sites of virus assembly. BTV-1 S8.C VIBs are smaller and fewer, which could be a limiting factor early in replication. A disruption in inclusion body formation affecting virus replication has previously been demonstrated with thiazolide drugs[245].

The *in vivo* data clearly showed that the mutations affected virus replication, but not the actual effect on RNA binding or NS2 oligomerisation. This was investigated *in vitro* with the generation of a recombinant baculovirus expressing NS2 with the same mutations as BTV-1 S8.C. The transfer plasmid pAcYM1-H/GST NS2.C was generated by an In-Fusion cloning method, and resulted in 100% successful transformation. Transfection of pAcYM1-H/GST NS2.C and bacmid DNA was performed and like NS2.N, the resulting recombinant virus had lost the purification tag. As previously described [156,161,237] NS2 was purified by ion exchange chromatography [164] which bound NS2 due

to the negative charge. Proteins were eluted from the column with increasing concentrations of NaCl-NS2 elution buffer; the negative ions in the salt compete with the proteins and eventually out compete, which results in the elution of the protein. The eluted fractions were collected and analysed to show that fraction 13 contained the highest concentration of NS2.C. While there are some non-specific bands in this fraction, NS2.C is by far the dominant protein. The sample was de-salted and concentrated resulting in highly pure NS2.C. A single protein band can be seen at ~25 kDa; this band is also present in the earlier western blot, suggesting it was a protein degradation product similar to one seem previously [159]. Even at highly purified >3 µg/µl quantities, WT NS2 and NS2.C did not form excessive aggregates, unlike previously published work [159].

To investigate if NS2.C mutation had an effect on RNA binding, an electrophoretic mobility shift assay was undertaken. WT NS2 and NS2.C both demonstrated a protein concentration dependent increase in BTV specific ssRNA binding. The specific ssRNA binding of the NS2.C mutant was, however, greatly reduced compared to WT. 15 µg NS2.M was able to bind 9% of the ssRNA, whereas WT was able to bind 99% at the same concentration. Neither 1 µg NS2.C nor WT NS2 was recorded as binding any RNA. Given the binding of NS2 to RNA at larger quantities it was probable that 1 µg NS2 is binding RNA, but at insufficient amounts to be detected, despite the use of radioactive labelling being used for detection due to its high sensitivity [239].

It has been suggested that oligomerisation of NS2 is triggered by the binding of RNA [151]. In order to investigate the oligomerisation NS2.C and WT NS2 in the presence and

absence of RNA, the complexes formed were examined by sedimentation analysis. NS2.C was predominantly detected in fraction 5 which equates to ~8S complexes, but was also present in large amounts in fractions 4-10 (7-10S) which relates to 6 (+/-2) copies of NS2. This was similar to the NS2 complexes formed by WT NS2 , previously published work on NS2 [154,167] and some *Reoviridae* family NS2 homologs [167]. The addition of RNA was shown to form a wide range of NS2.C complexes found in fractions 3–12 (6–22S). The quantification of the gels show that these complexes fall into two groups: the largest group of complexes fall within 6–10s, which was typical of NS2 unbound to RNA, and a second, smaller group of complexes in the 18–22S range, which equates to the complexes formed when NS2 was bound to RNA [154].

It was shown that WT NS2 forms 7-10S complexes in the absence of RNA, and 18-22S complexes in the presence of RNA, similar to published work, which is in contrast with an NS2.C mutant which has impaired RNA binding ability. It formed the typical 7-10S complexes in the absence of RNA and far fewer of the 18-22S complexes in the presence of RNA, with the remaining NS2.C retaining 7–10S form. The separation of NS2 complexes into two different oligomeric forms has previously been caused by the limiting of RNA to which the NS2 can bind [160], which suggested that the binding of RNA was a limiting factor of the formation of the larger oligomeric complexes.

The *in vitro* characterisation of NS2.C showed that the designed mutations severely impaired RNA binding compared to WT NS2. NS2.C oligomerisation was similar to WT NS2 in the absence of RNA but the impaired binding of RNA resulted in the formation of few of the larger 18–22S complexes in the presence of RNA, with the greatest

amount of NS2.C forming 7–10S complexes without RNA. When analysed with the *in vivo* characterisation of BTV-1 S8.C, which showed that the mutations delayed and reduced virus growth and effected VIB formation, it was clear that the C-terminal RNA binding domain is important in BTV replication and that binding of RNA in general is important in the efficient replication of the virus. Importantly, the delay in virus assembly but not production of component parts or the later rate of growth implied that the mutation in the ssRNA binding domain affected NS2s role in the concentration of viral components during assembly [153].

Chapter 6

Discussion and Conclusion

6.1 General discussion

This thesis aimed to map the role of NS2 RNA binding domains during virus replication. Both *in vivo* and *in vitro* investigations were undertaken to determine the degree of NS2-RNA interaction required for virus replication.

The NS2 coding region of 354 aa has three putative RNA binding regions dispersed throughout the N-terminal, C-terminal and middle region [158]. The N-terminal domain is located between 2–11 aa, the middle domain between 153 – 166 aa and the C-terminal domain between 274–286 aa. *E. coli* expressed, single deletion mutants BTV-17 $NS2_{2\text{-}11}$, BTV-17 $NS2_{153–166}$ and BTV-17 $NS2_{274–286}$ were used in non-BTV specific ssRNA EMSAs and all showed that the deletion mutants were less able to bind ssRNA compared to WT NS2 [158]. BTV-17 $NS2_{153–166}$ was described as having a higher affinity for RNA in the binding assays compared to the other deletion mutants, which suggests a less important role for this domain in the overall binding of RNA to NS2. Double deletion mutants and a triple deletion mutant to these putative regions were analysed and their ability to bind RNA explored [158]. It seemed that there was a degree of interaction between the three domains. A less important role for the 2–11 aa binding domain was described when examined as part of a double deletion mutant. Double deletion mutants BTV-17 $NS2_{2\text{-}11/153\text{-}166}$ and BTV-17 $NS2_{2\text{-}11/274\text{-}286}$ showed a greater affinity for RNA than the BTV-17 $NS2_{153\ \text{-}166/\ 274\text{-}286}$ mutant. The triple mutant was sufficient for a complete cessation of RNA binding.

The experiments in this thesis were undertaken to investigate the NS2 ssRNA binding

domain between residues 2 – 11, 153 – 166 and 274 – 286. The reverse genetics system developed in the lab was used to generate a BTV-1 mutant with specific mutations designed to disrupt RNA binding in this region. Both positively and negatively charged amino acids were considered as mutation candidates because only mutating the positively charged amino acids, likely to be involved in RNA binding, would result in the region having a net negative charge and possibly repel RNA. Due to the fact that the aim of this study was to examine the RNA binding of the three putative RNA binding domains, creating a region which could actively repel RNA would generate limited data.

Some amino acids were discounted from the mutation design due to proximity to a variable amino acid or a less clustered position, while E_2 was included in the design of the N-terminal domain mutant despite previously being shown not to be essential for RNA binding [158]. E_2 was included in the mutant so the putative RNA binding domain would have an overall neutral charge. The designed mutants substituted lysine, arginine and aspartic acids which have been shown to be involved in the binding nucleic acids [233 250].

The amino acid alignment of 26 serotypes of NS2, on which the mutational design was based, used mostly South African reference strains. This did not take into consideration the intra-serotype variation shown by the 'eastern' and 'western' topotypes. It could have been more representable of actual NS2 amino acid diversity if a split of eastern and western types was used. A wider comparison of NS2 variation may have identified other potential sites for mutation within the RNA binding regions.

In conjunction to the generation of mutant bluetongue viruses for the *in vivo* investigation of the RNA binding domains, identical NS2 mutants were produced with a recombinant baculovirus expression system. This recombinant purified protein allowed the *in vitro* study of the NS2 RNA binding domain mutants to further develop the findings of the *in vivo* study and to confirm that the mutations had not altered the overall protein structure, but instead targeted the function of specific domains.

6.1.1 The effects of the S8.N, S8.M and S8.C mutations on *in vivo* replication

The mutants were either generated by the reverse genetics system (BTV-1 S8.N and BTV-1 S8.C) or obtained from the lab (BTV-1 S8.M), confirmed through RT-PCR and sequencing to contain the designed alanine substitutions and characterised to explore the effects of the mutations on the growth of the virus and the formation of the VIBs.

Initial plaque assays of BTV-1 S8.M and BTV-1 S8.C demonstrated a distinct mutant plaque phenotype in BSR cells, which was smaller than those generated by WT BTV-1. BTV-1 S8.N showed no plaque formation in BSR cells, which was the first indication that the S8.N mutation was lethal. When these viruses were grown in the complementary cell line BSR-S8, the mutant plaque phenotype reverted to a WT BTV-1 plaque phenotype for all these mutant viruses. The differences demonstrated in plaque phenotype when compared to WT are most likely to be due to the mutations in the NS2 proteins, because plaque formation was reversed to a WT-like phenotype when a functional version of the NS2 protein was supplied *in trans* with the complementary cell line.

Plaque formation is an indication of virus growth but was incapable of providing detailed data on virus growth, because of this the growth kinetics were further investigated with a time course of virus growth and protein production. BTV-1 S8.N demonstrated a complete inhibition of growth in BSR cells. BTV-1 S8.M showed inhibited growth with maximum average tire of 3.3 $x10^6$ when compared to a maximum titre for WT BTV-1 grown in BSR (2.3 x 10^7) and BSR-S8 cells (2.5 $x10^7$). With this in mind, BTV-1 S8.C growth is more accurately described as a delay. A maximum titre of 8.3 x 10^6 demonstrated a slight reduction compared to WT (2.5 $x10^7$ and 2.3 x 10^7) but this was shown at 72 hpi whereas all the other maximum titres are at 36 hpi.

It has previously been published that the titre of WT BTV infection of BSR cells decreases at 2 hpi compared to initial infection [73]. 2 hpi was not analysed, but it could be presumed that the initial decrease in the S8.M and S8.C mutants' titre was an extension of this initial decrease. The initial delay in virus growth affected the overall growth of BTV-1 S8.M with titres (3.3 $x10^6$) never reaching the maximum titre seen in the WT BTV (2.5 $x10^7$ and 2.3 x 10^7), while the delay was continued throughout the time course for BTV-1 S8.C which demonstrated a the maximum titre at 72 hpi compared to 36 hpi. This reduction may be due to BSR cells being infected at almost 100 % confluence, and thus at 36 hours post infection the cells would be overgrown and not replicating as efficiently, limiting the replication.

As with the plaque phenotypes described above, mutant BTV-1 S8 growth in BSR-S8 cells reverted to similar levels as WT BTV due to the presence of functional NS2

supplied by the complementary cells. To further characterise the mutant's replication *in vivo*, protein samples were taken in parallel to the growth curve.

Differences in protein production of WT and the BTV-1 S8.M and BTV-1 S8.C mutants were detected between the time points but no major deficiencies in overall levels of protein production were detected in comparison to the lysate from WT infected cells, similar to that which was reported previously [73]. The differences in the time of protein production reflected the growth curves of the viruses. The protein analysis would show constantly reduced levels of protein if the reduction in growth was due to impairment in protein production. This is not the case because while protein production was delayed for all three of the proteins studied; the level of NS2 production was similar between WT and the mutants. Levels of NS1 and VP5 were reduced but this could be because the lower titre of mutant virus produces less protein. The western blot analysis also showed that BTV-1 S8.M and BTV-1 S8.C NS2 was recognised by a specific anti-BTV-10 NS2 antibody and was indistinguishable in size and antigenicity to wild-type BTV. NS2 protein was detected higher than the 42kDa published because it is phosphorylated and forms multimers; both of which are factors which can contribute to the actual band size differing from that predicted [154,162].

The fact that the largest increases in growth rate were seen for BTV-1 S8.M (2.5 log increase) and BTV-1 S8.C (2 log increase) at 16 hpi in BSR cells implied that the mutations the these regions did not adversely affect the rate of growth but instead, given NS2s role in the concentration of RNA and core protein during assembly [153], retards the assembly of progeny virus. This possibly allowed the component viral

structural proteins and RNA to reach such copious levels within the cell that once the retardation is overcome; there was no delay in assembly which resulted in the high growth rates shown. The exact mechanism of this must be further investigated within this thesis.

The mutation in BTV-1 S8.N however, significantly impaired growth as shown by the lack of plaques or protein to detectable levels in BSR cells. This suggested that the BTV-1 S8.N mutation had a substantial effect which is not overcome later in infection, unlike BTV-1 S8.M and BTV-1 S8.C; and supported the findings that a functional NS2 is essential for replication [153].

As the RNA binding mutations have been shown to delay virus assembly and significantly impair overall growth, an immuno fluorescence assay was undertaken to visualise and analyse the VIBs produced. This was done to investigate if the mutants formed different VIBs compared to WT. VIBs were examined because they are predominantly composed of NS2 and are the sites of immature progeny virus assembly. The labelling and fluorescence of viral structural protein VP7 demonstrated that WT BTV-1 and all three of the mutants were present within the BSR cells.

Labelling of NS2 visualised VIBs, BTV-1 formed VIBs comparable to those previously published [150]. BTV VIBs are often described as having a perinuclear location late in infection[133,148,152]. The images described here however, displayed WT and mutant VIBs throughout the cytoplasm. It is most clearly demonstrated in the mutant virus images but also in the WT BTV-1 infections. If this general cytoplasmic distribution was just attributed to the mutants it could be explained as a possible phenotypic difference but

it was also present in the positive control of WT BTV-1. The distribution displayed was more cytoplasmic, like that of a Negri body produced in Rabies virus infection [251]. BTV-1 S8.N was also shown to occasionally not form the typical, distinct, punctuate VIB structures; instead a diffuse staining of NS2 was observed which, as VIBs are the sites of core assembly, could account for the impairment in growth.

Visual inspection of the images indicated the mutant viruses formed VIBs which were both smaller in size and fewer in number when compared to WT BTV-1 VIBs. The following quantification revealed that WT BTV-1 infection of BSR cells at MOI 10 produced an average of 257 VIBs per frame with an average size of 1.38 μm^2, while collectively the mutants are fewer and smaller.

On average BTV-1 S8.N produced the smallest and fewest VIBS at 45 VIBs per frame with an average size of 0.78 μm^2. Compared to WT BTV-1 this was an 82% reduction in total number of VIBs and a 43% reduction in VIB size. Under the same conditions BTV-1 S8.M produced an average of 88 VIBs (66% reduction in number) with an average size of 1.05 μm^2 (25% reduction in VIB size). BTV-1 S8.C produced slightly fewer VIB than BTV-1 S8.M at 80 VIBs, a 69% reduction compared to WT. The average size of those VIBs was however, slightly larger than those produced by BTV-1 S8.M. The average size of BTV-1 S8.C VIB was 1.07 μm^2 which was 23 % reduction in VIB size compared to WT. BTV-1 S8.C also has a higher maximum titre (8.3 $x10^6$) than BTV-1 S8.M (3.3 $x10^6$) which could indicate that the size of the VIBs is more important than the quantity during replication.

Previous characterisation of BTV VIBs [148] showed that the average size of VIB was 1.1 μm^2 at 24 hpi, which was closer to the average size of BTV-1 S8.M (1.05 μm^2) and BTV-1 S8.C (1.07 μm^2) VIBs than BTV-1 VIBs (1.38 μm^2). Both investigations used the same MOI 10 but Brookes *et al* (1993) used SVP cells derived from porcine stable (PS) cells [244] rather than BSR cells, also this thesis analysed considerably more structures. The previous study used electron micrographs to measure the VIBs. The samples were fixed and stained which would have altered the size of the VIBs. It was probably the large sample size and more accurate computer measurement of this thesis which is the reason for this difference.

The maximum size of VIB varied greatly within the same virus infection type. This was shown by the large upper and lower confidence levels of the WT and mutant maximum size graphs. The maximum size of VIB also differed greatly between WT BTV-1 and the mutants. The BTV-1 average maximum VIB size was 19.66 μm^2, which is far larger than the average maximum VIB size for BTV-1 S8.M (7.48 μm^2) and BTV-1 S8.C (7.22 μm^2). The smallest maximum VIB size was 4.36 μm^2 for BTV-1 S8.N, a 40 % reduction compared to the other mutants. The minimum size for WT BTV-1, BTV-1 S8.N, BTV-1 S8.M and BTV-1 S8.C VIBs were very similar at 0.12 μm^2, 0.11 μm^2, 0.13 μm^2 and 0.13 μm^2, respectively and as such might represent the minimal structure detectable or the minimal structure of a VIB.

VIBs size, location and number is dynamic and changes throughout infection [148,240]. It has been reported previously that a greater number of inclusion bodes are seen early in infection, these then fuse to form fewer but larger bodies over time. The work

described here is a characterisation of VIB size and number at a specific time post infection. Due to the dynamic nature of VIBs, the differences displayed between WT and the mutants, and those shown between the mutants, were unable to confirm if this was transient or a true depiction of phenotype throughout infection. If this was a true depiction of phenotype it could be reasoned that RNA binding was important for VIB formation because when RNA binding was impaired, the resulting VIBs are smaller and fewer in number.

This data demonstrated the N-terminal RNA binding domain is more important in VIB formation than the middle domain and the C-terminal domain because the BTV-1 S8.N mutation resulted in considerably smaller and fewer VIBs. There was a correlation between VIB size and number, and replication. Given that VIBs are the sites of assembly this was not surprising.

The *in vivo* characterisation of the NS2 RNA binding mutants BTV-1 S8.N, BTV-1 S8.M and BTV-1 S8.C revealed significant differences in virus growth and VIBs formation, both between the mutants and WT BTV-1 and between the three mutants.

BTV-1 S8.N was the mutant most significantly affected. It demonstrated no detectable replication or protein production in BSR cells, which could be due to the differences seen in the VIBs. BTV-1 S8.N sometimes did not form the typical punctuate VIBs structures, instead a diffuse visualisation of NS2 was observed. When VIBs were formed they were 43% smaller and 82% fewer than WT which could be an essential factor in replication.

The BTV-1 S8.M mutant showed that the designed mutations affected virus growth and VIB formation. The growth was retarded early in infection which resulted in a lower maximum virus titre than WT but did not adversely affect the rate of virus replication or protein production. The delay in virus assembly but not production of component parts could be due to the differences seen in the VIBs, which are the sites of virus assembly. The 66 % fewer and 25% smaller VIBs could be a limiting factor early in replication.

BTV-1 S8.C was very similar to BTV-1 S8.M in both levels of virus growth and VIB formation. BTV-1 S8.C differ from BTV-1 S8.M however in that the growth was retarded early in infection which resulted in a 36 hour delay in maximum virus titre. This did not adversely affect the rate of virus replication or virus protein synthesis. This delay in virus assembly but not rate of replication could also be due to the differences seen in the VIBs which were 23% smaller and 70 % fewer.

6.1.2 The effects of the NS2.N, NS2.M and NS2.C mutations *in vitro*

The *in vivo* data clearly showed that the mutations in the RNA binding domains were affecting virus growth and VIB formation but it required further investigation in order to associate these changes with impairment in RNA binding, rather than a structural change. *In vitro* studies were performed in order to clarify if the mutations were affecting RNA binding as they were designed to do or if this was due to a structural change. Also the effect of the mutations on NS2 oligomerisation was investigated. It has been proposed that NS2 requires RNA to act either an initiator or as a supporting

scaffold to form the larger NS2 multimers. If RNA is required to form the large NS2 multimers, an impairment in RNA binding would produce smaller protein oligomers.

In vitro investigation required the generation of a recombinant baculoviruses expressing WT NS2 and the RNA binding mutants discussed above. The previous study of NS2 binding sites were performed in *E. coli*, which although is cost effective and quick, has the inherent limitations of prokaryotic expression. The baculovirus expression system was chosen because of the post-translational modifications conferred by mammalian eukaryotic cells, the reliability of successful recombination and high levels of protein production. Baculovirus expression ensures that the proteins would be phosphorylated, which is essential for NS2 because phosphorylation is essential for VIB formation [151]. An In-Fusion cloning method was also chosen for the generation of the transfer plasmids: pAcYM1-H/GST NS2.N, pAcYM1-H/GST NS2.M and pAcYM1-H/GST NS2.C, and resulted in the generation and selection of colonies with 100% containing the expected insert.

The production of NS2.N, NS2.M and NS2.C by the selected recombinant viruses was initially confirmed via the detection of a band at 65kDa, the correct size for the expression of NS2 with His/GST tags attached to the 5' end via a flexible linker. Trial purification of two of the three proteins (NS2.N and NS2.C) using the His and GST tags failed to produce any purified protein. Further investigation using western immuno blot and a specific NS2 antibody, revealed a protein band at 42kDa and thus the absence of the tags. The 65 kDa band detected was probably baculovirus protein GP64, an envelope fusion protein [246] which is produced to high levels during infection and has

a size of 65 kDa[247]. The addition of uninfected cell and baculovirus only infected cell controls would have made identification of these false positive bands easier.

Other members of the lab also obtained a similar loss of purification tags from this plasmid (personal communication). This is possibly due to repeats in the flexible sequence linking the tags and the protein of interest the large size of the tag. Protein bands were detected at ~25 kDa in the purified NS2.N and NS2.C samples. This band was also present in the western blots, which due to the specific nature of the NS2 antibody suggested it was most likely a degradation product, despite the use of protease inhibitors during the purification process. The C-terminal domain of NS2 has previously been shown to degrade rapidly at 4 °C, both with and without a protease inhibitor, to produce a major degradation product of 25 kDa and smaller fragments [159]. AcMNPV YM1-H/GST NS2.M retained the His and GST tags and purification was undertaken with Ni and GST beads.

All protein samples were RNaseA treated overnight prior to purification. Without RNase treatment the protein would remain bound to RNA which would interfere with the planned RNA binding assays and oligomerisation assays.

All mutant proteins were soluble, which was an indication that the inserted mutations had not affected the overall structure. This in turn confirmed that the differences displayed when compared to WT were due to a functional deficiency, rather than a structural one.

WT controls of AcMNPV YM1-H/GST NS2 and AcMNPV BTV-10 NS2 were purified by His/GST bead purification and HiTrap Q HP anion exchange column, respectively. These

purified proteins were used as comparison controls for the mutant proteins purified in the same way to eliminate any variation in the purification process.

All proteins were purified to at least 2 µg/µl quantities. Even at these high levels, WT NS2, NS2.N, NS2.M and NS2.C did not form aggregates. This is unlike previously reported attempts of NS2 purification, which resulted in aggregates of full-length NS2 with concentrations higher than 2 µg/µl [159].

Each of the mutants was designed to impair a specific RNA binding region. To investigate this, an electrophoretic mobility shift assay was undertaken. An EMSA was chosen because it has previously been successfully used to show NS2-RNA binding [160,161]. The initial EMSAs for all the RNA binding mutants were performed with 1, 5, 10 and 15 µg which demonstrated that 15 µg WT NS2 purified by His/GST bead purification and HiTrap Q HP anion exchange column was sufficient to bind 97–99 % of the RNA present and to visually result in a complete shift of all RNA to a bound position. The variation seen between 97% and 99% binding efficiency was found within the HiTrap Q HP anion exchange column purified WT NS2 and not between different purification methods. The variation was probably due to quantification error because visual analysis showed a complete shift and all variables remained the same between the assays. Generally, the two purification methods for WT NS2 resulted in similar gel shifts. This showed that the different purification methods had little effect on subsequent RNA binding and that the mutants purified by these methods could similarly be compared accurately. The only slight variation between purification methods was shown at 10 µg which was quantified to shift 30% of the His/GST bead

purified NS2 while the HiTrap Q HP anion exchange column purified NS2 shifted 31% of the RNA. An approximate margin of error of +/- 2 % could therefore be applied in the current absence of assay repeats but all the WT controls were sufficiently similar that all results were able to be compared with each other.

When this +/- 2 % margin of error is applied to NS2.M and NS2.C it showed that the two mutants demonstrated reduced BTV specific ssRNA binding to similar levels. 15 µg of NS2.M and NS2.C was able to bind 10% and 8%, respectively while WT shifted 99% of the RNA present. This was an overall reduction of approximately 90% which confirmed that the designed mutations have the intended effect of disrupting RNA binding.

In contrast to 15 µg NS2.M and NS2.C, 15 µg NS2.N was insufficient to bind any of the RNA. This was further investigated by increasing the concentration of NS2.N and WT NS2 to 25 µg. Quantification 25 µg NS2.N suggested that the mutant was able to bind RNA with 1% of the RNA in the bound position. Given the margin of error of +/-2 % this could be a false positive. Close examination of the EMSA image showed no binding of ssRNA. This indicated that the mutation in the N-terminal domain has abrogated the NS2 BTV specific ssRNA binding. The mutations in the middle domain and the C-terminal domain resulted in a large decrease in RNA binding but not as substantial as the N-terminal mutants. This result was partially similar to the findings of Zhao *et al* 1994 [231] in that the N-terminal was identified as important for ssRNA binding and these findings indicated that NS2.N is the most important RNA binding region. This data however, demonstrated that other domains are also involved in RNA binding but to a

lesser degree; whilst Zhao *et al* 1994 specified that the C-terminal was not at all involved in RNA binding. The work described here supported the presence of three RNA binding domains [158] but disagreed on the relative importance of each domain. The variations between the findings here and those of Fillmore *et al* (2002) could be due to differences in the experimental methods. This work focused on specific BTV ssRNA binding while Fillmore *et al* (2002) used general ssRNA size markers or yeast RNA.

The differences demonstrated in domain importance could reflect a role of the N-terminal RNA binding domain in BTV ssRNA specificity.

It was suggested that oligomerisation of NS2 was triggered by the binding of RNA [151]. An exploration of this hypothesis using the three RNA binding mutants has generated novel data on the extent of RNA importance during NS2 oligomerisation. NS2 forms large homomultimers but the exact oligomeric form of NS2 is disputed [154,160,168] or could vary. In order to investigate this, the oligomerisation of the three RNA binding mutants: NS2.N, NS2.M and NS2.C; and WT NS2 were studied by sedimentation analysis in the presence and absence of RNA.

WT NS2 was predominantly detected in fraction 4 which equates to 7S complexes, but NS2 is also present in large amounts in fraction 5 (~8S). This strongly supports the previous reports of a 7S complex comprised of 6 copies of 42 kDa baculovirus expressed NS2 [167], and partially supports the published 8-10S complexes of 6 (+/-2) copies of bacterially expressed NS2. This is maintained throughout the *Reoviridae* family with NS2 homologs also forming 7S minimal complexes [167]. The addition of RNA was shown to form larger NS2 complexes found in fractions 9–12 forming 18–22S

complexes of NS2, this is a verification of previously published work which found that BTV-1 NS2 forms a variety of larger complexes in the presence of RNA [154]. The strongest signal indicated in this thesis was from fraction 11 indicating predominantly 20 – 22S complexes which aligns closer to the findings of Huismans *et al* 1987 [160].It has been suggested that 8 – 10S (140 – 152 kDa) would consist of 6 (+/-2) units of NS2 [154], which is contradictory to the proposed structure of NS2 which indicated that the full-length protein could assemble as multimers of 10–11 subunits to form ring-like structures [168], but somewhat similar to P9-1 Rice Black Streak Dwarf Virus (RBSDV) [171] and NSP2 Rotavirus [172], which have low sequence homology but form oligomers in ring-like structures as NS2 is reported to do.

In the absence of RNA all three of the mutants were predominantly detected in fractions 4, 5 and 6 which equates to 7 - 10S complexes or 6 (+/-2) copies of bacterially expressed NS2 this was similar to the NS2 complexes formed by WT NS2 and the previously published work [154,167]. Some protein was also detected in fractions 3 and 7 but this is minimal compared to the majority of the protein. This data confirmed that the mutations had not greatly altered the overall protein structure.

The addition of RNA demonstrated differences between the NS2.N complexes and WT NS2. NS2.N complexes were found in fractions 3 – 7 (5 – 12S). The quantification of the gels showed that these complexes were predominantly found in fractions 4 and 5 (7 – 8S) which is similar to the size seen without RNA. Some larger complexes were detected in fractions 7 and 8 (11-12S) by the addition of RNA which are not present in samples without RNA but these were at a far lower intensity. Generally there was no

difference in the NS2.N multimers formed in either the presence or absence of. The severe RNA binding impairment of NS2.N demonstrated in the EMSAs was shown here as an absence of the large homomultimers.

NS2.M and NS2.C formed complexes which were notably different from both NS2.N and WT NS2. The addition of RNA formed a wide range of NS2.M and NS2.C complexes, these were identified in fractions 3–12 (6–22S). The quantification of the gels showed that these complexes fall into two groups: the largest group of complexes fall within 6–10S, which was typical of NS2 unbound to RNA; and a second, smaller group of complexes in the 18–22S range, which equated to the complexes formed when NS2 is bound to RNA.

The reduction in the ability of NS2.M and NS2.C to bind RNA seen in the EMSAs is illustrated here by the formation of a fewer 18–22S complexes compared to WT. The remaining NS2.M or NS2.C retains a smaller, unbound 7–10S form. The separation of NS2 complexes into two different oligomeric forms had previously been caused by the limiting of RNA from which the NS2 can bind to [160]. This suggests that the binding of RNA is a limiting factor of the formation of the larger oligomeric complexes.

The work undertaken here has not clarified if the oligomerisation of NS2 is triggered by the binding of RNA or if RNA binding simply supports larger structures. It has shown that the addition of RNA results in larger NS2 complexes and that an RNA binding impairment forms fewer of these large complexes. Most notably, a severe deficiency in RNA binding resulted in none of the large homomultimers; indicating that the binding of RNA is essential for their formation.

The *in vitro* characterisation of NS2.N showed that the designed mutations severely compromised the proteins ability to bind RNA compared to WT NS2. 25 µg NS2.N was unable to bind 1% of the RNA while 15 µg WT NS2 was sufficient to bind 97%. NS2.N oligomerisation was normal in the absence of RNA. The mutation impaired binding of RNA which resulted in no difference in complexes formed in the presence of RNA, with the greatest amount of NS2.N forming 7 – 8S complexes with and without RNA.

The *in vitro* characterisation of NS2.M revealed that the mutations severely impaired RNA binding as it was designed to do. 15 µg NS2.M was able to bind 10 % of the RNA while 15 µg WT NS2 was sufficient to bind 99 %. NS2.M oligomerisation was normal in the absence of RNA but the mutations and the impaired binding of RNA resulted in the formation of few of the larger 18 – 22S complexes in the presence of RNA, with the greatest amount of NS2.M forming 7 – 10S complexes without RNA.

The *in vitro* characterisation of NS2.C showed that the designed mutations severely impaired RNA binding compared to WT NS2 with 15 µg NS2.C able to bind 8 % of the RNA while 15 µg WT NS2 was sufficient to bind 99 % of the RNA. NS2.C oligomerisation was normal in the absence of RNA but the mutations and the impairment of RNA binding resulted in the formation of few of the larger 18 – 22S complexes in the presence of RNA, with the greatest amount of NS2.C forming 7 – 10S complexes without RNA.

6.2 Conclusion

This thesis describes the first *in vivo* and *in vitro* investigation into NS2, a key protein involved in BTV replication and assembly. This dual investigation into the RNA binding domains of NS2 through the generation of alanine substitution mutants has not only characterised the individual RNA binding domains, but also produced new data on the relevance of each domain during BTV assembly. It was only through the *in vivo* study of the effect on virus growth coupled with the *in vitro* study of the effect on NS2, that a complete explanation could be generated.

The middle domain and C-terminal domain mutants showed a reduction in BTV specific ssRNA binding ability which is proposed to result in the reduction of virus growth shown for both mutants. This could be due to BTV RNA being essential for virus assembly *in vivo*. Alternatively, the binding of ssRNA is necessary to stabilise the NS2 oligomerisation and formation of VIBs; VIBs act as concentrators and as such this function may be essential.

It was shown by the EMSAs that the middle domain and C-terminal domain mutants were able to bind BTV specific ssRNA, but this is seen at higher concentrations than needed by WT NS2. The mutations in the N-terminal domain however result in a complete abrogation of BTV ssRNA binding. Through the comparison of this data with WT, NS2.M andNS2.C, it was suggested that the N-terminal domain was responsible for the specific binding of BTV ssRNA. NS2 also has non-specific RNA binding which, given their less important effect on growth and VIB formation, could be located in the middle and C-terminal domains.

The data generated here would seem to support the previous work which linked the N-terminal with RNA binding [231]. It is worth considering however that the BTV-1 S8.N mutant substitutes all the charged amino acids within the domain, while BTV-1 S8.M and BTV-1 S8.C substitutes only a portion which could explain the differences indicated here. BTV-1 S8.M and BTV-1 S8.C have different numbers of charged amino acids which were omitted from the mutant design but displayed very similar results in all investigations which suggests that effects described here are not dependant on number of residues that were not mutated.

It is possible that NS2's role as a viral component concentrator during replication is linked to the formation or size of the VIB's as the sites of core formation. When RNA binding is impaired (as with the Middle domain and C-terminal mutants), oligomerisation is reduced and the resulting VIB's are smaller and fewer. This mutant VIB phenotype is less able to concentrate all the viral components needed for effective replication and results in the BTV-1 S8.M and BTV-1 S8.C impaired replication. The more severe growth defects of BTV-1 S8.N could be due to its potential role as the site of BTV-specific ssRNA binding and the essential nature of BTV ssRNA during virus replication. All the experiments described within this thesis used BTV-specific ssRNA and BTV-1 S8.N was unable to bind any of the RNA.

The work described within this thesis could not clarify if RNA binding triggers oligomerisation through acting as a supporting scaffold as previously proposed. It is unlikely that the mutations directly affect oligomerisation because the different mutations of NS2.M and NS2.C do generate the larger oligomeric structures formed by

WT, but at a lower proportion similar to the lower proportion of RNA binding exhibited by the NS2.M and NS2.C mutants. NS2.N is unable to bind RNA or form large oligomers but further work investigating the structure is needed to fully demonstrate that this is not due to a change in secondary structure or an unknown essential NS2-NS2 oligomerisation site.

This thesis has confirmed that NS2 contains 3 RNA binding sites and suggests that the N-terminal domain is BTV ssRNA specific. It employed a unique *in vivo* and *in vitro* approach to link actual WT and mutant virus growth with the potential molecular mechanisms behind them. It expands on previous studies which suggested that NS2 oligomerisation is triggered by RNA binding through the generation of RNA binding mutants and comparison with WT oligomerisation.

6.3 Future research

Further work using the BTV-1 S8.N, BTV-1 S8.M and BTV-1 S8.C mutants could include live cell imaging. A recently developed tagged virus has permitted the visualisation of BTV in live cell infection [185]. By using this virus as a positive WT control and generating BTV-1 S8.N, BTV-1 S8.M and BTV-1 S8.C viruses with the tag, it would be possible to visualise where the viruses are located during infection and identify the differences in replication. Another option would be to perform Immuno fluorescence assays (IFAs) with labelled RNA. This would further support the EMSA data generated here and visually show the locations and interactions of RNA with the mutants.

Given the large amounts of pure full-length WT NS2 generated by both recombinant baculoviruses AcMNPV YM1-H/GST NS2 and AcMNPV BTV-10 S8, crystallography could be undertaken to elucidate the structure of full-length NS2. Previously published work focused on the N-terminal and C-terminal separately and made the assumption that these two domains would not form difference structures when expressed separately [168]. The purified WT NS2 showed minimal degradation products and did not form aggregates, both of which have previously inhibited the study of the crystal structure on NS2.

One of the main areas of future work would be the expansion of the current investigation to include all the charged amino acids found in the middle and C-terminal RNA binding domains. Currently, some were omitted from the mutation design which has led to a limited ability to identify if the different domains have different relevance during replication.

The generation of mutants spanning the complete domains could identify if a single region is responsible for BTV RNA specificity through the use of competitive EMSAs with BTV specific and non-BTV ssRNA. Investigations with these mutations could reveal if the domains are involved in BTV segment selection. RNA segments have been shown to contain secondary structures [156] but the individual domains role in segment selection has yet to be investigated. Alternatively, it could definitively show if one domain is more important in the binding of RNA, which is currently debated [158,231].

Also of interest would be the generation of a triple mutant which was previously shown to be needed for complete elimination of the binding of RNA by NS2 [158]. This is dissimilar to the data described here, which showed that mutation of the N-terminal domain was sufficient to effectively eliminate RNA binding.

Phosphorylation is essential for VIB formation but not necessary for RNA binding [151]. Amino acids S_{249} and S_{259} have been identified as the sites of NS2 phosphorylation and as such will be the target of mutations. Mutants could be characterised and the effect on NS2 oligomerisation, VIB formation and BTV replication and assembly examined with *in vivo* and *in vitro* investigation.

Currently, the NTPase activity domain of NS2 have not been identified although it has been shown not to be located in the first 177aa due to previous mutational work which reported that NS2 missing this portion was still able to hydrolyse NTP'S [237]. A series of deletion mutants could be used to map this domain. This could be followed by an investigation using the method described here to potentially reveal if NTPase activity is essential for virus replication.

An in depth understanding of the mechanisms involved in VIB formation, viral component sequestration, RNA segment selection, assembly and release of core particles from the VIBs could be used to design a new vaccine. BTV is the prototype virus of the *Orbivirus* genus, information gained here could be used as the basis for further studies in related viruses.

References

1. Mellor, P. S. & Boorman, J. The transmission and geographical spread of African horse sickness and bluetongue viruses. *Ann. Trop. Med. Parasitol.* **89,** 1–15 (1995).

2. Gorman, B. M. The bluetongue viruses. *Curr. Top. Microbiol. Immunol.* **162,** 1–19 (1990).

3. Elbers, A. R. W. *et al.* Field observations during the bluetongue serotype 8 epidemic in 2006. I. Detection of first outbreaks and clinical signs in sheep and cattle in Belgium, France and the Netherlands. *Prev. Vet. Med.* **87,** 21–30 (2008).

4. Alexander, K. A. *et al.* Evidence of natural bluetongue virus infection among African carnivores. *Am. J. Trop. Med. Hyg.* **51,** 568–76 (1994).

5. *Fields' Virology, Volume 2*. (Lippincott Williams & Wilkins, 2001). at <http://books.google.com/books?id=NH_KoAEACAAJ&pgis=1>

6. Maan, S. *et al.* Analysis and phylogenetic comparisons of full-length VP2 genes of the 24 bluetongue virus serotypes. *J. Gen. Virol.* **88,** 621–30 (2007).

7. Hofmann, M. A. *et al.* Genetic characterization of toggenburg orbivirus, a new bluetongue virus, from goats, Switzerland. *Emerg. Infect. Dis.* **14,** 1855–61 (2008).

8. Maan, S. *et al.* Novel bluetongue virus serotype from Kuwait. *Emerg. Infect. Dis.* **17,** 886–9 (2011).

9. Jenckel, M. *et al.* Complete coding genome sequence of putative novel bluetongue virus serotype 27. *Genome Announc.* **3,** (2015).

10. OIE. OIE Technical Disease Cards Bluetongue. (2014). at <http://www.oie.int/fileadmin/Home/eng/Animal_Health_in_the_World/docs/pdf/Disease_cards/BLUETONGUE.pdf>

11. Mellor, P. S. & Wittmann, E. J. Bluetongue virus in the Mediterranean Basin 1998-2001. *Vet. J.* **164,** 20–37 (2002).

12. Calistri, P., Goffredo, M., Caporale, V. & Meiswinkel, R. The distribution of Culicoides imicola in Italy: application and evaluation of current Mediterranean models based on climate. *J. Vet. Med. B. Infect. Dis. Vet. Public Health* **50,** 132–8 (2003).

13. Commission, E. Bluetongue. at <http://ec.europa.eu/food/animal/diseases/controlmeasures/bluetongue_en.htm>

14. Webb, D. *The economic and social impact of the Institute for Animal Health*"*s work on Bluetongue disease (BTV - 8)*. (2008). at <http://www.pirbright.ac.uk/ecosoc/docs/Blue-Tongue-case-study.pdf>

15. SABIN, A. B. Reoviruses. A new group of respiratory and enteric viruses formerly classified as ECHO type 10 is described. *Science* **130,** 1387–9 (1959).

16. Attoui, H. *et al.* Expansion of family Reoviridae to include nine-segmented dsRNA viruses: isolation and characterization of a new virus designated Aedes pseudoscutellaris reovirus assigned to a proposed genus (Dinovernavirus). *Virology* **343,** 212–23 (2005).

17. Attoui, H. *et al.* Common evolutionary origin of aquareoviruses and orthoreoviruses revealed by genome characterization of Golden shiner reovirus, Grass carp reovirus, Striped bass reovirus and golden ide reovirus (genus Aquareovirus, family Reoviridae). *J. Gen. Virol.* **83,** 1941–1951 (2002).

18. Kapoor, A. *et al.* A novel mosquito-borne Orbivirus species found in South-east Asia. *J. Gen. Virol.* **94,** 1051–7 (2013).

19. Estes, M. K. & Cohen, J. Rotavirus gene structure and function. *Microbiol. Mol. Biol. Rev.* **53,** 410–449 (1989).

20. Murphy, F. A., Coleman, P. H., Harrison, A. K. & Gary, G. W. Colorado tick fever virus: An electron microscopic study. *Virology* **35,** 28–40 (1968).

21. Carstens, E. B. Ratification vote on taxonomic proposals to the International Committee on Taxonomy of Viruses (2009). *Arch. Virol.* **155,** 133–46 (2010).

22. ICTV Virus Taxonomy 2009. *Virus Taxonomy:2009 Release* (2009). at <http://ictvonline.org/virusTaxonomy.asp?msl_id=25>

23. Mellor, P. S., Baylis, M. & Mertens, P. P. C. *Bluetongue*. *Bluetongue* (Elsevier, 2009). doi:10.1016/B978-012369368-6.50001-0

24. *Virus Taxonomy*. *Virus Taxonomy* (Elsevier, 2012). doi:10.1016/B978-0-12-384684-6.00051-3

25. Maan, S. *et al.* Analysis and phylogenetic comparisons of full-length VP2 genes of the 24 bluetongue virus serotypes. *J. Gen. Virol.* **88,** 621–30 (2007).

26. OIE. OIE Technical Disease Cards African Horse Virus Sickness. (2014). at <http://www.oie.int/fileadmin/Home/eng/Animal_Health_in_the_World/docs/pdf/Disease_cards/AFRICAN_HORSE_SICKNESS.pdf>

27. Sánchez-Vizcaíno, J. M. Control and eradication of African horse sickness with vaccine. *Dev. Biol. (Basel).* **119,** 255–8 (2004).

28. Shope, R. E., Macnamara, L. G. & Mangold, R. A VIRUS-INDUCED EPIZOOTIC HEMORRHAGIC DISEASE OF THE VIRGINIA WHITE-TAILED DEER (ODOCOILEUS VIRGINIANUS). *J. Exp. Med.* **111,** 155–70 (1960).

29. Omori, T., Inaba, Y., Morimoto, T., Tanaka, Y. & Ishitani, R. Ibaraki virus, an agent of epizootic disease of cattle resembling bluetongue. I. Epidemiologic, clinical and pathologic observations and experimental transmission to calves. *Jpn. J. Microbiol.* **13,** 139–57 (1969).

30. Ruder, M. G. *et al.* Susceptibility of white-tailed deer (Odocoileus virginianus) to experimental infection with epizootic hemorrhagic disease virus serotype 7. *J. Wildl. Dis.* **48,** 676–85 (2012).

31. HOUSE, C., SHIPMAN, L. D. & WEYBRIGHT, G. Serological Diagnosis of Epizootic Hemorrhagic Disease in Cattle in the USA with Lesions Suggestive of Vesicular Disease. *Ann. N. Y. Acad. Sci.* **849,** 497–500 (1998).

32. Hamblin, C., Salt, J. S., Graham, S. D., Hopwood, K. & Wade-Evans, A. M. Bluetongue virus serotypes 1 and 3 infection in Poll Dorset sheep. *Aust. Vet. J.* **76,** 622–9 (1998).

33. Walker, A. R. & Davies, F. G. A preliminary survey of the epidemiology of bluetongue in Kenya. *J. Hyg. (Lond).* **69,** 47–60 (1971).

34. Gibbs, E. P., Lawman, M. J. & Herniman, K. A. Preliminary observations on transplacental infection of bluetongue virus in sheep-a possible overwintering mechanism. *Res. Vet. Sci.* **27,** 118–20 (1979).

35. Darpel, K. E. *et al.* Transplacental transmission of bluetongue virus 8 in cattle, UK. *Emerg. Infect. Dis.* **15,** 2025–8 (2009).

36. Van der Sluijs, M. *et al.* Transplacental transmission of Bluetongue virus serotype 8 in ewes in early and mid gestation. *Vet. Microbiol.* **149,** 113–25 (2011).

37. Richardson, C., Taylor, W. P., Terlecki, S. & Gibbs, E. P. Observations on transplacental infection with bluetongue virus in sheep. *Am. J. Vet. Res.* **46,** 1912–22 (1985).

38. Nusinovici, S., Souty, C., Seegers, H., Beaudeau, F. & Fourichon, C. Decrease in milk yield associated with exposure to bluetongue virus serotype 8 in cattle herds. *J. Dairy Sci.* **96,** 877–88 (2013).

39. Nusinovici, S., Monestiez, P., Seegers, H., Beaudeau, F. & Fourichon, C. Using animal performance data to evidence the under-reporting of case herds during an epizootic: application to an outbreak of bluetongue in cattle. *PLoS One* **9,** e100137 (2014).

40. Gould, A. R. The complete nucleotide sequence of bluetongue virus serotype l RNA3 and a comparison with other geographic serotypes from Australia, South Africa and the United States of America, and with other orbivirus isolates. *Virus Res.* **7,** 169–183 (1987).

41. Maan, S. *et al.* Analysis and phylogenetic comparisons of full-length VP2 genes of the 24 bluetongue virus serotypes. *J. Gen. Virol.* **88,** 621–30 (2007).

42. Mertens, P. P. C. *et al.* Design of primers and use of RT-PCR assays for typing European bluetongue virus isolates: differentiation of field and vaccine strains. *J. Gen. Virol.* **88,** 2811–23 (2007).

43. Mertens, P. P. C., Attoui, H. & Bamford, D. H. The geographical distribution of different BTV serotypes. *reoviridae.org* at <http://www.reoviridae.org/dsrna_virus_proteins/btv-serotype-distribution.htm>

44. Mehlhorn, H. *et al.* First occurrence of Culicoides obsoletus-transmitted Bluetongue virus epidemic in Central Europe. *Parasitol. Res.* **101,** 219–28 (2007).

45. Caracappa, S. *et al.* Identification of a novel bluetongue virus vector species of Culicoides in Sicily. *Vet. Rec.* **153,** 71–4 (2003).

46. Osmani, A. *et al.* Evidence for the presence of bluetongue virus in Kosovo between 2001 and 2004. *Vet. Rec.* **158,** 393–6 (2006).

47. Slingenbergh, J. I., Gilbert, M., de Balogh, K. I. & Wint, W. Ecological sources of zoonotic diseases. *Rev. Sci. Tech.* **23,** 467–84 (2004).

48. N.J. Knowles and P.R. Davies. *Origin of recent outbreaks of foot-and-mouth disease in North Africa, the Middle East and Europe*. (2000). at <http://www.fao.org/ag/againfo/commissions/docs/research_group/borovet/app03.pdf>

49. Losson, B. *et al.* Biting midges overwintering in Belgium. *Vet. Rec.* **160,** 451–2 (2007).

50. International Society for Infectious Diseases. *Bluetongue—Europe (14): BTV-8, Germany (Nordrhein-Westfalen), confirmed.* (2007). at <http://www.promedmail.org/?p=2400:1001:2689187839676304::::F2400_P1001_BACK_PAGE,F2400_P1001_ARCHIVE_NUMBER,F2400_P1001_USE_ARCHIVE:1001,20070613.1928,Y>

51. International Society for Infectious Diseases. *No TitleBLUETONGUE - EUROPE (42): BTV-8, DENMARK, Archive Number: 20071014.3375*. (2007).

52. International Society for Infectious Diseases. *Bluetongue - Europe (49): BTV-8, Switzerland Archive Number: 20071028.3504*. (2007).

53. International Society for Infectious Diseases. *Bluetongue - Europe (16): BTV-8, Czech Rep. Archive Number: 20080320.1065*. (2007).

54. International Society for Infectious Diseases. *Europe (10): BTV-8, UK Archive Number: 20080223.0743*. (2008).

55. International Society for Infectious Diseases. *Bluetongue, ovine - Morocco (02) Archive Number: 20061121.3316*. (2006).

56. International Society for Infectious Diseases. *Bluetongue, ovine - Tunisia: OIE Archive Number: 20061130.3393*. (2006).

57. International Society for Infectious Diseases. *Bluetongue, sheep - Algeria (02): OIE Archive Number: 20060925.2735*. (2006).

58. World Organisation for Animal Health. *Bluetongue, Spain (Immediate notification : 26/07/2007)*. (2007). at <http://www.oie.int/wahis_2/public%5C..%5Ctemp%5Creports/en_imm_0000005799_20070726_123322.pdf>

59. World Organisation for Animal Health. *Bluetongue, Portugal (Follow-up Report 13 : 21/09/2007)*. (2007). at <http://www.oie.int/wahis_2/public%5C..%5Ctemp%5Creports/en_fup_0000006235_20070921_173054.pdf>

60. World Organisation for Animal Health. *Bluetongue, France (Immediate notification : 27/11/2007)*. (2007). at <http://www.oie.int/wahis_2/public%5C..%5Ctemp%5Creports/en_imm_0000006498_20071127_165409.pdf>

61. World Organisation for Animal Health. *Bluetongue, Netherlands (Immediate notification : 27/10/2008)*. (2008). at <http://www.oie.int/wahis_2/public%5C..%5Ctemp%5Creports/en_imm_0000007458_20081027_163408.pdf>

62. World Organisation for Animal Health. *Bluetongue, Germany (Immediate notification : 06/11/2008)*. (2008). at <http://www.oie.int/wahis_2/public%5C..%5Ctemp%5Creports/en_imm_0000007490_20081106_174647.pdf>

63. International Society for Infectious Diseases. *Bluetongue - Europe (03): Belgium, BTV-11 Archive Number: 20090205.0516*. (2009).

64. Defra. Archive: Bluetongue Surveillance and Control. at <http://archive.defra.gov.uk/foodfarm/farmanimal/diseases/atoz/bluetongue/control/>

65. Pearson, L. D. & Roy, P. Genetically engineered multi-component virus-like particles as veterinary vaccines. *Immunol. Cell Biol.* **71 (Pt 5),** 381–9 (1993).

66. Batten, C. A., Maan, S., Shaw, A. E., Maan, N. S. & Mertens, P. P. C. A European field strain of bluetongue virus derived from two parental vaccine strains by genome segment reassortment. *Virus Res.* **137,** 56–63 (2008).

67. Veronesi, E., Hamblin, C. & Mellor, P. S. Live attenuated bluetongue vaccine viruses in Dorset Poll sheep, before and after passage in vector midges (Diptera: Ceratopogonidae). *Vaccine* **23,** 5509–16 (2005).

68. Savini, G. *et al.* Risk factors associated with the occurrence of undesired effects in sheep and goats after field vaccination with modified-live vaccine against bluetongue virus serotypes 2, 4 and 16. *Vet. Microbiol.* **146,** 44–50 (2010).

69. González, J. M. *et al.* Possible adverse reactions in sheep after vaccination with inactivated BTV vaccines. *Vet. Rec.* **166,** 757–8 (2010).

70. Capua, I., Terregino, C., Cattoli, G., Mutinelli, F. & Rodriguez, J. F. Development of a DIVA (Differentiating Infected from Vaccinated Animals) strategy using a vaccine containing a heterologous neuraminidase for the control of avian influenza. *Avian Pathol.* **32,** 47–55 (2003).

71. Bhanuprakash, V., Indrani, B. K., Hosamani, M., Balamurugan, V. & Singh, R. K. Bluetongue vaccines: the past, present and future. *Expert Rev. Vaccines* **8,** 191–204 (2009).

72. Boyce, M., Celma, C. C. P. & Roy, P. Development of reverse genetics systems for bluetongue virus: recovery of infectious virus from synthetic RNA transcripts. *J. Virol.* **82,** 8339–48 (2008).

73. Matsuo, E. *et al.* Generation of replication-defective virus-based vaccines that confer full protection in sheep against virulent bluetongue virus challenge. *J. Virol.* **85,** 10213–21 (2011).

74. Fukusho, A., Yu, Y., Yamaguchi, S. & Roy, P. Completion of the sequence of bluetongue virus serotype 10 by the characterization of a structural protein, VP6, and a non-structural protein, NS2. *J. Gen. Virol.* **70 (Pt 7),** 1677–89 (1989).

75. Nason, E. L. *et al.* Interactions between the inner and outer capsids of bluetongue virus. *J. Virol.* **78,** 8059–67 (2004).

76. Huismans, H., van Dijk, A. A. & Els, H. J. Uncoating of parental bluetongue virus to core and subcore particles in infected L cells. *Virology* **157,** 180–8 (1987).

77. Martin, S. A. & Zweerink, H. J. Isolation and characterization of two types of bluetongue virus particles. *Virology* **50,** 495–506 (1972).

78. Verwoerd, D. W., Els, H. J., De Villiers, E. M. & Huismans, H. Structure of the bluetongue virus capsid. *J. Virol.* **10,** 783–94 (1972).

79. French, T. J. & Roy, P. Synthesis of bluetongue virus (BTV) corelike particles by a recombinant baculovirus expressing the two major structural core proteins of BTV. *J. Virol.* **64,** 1530–6 (1990).

80. French, T. J., Marshall, J. J. & Roy, P. Assembly of double-shelled, viruslike particles of bluetongue virus by the simultaneous expression of four structural proteins. *J. Virol.* **64,** 5695–700 (1990).

81. Loudon, P. T. & Roy, P. Assembly of five bluetongue virus proteins expressed by recombinant baculoviruses: inclusion of the largest protein VP1 in the core and virus-like proteins. *Virology* **180,** 798–802 (1991).

82. Lawton, J. A., Estes, M. K. & Prasad, B. V. Mechanism of genome transcription in segmented dsRNA viruses. *Adv. Virus Res.* **55,** 185–229 (2000).

83. Schoehn, G., Moss, S. R., Nuttall, P. A. & Hewat, E. A. Structure of Broadhaven virus by cryoelectron microscopy: correlation of structural and antigenic properties of Broadhaven virus and bluetongue virus outer capsid proteins. *Virology* **235,** 191–200 (1997).

84. Hewat, E. A., Booth, T. F. & Roy, P. Structure of bluetongue virus particles by cryoelectron microscopy. *J. Struct. Biol.* **109,** 61–9

85. Maan, S. *et al.* Complete genome characterisation of a novel 26th bluetongue virus serotype from Kuwait. *PLoS One* **6,** e26147 (2011).

86. Ghiasi, H., Fukusho, A., Eshita, Y. & Roy, P. Identification and characterization of conserved and variable regions in the neutralization vp2 gene of bluetongue virus. *Virology* **160,** 100–109 (1987).

87. Huismans, H., van der Walt, N. T., Cloete, M. & Erasmus, B. J. Isolation of a capsid protein of bluetongue virus that induces a protective immune response in sheep. *Virology* **157,** 172–9 (1987).

88. Hassan, S. S. & Roy, P. Expression and Functional Characterization of Bluetongue Virus VP2 Protein: Role in Cell Entry. *J. Virol.* **73,** 9832–9842 (1999).

89. Zhang, X. *et al.* Bluetongue virus coat protein VP2 contains sialic acid-binding domains, and VP5 resembles enveloped virus fusion proteins. *Proc. Natl. Acad. Sci. U. S. A.* **107,** 6292–7 (2010).

90. Isa, P., Lopez, S., Segovia, L. & Arias, C. Functional and structural analysis of the sialic acid-binding domain of rotaviruses. *J. Virol.* **71,** 6749–6756 (1997).

91. Dormitzer, P. R., Sun, Z.-Y. J., Wagner, G. & Harrison, S. C. The rhesus rotavirus VP4 sialic acid binding domain has a galectin fold with a novel carbohydrate binding site. *EMBO J.* **21,** 885–97 (2002).

92. Forzan, M., Marsh, M. & Roy, P. Bluetongue virus entry into cells. *J. Virol.* **81,** 4819–27 (2007).

93. Gold, S., Monaghan, P., Mertens, P. & Jackson, T. A Clathrin Independent Macropinocytosis-Like Entry Mechanism Used by Bluetongue Virus-1 during Infection of BHK Cells. *PLoS One* **5,** e11360 (2010).

94. Maréchal, V. *et al.* Human immunodeficiency virus type 1 entry into macrophages mediated by macropinocytosis. *J. Virol.* **75,** 11166–77 (2001).

95. Raghu, H., Sharma-Walia, N., Veettil, M. V., Sadagopan, S. & Chandran, B. Kaposi's sarcoma-associated herpesvirus utilizes an actin polymerization-dependent macropinocytic pathway to enter human dermal microvascular endothelial and human umbilical vein endothelial cells. *J. Virol.* **83,** 4895–911 (2009).

96. Amstutz, B. *et al.* Subversion of CtBP1-controlled macropinocytosis by human adenovirus serotype 3. *EMBO J.* **27,** 956–69 (2008).

97. Hassan, S. H., Wirblich, C., Forzan, M. & Roy, P. Expression and functional characterization of bluetongue virus VP5 protein: role in cellular permeabilization. *J. Virol.* **75,** 8356–67 (2001).

98. Forzan, M., Wirblich, C. & Roy, P. A capsid protein of nonenveloped Bluetongue virus exhibits membrane fusion activity. *Proc. Natl. Acad. Sci. U. S. A.* **101,** 2100–5 (2004).

99. CASPAR, D. L. & KLUG, A. Physical principles in the construction of regular viruses. *Cold Spring Harb. Symp. Quant. Biol.* **27,** 1–24 (1962).

100. Hewat, E. A., Booth, T. F., Loudon, P. T. & Roy, P. Three-dimensional reconstruction of baculovirus expressed bluetongue virus core-like particles by cryo-electron microscopy. *Virology* **189,** 10–20 (1992).

101. Prasad, B. V, Yamaguchi, S. & Roy, P. Three-dimensional structure of single-shelled bluetongue virus. *J. Virol.* **66,** 2135–2142 (1992).

102. Grimes, J. M. *et al.* An atomic model of the outer layer of the bluetongue virus core derived from X-ray crystallography and electron cryomicroscopy. *Structure* **5,** 885–93 (1997).

103. Grimes, J. M. *et al.* The atomic structure of the bluetongue virus core. *Nature* **395,** 470–8 (1998).

104. Urakawa, T., Ritter, D. G. & Roy, P. Expression of largest RNA segment and synthesis of VP1 protein of bluetongue virus in insect cells by recombinant baculovirus: association of VP1 protein with RNA polymerase activity. *Nucleic Acids Res.* **17,** 7395–401 (1989).

105. Boyce, M., Wehrfritz, J., Noad, R. & Roy, P. Purified recombinant bluetongue virus VP1 exhibits RNA replicase activity. *J. Virol.* **78,** 3994–4002 (2004).

106. Patton, J. T., Jones, M. T., Kalbach, A. N., He, Y. W. & Xiaobo, J. Rotavirus RNA polymerase requires the core shell protein to synthesize the double-stranded RNA genome. *J. Virol.* **71,** 9618–26 (1997).

107. Matsuo, E. & Roy, P. Bluetongue virus VP1 polymerase activity in vitro: template dependency, dinucleotide priming and cap dependency. *PLoS One* **6,** e27702 (2011).

108. Ramadevi, N., Burroughs, N. J., Mertens, P. P. C., Jones, I. M. & Roy, P. Capping and methylation of mRNA by purified recombinant VP4 protein of bluetongue virus. *Proc. Natl. Acad. Sci.* **95,** 13537–13542 (1998).

109. Liu, M., Mattion, N. M. & Estes, M. K. Rotavirus VP3 expressed in insect cells possesses guanylyltransferase activity. *Virology* **188,** 77–84 (1992).

110. Venkatesan, S., Gershowitz, A. & Moss, B. Modification of the 5' end of mRNA. Association of RNA triphosphatase with the RNA guanylyltransferase-RNA (guanine-7-)methyltransferase complex from vaccinia virus. *J. Biol. Chem.* **255,** 903–8 (1980).

111. Furuichi, Y., Muthukrishnan, S., Tomasz, J. & Shatkin, A. J. Mechanism of formation of reovirus mRNA 5'-terminal blocked and methylated sequence, m7GpppGmpC. *J. Biol. Chem.* **251,** 5043–53 (1976).

112. Ramadevi, N. & Roy, P. Bluetongue virus core protein VP4 has nucleoside triphosphate phosphohydrolase activity. *J. Gen. Virol.* **79 (Pt 10,** 2475–80 (1998).

113. Martinez-Costas, J., Sutton, G., Ramadevi, N. & Roy, P. Guanylyltransferase and RNA 5'-triphosphatase activities of the purified expressed VP4 protein of bluetongue virus. *J. Mol. Biol.* **280,** 859–66 (1998).

114. Kar, A. K. & Roy, P. Defining the structure-function relationships of bluetongue virus helicase protein VP6. *J. Virol.* **77,** 11347–56 (2003).

115. Stäuber, N., Martinez-Costas, J., Sutton, G., Monastyrskaya, K. & Roy, P. Bluetongue virus VP6 protein binds ATP and exhibits an RNA-dependent ATPase function and a helicase activity that catalyze the unwinding of double-stranded RNA substrates. *J. Virol.* **71,** 7220–6 (1997).

116. Roy, P., Adachi, A., Urakawa, T., Booth, T. F. & Thomas, C. P. Identification of bluetongue virus VP6 protein as a nucleic acid-binding protein and the localization of VP6 in virus-infected vertebrate cells. *J. Virol.* **64,** 1–8 (1990).

117. Sedman, J. & Stenlund, A. The Papillomavirus E1 Protein Forms a DNA-Dependent Hexameric Complex with ATPase and DNA Helicase Activities. *J. Virol.* **72,** 6893–6897 (1998).

118. Gogol, E. P., Seifried, S. E. & von Hippel, P. H. Structure and assembly of the Escherichia coli transcription termination factor rho and its interaction with RNA. I. Cryoelectron microscopic studies. *J. Mol. Biol.* **221,** 1127–38 (1991).

119. Ratinier, M. *et al.* Bluetongue virus 1 strain RSArrrr/01 segment 1, complete sequence - Nucleotide - NCBI. at <http://www.ncbi.nlm.nih.gov/nuccore/JX680457.1>

120. Ratinier, M. *et al.* Bluetongue virus 1 strain RSArrrr/01 segment 10, complete sequence - Nucleotide - NCBI. at <http://www.ncbi.nlm.nih.gov/nuccore/JX680466.1>

121. Belhouchet, M. *et al.* Detection of a fourth orbivirus non-structural protein. *PLoS One* **6,** e25697 (2011).

122. Ratinier, M. *et al.* Identification and characterization of a novel non-structural protein of bluetongue virus. *PLoS Pathog.* **7,** e1002477 (2011).

123. Mertens, P. P., Brown, F. & Sangar, D. V. Assignment of the genome segments of bluetongue virus type 1 to the proteins which they encode. *Virology* **135,** 207–17 (1984).

124. Gould, A. R. Nucleotide sequence of the Australian bluetongue virus serotype 1 RNA segment 10. *J. Gen. Virol.* **69 (Pt 4),** 945–9 (1988).

125. Rao, C. D., Kiuchi, A. & Roy, P. Homologous terminal sequences of the genome double-stranded RNAs of bluetongue virus. *J. Virol.* **46,** 378–83 (1983).

126. Van Dijk, A. A. & Huismans, H. The in vitro activation and further characterization of the bluetongue virus-associated transcriptase. *Virology* **104,** 347–56 (1980).

127. Van Dijk, A. A. & Huismans, H. In vitro transcription and translation of bluetongue virus mRNA. *J. Gen. Virol.* **69 (Pt 3),** 573–81 (1988).

128. Huismans, H. Protein synthesis in bluetongue virus-infected cells. *Virology* **92,** 385–96 (1979).

129. Urakawa, T. & Roy, P. Bluetongue virus tubules made in insect cells by recombinant baculoviruses: expression of the NS1 gene of bluetongue virus serotype 10. *J. Virol.* **62,** 3919–27 (1988).

130. Hewat, E. A., Booth, T. F., Wade, R. H. & Roy, P. 3-D reconstruction of bluetongue virus tubules using cryoelectron microscopy. *J. Struct. Biol.* **108,** 35–48

131. Huismans, H. & Els, H. J. Characterization of the tubules associated with the replication of three different orbiviruses. *Virology* **92,** 397–406 (1979).

132. Owens, R. J., Limn, C. & Roy, P. Role of an arbovirus nonstructural protein in cellular pathogenesis and virus release. *J. Virol.* **78,** 6649–56 (2004).

133. Eaton, B. T., Hyatt, A. D. & White, J. R. Localization of the nonstructural protein NS1 in bluetongue virus-infected cells and its presence in virus particles. *Virology* **163,** 527–37 (1988).

134. Boyce, M., Celma, C. C. P. & Roy, P. Bluetongue virus non-structural protein 1 is a positive regulator of viral protein synthesis. *Virol. J.* **9,** 178 (2012).

135. Lecatsas, G. Electron microscopic study of the formation of bluetongue virus. *Onderstepoort J. Vet. Res.* **35,** 139–49 (1968).

136. Hyatt, A. D., Gould, A. R., Coupar, B. & Eaton, B. T. Localization of the non-structural protein NS3 in bluetongue virus-infected cells. *J. Gen. Virol.* **72,** 2263–2267 (1991).

137. Bhattacharya, B., Noad, R. J. & Roy, P. Interaction between Bluetongue virus outer capsid protein VP2 and vimentin is necessary for virus egress. *Virol. J.* **4,** 7 (2007).

138. Bhattacharya, B. & Roy, P. Bluetongue virus outer capsid protein VP5 interacts with membrane lipid rafts via a SNARE domain. *J. Virol.* **82,** 10600–12 (2008).

139. Bhattacharya, B. & Roy, P. Role of lipids on entry and exit of bluetongue virus, a complex non-enveloped virus. *Viruses* **2,** 1218–35 (2010).

140. Waheed, A. A. & Freed, E. O. Lipids and membrane microdomains in HIV-1 replication. *Virus Res.* **143,** 162–76 (2009).

141. Bavari, S. Lipid Raft Microdomains: A Gateway for Compartmentalized Trafficking of Ebola and Marburg Viruses. *J. Exp. Med.* **195,** 593–602 (2002).

142. Manie, S. N., Debreyne, S., Vincent, S. & Gerlier, D. Measles Virus Structural Components Are Enriched into Lipid Raft Microdomains: a Potential Cellular Location for Virus Assembly. *J. Virol.* **74,** 305–311 (2000).

143. Hyatt, A. D., Zhao, Y. & Roy, P. Release of bluetongue virus-like particles from insect cells is mediated by BTV nonstructural protein NS3/NS3A. *Virology* **193,** 592–603 (1993).

144. Wechsler, S. J. & McHolland, L. E. Susceptibilities of 14 cell lines to bluetongue virus infection. *J. Clin. Microbiol.* **26,** 2324–7 (1988).

145. Celma, C. C. P. & Roy, P. Interaction of calpactin light chain (S100A10/p11) and a viral NS protein is essential for intracellular trafficking of nonenveloped bluetongue virus. *J. Virol.* **85,** 4783–91 (2011).

146. Beaton, A. R., Rodriguez, J., Reddy, Y. K. & Roy, P. The membrane trafficking protein calpactin forms a complex with bluetongue virus protein NS3 and mediates virus release. *Proc. Natl. Acad. Sci. U. S. A.* **99,** 13154–9 (2002).

147. Firth, A. E. Bioinformatic analysis suggests that the Orbivirus VP6 cistron encodes an overlapping gene. *Virol. J.* **5,** 48 (2008).

148. Brookes, S. M., Hyatt, A. D. & Eaton, B. T. Characterization of virus inclusion bodies in bluetongue virus-infected cells. *J. Gen. Virol.* **74 (Pt 3),** 525–30 (1993).

149. Eaton, B. T., Hyatt, A. D. & White, J. R. Association of bluetongue virus with the cytoskeleton. *Virology* **157,** 107–16 (1987).

150. Kar, A. K., Bhattacharya, B. & Roy, P. Bluetongue virus RNA binding protein NS2 is a modulator of viral replication and assembly. *BMC Mol. Biol.* **8,** 4 (2007).

151. Modrof, J., Lymperopoulos, K. & Roy, P. Phosphorylation of bluetongue virus nonstructural protein 2 is essential for formation of viral inclusion bodies. *J. Virol.* **79,** 10023–31 (2005).

152. Hyatt, A. D. & Eaton, B. T. Ultrastructural distribution of the major capsid proteins within bluetongue virus and infected cells. *J. Gen. Virol.* **69 (Pt 4),** 805–15 (1988).

153. Matsuo, E. & Roy, P. Minimum requirements for bluetongue virus primary replication in vivo. *J. Virol.* **87,** 882–9 (2013).

154. Taraporewala, Z. F., Chen, D. & Patton, J. T. Multimers of the bluetongue virus nonstructural protein, NS2, possess nucleotidyl phosphatase activity: similarities between NS2 and rotavirus NSP2. *Virology* **280,** 221–31 (2001).

155. Thomas, C. P., Booth, T. F. & Roy, P. Synthesis of bluetongue virus-encoded phosphoprotein and formation of inclusion bodies by recombinant baculovirus in insect cells: it binds the single-stranded RNA species. *J. Gen. Virol.* **71 (Pt 9),** 2073–83 (1990).

156. Lymperopoulos, K. *et al.* Specific binding of Bluetongue virus NS2 to different viral plus-strand RNAs. *Virology* **353,** 17–26 (2006).

157. Gould, A. R., Hyatt, A. D. & Eaton, B. T. Morphogenesis of a bluetongue virus variant with an amino acid alteration at a neutralization site in the outer coat protein, VP2. *Virology* **165,** 23–32 (1988).

158. Fillmore, G. C., Lin, H. & Li, J. K. K. Localization of the single-stranded RNA-binding domains of bluetongue virus nonstructural protein NS2. *J. Virol.* **76,** 499–506 (2002).

159. Mumtsidu, E., Makhov, A. M., Roessle, M., Bathke, A. & Tucker, P. A. Structural features of the Bluetongue virus NS2 protein. *J. Struct. Biol.* **160,** 157–67 (2007).

160. Huismans, H., van Dijk, A. A. & Bauskin, A. R. In vitro phosphorylation and purification of a nonstructural protein of bluetongue virus with affinity for single-stranded RNA. *J. Virol.* **61,** 3589–95 (1987).

161. Lymperopoulos, K., Wirblich, C., Brierley, I. & Roy, P. Sequence specificity in the interaction of Bluetongue virus non-structural protein 2 (NS2) with viral RNA. *J. Biol. Chem.* **278,** 31722–30 (2003).

162. Theron, J. & Nel, L. H. Stable protein-RNA interaction involves the terminal domains of bluetongue virus mRNA, but not the terminally conserved sequences. *Virology* **229,** 134–42 (1997).

163. Devaney, M. A., Kendall, J. & Grubman, M. J. Characterization of a nonstructural phosphoprotein of two orbiviruses. *Virus Res.* **11,** 151–64 (1988).

164. Horscroft, N. J. & Roy, P. NTP binding and phosphohydrolase activity associated with purified bluetongue virus non-structural protein NS2. *J. Gen. Virol.* **81,** 1961–5 (2000).

165. Mancini, E. J. *et al.* Atomic snapshots of an RNA packaging motor reveal conformational changes linking ATP hydrolysis to RNA translocation. *Cell* **118,** 743–55 (2004).

166. Yao, W., Adelman, K. & Bruenn, J. A. In vitro selection of packaging sites in a double-stranded RNA virus. *J. Virol.* **71,** 2157–62 (1997).

167. Uitenweerde, J. M., Theron, J., Stoltz, M. A. & Huismans, H. The multimeric nonstructural NS2 proteins of bluetongue virus, African horsesickness virus, and epizootic hemorrhagic disease virus differ in their single-stranded RNA-binding ability. *Virology* **209,** 624–32 (1995).

168. Butan, C. & Tucker, P. Insights into the role of the non-structural protein 2 (NS2) in Bluetongue virus morphogenesis. *Virus Res.* **151,** 109–17 (2010).

169. Butan, C., Van Der Zandt, H. & Tucker, P. A. Structure and assembly of the RNA binding domain of bluetongue virus non-structural protein 2. *J. Biol. Chem.* **279,** 37613–21 (2004).

170. Jiang, X. *et al.* Cryoelectron microscopy structures of rotavirus NSP2-NSP5 and NSP2-RNA complexes: implications for genome replication. *J. Virol.* **80,** 10829–35 (2006).

171. Akita, F. *et al.* Crystallographic analysis reveals octamerization of viroplasm matrix protein P9-1 of Rice black streaked dwarf virus. *J. Virol.* **86,** 746–56 (2012).

172. Jayaram, H., Taraporewala, Z., Patton, J. T. & Prasad, B. V. V. Rotavirus protein involved in genome replication and packaging exhibits a HIT-like fold. *Nature* **417,** 311–5 (2002).

173. Taraporewala, Z., Chen, D. & Patton, J. T. Multimers formed by the rotavirus nonstructural protein NSP2 bind to RNA and have nucleoside triphosphatase activity. *J. Virol.* **73,** 9934–43 (1999).

174. Becker, M. M. *et al.* Reovirus sigmaNS protein is required for nucleation of viral assembly complexes and formation of viral inclusions. *J. Virol.* **75,** 1459–75 (2001).

175. Antczak, J. B. & Joklik, W. K. Reovirus genome segment assortment into progeny genomes studied by the use of monoclonal antibodies directed against reovirus proteins. *Virology* **187,** 760–76 (1992).

176. Helmberger-Jones, M. & Patton, J. T. Characterization of subviral particles in cells infected with simian rotavirus SA11. *Virology* **155,** 655–65 (1986).

177. Petrie, B. L., Greenberg, H. B., Graham, D. Y. & Estes, M. K. Ultrastructural localization of rotavirus antigens using colloidal gold. *Virus Res.* **1,** 133–52 (1984).

178. Gillian, A. L., Schmechel, S. C., Livny, J., Schiff, L. A. & Nibert, M. L. Reovirus protein sigmaNS binds in multiple copies to single-stranded RNA and shares properties with single-stranded DNA binding proteins. *J. Virol.* **74,** 5939–48 (2000).

179. Noble, S. & Nibert, M. L. Core protein mu2 is a second determinant of nucleoside triphosphatase activities by reovirus cores. *J. Virol.* **71,** 7728–35 (1997).

180. Brentano, L., Noah, D. L., Brown, E. G. & Sherry, B. The reovirus protein mu2, encoded by the M1 gene, is an RNA-binding protein. *J. Virol.* **72,** 8354–7 (1998).

181. Mbisa, J. L., Becker, M. M., Zou, S., Dermody, T. S. & Brown, E. G. Reovirus mu2 protein determines strain-specific differences in the rate of viral inclusion formation in L929 cells. *Virology* **272,** 16–26 (2000).

182. Fabbretti, E., Afrikanova, I., Vascotto, F. & Burrone, O. R. Two non-structural rotavirus proteins, NSP2 and NSP5, form viroplasm-like structures in vivo. *J. Gen. Virol.* **80 (Pt 2),** 333–9 (1999).

183. Boyce, M. & Roy, P. Recovery of infectious bluetongue virus from RNA. *J. Virol.* **81,** 2179–86 (2007).

184. Lourenco, S. & Roy, P. In vitro reconstitution of Bluetongue virus infectious cores. *Proc. Natl. Acad. Sci. U. S. A.* **108,** 13746–51 (2011).

185. Du, J., Bhattacharya, B., Ward, T. H. & Roy, P. Trafficking of Bluetongue virus visualized by recovery of tetracysteine-tagged virion particles. *J. Virol.* (2014). doi:10.1128/JVI.01815-14

186. Diprose, J. M. *et al.* Translocation portals for the substrates and products of a viral transcription complex: the bluetongue virus core. *EMBO J.* **20,** 7229–39 (2001).

187. Mertens, P. P. C. & Diprose, J. The bluetongue virus core: a nano-scale transcription machine. *Virus Res.* **101,** 29–43 (2004).

188. Matsuo, E. & Roy, P. Bluetongue virus VP6 acts early in the replication cycle and can form the basis of chimeric virus formation. *J. Virol.* **83,** 8842–8 (2009).

189. Celma, C. C. P. & Roy, P. A viral nonstructural protein regulates bluetongue virus trafficking and release. *J. Virol.* **83,** 6806–16 (2009).

190. Racaniello, V. R. & Baltimore, D. Cloned poliovirus complementary DNA is infectious in mammalian cells. *Science* **214,** 916–9 (1981).

191. Baltimore, D. Expression of animal virus genomes. *Bacteriol. Rev.* **35,** 235–41 (1971).

192. Kitamura, N. *et al.* Primary structure, gene organization and polypeptide expression of poliovirus RNA. *Nature* **291,** 547–553 (1981).

193. Kaplan, G., Lubinski, J., Dasgupta, A. & Racaniello, V. R. In vitro synthesis of infectious poliovirus RNA. *Proc. Natl. Acad. Sci. U. S. A.* **82,** 8424–8 (1985).

194. Boyer, J. C. & Haenni, A. L. Infectious transcripts and cDNA clones of RNA viruses. *Virology* **198,** 415–26 (1994).

195. Schnell, M. J., Mebatsion, T. & Conzelmann, K. K. Infectious rabies viruses from cloned cDNA. *EMBO J.* **13,** 4195–203 (1994).

196. Radecke, F. *et al.* Rescue of measles viruses from cloned DNA. *EMBO J.* **14,** 5773–84 (1995).

197. Bridgen, A. & Elliott, R. M. Rescue of a segmented negative-strand RNA virus entirely from cloned complementary DNAs. *Proc. Natl. Acad. Sci. U. S. A.* **93,** 15400–4 (1996).

198. Rohrmann, G. F. Baculovirus Molecular Biology. (2013). at <http://www.ncbi.nlm.nih.gov/books/NBK114593/>

199. Kuroda, K., Hauser, C., Rott, R., Klenk, H. D. & Doerfler, W. Expression of the influenza virus haemagglutinin in insect cells by a baculovirus vector. *EMBO J.* **5,** 1359–65 (1986).

200. Blissard, G. W. & Rohrmann, G. F. Baculovirus diversity and molecular biology. *Annu. Rev. Entomol.* **35,** 127–55 (1990).

201. Kost, T. A., Condreay, J. P. & Jarvis, D. L. Baculovirus as versatile vectors for protein expression in insect and mammalian cells. *Nat. Biotechnol.* **23,** 567–75 (2005).

202. Todd, J. W., Passarelli, A. L., Lu, A. & Miller, L. K. Factors regulating baculovirus late and very late gene expression in transient-expression assays. *J. Virol.* **70,** 2307–17 (1996).

203. Smith, G. E., Summers, M. D. & Fraser, M. J. Production of human beta interferon in insect cells infected with a baculovirus expression vector. *Mol. Cell. Biol.* **3,** 2156–65 (1983).

204. Bishop, D. H. Gene expression using insect cells and viruses. *Curr. Opin. Biotechnol.* **1,** 62–7 (1990).

205. Matsuura, Y., Possee, R. D., Overton, H. A. & Bishop, D. H. Baculovirus expression vectors: the requirements for high level expression of proteins, including glycoproteins. *J. Gen. Virol.* **68 (Pt 5),** 1233–50 (1987).

206. Hu, Y. Baculovirus as a highly efficient expression vector in insect and mammalian cells. *Acta Pharmacol. Sin.* **26,** 405–16 (2005).

207. Ooi, B. G., Rankin, C. & Miller, L. K. Downstream sequences augment transcription from the essential initiation site of a baculovirus polyhedrin gene. *J. Mol. Biol.* **210,** 721–36 (1989).

208. Vialard, J. *et al.* Synthesis of the membrane fusion and hemagglutinin proteins of measles virus, using a novel baculovirus vector containing the beta-galactosidase gene. *J. Virol.* **64,** 37–50 (1990).

209. Kitts, P. A., Ayres, M. D. & Possee, R. D. Linearization of baculovirus DNA enhances the recovery of recombinant virus expression vectors. *Nucleic Acids Res.* **18,** 5667–72 (1990).

210. Zhao, Y., Chapman, D. A. G. & Jones, I. M. Improving baculovirus recombination. *Nucleic Acids Res.* **31,** E6–6 (2003).

211. Vaughn, J. L., Goodwin, R. H., Tompkins, G. J. & McCawley, P. The establishment of two cell lines from the insect Spodoptera frugiperda (Lepidoptera; Noctuidae). *In Vitro* **13,** 213–7 (1977).

212. Summers, M. & Smith, G. E. *A Manual of Methods for Baculovirus Vectors and Insect Cell Culture Procedures, Issue 1555*. (Texas Agricultural Experiment Station, 1987). at <http://books.google.co.uk/books/about/A_Manual_of_Methods_for_Baculovirus_Vect.html?id=uM7zGAAACAAJ&pgis=1>

213. Sambrook, J. & Russell, D. W. *Molecular Cloning: A Laboratory Manual, Volume 1*. (CSHL Press, 2001). at <http://books.google.co.uk/books/about/Molecular_Cloning.html?id=YTxKwWUiBeUC&pgis=1>

214. Hemsley, A., Arnheim, N., Toney, M. D., Cortopassi, G. & Galas, D. J. A simple method for site-directed mutagenesis using the polymerase chain reaction. *Nucleic Acids Res.* **17,** 6545–51 (1989).

215. Islam, M. K., Miyoshi, T., Yamada, M. & Tsuji, N. Pyrophosphatase of the roundworm Ascaris suum plays an essential role in the worm's molting and development. *Infect. Immun.* **73,** 1995–2004 (2005).

216. Chomczynski, P. & Sacchi, N. Single-step method of RNA isolation by acid guanidinium thiocyanate-phenol-chloroform extraction. *Anal. Biochem.* **162,** 156–159 (1987).

217. Chomczynski, P. & Sacchi, N. The single-step method of RNA isolation by acid guanidinium thiocyanate-phenol-chloroform extraction: twenty-something years on. *Nat. Protoc.* **1,** 581–5 (2006).

218. Palmiter, R. D. Magnesium precipitation of ribonucleoprotein complexes. Expedient techniques for the isolation of undergraded polysomes and messenger ribonucleic acid. *Biochemistry* **13,** 3606–15 (1974).

219. Haider, S. R., Sharp, B. L. & Reid, H. J. A comparison of Tris-glycine and Tris-tricine buffers for the electrophoretic separation of major serum proteins. *J. Sep. Sci.* **34,** 2463–7 (2011).

220. Laemmli, U. K. Cleavage of structural proteins during the assembly of the head of bacteriophage T4. *Nature* **227,** 680–5 (1970).

221. Bradford, M. M. A rapid and sensitive method for the quantitation of microgram quantities of protein utilizing the principle of protein-dye binding. *Anal. Biochem.* **72,** 248–54 (1976).

222. Lorentzen, E. *et al.* The archaeal exosome core is a hexameric ring structure with three catalytic subunits. *Nat. Struct. Mol. Biol.* **12,** 575–81 (2005).

223. Symmons, M. F., Jones, G. H. & Luisi, B. F. A Duplicated Fold Is the Structural Basis for Polynucleotide Phosphorylase Catalytic Activity, Processivity, and Regulation. *Structure* **8,** 1215–1226 (2000).

224. Valentine, R. C., Thang, M. N. & Grunberg-Manago, M. Electron microscopy of Escherichia coli polynucleotide phosphorylase molecules and polyribonucleotide formation. *J. Mol. Biol.* **39,** 389–91 (1969).

225. Monzingo, A. F., Gao, J., Qiu, J., Georgiou, G. & Robertus, J. D. The X-ray structure of Escherichia coli RraA (MenG), A protein inhibitor of RNA processing. *J. Mol. Biol.* **332,** 1015–24 (2003).

226. Törö, I. *et al.* RNA binding in an Sm core domain: X-ray structure and functional analysis of an archaeal Sm protein complex. *EMBO J.* **20,** 2293–303 (2001).

227. Collins, B. M. *et al.* Crystal structure of a heptameric Sm-like protein complex from archaea: implications for the structure and evolution of snRNPs. *J. Mol. Biol.* **309,** 915–23 (2001).

228. Stein, A. J., Fuchs, G., Fu, C., Wolin, S. L. & Reinisch, K. M. Structural insights into RNA quality control: the Ro autoantigen binds misfolded RNAs via its central cavity. *Cell* **121,** 529–39 (2005).

229. Pruijn, G. J. M. Doughnuts dealing with RNA. *Nat. Struct. Mol. Biol.* **12,** 562–4 (2005).

230. Kilic, T., Thore, S. & Suck, D. Crystal structure of an archaeal Sm protein from Sulfolobus solfataricus. *Proteins* **61,** 689–93 (2005).

231. Zhao, Y., Thomas, C., Bremer, C. & Roy, P. Deletion and mutational analyses of bluetongue virus NS2 protein indicate that the amino but not the carboxy terminus of the protein is critical for RNA-protein interactions. *J. Virol.* **68,** 2179–85 (1994).

232. Lin, D., Lan, J. & Zhang, Z. Structure and function of the NS1 protein of influenza A virus. *Acta Biochim. Biophys. Sin. (Shanghai).* **39,** 155–62 (2007).

233. Waksman, G., Shoelson, S. E., Pant, N., Cowburn, D. & Kuriyan, J. Binding of a high affinity phosphotyrosyl peptide to the Src SH2 domain: crystal structures of the complexed and peptide-free forms. *Cell* **72,** 779–90 (1993).

234. Du Prel, J.-B., Hommel, G., Röhrig, B. & Blettner, M. Confidence interval or p-value?: part 4 of a series on evaluation of scientific publications. *Dtsch. Arztebl. Int.* **106,** 335–9 (2009).

235. Sauro, J. & Lewis, J. R. *Quantifying the User Experience*. *Quantifying the User Experience* (Elsevier, 2012). doi:10.1016/B978-0-12-384968-7.00003-5

236. Payton, M. E., Greenstone, M. H. & Schenker, N. Overlapping confidence intervals or standard error intervals: what do they mean in terms of statistical significance? *J. Insect Sci.* **3,** 34 (2003).

237. Horscroft, N. J. & Roy, P. NTP binding and phosphohydrolase activity associated with purified bluetongue virus non-structural protein NS2. *J. Gen. Virol.* **81,** 1961–1965 (2000).

238. Fried, M. & Crothers, D. M. Equilibria and kinetics of lac repressor-operator interactions by polyacrylamide gel electrophoresis. *Nucleic Acids Res.* **9,** 6505–25 (1981).

239. Hellman, L. M. & Fried, M. G. Electrophoretic mobility shift assay (EMSA) for detecting protein-nucleic acid interactions. *Nat. Protoc.* **2,** 1849–61 (2007).

240. Eichwald, C. *et al.* Rotavirus viroplasm fusion and perinuclear localization are dynamic processes requiring stabilized microtubules. *PLoS One* **7,** e47947 (2012).

241. Altenburg, B. C., Graham, D. Y. & Estes, M. K. Ultrastructural study of rotavirus replication in cultured cells. *J. Gen. Virol.* **46,** 75–85 (1980).

242. Parker, J. S. L., Broering, T. J., Kim, J., Higgins, D. E. & Nibert, M. L. Reovirus core protein mu2 determines the filamentous morphology of viral inclusion bodies by interacting with and stabilizing microtubules. *J. Virol.* **76,** 4483–96 (2002).

243. RHIM, J. S., JORDAN, L. E. & MAYOR, H. D. Cytochemical, fluorescent-antibody and electron microscopic studies on the growth of reovirus (ECHO 10) in tissue culture. *Virology* **17,** 342–55 (1962).

244. Della-Porta, A. J. & Snowdon, W. A. An experimental inactivated virus vaccine against bovine ephemeral fever 1. Studies of the virus. *Vet. Microbiol.* **4,** 183–195 (1979).

245. La Frazia, S. *et al.* Thiazolides, a New Class of Antiviral Agents Effective against Rotavirus Infection, Target Viral Morphogenesis, Inhibiting Viroplasm Formation. *J. Virol.* **87,** 11096–11106 (2013).

246. Oomens, A. G., Monsma, S. A. & Blissard, G. W. The baculovirus GP64 envelope fusion protein: synthesis, oligomerization, and processing. *Virology* **209,** 592–603 (1995).

247. Ayres, M. D., Howard, S. C., Kuzio, J., Lopez-Ferber, M. & Possee, R. D. The complete DNA sequence of Autographa californica nuclear polyhedrosis virus. *Virology* **202,** 586–605 (1994).

248. Gomatos, P. J., Prakash, O. & Stamatos, N. M. Small reovirus particle composed solely of sigma NS with specificity for binding different nucleic acids. *J. Virol.* **39,** 115–24 (1981).

249. Ferron, F. *et al.* The hexamer structure of Rift Valley fever virus nucleoprotein suggests a mechanism for its assembly into ribonucleoprotein complexes. *PLoS Pathog.* **7,** e1002030 (2011).

250. Méthot, N., Song, M. S. & Sonenberg, N. A region rich in aspartic acid, arginine, tyrosine, and glycine (DRYG) mediates eukaryotic initiation factor 4B (eIF4B) self-association and interaction with eIF3. *Mol. Cell. Biol.* **16,** 5328–34 (1996).

251. Lahaye, X. *et al.* Functional characterization of Negri bodies (NBs) in rabies virus-infected cells: Evidence that NBs are sites of viral transcription and replication. *J. Virol.* **83,** 7948–58 (2009).

Appendix 1.

Alignment of 26 serotypes of NS2.

```
gi|480327480|gb|AGJ83578.1|      MEQKQRRFTKNIFVLDAAAKTLCGVIAKLSSQPYCQIKIGRVIAFKPVKNPEPKGYVLNV  60
gi|385722006|gb|AFI73131.1|      MEQKQRRFTKNIFVLDVTAKTLCGAIAKLSSQPYCQIKIGRVVAFKPVKNPEPKGYVLNV  60
gi|480327600|gb|AGJ83638.1|      MEQKQRRFTKNIFVLDVNSKTLCGAIAKLSSQPYCQIKIGRVVAFKPVKNPEPKGYVLNV  60
gi|410444351|gb|AFV68257.1|      MEQKQRRFTKNIFVLDANAKTLCGAIAKLSSQPYCQIKIGRVIAFKPVKNPEPKGYVLDV  60
gi|480327500|gb|AGJ83588.1|      MEQKQRRFTKNIFVLDANAKTLCGAIAKLSSQPYCQIKIGRVIAFKPVKNPEPKGYVLNV  60
gi|480327440|gb|AGJ83558.1|      MEQKQRRFTKNIFVLDANAKTLCGAIAKLSSQPYCQIKIGRVIAFKPVKNPEPKGYVLNV  60
gi|480327360|gb|AGJ83518.1|      MEQKQRRFTKNIFVLDANAKTLCGAIAKLSSQPYCQIKIGRVIAFKPVKNPEPKGYVLNV  60
gi|480327200|gb|AGJ83438.1|      MEQKQRRFTKNIFVLDANAKTLCGAIAKLSSQPYCQIKIGRVIAFKPVKNPEPKGYVLNV  60
gi|480327520|gb|AGJ83598.1|      MEQKQRRFTKNIFVLDANAKTLCGAIAKLSSQPYCQIKIGRVIAFKTVKNPEPKGYVLNV  60
gi|480327400|gb|AGJ83538.1|      MEQKQRRFTKNIFVLDANAKTLCGAIAKLSSQPYCQIKIGRVIAFKPVKNPEPKGYVLNV  60
gi|480327380|gb|AGJ83528.1|      MEQKQRRFTKNIFVLDANAKTLCGAIAKLSSQPYCQIKIGRVIAFKPVKNPEPKGYVLNV  60
gi|480327280|gb|AGJ83478.1|      MEQKQRRFTKNIFVLDANAKTLCGAIAKLSSQPYCQIKIGRVIAFKPVKNPEPKGYVLNV  60
gi|557882471|gb|AEO19765.2|      MEQKQRRFTKNIFVLDANAKTLCGAIAKLSSQPYCQIKIGRIIAFKPVKNPEPKGYVLNV  60
gi|480327640|gb|AGJ83658.1|      MEQKQRRFTKNIFVLDANAKTLCGAIAKLSSQPYCQIKIGRVIAFKPVKNPEPKGYVLNV  60
gi|480327420|gb|AGJ83548.1|      MEQKQRRFTKNIFVLDANAKTLCGAIAKLSSQPYCQIKIGRVIAFKPVKNPEPKGYVLNV  60
gi|480327240|gb|AGJ83458.1|      MEQKQRRFTKNIFVLDANAKTLCGAIAKLSSQPYCQIKIGRVIAFKPVKNPEPKGYVLNV  60
gi|480327260|gb|AGJ83468.1|      MEQKQRRFTKNIFVLDANAKTLCGAIAKLSSQPYCQIKIGRVIAFKPVKNPEPKGYVLNV  60
gi|410443430|gb|AFV67789.1|      MEQKQRKFTKNIFVLDVNAKTLCGVIAKQSSQPYCQIKIGRVIAFKPVKNPEPKGYVLNV  60
gi|443411621|gb|AGC83568.1|      MEQKQRKFTKNIFVLDVNAKTLCGVIAKQSSQPYCQIKIGRVIAFKPVKNPEPKGYVLNV  60
gi|557882457|gb|AEO19789.2|      MEQKQRKFTKNIFVLDVNAKTLCGVIAKQSSQPYCQIKIGRVIAFKPVKNPEPKGYVLNV  60
gi|545290061|gb|AGW27487.1|      MEQKQRKFTKNIFVLDVNAKTLCGVIAKQSSQPYCQIKIGRVIAFKPVKNPEPKGYVLNV  60
gi|545290083|gb|AGW27499.1|      MEQKQRKFTKNIFVLDVNAKTLCGVIAKQSSQPYCQIKIGRVIAFKPVKNPEPKGYVLNV  60
gi|389616810|gb|AFK91775.1|      MEQKQRKFTKNIFVLDVNAKTLCGVIAKQSSQPYCQIKIGRVIAFKPVKNPEPKGYVLNV  60
gi|480327560|gb|AGJ83618.1|      MEQKQRKFTKNIFVLDVNAKTLCGVIAKQSSQPYCQIKIGRVIAFKPVKNPEPKGYVLNV  60
gi|210076696|gb|ACJ06706.1|      MEQRQRRFTKNIFVFDVNAKTICGIIAKQNALPYCQVRIGRVIAFKPVKNPEPKGYVLSV  60
gi|355346214|gb|AER60537.1|      MEQRQRRFTKKVFVLEPGAKTLCGVIAKQSSMPYCQIQIGRVYAFKPTKNPEPKGYVLSI  60
                                 ***:**:***::**::  :**:** *** .: ****::***: *** .**********.:

gi|480327480|gb|AGJ83578.1|      PGPGAYRIQDGQDIISLMLTPYGVEATTERWEEWKFEGVSVTPLATRVQHNGVMVDAEIK  120
gi|385722006|gb|AFI73131.1|      PGPGAYRIQDGQDIISLMLTPHGVEATTERWEEWKFEGVSVTPMATRVQYNGVMVDAEIK  120
gi|480327600|gb|AGJ83638.1|      PGPGAYRIQDGQDIISLMLTPHGVEATTERWEEWKFEGVSVTPMATRVQHNGVMVDAEIK  120
gi|410444351|gb|AFV68257.1|      PGPGAYRIQDGQDIISLMLTPHGVEATTERWEEWKFEGVSVTPMATRVQHNGVMVDAEIK  120
gi|480327500|gb|AGJ83588.1|      PGPGAYRIQDGQDIISLMLTPHGVEATTERWEEWKFEGVSVTPMATRVQHNGVMVDAEIK  120
gi|480327440|gb|AGJ83558.1|      PGPGAYRIQDGQDIISLMLAPHGVEATTERWEEWKFEGVSVTPMATRVQHNGVMVDAEIK  120
gi|480327360|gb|AGJ83518.1|      PGPGAYRIQDGQDIISLMLTPHGVEATTERWEEWKFEGVSVTPMATRVQHNGVMVDAEIK  120
gi|480327200|gb|AGJ83438.1|      PGPGAYRIQDGQDIISLMLTPHGVEATTERWEEWKFEGVSVTPMATRVQHNGVMVDAEIK  120
gi|480327520|gb|AGJ83598.1|      PGPGAYRIQDGQDIISLMLTPHGVEATTERWEEWKFEGVSVTPMATRVQHNGVMVDAEIK  120
gi|480327400|gb|AGJ83538.1|      PGPGAYRIQDGQDIISLMLTPHGVEATTERWEEWKFEGVSVTPMATRVQHNGVMVDAEIK  120
gi|480327380|gb|AGJ83528.1|      PGPGAYRIQDGQDIISLMLTPHGVEATTERWEEWKFEGVSVTPMATRVQHNGVMVDAEIK  120
gi|480327280|gb|AGJ83478.1|      PGPGAYRIQDGQDIISLMLTPYGVEATTERWEEWKFEGVSVTPMATRVQHNGVMVDAEIK  120
gi|557882471|gb|AEO19765.2|      PGPGAYRIQDGQDIISLMLTPHGVEATTERWEEWKFEGVSVTPMATRVQHNGVMVDAEIK  120
gi|480327640|gb|AGJ83658.1|      PGPGAYRIQDGQDIISLMLTPHGVEATTERWEEWKFEGVSVTPMATRVQHNGVMVDAEIK  120
gi|480327420|gb|AGJ83548.1|      PGPGAYRIQDGQDIISLMLTPHGVEATTERWEEWKFEGVSVTPMATRVQHNGVMVDAEIK  120
gi|480327240|gb|AGJ83458.1|      PGPGAYRIQDGQDIISLMLTPHGVEATTERWEEWKFEGVSVTPMATRVQHNGVMVDAEIK  120
gi|480327260|gb|AGJ83468.1|      PGPGAYRIQDGQDIISLMLTPHGVEATTERWEEWKFEGVSVTPMATRVQHNGVMVDAEIK  120
gi|410443430|gb|AFV67789.1|      PGPGAYRIQDGQDIISMMLTSSGVEATTERWEEWKFEGVSVTPMATRVQHNGVMVDAEIK  120
gi|443411621|gb|AGC83568.1|      PGPGAYRIQDGQDIISIMLTPNGVEATTERWEEWKFEGVSVTPMATRVQHNGVMVDAEIK  120
gi|557882457|gb|AEO19789.2|      PGPGAYRIQDGQDIISIMLTPSGVEATTERWEEWKFEGVSVTPMATRVQHNGVMVDAEIK  120
gi|545290061|gb|AGW27487.1|      PGPGAYRIQDGQDIISIMLTPSGVEATTERWEEWKFEGVSVTPMATRVQHNGVMVDAEIK  120
gi|545290083|gb|AGW27499.1|      PGPGAYRIQDGQDIVSIMLTPSGVEATTERWEEWKFEGVSVTPMATRVQHNGVMVDAEIK  120
gi|389616810|gb|AFK91775.1|      PGPGAYRIQDGQDIISIMLTSCGVEATTERWEEWKFEGVSVTPMATRVQHNGVMVDAEIK  120
gi|480327560|gb|AGJ83618.1|      PGPGAYRIQDGQDVISVMLTLCGVEATTERWEEWKFEGVSVTPMATRVQHNGVMVDAEIK  120
gi|210076696|gb|ACJ06706.1|      SGPGAYRILDGQDVISMMLTSTGVEATTERWEEWKFESVSVTPMATRIQHNGVMVDAEIK  120
gi|355346214|gb|AER60537.1|      PGPGAYRILDGQDVISVMITMTGIEATTERWEEWKFESVSVTPMATRIQHNGVMVDAEIK  120
                                  ******* ****:::*::*::  *:**************.*****:***:*:**********

gi|480327480|gb|AGJ83578.1|      YCKGMGIVQPYMRNDFDRSEMPDLPGVMRSNYDVRELRQKIKNERESAPRLQVQNVAPKE  180
gi|385722006|gb|AFI73131.1|      YCKGMGIVQPYMRNDFDRNEMPDLPGVMRSNYDIRELRQKIKNERESAPRLQVHSVAPRE  180
gi|480327600|gb|AGJ83638.1|      YCKGMGIVQPYMRNDFDRNEMPDLPGVMRSNYDVRELRQKIKNERESAPRLQVQSVAPRE  180
gi|410444351|gb|AFV68257.1|      YCKGMGIVQPYMRNDFDRNEMPDLPGVMRSNYDVRELRQKIKNERESAPRLQVQSVAPRE  180
gi|480327500|gb|AGJ83588.1|      YCKGMGIVQPYMRNDFDRNEMPDLPGVMRSNYDVRELRQKIKNERESAPRLQVQSVAPRE  180
gi|480327440|gb|AGJ83558.1|      YCKGMGIVQPYMRNDFDRNEMPDLPGVMRSNYDVRELRQKIKNERESAPRLQVQSVAPRE  180
gi|480327360|gb|AGJ83518.1|      YCKGMGIVQPYMRNDFDRNEMPDLPGVMRSNYDVRELRQKIKNERESAPRLQVQSVAPRE  180
gi|480327200|gb|AGJ83438.1|      YCKGMGIVQPYMRNDFDRNEMPDLPGVMRSNYDVRELRQKIKNERESAPRLQVQSVAPRE  180
gi|480327520|gb|AGJ83598.1|      YCKGMGIVQPYMRNDFDRNEMPELPGVMRSNYDVRELRQKIKNERESAPRLQVQSVAPRE  180
gi|480327400|gb|AGJ83538.1|      YCKGMGIVQPYMRNDFDRNEMPDLPGVMRSNYDVRELRQKIKNERESAPRLQVQSVAPRE  180
gi|480327380|gb|AGJ83528.1|      YCKGMGIVQPYMRNDFDRNEMPDLPGVMRSNYDVRELRQKIKNERESAPRLQVQSVAPRE  180
gi|480327280|gb|AGJ83478.1|      YCKGMGIVQPYMRNDFDRNEMPDLPGVMRSNYDVRELRQKIKNERESAPRLQVQSVAPRE  180
gi|557882471|gb|AEO19765.2|      YCKGMGIVQPYMRNDFDRNEMPDLPGVMRSNYDVRELRQKIKNERESAPRLQVQSVAPRE  180
gi|480327640|gb|AGJ83658.1|      YCKGMGIVQPYMRNDFDRNEMPDLPGVMRSNYDVRELRQKIKNERESAPRLQVQSVAPRE  180
gi|480327420|gb|AGJ83548.1|      YCKGMGIVQPYMRNDFDRNEMPDLPGVMRSNYDVRELRQKIKNERESAPRLQVQSVAPRE  180
gi|480327240|gb|AGJ83458.1|      YCKGMGIVQPYMRNDFDRNEMPDLPGVMRSNYDVRELRQKIKNERESAPRLQVQSVAPRE  180
gi|480327260|gb|AGJ83468.1|      YCKGMGIVQPYMRNDFDRNEMPDLPGVMRSNYDVRELRQKIKNERESAPRLQVQSVAPRE  180
```

```
gi|410443430|gb|AFV67789.1|      YCKGMGIVQPYMKNDFDRNEMPDLPGVMRSNYDIRELRQKIKSEREMAPRPQIQSAAPRE  180
gi|443411621|gb|AGC83568.1|      YCKGMGIVQPYMRNDFDRNEMPDLPGVMRSNYDIRELRQKIKSEREMAPRSQIQSAAPRE  180
gi|557882457|gb|AEO19789.2|      YCKGMGIVQPYMRNDFDRNEMPDLPGVMRSNYDIRELRQKIKNEREMAPRPQIQSAAPRE  180
gi|545290061|gb|AGW27487.1|      YCKGMGIVQPYMRNDFDRNEMPDLPGVMRSNYDIRELRQKIKNEREMAPRPQIQSAAPRE  180
gi|545290083|gb|AGW27499.1|      YCKGMGIVQPYMRNDFDRNEMPDLPGVMRSNYDIRELRQKIKNEREMAPRPQFQSAAPRE  180
gi|389616810|gb|AFK91775.1|      YCKGMGIVQPYMKNDFDRNEMPNLPGVMRSNYDIRELRQKIKNEREMAPRPQVQSAVPRE  180
gi|480327560|gb|AGJ83618.1|      YCKGMGIVQPYMKNDFDRNEMPDLPGVMRSSYDIRELRQKIKNEREMAPRPQVQSTVSRE  180
gi|210076696|gb|ACJ06706.1|      YCKGMGIVTPYMRNDFDRTEVPELPGVMKSHYDIRELRQKIRSEREQVPRFQVQNVAQKE  180
gi|355346214|gb|AER60537.1|      YCKGMGIVTPYMRNDFDRTEMPELPGVQRSHYDVRELRQKIRSEREQAPRFQVQSATQKG  180
                                 ******** ***:*****.*:*:**** :* **:*******:.*** .** *.:... :

gi|480327480|gb|AGJ83578.1|      ESRWMDDDEAKVDEEAKEMIPGPSRLEKLREARGNVLKELEAGINWNLDEGDKGDRDEQE  240
gi|385722006|gb|AFI73131.1|      ESRWMDDDEAKVDDEAKEIVPGTSGLEKLREARSNVFKEVEAVINWNLDERDEGDRDERG  240
gi|480327600|gb|AGJ83638.1|      ELRWMDDDEVKVDEEAKGMIPGTSRLEKLREARSNVFKEVEAGINWNLDEKDDEGGSERE  240
gi|410444351|gb|AFV68257.1|      ESRWMDDDEAKVDEEAKEMIPGTSRLEKLREARNNVFKEVEAGINWNLDEKDEEDRGERE  240
gi|480327500|gb|AGJ83588.1|      ESRWMDDDEAKVDEEAKEMIPGTSRLEKLRETRNNVFKEVEAGINWNLDEKDEEDRDERE  240
gi|480327440|gb|AGJ83558.1|      ESRWMDDDEAKVDEEAKEMIPGTSRLEKLREARSNVFKEVEAGINWNLDEKDVEDRDERG  240
gi|480327360|gb|AGJ83518.1|      ESRWMDDDEAKVDEEAKEMIPGTSRLEKLREARSNVFKEVEAGINWNLDEKDDEDRDEQE  240
gi|480327200|gb|AGJ83438.1|      ESRWMDDDEAKVDEEAKEMIPGTSRLEKLREARSNVFKEVEAGINWNLDEKDKEDRDERE  240
gi|480327520|gb|AGJ83598.1|      ESRWMDDDEAKVDEEAKEMIPGTSRLEKLREARSNVFKEVEAGINWNLDEKDEEDRDERE  240
gi|480327400|gb|AGJ83538.1|      ESRWMDDDEAKVDEEAREMIPGTSRLDKLREARSNVFKEVEAGINWNLDEKDEEDRDERE  240
gi|480327380|gb|AGJ83528.1|      ESRWMDDDEAKVDEEAKEMIPGTSRLEKLREARNNVFKEVEAGINWNLDEKDEEDRDERG  240
gi|480327280|gb|AGJ83478.1|      ESRWMDDDEAKVDEEAKEMVPGTSRLEKLREARSNVFKEVEAGINWNLDEKDEEDRDERE  240
gi|557882471|gb|AEO19765.2|      ESRWMDDDEAKVDEEAKEMIPGTSRLEKLREARGNVFKEVEAGINWNLDEKDEEDRDERE  240
gi|480327640|gb|AGJ83658.1|      ESRWMDDDEAKVDEEAKEMIPGTSRLEKLREARSNVFKEVEAGINWNLDEKDEEDRDERE  240
gi|480327420|gb|AGJ83548.1|      ESRWMDDDEAKVDEEAKEMIPGTSRLEKLREARSNVFKEVEAGINWNLDEKDEEDRDERE  240
gi|480327240|gb|AGJ83458.1|      ESRWMDDDEAKVDEEAKEMIPGTSRLEKLREARSNVFKEVEAGINWNLDEKDEEDRDERE  240
gi|480327260|gb|AGJ83468.1|      ESRWMDDDEAKVDEEAKEMIPGTSRLEKLREARSNVFKEVEAGINWNLDEKDEEDRDERE  240
gi|410443430|gb|AFV67789.1|      ESRWMDEDEERVNEEIKEAASNVGRLEKLREARTNMFKEVEAGVSWNLNHQSEEEADGDE  240
gi|443411621|gb|AGC83568.1|      ESRWMDEDEARVNEEIKEAASSVGRLERLREARTNMFKEVEAGVSWNLDHQSEEEADGDE  240
gi|557882457|gb|AEO19789.2|      ESRWMDEDEARVNEEIKEAASSVGRLERLREARTNMFREVEAGVSWNLDHQSEEEADGDE  240
gi|545290061|gb|AGW27487.1|      ESRWMDEDEARVDEEIKEAASSVGRLERLREARTNMFKEVEAGVSWNLNHQSEEEADGDE  240
gi|545290083|gb|AGW27499.1|      ESRWMDEDEARVDEEIKEASSSVGRLERLREARTNMFKEVEAGVSWNLNHQSEEEADGDE  240
gi|389616810|gb|AFK91775.1|      ESRWMDEDEARVSEEMKEAASSASRLERLREARANMFKEVEAGVSWSLSHQGEERADEDV  240
gi|480327560|gb|AGJ83618.1|      ESRWMDEDEARVSEEMKEAASSVSRLEGLREARANMFKEVEVGVSWNLSHQGEERADKDE  240
gi|210076696|gb|ACJ06706.1|      GLRWMDEDEAKANDESEDAISTETETVTLQTLGGDEFKKVELGDNWSLHKSDVSTENDGK  240
gi|355346214|gb|AER60537.1|      ELRWMDEDEAKVNDEVDEATAEKPKPMRPRMLKVEGFKKVEPGVNWNPEKDSVSEGEEEE  240
                                   ****:** :..:*              :    : ::::*   .*.  .

gi|480327480|gb|AGJ83578.1|      DEEEVKALSDDDERGEDASDDEHLKTHITKEYIEKVAKQIKLKDERFMSLSSAMPQASGG  300
gi|385722006|gb|AFI73131.1|      DEEQVKTLSDDDDQGEDASDDEHPKTHITKEYIEKVAKQIKLKDERFMSLSSAMPQASGG  300
gi|480327600|gb|AGJ83638.1|      AEEQVKTQSDDDEQGEDASDDEHPKTHITKEYIEKVAKQIKLKDERFMSLSSAMPQASGG  300
gi|410444351|gb|AFV68257.1|      NEEQVKNLSDDDEQGEDASDDEHPRTHITKEYIEKVAKQIKLKDERFMSLSSAMPQASGG  300
gi|480327500|gb|AGJ83588.1|      DEEQVKALSDDDEQGEDASDDEHPKTHITKEYIEKVAKQIKLKDERFMSLSSAMPQASGG  300
gi|480327440|gb|AGJ83558.1|      DEEQVKTLSDDDEQGEDASDDEHPKTHITKEYIEKVAKQIKLKDERFMSLSSAMPQASGG  300
gi|480327360|gb|AGJ83518.1|      DEGRVKTLSDDDEQGEDASDDEHPKTHITKEYIEKVAKQIKLKDERFMSLSSAMPQASGG  300
gi|480327200|gb|AGJ83438.1|      DEERVKTLSDDDEQGEDASDDEHPKTHITKEYIEKVAKQIKLKDERFMSLSSAMPQASGG  300
gi|480327520|gb|AGJ83598.1|      DEEQVKTLSDDDEQGEDASDDEHPKTHITKEYIEKVAKQIKLKDERFMSLSSAMPQASGG  300
gi|480327400|gb|AGJ83538.1|      DEERVKTLSDDDEQGEDASDDEHPKTHITKEYIEKVAKQIKLKDERFMSLSSAMPQASGG  300
gi|480327380|gb|AGJ83528.1|      DEEQVKTLSDDDEQGEDASDDEHPKTHITKEYIEKVAKQIKLKDERFMSLSSAMPQASGG  300
gi|480327280|gb|AGJ83478.1|      DEERVKTLSDDDEQGEDASDDEHPKTHITKEYIEKVAKQIKLKDERFMSLSSAMPQASGG  300
gi|557882471|gb|AEO19765.2|      DEEQVKTLSDDDEQGEDASDDEHPKTHITKEYIEKVAKQIKLKDERFMSLSSAMPQASGG  300
gi|480327640|gb|AGJ83658.1|      NEERVKTLSDDDEQGEDASDDEHPKTHITKEYIEKVAKQIKLKDERFMSLSSAMPQASGG  300
gi|480327420|gb|AGJ83548.1|      DEERVKTLSDDEEQGEDASDDEHPKTHITKEYIEKVAKQIKLKDERFMSLSSAMPQASGG  300
gi|480327240|gb|AGJ83458.1|      DEERVKTLSDDDEQGEDASDDEHPKTHITKEYIEKVAKQIKLKDERFMSLSSAMPQASGG  300
gi|480327260|gb|AGJ83468.1|      DEEQVKTLSDDDEQGEDASDDEHPKTHITKEYIEKVAKQIKLKDERFMSLSSAMPQASGG  300
gi|410443430|gb|AFV67789.1|      DGDRVDHQVDEDEQGEDASDDEHPKTHITKEYIEKVAKQVKLKDERFMSLSSAMPQASGG  300
gi|443411621|gb|AGC83568.1|      DGDHANHQSDEDEQGEDASDDEHPKTHITKEYIEKVAKQVKLKDERFMSLSSAMPQASGG  300
gi|557882457|gb|AEO19789.2|      DGDHANHQADEDEQGEDASDDEHPKTHITKEYIEKVAKQVKLKDERFMSLSIAMPQASGG  300
gi|545290061|gb|AGW27487.1|      DGDHANHQADEDEQGEDASDDELPKTHITKEYIEKVAKQVKLKDERFMSLSSAMPQASGG  300
gi|545290083|gb|AGW27499.1|      DGDHANHQADEDEQGEDASDDEHPKTHITKEYIEKVAKQVKLKDERFMSLSSAMPQASGG  300
gi|389616810|gb|AFK91775.1|      DEDHDDHQADEDEQDEDASDDEQLKTHITKEYIEKVAKQVKLKDERFMSLSSAMPQASGG  300
gi|480327560|gb|AGJ83618.1|      DEDHDDYRADEDERGEDASDDEQLKTHITKEYIEKVAKQVKLKDERFMSLSSAMPQASGG  300
gi|210076696|gb|ACJ06706.1|      D-KCGEEQNDDEDEEETSEDEVPKTHLTKEYIEKVSKQLKSKDERLMSLSGAMPQASGN  299
gi|355346214|gb|AER60537.1|      P-RNAGLQGREIESDEGSSGEGEQETHMTKEYIEKVSKHMKSNDERFMSLSGAMPQVNGG  299
                                           : :  * :* :   .**:********:*::* :***:**** ****..*

gi|480327480|gb|AGJ83578.1|      FDRMIVTKKLKWQNVPLYCFDESSKRYELQCVGACERVAFVSKDMSLIILPVGV        354
gi|385722006|gb|AFI73131.1|      FDRMIVTKKLKWQNVPLYCFDESLKRYELQCVGACERVAFVSKDMSLIILPVGV        354
gi|480327600|gb|AGJ83638.1|      FDRMIVTKKLKWHNVPLYCFDESSKRYELQCVGACERVAFVSKDMSLITLPVGV        354
gi|410444351|gb|AFV68257.1|      FDRMIVTKKLKWQNVPLYCFDESSKRYELQCVGACERVAFVSKDMSLIILPVGV        354
gi|480327500|gb|AGJ83588.1|      FDRMIVTKKLKWQNVPLYCFDESSKRYELQCVGACERVAFVSKDMSLIILPVGV        354
gi|480327440|gb|AGJ83558.1|      FDRMIVTKKLKWQNVPLYCFDESSKRYELQCVGACERVAFVSKDMSLIILPVGV        354
gi|480327360|gb|AGJ83518.1|      FDRMIVTKKLKWQNVPLYCFDESSKRYELQCVGACERVAFVSKDMSLIILPVGV        354
gi|480327200|gb|AGJ83438.1|      FDRMIVTKKLKWRNVPLYCFDESSKRYELQCVGTCERVAFVSKDMSLIILPVGV        354
gi|480327520|gb|AGJ83598.1|      FDRMIVTKKLKWQNVPLYCFDESSKRYELQCVGACERVAFVSKDMSLIILPVGV        354
gi|480327400|gb|AGJ83538.1|      FDRMIVTKKLKWQNVPLYCFDESSKRYELQCVGACERVAFVSKDMSLIILPVGV        354
gi|480327380|gb|AGJ83528.1|      FDRMIVTKKLKWQNVPLYCFDESSKRYELQCVGACERVAFVSKDMSLIILPVGV        354
gi|480327280|gb|AGJ83478.1|      FDRMIVTKKLKWQNVPLYCFDESSKRYELQCVGACERVAFVSKDMSLIILPVGV        354
gi|557882471|gb|AEO19765.2|      FDRMIVTKKLKWQNVPLYCFDESSKRYELQCVGACERVAFVSKDMSLIILPVGV        354
gi|480327640|gb|AGJ83658.1|      FDRMIVTKKLKWQNVPLYCFDESSKRYELQCVGACERVAFVSKDMSLIILPVGV        354
gi|480327420|gb|AGJ83548.1|      FDRMIVTKKLKWQNVPLYCFDESSKRYELQCVGACERVAFVSKDMSLIILPVGV        354
gi|480327240|gb|AGJ83458.1|      FDRMIVTKKLKWQNVPLYCFDESSKRYELQCVGACERVAFVSKDMSLIILPVGV        354
gi|480327260|gb|AGJ83468.1|      FDRMIVTKKLKWQNVPLYCFDESSKRYELQCVGACERVAFVSKDMSLIILPVGV        354
```

```
gi|410443430|gb|AFV67789.1|      FDRMIVTKKLKWQNVPLYCFDESTKRYELQCVGACERVAFVSKDMSLIILPVGV       354
gi|443411621|gb|AGC83568.1|      FDRMIVTKKLKWQNVPLYCFDESTKRYELQCVGACERVAFVSKDMSLIILPVGV       354
gi|557882457|gb|AEO19789.2|      FDRMIVTKKLKWQNVPLYCFDESTKRYQLQCVGACERVAFVSKDMSLIILPVGV       354
gi|545290061|gb|AGW27487.1|      FDRMIVTKKLKWQNVPLYCFDESTKRYELQCVGACERVAFVSKDMSLIILPVGV       354
gi|545290083|gb|AGW27499.1|      FDRMIVTKKLKWQNVPLYCFDESTKRYELQCVGACERVAFVSKDMSLIILPVGV       354
gi|389616810|gb|AFK91775.1|      FDRMIVTKKLKWQNVPLYCFDESTKRYELQCVGACERVAFVSKDMSLIILPVGV       354
gi|480327560|gb|AGJ83618.1|      FDRMIVTKRLKWQNVPLYCFDESTKRYELQCVGACERVAFVSKDMSLIILPVGV       354
gi|210076696|gb|ACJ06706.1|      FDHVIVIKKLKWQNVPLFCLDESSKRYDLQCVGACERVAFVSKDLSLLTLPIGV       353
gi|355346214|gb|AER60537.1|      FDRVIVIKKLKWQNVPLYCIDESSKKYELQCVGACERVAFVSKDMSLIILPVGV       353
                                 **::** *:***:****:*:*** *:*:*****:**********:**: **:**
```